Harnessing senescence to control PI3K/AKT/mTORC pathway-driven cancer through metabolic intervention

Haoran Zhu

ORCID: 0000-0003-3879-0389

Submitted in total fulfillment of the requirements of the degree of Doctor of Philosophy

May 2020

Faculty of Medicine, Dentistry and Health Sciences
Sir Peter MacCallum Department of Oncology
The University of Melbourne

Abstract

Oncogene-induced senescence (OIS) is a critical anti-tumour mechanism by arresting cell proliferation following oncogenic activation in normal cells. Cell cycle withdrawal along with senescence-associated secretory phenotype, deregulated metabolism and macromolecular changes are the hallmarks of cellular senescence. The PI3K/AKT/mTORC1 pathway is a key signalling pathway for homeostatic control of cell growth, proliferation, and survival. Molecular aberrations in the PI3K/AKT/mTORC1 signalling pathway have been identified in one third of solid tumours and more than 40 cancer types. Paradoxically, PI3K/AKT/mTORC1 hyperactivation causes a senescence-like phenotype in non-transformed cells. While most studies have focused on RAS/MAPK-induced senescence (RIS), little is known about the mechanisms regulating AKT-induced senescence (AIS) and its potential tumour-suppressive function. We hypothesise that understanding the molecular requirements for AIS and determining the essential regulators involved in AIS will identify therapeutic vulnerabilities for treatment of PI3K/AKT/mTORC1-driven cancer.

To characterise the molecular landscape of AIS, we performed the RNA-seq and metabolomics analysis in BJ-TERT human skin fibroblasts overexpressing AKT1 or $HRAS^{G12V}$ in Chapter 3. Compared to normal proliferating cells, AIS and RIS cells exhibited distinct metabolomes and transcriptomes, supporting metabolic and transcriptional reprogramming in OIS. The common molecular signatures in both AIS and RIS cells well represent the hallmarks of senescence and the molecular signatures that are unique for AIS or RIS are associated with the distinct molecular mechanisms underpinning these two types of OIS. The similar metabolic profile presented by the AIS and RIS cells with enhanced glycolysis, TCA cycle and oxidative phosphorylation to maximise energy production indicates a highly active metabolic status in OIS.

To gain more insight of metabolic dependency of AIS, we utilised Cystathionine β-Synthase (CBS), one of the top candidates in an RNAi screen we recently performed to identify key regulators of AIS and characterised its role in AIS maintenance in chapter 4. CBS acts as a hub for coordinating the transsulfuration and transmethylation pathways, regulating the biosynthesis of hydrogen sulfide (H_2S) and glutathione (GSH) and

modulating mitochondrial functions and cellular bioenergetics. We demonstrated that 1) the upregulation of transsulfuration pathway activity is an AIS-specific antioxidant response. 2) the metabolic reprogramming potentially couples to epigenetic alterations to maintain AIS. 3) CBS depletion releases oxidative stress through suppression of mitochondrial oxidative phosphorylation and causes AIS escape. The finding of loss of CBS resulting in the release of the senescence brake engaged by AKT hyperactivation promoted us to further evaluate the potential tumour suppressor role of CBS in gastric cancer. We provided *in vitro* and *in vivo* evidence to support that CBS depletion synergises with PI3K pathway activation to promote gastric cancer initiation and restoration of CBS inhibited gastric tumour growth via H_2S. These findings provided an example of harnessing metabolic vulnerabilities therapeutically for treating cancer.

Overall, our study provides novel mechanistic insights into AIS maintenance and more importantly, reveals the essential role of the metabolic reprogramming in AIS maintenance and escape. Further investigation of the molecular mechanisms underpinning PI3K/AKT/mTORC1-driven senescence and tumorigenesis will facilitate developing appropriate strategies to improve human health in aging, aging-related diseases, and cancer.

Declaration

This is to certify that:

1. This thesis comprises only original work towards Doctor of Philosophy where indicated in the preface.

2. Due acknowledgement has been made in the text to all other material used.

3. This thesis is fewer than 100,000 words in length, exclusive of tables, maps, bibliographies and appendices.

Haoran Zhu

1 Sep 2020

Preface

The majority of the work described in this thesis was designed, performed and analysed by the candidate under the supervision of Prof Richard Pearson and Dr Jian Kang.

Dr. Keefe Chan, Mr. Shaun Blake, Ms. Natalie Brajanovski, Mr. Elhadi Iich (Peter MacCallum Cancer Centre (PMCC), Australia), Mr. David De Souza, Dr. Vinod Narayana (Metabolomics Australia, Australia), Dr. Darren Creek and Ms. Dovile Anderson (Monash Institute of Pharmaceutical Sciences (MIPS), Australia), A/Prof Claudia Fu (Zhejiang Sci-Tech University, China) provided material and/or technical support.

cDNA library preparation and RNA sequencing were performed with assistance of by the Molecular Genomics Core Facility (PMCC, Australia). Bioinformatics analysis was performed with the assistance of Dr. Anna Trigos and Dr. Maria Doyle (PMCC, Australia). Tissue microarray was conducted with the assistance of A/Prof. Sarah Ellis and her team (Centre for Advanced Histology and Microscopy, PMCC, Australia) In vivo animal experiments were conducted with the assistance of A/Prof. Carleen Cullinane and her team (Translational Research Laboratory, PMCC, Australia) and PMCC's Animal Facility staff members. Dr. Keefe Chan and Dr. Elaine Sanij assisted with study design.

Original work from this study has been included in the following publications:

Zhu, H., Blake, S., Chan, K. T., Pearson, R. B. & Kang, J. Cystathionine beta-Synthase in Physiology and Cancer. *Biomed Res Int,* 2018, doi:10.1155/2018/3205125. (this publication is included as a section in Chapter 1 of this thesis (Appendix 1). The candidate planned, designed, organised and wrote all section of the manuscript, and performed subsequent edits suggested based on the coauthors' suggestions. Estimated contribution: 60%)

Zhu, H., Chan, K. T., Blake, S., Ellis, S., Cullinane, C., Sanij, E., Kang, J. & Pearson, R. B. CBS is an essential metabolic regulator in AKT-induced senescence and suppresses

oncogenic transformation and progression. (Sections in Chapter 4 of this thesis were adapted for inclusion in this publication. Estimated contribution: 60%)

Zhu, H.*, Blake, S.*, Kusuma, F. K., Pearson, R. B., Kang, J. [§] & Chan, K. T. [§] Oncogene-Induced Senescence: from Biology to Therapy. Mech Ageing Dev, 2020, doi: 10.1016/j.mad.2020.111229. *[§]these authors contributed equally. (Sections and figures in Chapter 1 of this thesis were adapted for inclusion in this publication. Inclusion of contents in a thesis is permitted by Elsevier.)

Chan, K. T., Blake, S., **Zhu, H.**, Kang, J., Trigos, A. S., Madhamshettiwar, P. B., Diesch, J., Paavolainen, L., Horvath, P., Hannan, R. D., George, A. J., Sanij, E., Hannan, K. M., Simpson, K. J., and Pearson, R. B. A functional genetic screen defines the AKT-induced senescence signaling network. Cell Death Differ, 2019, doi:10.1038/s41418-019-0384-8. (Sections in Chapter 3 of this thesis were adapted for inclusion in this publication.)

Other publications not included as part of this thesis:

Lee, E. F., Harris, T. J., Tran, S., Evangelista, M., Arulananda, S., John, T., Ramnac, C., Hobbs, C., **Zhu, H.**, Gunasingh, G., Segal, D., Behren, A., Cebon, J., Dobrovic, A., Mariadason, J. M., Strasser, A., Rohrbeck, L., Haass, N. K., Herold, M. J. and Fairlie, W. D. BCL-XL and MCL-1 are the key BCL-2 family proteins in melanoma cell survival, Cell Death Dis, 2019, doi:10.1038/s41419-019-1568-3.

No work presented in this thesis has been submitted for any other qualification or performed prior to candidature enrolment

No third party editorial assistance was used in the writing of any section of this thesis.

Acknowledgements

I gratefully acknowledge the financial support I received from the University of Melbourne (Melbourne Research Scholarship).

I would like to thank my supervisors for their enlightenment and unwavering support throughout my PhD program. Thank you to Prof. Rick Pearson for his guidance and insightful input, and for his Australian style humour encouraging me beyond my PhD life. I thank Dr. Jian Kang for her patience and extensive effort she has put into my project, and for her life advices provided from whom sharing a similar cultural background. Thank you to my unofficial supervisor Dr. Keefe Chan for his continuous dedication and support. All of them have certainly played critical roles in my growth.

To my mentors, A/Prof. Douglas Fairlie and Dr. Erinna Lee (Olivia Newton-John Cancer Research Institute), thank you for your supports, career advice, ideas and times attending my committee meetings. You helped and guided me growing from a naïve student to a scientist.

Thank you to all of the past and present members of the Pearson Lab who have made critical contributions to my PhD journey. It was a great pleasure to work with you all. To Dr Elaine Sanij, Shaun Blake, Allison Ogden, Natalie Brajanovski, Jessica Ahern and Diana Motion thank you for your generous intellectual and technical support. To my fellow PhD students: Xin Du, Elhadi Iich, Anthony Xuan, Dr. Eric Kusnadi, Dr. Jinbae Son, Dr. Shunfei Yan, Dr. Jirawas Sornkom, Dr. Shatha Abuhammad and Dr. Anna Trigos; thank you for your friendship and I feel privileged to have shared this ride with you.

My thanks to staff members at Peter Mac who assisted me during this project: A/Prof. Caroline Owen, Niranga Nawagamuwa and Dr. Erika Cretney (Research Education); Dr. Kristin Brown, Dr. Andrew Cox, and Dr. Lev Kats (PMCC); A/Prof. Sarah Ellis and Dr. Metta Jana (Centre for Advanced Histology and Microscopy); Dr Gisela Mir Arnau and Maria Doyle (Molecular Genomic Core); Dr Carleen Cullinane, Kerry Ardley, Rachel Walker and

Susan Jackson (Translational Research Lab); Ralph Rossi, Sophie Curcio and Viki Milovac (FACS Facility) and the Media Kitchen.

Beyond Peter Mac, thanks to: David De Souza and Dr. Vinod Narayana (Metabolomics Australia); Dr. Darren Creek and Dovile Anderson (Monash Institute of Pharmaceutical Sciences); Prof. Bruce Kemp and Dr. Dingyi Yu (St. Vincent's Institute of Medical Research), I truly appreciate all the support and advice you have provided me.

To my friends and extended family in Australia and China, thank you for your kind support and encouragement over the past years. Finally, my deepest thanks go to my beautiful wife, Wenyuan Lyu, for her unconditional love and steadfast consolation. She is the one who began, conquered and finished this long journey together with me.

Table of Contents

ABSTRACT ..... **III**

DECLARATION ..... **V**

PREFACE ..... **VII**

ACKNOWLEDGEMENTS ..... **IX**

TABLE OF CONTENTS ..... **XI**

LIST OF FIGURES ..... **XIII**

LIST OF TABLES ..... **XIV**

CHAPTER 1 INTRODUCTION **1**

1.1 Cellular senescence: from Biology to therapy 1
1.1.1 DNA damage response (DDR) and pRb-p53 tumour suppressor networks during OIS *2*
1.1.2 The senescence-associated secretory phenotype (SASP) and immune response during OIS *5*
1.1.3 Epigenetic regulation and chromatin remodelling *9*
1.1.4 Autophagy *11*
1.1.5 Experimental approaches to investigate OIS *13*
1.1.6 Therapeutic exploitation of OIS to treat cancer *19*
1.1.7 Concluding remarks *23*
1.2 Metabolic reprogramming in cellular senescence 24
1.2.1 Energy metabolism in senescence *25*
1.2.2 Reactive oxygen species-induced signalling in senescence *30*
1.2.3 Anabolic reprogramming in senescence *33*
1.2.4 Concluding remarks *36*
1.3 Cystathionine β-Synthase in Physiology and Cancer 37
1.4 Hypothesis and aims 38

CHAPTER 2 METHODS AND MATERIALS **39**

2.1 Mammalian cell culture 39
2.2 Pharmacological compounds 40
2.3 Plasmids cloning & amplification 40
2.4 Plasmid transfection, virus concentration & transduction 42
2.4.1 CRISPR/Cas-9 gene deletion of PTEN *43*
2.5 Fluorescence-activated cell sorting 43
2.6 siRNA transfection of BJ-TERT and IMR-90 fibroblasts 43
2.7 Gene expression analysis 44
2.7.1 RNA extraction *44*
2.7.2 Quantitative Real-Time Polymerase Chain Reaction (qRT-PCR) *44*
2.7.3 Methylation-specific PCR (MSP) *45*
2.8 Protein extraction & Western blotting 46
2.9 Cell proliferation, clonogenic & anchorage-independent growth assays 47
2.9.1 Cell proliferation assay *47*
2.9.2 Colony formation assay *47*
2.9.3 Anchorage-independent growth assay *48*
2.10 Histopathology & Immunofluorescence (IF) Staining 48
2.10.1 Senescence-associated ß-galactosidase staining & EdU labelling *48*
2.10.2 IF staining for cells *49*
2.11 Tissue Microarray (TMA) 50
2.12 Intracellular H_2S production measurement 51
2.13 Glutathione (GSH) detection assay 52
2.14 Metabolomics 52
2.14.1 Gas chromatography-mass spectrometry (GC/MS) based Metabolomics *52*
2.14.2 Thiol derivatization & detection using Liquid chromatography-mass spectrometry (LC/MS) based Metabolomics *53*

2.15 RNA-sequencing and analysis 54
2.16 Mouse xenograft model establishment 54
2.17 Chapter 2 Tables 56

CHAPTER 3 THE TRANSCRIPTIONAL AND METABOLIC PROFILING OF AKT-INDUCED SENESCENCE 65

3.1 Preface 65
3.2 Introduction 65
3.3 Results 66
3.3.1 Human skin fibroblasts (BJ-T cells) with hyperactivation of AKT and RAS develop senescence with distinct kinetics 66
3.3.2 Transcriptomic analysis identified the key molecular signatures of AIS 70
3.3.3 The dynamic transcriptomic changes during AIS 73
3.3.4 Metabolic reprogramming during OIS. 75
3.3.5 Mitochondrial hyperactivation and oxidative stress in AIS cells 80
3.3.6 A genome-wide RNAi screen identifies novel mediators of AIS 83
3.4 Discussion 87
3.4.1 The hallmarks of senescence shared by AIS and RIS 87
3.4.2 The distinct molecular mechanisms underpinning AIS and RIS 91
3.4.3 AIS and RIS exhibit similar metabolic phenotypes 93
3.5 Chapter 3 Tables 96

CHAPTER 4 CBS IS AN ESSENTIAL METABOLIC REGULATOR IN AKT-INDUCED SENESCENCE AND SUPPRESSES ONCOGENIC TRANSFORMATION AND PROGRESSION 102

4.1 Preface 102
4.2 Introduction 102
4.3 Results 105
4.3.1 Inhibition of CBS promotes escape from AKT-induced senescence (AIS) 105
4.3.2 Upregulated transsulfuration and transmethylation pathways in AIS cells are not affected by CBS deficiency. 111
4.3.3 CBS depletion reduces DNA and histone methylation in AIS cells. 117
4.3.4 CBS deficiency releases oxidative stress in AIS cells. 119
4.3.5 CBS deficiency induces transcriptional changes in AIS cells 123
4.3.6 Loss of CBS synergises with PI3K pathway activation to promote gastric tumour initiation. 127
4.3.7 CBS restoration suppresses gastric tumour growth through H_2S 133
4.4 Discussion 138
4.4.1 Upregulation of transsulfuration pathway functions as an AIS-specific antioxidant response 138
4.4.2 Metabolic reprogramming is coupled to epigenetic alterations during AIS and escape 140
4.4.3 CBS is a novel tumour suppressor in gastric cancer. 141
4.5 Chapter 4 Table 145

CHAPTER 5 OVERALL DISCUSSION AND FUTURE DIRECTIONS 146

5.1 Introduction 146
5.2 Transmethylation pathway and epigenetic modifications in AIS 148
5.3 Oxidative stress, antioxidant defence and transsulfuration pathway in senescence 149
5.4 PI3K/AKT/mTORC1 signalling pathway-induced senescence and cancer 150
5.5 Conclusion 152

BIBLIOGRAPHY 154

APPENDICES 175

List of Figures

Chapter 1

FIGURE 1. 1 4
FIGURE 1. 2 24

Chapter 3

FIGURE 3.1. 1 68
FIGURE 3.1. 2 69

FIGURE 3.2 72

FIGURE 3.3 74

FIGURE 3.4. 1 78
FIGURE 3.4. 2 79

FIGURE 3.5 82

FIGURE 3.6 85

FIGURE 3.7 90

Chapter 4

FIGURE 4.1. 1 104
FIGURE 4.1. 2 106
FIGURE 4.1. 3 108
FIGURE 4.1. 4 110

FIGURE 4.2. 1 113
FIGURE 4.2. 2 115

FIGURE 4.3 118

FIGURE 4.4 121

FIGURE 4.5. 1 125
FIGURE 4.5. 2 126

FIGURE 4.6. 1 129
FIGURE 4.6. 2 131

FIGURE 4.7. 1 135
FIGURE 4.7. 2 137

Chapter 5

FIGURE 5. 1 147

List of Tables

Chapter 2

TABLE 2. 1 56
TABLE 2. 2 57
TABLE 2. 3 58
TABLE 2. 4 59
TABLE 2. 5 61
TABLE 2. 6 63
TABLE 2. 7 64

Chapter 3

TABLE 3. 1 96
TABLE 3. 2 98
TABLE 3. 3 99
TABLE 3. 4 100
TABLE 3. 5 101

Chapter 4

TABLE 4. 1 145

CHAPTER 1 Introduction

1.1 Cellular senescence: from Biology to therapy

Cellular senescence is characterised as a state of permanent cell cycle arrest, initially described in 1961 by Hayflick and Moorhead who demonstrated that cultured human diploid cells ceased to proliferate after a finite number of cell divisions [1]. This replicative senescence is associated with telomere erosion due to the 'end replication problem', the inability of DNA polymerases to completely replicate the lagging DNA strand [2] [3] [4], which triggers a DNA damage checkpoint response [5] [6]. Subsequent investigation has demonstrated that several stressors can induce a similar phenotypic change, thus extending the definition of senescence to include a complex cellular response to stress. Since then, extensive investigations have established that senescence is a cellular response to a variety of stressors, including oncogene activation, hypoxia, reactive oxygen species and genotoxic agents [7].

Senescent cells display striking morphologic, structural and functional changes that are distinct from those observed in quiescent or terminally differentiated cells [8] [9] [10]. They typically display a large and flattened morphology with markedly increased lysosomal contents which allows the colourimetric staining of senescence-associated beta-galactosidase (SA-βGal) activity as a gold standard for identifying senescent cells [11] [12] [13]. Senescent cells also display persistent DNA damage and deregulated energy, protein and lipid homeostasis resulting in a distinct senescence-associated metabolic profile. More importantly, senescent cells secrete several extracellular matrix components and soluble factors, which are associated with autocrine and paracrine activities termed the senescence-associated secretory phenotype (SASP) [14] [15]. Senescent cells exhibit either all or just a subset of these phenotypes depending on the type of stimuli [5] [16].

Hyperactivation of oncogenes or loss of certain tumour suppressor genes in normal cells can lead to oncogene-induced senescence (OIS), which is considered as a potent tumour suppressive machinery. The first evidence for OIS was provided by studies that

transduced an activated Harvey rat sarcoma viral oncogene homolog *HRAS*^{G12V} allele in primary diploid fibroblasts, which resulted in an enlarged, flattened morphology and stalled mitotic activity [8]. Several landmark studies published in 2005 reported *in vivo* models of OIS. (1) Using a transgenic KRAS^{G12V}-driven murine lung cancer model, Collado and colleagues identified several novel senescence markers including p15^{INK4b}, Bhlhb2 (Dec1), and Tnfrsf10d (DcR2), which were observed in premalignant lung adenomas but not in malignant adenocarcinomas [17]. (2) Besides, hypo-phosphorylated retinoblastoma (Rb) protein, bound to growth-promoting E2F transcription factors, may recruit H3K9 methyltransferase such as Suv39h1 to direct heterochromatinization to the vicinity of E2F-responsive promoters, thus silencing S-phase genes during OIS [18]. (3) The oncogenic V600E mutation in *BRAF* triggered cell cycle arrest and SA-βGal activity in human naevi [19]. Intriguingly, expression of p16 without p53 upregulation or telomere attrition in these naevi suggested that other mechanisms may be involved in senescence induction. (4) Finally, while pharmacological inhibition of PTEN drives senescence [20], deletion of *Pten* in the mouse prostate cells led to the formation of benign prostatic intraepithelial neoplasia (PIN) and further loss of *Trp53* in *Pten*$^{-/-}$ mice caused invasive prostate cancer and lethal disease [21]. Taken together, these studies are consistent with OIS acting as a critical 'brake' against tumourigenesis in a variety of mammalian tissues. Moreover, depending on cell type and oncogenic stimulus, senescence is established through overlapping and distinct mechanisms [22]. The mechanistic understanding of OIS induction and maintenance will be critical for identification of potential novel strategies for treatment of oncogene-driven cancers in which the senescence 'brake' is released [23]. In this chapter, we discuss key mechanisms that control OIS, summarise current experimental approaches to investigate OIS, and overview recent advances in exploiting senescence to treat cancer.

1.1.1 DNA damage response (DDR) and pRb-p53 tumour suppressor networks during OIS

DNA damage is one of the most robust stimuli of senescence, which could be resulted from telomere dysfunction, chromatin aberrations, ultraviolet (UV)- or γ-irradiation, reactive oxygen species (ROS), or potent mitogenic signals [24] [25]. Activated oncogenes, for example HRAS^{G12V}, promote hyperproliferative growth and error-prone DNA replication [26]. DNA replication stress triggers the DDR pathways through the ATM

and ATR kinases [26] [15]. In response to DNA damage, p53 is phosphorylated by ATM and ATR at serine 15 to facilitate its transactivation [27]. p21 is the main downstream target of p53 upon DNA damage, which is another key mediator of senescence and functions as an inhibitor of CDK2 and CDK4 to induce cell cycle arrest [24] (Fig. 1.1). In murine cells, p53 can also be activated by p19/Arf in response to activation of Myc, Ras, E2f1 and E1a [8]. p19/Arf is transcribed from the Ink4a locus which also encodes p16 through a different open reading frame [28]. Arf stabilises p53 protein through binding to the E3 ubiquitin ligase Mdm2 [29]. However, evidence suggests this pathway is not conserved in human cells. Different from murine cells, upon ectopic expression of oncogenes such as RAS or MYC, human cells exit cell cycle by upregulating p16 instead of ARF [30] [19]. Although the mechanism of p16 activation is not well understood, p16/INK4a inhibits CDK4 and CDK2 by reassortment of Cyclin-CDK-Inhibitor Complexes [31]. This relieves inhibition of pRB, thereby repressing the E2F family of transcription factors which controlling transcription of cyclins and CDKs [32] (Fig. 1.1).

In contrast to RAS-induced senescence (RIS), activation of PI3K/AKT pathway induces senescence in the absence of DDR, including DNA damage foci or Senescence-Associated Heterochromatin Foci (SAHF), and displaying p53 induction rather than p16 [33] (Fig. 1.1). Moreover, we have demonstrated that PI3K/AKT signalling hyperactivation can trigger the PML/p19ARF-independent sequestration of MDM2 [34]. It is hypothesized that OIS can induce nucleolar stress response which leads to the release of ribosomal proteins RPL5/11 from the nucleolus into the nucleoplasm to sequester MDM2 [35] [36] [37]. In the absence of free MDM2, p53 accumulation subsequently increases p21 transcription independent of its phosphorylation status [38] [39]. We and others have shown that depletion of p53 by RNAi allowed AKT-induced senescent cells to escape senescence *in vitro* [34]. Furthermore, while Pten depletion in the mouse prostate results in the formation of benign neoplastic lesions with the presence of senescent cells [40], further deletion Trp53 leads to loss of senescent cells and invasive adenocarcinoma [21], supporting p53 is a key regulator of AKT-induced senescence (AIS).

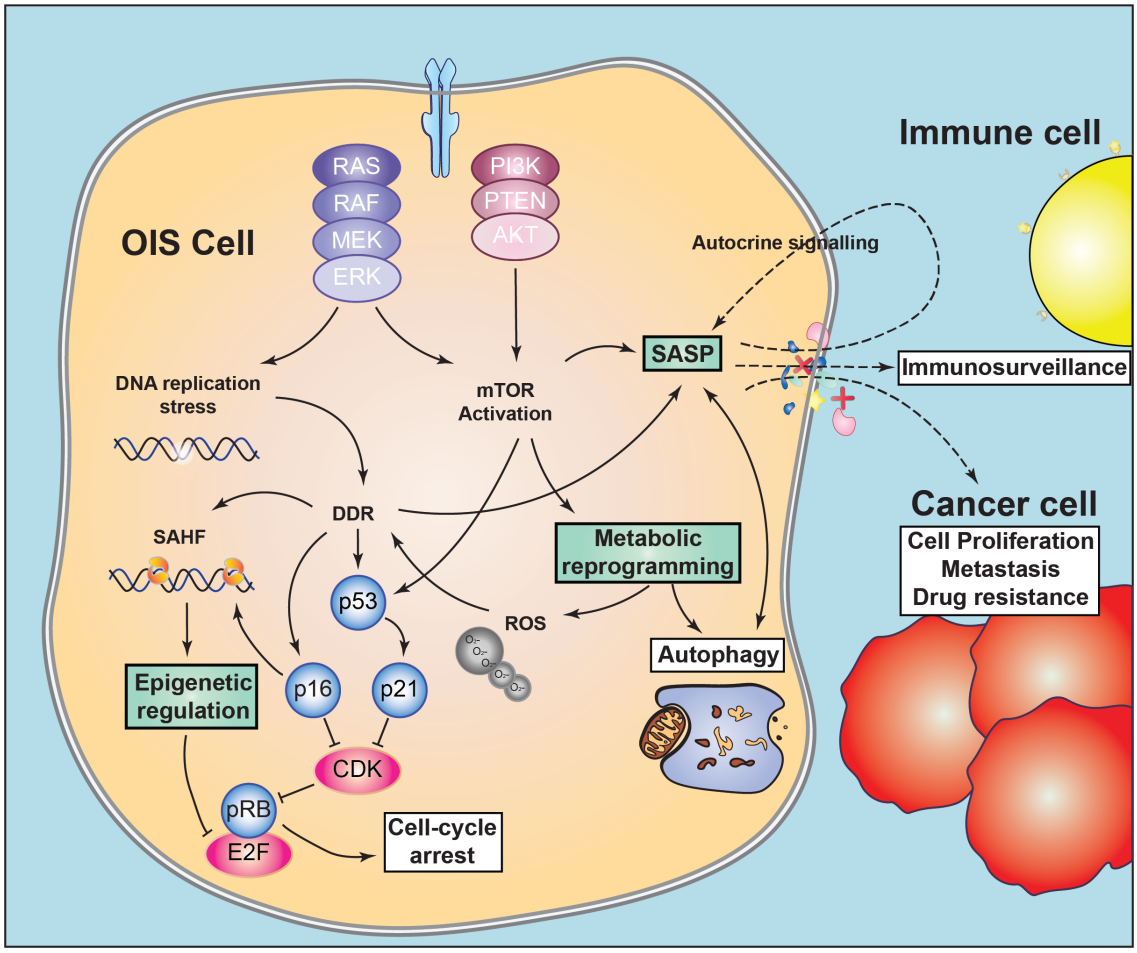


Figure 1.1 Cellular and molecular markers of RAS vs AKT oncogene-induced senescence.

(Figure reused from Zhu & Blake et al., 2020, Mech Ageing Dev. doi: 10.1016/j.mad.2020.111229. Inclusion of figures in a thesis is permitted by Elsevier)

Schematic representing the mechanisms of OIS induced by either the RAS/RAF/MEK/ERK or PI3K/AKT/mTORC1 pathway activation. Normal cells senesce upon oncogene hyperactivation, resulting in phenotypic changes. RAS-OIS shows active DDR, Senescence Associated Heterochromatic Foci, p16/pRB, where AKT-OIS occurs without DDR and is p53/p21-dependent. Subsequent inhibition of CDKs activates Rb to prevent pro-proliferative gene transcription and enforce cell-cycle arrest. Senescent cells exhibit senescence-associated secretory phenotype (SASP) and regulate microenvironment through autocrine, paracrine signalling. SASP can be activated through different mechanisms such as mTORC1 signalling, cGAS-cGAMP-STING pathway signalling as a result of DDR, impaired autophagy. Metabolic reprogramming, a hallmark of senescent cells, can be triggered directly by mTOR activation. Rewire metabolic pathways reinforces senescence by regulating autophagy or DDR through ROS production.

1.1.2 The senescence-associated secretory phenotype (SASP) and immune response during OIS

Different from quiescence and terminal differentiation, despite cell cycle arrest, senescent cells still actively interact with the microenvironment via SASP [14] [15]. The SASP is an important non-cell autonomous effect of senescence, comprising a secretome of cytokines, chemokines, growth factors and proteolytic enzymes [14] (Fig. 1.1). However, SASP is a double-edged sword during tumourigenesis and exerts both tumourigenic and tumour suppressive effect. An elegant study by the Campisi group systematically used antibody arrays to compare the SASP profiles of epithelial cells and fibroblasts in different types of senescence including replicative senescence, chemotherapy-induced senescence, and RIS [14]. They identified novel epithelial-mesenchymal transition and invasiveness signatures stimulated by the interleukins (IL)-6 and IL-8, suggesting that in some contexts the SASP may be pro-tumourigenic. They further determined that IL-1α is the principal cytokine which drives the SASP [41]. FACS analysis illustrated that the expression of membrane-associated IL-1α was higher in senescent cells than in control cells and drove IL-6 and IL-8 secretion. IL-1α is one of the senescence-associated secretory phenotype (SASP) inflammatory cytokines. IL-1α binding to the receptor IL-1R induces formation of a signalling complex including IL-1R, IL-1RAcp and IRAK1, which ultimately promotes nuclear translocation of NK-kB. NF-kB transactivates the expression of IL-6 and IL-8, two major SASP cytokines [41]. IL-1α is therefore a key regulator of the SASP. Inactivation of IL-1a has been shown to promote tumour progression by suppressing SASP and impairing immune cell infiltration without affect cell cycle arrest in vivo, supporting the pro-tumorigenic role of IL-1a signalling [42]. Overexpression of IL-1α was sufficient to halt proliferation and induce a SASP-like response driving paracrine senescence [43]. IL-1α is known to mediate a positive feedback loop with NF-κB activation and cytokine secretion [44]. Polysome fractionation experiments showed that rapamycin blocks IL-1α translation despite the absence of a functional 5' terminal oligopyrimidine (TOP) motif.Conversely, inhibition of IL-1R signalling blocked paracrine senescence in several murine models including RIS in liver hepatocytes, $Braf^{V600E}$-driven colon adenoma, $KRAS^{G12D}$-driven PanIN lesions, highlighting the essential role of SASP in OIS maintenance.

A persistent DDR is thought to promote the SASP [14] [15]. This was borne from the observation that the SASP correlated with the degree of genotoxic stress [14]. Transient treatment of human fibroblasts with low dose irradiation triggered a DDR without inflammatory secretion. In contrast, treatment with high dose irradiation led to a persistent DDR and SASP [15]. Using simultaneous $HRAS^{G12V}$ activation and ATM depletion in p53-deficient HCA2 colon cancer cells, the authors determined that IL-6 secretion was ATM-dependent and p53-independent, suggesting a direct association of SASP with DDR. Insight into the mechanism directly linking DDR to the SASP was recently uncovered [45]. In response to DNA damaging compounds that induce senescence, cytoplasmic DNA accumulates which can bind the cGMP-AMP (cGAMP) synthase (cGAS). Cytosolic DNA initiates cGAS to upregulate the cGAMP that interacts with the stimulator of interferon genes (STING) adaptor protein. This mediates an innate immune response and secretion of SASP components such as IL-1β, IL-8 and MMP12. Takahashi et al. have recently demonstrated that downregulation of DNases in senescent cells is responsible for the accumulated cytoplasmic nuclear DNA [46]. Similarly in OIS, loss of cGAS-cGAMP-STING pathway impaired senescence surveillance and promoted tumourigenesis in the liver OIS model induced by $NRAS^{G12V}$ [47] [48]. On the other hand, prolonged cGAS-cGAMP-STING pathway activation and SASP secretion may promote tumourigenesis and metastasis through chronic inflammation [49]. Taken together, persistent DDR promotes SASP through cGAS-cGAMP-STING pathway, and SASP can be either tumourigenic or tumour suppressive depending on cellular context.

Apart from cGAS-cGAMP-STING pathway triggered by DDR, SASP could also occur via p38 mitogen-activated protein kinase (MAPK) in the absence of a DDR. p38MAPK can be activated in response to oncogenic stress by $HRAS^{G12V}$ [50] [51]. During oncogenic stress, enhanced ROS production likely mediates p38MAPK induction [52, 53] [54]. Pharmacological inhibition of p38MAPK reduces the majority of SASP factor secretion [55]. In addition, activation of the upstream p38MAPK kinases (MKK)3 and MKK6 is sufficient to induce senescence by increase of nuclear factor kappa B (NF-κB) DNA-binding activity to promote transcription of SASP genes.

The serine/threonine kinase mammalian target of rapamycin (mTOR) drives cell growth and proliferation in response to growth factors, nutrients, and environmental cues [56]. mTOR signalling regulates the SASP at the levels of DNA transcription, mRNA translation, and mRNA degradation. Treatment with mTORC1 inhibitor Rapamycin in senescent cells induced by various stimuli (IR, doxorubicin, $HRAS^{G12V}$) significantly decreased the NF-κB pathway activity and reduced the secretion of 35% of SASP factors evaluated by enzyme-linked immunosorbent assay (ELISA) [57]. Given that IL-1α is known to initiate a positive feedback loop with cytokine secretion via NF-κB pathway, they further investigated how mTORC1 regulated the SASP via IL-1α [44]. Using polysome fractionation, they demonstrated that despite the absence of a functional 5' terminal oligopyrimidine (TOP) motif, rapamycin inhibited IL-1α translation. Furthermore, Herranz et al. identified that inhibitors of NF-κB signalling, IL-1 and mTOR could antagonize the SASP in RIS human lung fibroblasts through a compound screen [58] [59]. They further demonstrated that in OIS cells mTOR inhibition significantly downregulated translation of MAPK-activated protein kinase 2 (MAPKAPK2). MAPKAPK2 stabilises SASP mRNAs through phosphorylating and inhibiting ZFP36L1, a protein that mediates mRNA degradation. They thus proposed that mTOR activation during OIS inhibits ZFP36L1 via stimulating MAPKAPK2 translation, resulting in stabilisation of SASP-related mRNA.

Genetic knockdown studies together with SASP profiling and gene expression analysis demonstrate that the transcription of SASP genes is regulated by the NF-κB and CCAAT-enhancer binding protein β (C/EBPβ) transcription factors [60] [61] [62] [63] [64]. Inhibition of NF-κB pathway leads to bypass of OIS in fibroblasts [63]. However, NF-κB mediated SASP may either inhibit tumorigenesis or promote tumour progression dependent on genetic background and stage of disease. In a KRAS-driven model of pancreatic cancer, pancreatic-specific deletion of RelA, one NF-κB subunit, decreased survival by enhancing formation of pancreatic ductal adenocarcinoma (PDAC) [65]. RelA deletion led to an altered immune response characterized by infiltrating M2-polarised macrophages and CD11b(+)-Gr-1(+) myeloid-derived suppressor cells (MDSC), suggesting an anti-tumour role of NF-kB-mediated SASP is through immune surveillance. In contrast, during late-stage PDAC in the case of disengaged OIS by loss of p53 or p16

in conditional KRASG12D mice, knock out of RelA extended survival, supporting NF-kB mediated SASP plays a tumour-promoting role in late-stage tumorigenesis.

In addition to the transcriptional and translational regulation, the epigenetic reprogramming also involves in regulation SASP in OIS. Genome-wide ChIP-seq analysis identified loss of the repressive marker H3K27me3 from SASP genes contributed to the upregulation of SASP gene transcription [66]. Tasdemir and colleagues performed a genome-wide chromatin profiling of H3K27ac, a marker of active enhancers, and found a selective chromatin remodelling during RIS [67]. They reported that BRD4, the member of the bromodomain and extra terminal domain (BET) family of epigenetic modifiers, is recruited to superenhancer elements during OIS, and reside near SASP genes. Through genetic and pharmacologic inactivation of BRD4, they demonstrated that BRD4 is required for the paracrine function of the SASP but not involved in senescence proliferation arrest. Importantly, BRD4 inactivation impaired immune-mediated clearance of $NRAS^{G12D}$ senescent hepatocytes, highlighting a novel role for BRD4 in regulating the OIS program.

The SASP is thought to play a protective role by promoting immune surveillance and clearance of senescent cells from normal and tumour tissues (Fig. 1.1). However, chronic SASP secretion facilitates inflammation and tumourigenesis. Upon ectopic expression of $NRAS^{G12D}$ in the mouse liver cells, senescent hepatocytes were eliminated by natural killer (NK) cells while defective immune surveillance facilitated progression to hepatocellular carcinoma [68]. Furthermore, the Krizhanovsky group demonstrated that senescent cells upregulated MICA and ULBP2, which are the NK cell receptor (NKG2D) activating ligands, enabling their recognition by NK cells [69]. Conversely, knockout of Nkg2d in a mouse model of liver fibrosis induced by chronic CCl4 treatment led to a retention of senescent cells in the liver due to impaired clearance. Most recently, $Prf1^{-/-}$ mice with defective cell cytotoxicity showed increased senescent cell tissue burden and chronic inflammation, and exhibits age-related diseases and shortened lifespan [70]. In a murine prostate cancer model with Pten-deficiency, a CD11b(+)-Gr-1(+) tumour-infiltrating myeloid population kept tumour cells from becoming senescent, thereby leading to sustained tumour growth [71]. These Gr-1(+) cells suppressed the SASP by

secreting IL-1RA, the IL-1 receptor antagonist, which promotes senescence evasion and chemoresistance. Together, these studies highlight the complexity of the SASP in both inhibiting and promoting tumourigenesis. To reveal the therapeutic applicability of manipulating the SASP, it will therefore be essential to distinguish the pro- and anti-inflammatory arms through dissecting the molecular profiles of the SASP in a context-dependent manner.

1.1.3 Epigenetic regulation and chromatin remodelling

1.1.3.1 Senescence Associated Heterochromatic Foci during OIS

OIS cells display significant alterations in chromatin structures, including Senescence Associated Heterochromatic Foci (SAHF), the dense foci formed in the nucleus [72] [73]. Senescence Associated Heterochromatic Foci package proliferative genes including those silenced by pRB into heterochromatic domains, and contribute to the irreversibility of the senescence phenotype (Fig. 1.1). Senescence Associated Heterochromatic Foci formation in OIS is correlated to the upregulation of p16 ~~[~~74~~]~~ ~~[~~75~~]~~ ~~[~~72~~]~~, and depends on ATR expression and DNA replication. Inhibition of p53 or ATM leads to restoring of proliferation capacity of OIS cells while retaining increased heterochromatin induction ~~[~~74~~]~~. Senescence Associated Heterochromatic Foci formation may also restrain DDR signalling in OIS-cells, and perturbation of heterochromatin increases DDR signalling and leads to apoptosis [74].

Senescence Associated Heterochromatic Foci are enriched for many markers of heterochromatin, for example the heterochromatin protein 1 (HP1), the facultative heterochromatin histone variant macroH2A, H3K9me3 and H3K27me3 [73] [76]. A recent study revealed a multilayered structure of Senescence Associated Heterochromatic Foci composing of a core enriched for the histone mark H3K9me3 and an outer ring of H3K27me3 [76]. Furthermore, studies identified several effectors and structural components of Senescence Associated Heterochromatic Foci, such as HIRA/ASF1a [73], JARIDa/b [77], Cathepsin-L1 [78], HP1 proteins [72], and high mobility group A (HMGA) proteins [75]. Importantly, Yu et al. recently demonstrated that H3K9me3 is essential for OIS in melanocyte. Overexpression of H3K9 demethylases causes Ras/Braf-induced senescence escape and malignant transformation in both

mouse and zebrafish models [79]. Accumulating evidence supports that Senescence Associated Heterochromatic Foci formation is associated with a spatial restructure of pre-existing heterochromatin rather than a re-distribution or expansion of histone modification across the genome. However, Senescence Associated Heterochromatic Foci are not a common hallmark of cellular senescence and are rarely found *in vivo* [80]. Rather, they are preferentially formed following expression of specific oncogenes such as $HRAS^{G12V}$ and are not detected during replicative or stress-induced senescence.

In addition to Senescence Associated Heterochromatic Foci, global chromatin accessibility is changed in OIS cells. In RIS lung fibroblasts, a massive increase in chromatin accessibility has been detected by Assay for Transposase-Accessible Chromatin using sequencing (ATAC-seq). Different types of OIS display distinct profiles of accessible regions [81].

1.1.3.2 The nuclear lamina in OIS

The nuclear lamina has been implicated in chromatin nuclear positioning and transcriptional regulation. Lamina-associated domains (LADs), identified from a genome-wide mapping of Lamin B1, are transcriptionally silenced heterochromatin domains. During senescence, Lamin B1 is preferentially downregulated from H3K9me3-enriched regions of LADs [82], which may promote the spatial rearrangement of heterochromatin into Senescence Associated Heterochromatic Foci. More recently, two groups analysed the three-dimensional chromosomal structure through high-throughput chromatin conformation capture (3C) during OIS [76] and replicative senescence [83]. Both studies observed a relative decrease of long-range and increase of short-range chromatin contacts along an entire chromosome in both types of senescence compared to proliferating cells. Chandra and colleagues identified a focal increase of long-range interactions and a decrease of short-range interactions at the topologically associated domains (TAD), which is a genomic compartment in 3D chromatin space. Whether these focal changes of chromatin interactions are essential for Senescence Associated Heterochromatic Foci formation and how these chromosome structural modulations contribute to gene expression and cellular function during senescence remains unknown.

1.1.3.3 DNA and Histone modifications during OIS

Xie et al. characterised the DNA methylation changes during RIS and found that OIS cells displayed a minimal global DNA methylation reprogramming [84].In contrast, early studies in replicative senescence identified a global reduction of DNA methylation compared to the immortalised fibroblasts from rodents and humans [85, 86]. A whole genome single-nucleotide bisulfite-sequencing analysis demonstrated that human replicative senescent fibroblasts displayed a global DNA hypomethylation with focal hypermethylation [87]. The DNA hypomethylation associated with senescence is enriched at gene-poor, late-replicating sequences, and in nuclear (LADs), which are associated with heterochromatin histone markers. In contrast, focal hypermethylation is usually observed at CpG islands within gene promoters, resulting in suppression of pro-proliferative gene expression.

OIS cells also exhibit extensive histone modifications. Global remodelling of H3K27ac, an epigenetic marker of active enhancers, is significantly increased in OIS cells compared to proliferating cells [67]. During OIS the landscape of transcriptionally repressive marker at actively transcribed genes H4K20me1, is rewired at gene loci, including genes encoding ribosomal proteins (RPs) and RNAs, as well as p16INK4A, leading to the activation of nucleolar and mitochondrial functions [88]. Furthermore, the nucleosome-specific methyltransferase SETD8, which catalyses mono-methylation of histone H4 lysine 20, is downregulated in OIS cells. Depletion of SETD8 upregulated of ribosomal protein (RP) genes and mitochondrial activity, and mediated senescence in human fibroblasts. Together, these studies support that remodelling of the epigenome contributes to the complex suite of phenotypic changes associated with senescence.

1.1.4 Autophagy

Upon cellular senescence, organelles are often damaged as the result of ROS overproduction due to mitochondrial dysfunction [89]. In normal cells, autophagy eliminates the damaged organelle and facilitates the de novo organelle biosynthesis. To maintain intracellular homeostasis, macroautophagy, a catabolic pathway for degradation of cellular components through the lysosome, takes place in human cells to control organelle degradation [90]. This process starts with the formation of a double-

membrane cytosolic compartment containing cellular waste, termed autophagosome. Subsequently, the autophagosome fuses with the lysosome to form the phagolysosome, which digests contents requiring degradation [91]. During OIS, H_2O_2, one form of superoxide produced upon mitochondrial dysfunction, deactivates GSK3 and in turn triggers anabolism through SREBP1-mediated lipogenesis, eIF2B-mediated translation, and GS-mediated glycogenesis [92]. In contrast, GSK3 inactivation suppresses autophagy through TIP60/ULK signalling [93]. Moreover, inactivated GSK3 inhibits mitochondrial complex IV and leads to OXPHOS dysfunction and enhanced ROS production. Consequently, newly synthesized organelles through anabolism are immediately damaged due to the presence of oxidative stress. These findings explain how mitochondrial dysfunction interacts with autophagy in senescence via the production of ROS (Fig 1.1). Therefore, the elevated autophagic function appears to be required during OIS to counteract the cellular stress induced by mitochondrial dysfunction and ROS overproduction, which is discussed in later section 1.2.2.

How is autophagy activated during OIS? Young et al. demonstrated that the expression autophagy-related genes correlated with the SASP secretion, implicating a functional link between autophagy and SASP [94] (Fig. 1.1). It has been suggested that SASP leads to proteotoxic stress, thereby promoting the activation of the endoplasmic reticulum stress-UPR-autophagy cascade [95]. Indeed, the Elledge group identified a SASP regulator GATA4, which is stabilised in senescent human fibroblasts due to increased autophagic activity [96]. In turn, inhibiting autophagy suppresses IL-6 and IL-8 expression at the protein but not mRNA level, and delays cell proliferation arrest during OIS, supporting that autophagy promotes senescence establishment through facilitating SASP secretion [94]. Besides, oxidative stress may also mediate autophagic activation [97] [98] [99]. Consistent with a p38MAPK-dependent autophagic activation in ROS-induced senescence [100], a recent study established the direct link between ROS and autophagy in OIS. p38α signalling activation increases the autophagic flux through ULK1 phosphorylation, and mitochondrial ROS production is required for autophagy induction [101]. Finally, the downregulation of mTOR signalling, which is a major autophagy-suppressive pathway, has been linked to autophagy induction during RIS [102]. In response to RAS activation, mTORC1 and mTORC2 activity were initially activated

followed by suppression through a negative feedback loop: (1) The delayed suppression of mTORC1 signalling facilitates the expression of a key protein involved in autophagosome formation, termed ATG1 (human homolog ULK). (2) Activation of FoxO3a, a transcription factor controlling autophagy, was also observed and is thought to be associated with impaired mTORC2 activity. Together, these studies suggest that elevated autophagy is required for OIS induction.

How does autophagy maintain OIS? Studies suggest that autophagy accelerates senescence in the presence of oncogene activation. For example, one study visualized the increase of autophagic vacuoles together with SA-βGal activity in aging fibroblasts [103]. More importantly, the activity of autophagy is increased in oncogene-induced senescent fibroblasts through the upregulation of FoxO3A, a transcriptional activator [104]. Later studies showed that inhibition of autophagy delays the onset of OIS [94] [105]. In parallel, some findings indicate that autophagy not only facilitates senescence but is essential for senescence induction following stress stimuli. Inhibition of autophagy by depletion of one critical gene ATG7 failed to induce senescence after $HRAS^{G12V}$ overexpression [106], DNA-damaging agent and hydrogen peroxide treatment [107]. Taken together, these studies supposed that autophagy was required for OIS maintenance.

1.1.5 Experimental approaches to investigate OIS

We have summarised OIS from different aspects and revealed the complexity of senescence phenotypes. However, a few key questions about OIS remain to be answered: what are the essential regulators that governing OIS? Is it possible to target OIS cells therapeutically? How does senescent microenvironment influence tumourigenesis? Here, we review advanced approaches to study these questions over the past decade including gene expression profiling, high-throughput functional screens, epigenomics and proteomics analyses, and novel *in vivo* models.

1.1.5.1 Screening for senescence regulators

An initial study to screen for senescence regulators by comparing microarray expression data in human fibroblasts undergoing $HRAS^{G12V}$, replicative or H_2O_2-induced senescence,

identified exclusive upregulation of Ras-induced senescence 1 (Ris1) in RIS [108]. However, after performing extensive functional studies using mutant mice lacking Ris1, the authors concluded that despite the selective upregulation of Ris1 during RIS, it did not play a role in OIS and was not involved in tumour suppression [109]. These studies highlight the importance of functionally validating findings from gene expression datasets. Kuilman et al. screened for transcriptionally upregulated genes during B-RAF^{V600E}-OIS in TIG3 human fibroblasts through genome-wide microarray expression analysis [61]. Significant upregulations of C/EBPβ-dependent cytokines and chemokines were revealed by gene ontology analysis. They further demonstrated that IL-6 was required for B-RAF^{V600E}-OIS.

Several studies have employed cDNA overexpression screens to identify novel OIS regulators. Using MEFs deficient in a polycomb complex proto-oncogene Bmi1, Jacobs et al. transduced a cDNA library with replication-deficiency derived from a chorion carcinoma cell line named JEG3 and screened for genes that could confer immortalisation [110]. They determined that the transcription factor named Tbx2 was a novel negative regulator of Arf and a potential oncogene in breast cancer. In the context of RIS, Peeper and colleagues used the same cDNA overexpression library and identified DRIL1, a B-cell transcription factor that binds to the IgH locus [111]. Overexpression of DRIL transformed MEFs co-expressing the simian virus 40 (SV40) large T mutant and HRAS^{G12V}. To identify genes contributing to melanoma development, Lee et al. employed an inducible p16-expressing melanoma cell line transduced with a lentiviral overexpression library containing 17,030 ORFs [112]. They not only found the expected genes such as the human papillomavirus 18 E7 (HPV18E7), but also uncovered the novel genes including the HMGBs cooperating with p16 loss. Elledge and colleagues used a similar lentiviral overexpression approach with a ~15,000 human ORFeome 5.1 library [113] in BJ fibroblasts expressing the HPV E6 or E7, which inactivate the p53 or pRB pathway, respectively [114]. The authors characterised the role of the homeobox transcription factor DLX2. In particular, DLX2 expression attenuated signalling via the DDR kinases ATM and DNA-PK and p53 pathway activation, and correlated with tumour progression and prognosis in several human cancers. Conclusively, cDNA overexpression

screen is a powerful approach for identifying essential regulators that govern the senescence program.

To address the functional role of potential senescence regulators, the majority of OIS-rescue screens have employed genetic depletion by siRNA. The results from a functional genomics shRNA screen for extending lifespan of IMR-90 fibroblasts were applied to other types of senescence induced by $HRAS^{G12V}$ or DNA damage [60]. The authors found that CXCR2 knockdown delayed replicative senescence and that CXCR2 ligands were upregulated during OIS. They determined that NF-κB and C/EBPβ were activated during OIS, inducing the expression of CXCR2 ligands, which could reinforce senescence. To identify factors required for $BRAF^{V600E}$-mediated senescence, Wajapayee et al., performed a genome-wide shRNA bypass screen in BJ fibroblasts using a shRNAmir library consisting of ~62,400 shRNAs against ~28,000 genes [115]. The secreted insulin growth factor binding protein IGFBP7 was necessary and sufficient for $BRAF^{V600E}$-OIS. Furthermore, bisulfite sequencing revealed significant hypermethylation of the IGBP7 promoter during the transition from $BRAF^{V600E}$ naevi to melanoma, suggesting a role for IGBP7 in suppressing melanoma. However, another group later argued that IGFBP7 is not required for BRAF-Induced melanocyte senescence by showing BRAF signalling does not induce IGFBP7 expression, nor the expression of the IGFBP7 targets [116]. Kaplon et al. performed a screen targeting 15,000 genes using the near genome-wide lentiviral shRNA approach [117]. They identified the novel OIS regulator RAS and EF-hand domain containing (RASEF), whose promoter is hypermethylated in melanoma. RASEF depletion not only restored proliferation but also affected the SASP. Reactivation of both the IGBP7 and RASEF promoters by treatment of a DNA methyltransferase inhibitor named 5-aza-2'-deoxycytidine, mediated senescence in melanoma cell lines, implicating the role of epigenetic silencing in contributing to melanoma development. Thus, screens using genetic depletion through siRNA or shRNA can be utilised for identifying OIS regulators.

While these screens have focused on RAS/MAPK-induced senescence, little is known about the requirements for senescence induced by other oncogenes such as activated PI3K/AKT. Understanding the genetic requirements for PI3K/AKT-induced senescence

and determining their pathway specificity will be essential to identify in which contexts they can be manipulated to target cancer. Our group recently reported a siRNA escape screen from PI3K/AKT-induced senescence, which utilised multiparametric readouts including cell number, proliferation, and nuclear area, as well as a machine learning approach to phenotypically classify SA-βGal staining [118]. The inclusion of multiparametric readouts for OIS screening is becoming critical, as we previously reviewed that senescent cells do not display a single specific biomarker [119] [120]. We further identified the key signatures required to maintain AIS through a combination of transcriptome and metabolic profiling [121]. The new mechanistic insights into the regulation of AIS and identification of senescence regulators can provide potential therapeutic strategies to treat PI3K/AKT/mTORC1 pathway-driven tumours.

High-throughput drug screens are also exploited to explore the possibility of therapeutically targeting OIS. Alimonti et al. performed a screen to identify potential therapeutics that enhance senescence in $Pten^{-/-}$ MEFs, using a library of ~500 compounds in advanced preclinical development [122]. They identified and validated that casein kinase 2 (CK2) inhibitors enhanced senescence in $Pten^{-/-}$ by stabilising an essential senescence regulator Pml. Furthermore, the CK2 inhibitor CX-4945 induced senescence and prevented tumour progression in a prostate $Pten^{-/-}$ murine mouse model. However, the effects of this pro-senescence strategy on the SASP and immune response were not assessed. Due to the potentially deleterious effects of the SASP, future screens will be directed toward testing elimination of the SASP or selectively killing senescent cells.

Furthermore, recent advances in CRISPR (clustered, regulatory interspaced, short palindromic repeats) -Cas9 (CRISPR associated protein 9) technology have allowed gene editing in human cells [123]. Many genetic screens using CRISPR-Cas9 have interrogated protein-coding genes, but now it is possible to characterize endogenous enhancer elements. A functional genetic screen for endogenous p53-bound enhancers was performed in cells undergoing RIS [124]. Several enhancers were located proximal to the CDKN1A and its start site of transcription. Global run-on sequencing (GRO-seq) confirmed the induction of enhancer-associated RNAs. CRISPR-Cas9-mediated deletion

of a specific enhancer p53enh3507 resulted in the bypass of OIS as shown by increased BrdU labelling, decreased SA-βGal staining, and restoration of proliferation. More recently, a large-scale CRISPR screen was performed for therapy-induced senescence in parallel with RIS to identify SASP regulators [125]. The expression of SASP genes was enhanced upon CHEK2, HAS1, or MDK knockout, but was attenuated upon MTOR, CRISPLD2, or MORF4L1 knockout. Therefore, recent advances in CRISPR-knockout technology provides a great platform for studying OIS mechanisms.

In addition to genetic screening, an emerging approach involves the proteomics-based analysis of OIS. Mass spectrometry using Ti4+-IMAC enrichment identified phosphopeptides potentially contributing to the dynamic reprogramming of the phospho-proteome during B-RAF^{V600E}-OIS [126]. The Gil group has employed stable isotope labelling with amino acid in culture (SILAC)-based quantitative proteomics to profile the secretome from the conditioned medium of RIS cells [43] [58]. Given the hypothesis that selective mRNAs may be translated during OIS, a recent method used to investigate nascent protein synthesis is through the methionine analog L-azidohomoalanine (AHA) incorporation [127] [58]. Prospectively, future studies will integrate these proteomics and genetic screening datasets to provide a more complete picture of the senescence response.

1.1.5.2 The innovative approach to study OIS *in vivo*: Hydrodynamic transfection

In addition to murine models with tissue-specific expression of oncogenes to study OIS *in vivo*, an innovative approach utilises hydrodynamic transfection to deliver stable transposable elements harbouring NRAS^{G12V} into endogenous murine hepatocytes [68]. Given that the liver parenchyma is closely associated with the endothelial capillaries, a large volume, rapid tail vein injection introduces a hydrodynamic force sufficient to permeabilize the capillaries and generate pores in the parenchyma cells, allowing DNA introduction and stable transposon-mediated genomic integration [128]. After 6 days post-transfection, a subset of NRAS^{G12V}-expressing hepatocytes displayed staining for phosphorylated ERK as well as the senescence markers p21, p16, and SA-βGal [68]. Immunohistochemistry of NRAS^{G12V}-transduced livers revealed immune cell clusters consisting of CD4+ T cells, macrophages and neutrophils, and cytokine arrays indicated

that hepatocytes secreted several SASP cytokines. Immuno-deficient mice with defects in macrophage and NK cell function had significantly reduced the influx of innate immune cells, suggesting that innate immune cells play a critical role in clearing senescent cells. Strikingly, in longer-term (3 months) studies in these backgrounds, pre-malignant senescent hepatocytes progressed to hepatocellular carcinoma (HCC), supporting the observation that immune surveillance is critical for limiting tumour development. Similarly, Tasdemir et al. examined the effects of depleting BRD4 genetically or antagonising BRD4 using a compound termed I-BET762 (iBET), and illustrated that BRD4 is essential for the SASP secretion and immune surveillance [67].

Tordella and colleagues examined the role of another epigenetic regulator AT-rich Interaction Domain 1B (Arid1b) using the $NRAS^{G12V}$ liver OIS model [129]. Using a focused shRNA library of genes frequently deleted in HCC to screen for the bypass of replicative senescence in MEFs, they identified Arid1b, an element of the SWI/SNF chromatin-remodelling complex. Using hydrodynamic transfection into the liver, they found that knockdown of Arid1b cooperated with $NRAS^{G12V}$ to promote HCC formation. Overexpression of the Arid1b target gene Entpd7, a purine-converting enzyme, was sufficient to induce senescence and conferred vulnerability of $NRAS^{G12V}$-driven HCC to drugs that target nucleotide metabolism. Therefore, hydrodynamic transfection is a powerful non-viral approach for studying OIS in murine models.

It will be important to test the applicability of the hydrodynamic transfection approach to investigate senescence induced by other oncogenes such as constitutively active AKT. Indeed, the long latency (~6 months) of tumour induction [130] suggests that AIS may also play a role in limiting tumourigenesis. More recently, a spontaneous HCC mouse model was established to study tumour immune response through hydrodynamic transfection using AKT and NRAS [131]. CD8+ T cells were identified in HCC microenvironment; however, they were found exhausted due to the presence of Myeloid-derived suppressor cells and tumour-associated macrophage.

1.1.6 Therapeutic exploitation of OIS to treat cancer

Senescence is a protective mechanism in response to various stresses and plays beneficial roles in tumour suppression, tissue patterning, and wound healing [132] [133] [134]. However, it is becoming increasingly clear that when senescent cells accumulate in tissues, chronic SASP secretion may impair the functioning of neighbouring cells and contribute to aging, age-related diseases and cancer [135] [136]. It will be essential to identify the effects of the SASP in various contexts in order to harness it therapeutically. Key aspects of the "double-edged sword" of the SASP during OIS and potential strategies to combat the deleterious aspects of the SASP by either eliminating it or selectively killing senescent cells are reviewed.

1.1.6.1 Senostatics: Eliminating the SASP

The SASP in senescent cells either exerts a positive effect by promoting immune surveillance and prevent tumorigenesis or promotes inflammation, tissue dysfunction and tumorigenesis. To therapeutically exploit the SASP, the approaches including targeting the pathways that regulate the SASP or interfering specific SASP components, have been taken to preserve the protective effect and eliminate the harmful effect of the SASP. NF-κB pathway inhibition mediated apoptosis in a Trp53-depleted KRAS-driven murine lung cancer model [137]. However, NF-κB pathway inhibition also promoted chemoresistance in Bcl2-overexpressing Eμ-myc lymphomas [63]. Therefore, NF-κB inhibition may result in anti-tumour or pro-tumourigenic effects depending on the genetic background. Rapamycin, a mTORC1 inhibitor, has been demonstrated to extend lifespan in mice [138]. Considering that mTORC1 signalling is essential for the SASP, mTORC1 inhibitors may potentially be a therapeutic option for abrogating the SASP in cancer as well as aging-related diseases. Moreover, inhibition of BET using JQ1 or iBET attenuated the SASP during RIS in the liver [67]. BET inhibitors are in phase I or II clinical trials for treating several cancers, including NUT midline carcinoma, refractory Acute Myeloid Leukemia, lymphoma and haematological malignancies [139]. Moreover, existing agents that have already been used to treat immune diseases may be repurposed to target the SASP. For example, the IL-1R inhibitor anakinra or the IL-6R inhibitor tocilizumab are clinically approved to treat rheumatoid arthritis [140] [141]. Both agents may be repurposed to treat oncogene-driven cancers displaying chronic

inflammation. Moreover, the administration of JAK1/2 inhibitor ruxolitinib reduces SASP and systemic inflammation through blocking C/EBPβ activation in old age [142].

Several novel SASP regulators have been identified and may potentially be developed as senostatics. Recently, Kim et al. demonstrate that secretory carrier membrane protein 4 (SCAMP4) accumulated on the senescent cell surface, is required for secretion of SASP such as IL-6, IL-8, GDF-15, CXCL1 and IL-7 [143]. Furthermore, Georgilis et al. identified a novel SASP regulator PTBP1, which is involved in controlling intracellular trafficking [144]. PTBP1 inhibition alleviates the pro-inflammatory arm of SASP, decreases immune surveillance without accelerating tumourigenesis. Therefore, the idea of 'erasing the deleterious effects of the SASP but not re-activating the arrested cancer cell' is an exciting new aspect for discovering novel cancer therapeutics [145]. However, there are beneficial effects of SASP on wound healing, tissue patterning, and immune surveillance. Therefore, it is important to rigorously evaluate the long-term functional outcomes of SASP inhibition in order to prevent potential side effects.

1.1.6.2 Senolytic therapy: senescent cell selective killing

The SASP from OIS-cells may promote tumour growth and metastasis of neighbouring tumour cells by creating a tumour-suppressive microenvironment [146] [147] [148]. Senescent cells are resistant to apoptosis and thus provide a source of dormant cells that can be re-activated upon cessation of treatment resulting in disease relapse [149]. Indeed, despite cellular senescence being generally considered to be irreversible, several studies suggest that therapy-induced senescence can be bypassed and becoming highly tumourigenic cells [150] [151]. Therefore, the clearance of senescent cells in tumours not only suppresses tumour growth but also prevents drug resistance and disease relapse.

Is it possible to treat age-related pathologies and cancer by removing senescent cells? Van Deursen and colleagues provided the first proof-of-concept using fast-aging [152] and natural-aging murine models [135] expressing the transgene INK-ATTAC (INK-linked apoptosis through targeted activation of caspase). The INK-ATTAC allele allows the inducible deletion of cells carrying p16Ink4a, a senescence biomarker, upon addition of

the homo-dimerizing drug AP20187. Removal of p16Ink4a-positive cells decreased tumour incidence, extended median lifespan and attenuated age-related dysfunction of several organs and tissues, such as kidney, heart and fat tissue. Recently, Zhang et al. linked cellular senescence with neurodegenerative disease and demonstrated the beneficial effects of eliminating senescent cells using a senolytic cocktail of dasatinib plus quercetin (D + Q) [153]. In Alzheimer's disease (AD) patients and a murine model, senescent oligodendrocyte progenitor cells (OPCs) were induced due to the presence of amyloid-beta (Aβ) plaque, a pathological hallmark of AD. Senescent OPCs exhibits hyperactivated p21/p16 pathways and SAβ-Gal activity. Senolytic treatment selectively eliminated senescent OPCs in an *in vivo* AD model and relieved inflammation, Aβ deposition and cognitive deficits. Senolytics have also shown promising beneficial effects in other types of age-related diseases, such as CVD [154], osteoporosis [155] and fibrotic pulmonary disease [156]. These data strongly support that the accumulation of senescent cells contributes to age-related diseases and that clearance of senescent cells can attenuate or delay age-related diseases as in cancer.

The first potential senolytic drugs were identified by the Kirkland group through a viability screen [157]. The kinase inhibitors quercetin and dasatinib eliminated senescent cells by causing apoptosis; however, other groups later reported that these compounds were not specific for senescent cells [158] [159]. Recently, three studies identified the Bcl-2 family inhibitors such as ABT-263/ABT-737 to be selective for senescent cells [159] [160] [161]. These studies indicated that Bcl-2 family protein activation is a key molecular mechanism by which senescent cells show resistance to apoptotic stimuli. The pan-BCL inhibitors simultaneously inhibit several members of the BCL family of proteins: Bcl-2, Bcl-xL, and Bcl-w, but inhibition of the latter two seems to predominantly contribute to the cytotoxicity in senescent cells. Recently, Keizer and colleagues reported an alternative senolytic approach by disrupting the interaction between a PI3K/AKT-mediated transcription factor FOXO4 and p53 using a FOXO4 cell-penetrating peptide [158]. This approach selectively mediated p53 nuclear exclusion and cell-intrinsic apoptosis in senescent cells. In addition, a new drug delivery system designed by Munoz-Espin group enables selective senescent cell targeting. They coated cytotoxic drugs with galacto-oligosaccharides and showed that such drugs selectively

target senescent tumour cells *in vivo* based on their elevated SA-βGal activity [162]. Conclusively, different senolytic approaches have been developed to selectively target senescent cells, which may become novel therapeutics of cancer treatment.

Will senolytics provide more therapeutic benefits for cancer patients? The most promising senolytic agents to date are the pan-Bcl2 inhibitors. The toxicity and off-target effects on the immune and haematological systems [163] [164], and liver function [165] of pan-Bcl2 inhibitors would not be suitable for long term treatment of age-related diseases but could be acceptable for cancer treatment. Navitoclax (ABT-263) has been applied with success against small cell lung cancer [165] for metastatic and advanced solid tumours. As an alternative to targeting pro-survival pathways, Dorr et al. exploited the metabolic vulnerability of Therapy-Induced Senescent (TIS) cells to trigger cell death after a first treatment with cyclophosphamide (CTX) [95]. They found that high production of SASP factors promoted misfolded or toxic protein formation, which consequently activated the ER stress–UPR–ubiquitination autophagy cascade. Therefore, they used a synthetic lethal approach to inhibit glycolysis by 2-deoxyglucose (2DG) or antagonizing V-ATPases by bafilomycin A1 in SASP-producing TIS cells, resulting in further misfolded protein accumulation and triggering ER-stress related cell death. The benefits of senolytic therapy in relevant murine models have also been established. Treatment of dasatinib plus quercetin in chronologically aged mouse model selectively kills senescent cells, alleviates the secretion of pro-inflammatory cytokines, and improves physical dysfunction [166]. Similar evidence has been shown in murine tumour models, where selective elimination of chemotherapy-induced stromal senescent cells reduces the associated side effects, such as cardiac and liver dysfunction and general fatigue [158] [167]. In addition, Hubackova et al. recently documents that senescent cell selective elimination can also be achieved through targeting mitochondrial. Mitochondria-targeted tamoxifen (MitoTam) is commonly used as an anti-cancer therapy, and a low abundance of adenine nucleotide translocase-2 (ANT2) is required for the susceptibility of senescent cells to MitoTam. Restoring ANT2 in senescence cells leads to MitoTam resistance, while ANT2 depletion increases MitoTam sensitivity in normal cells [168]. Together, these studies provided strong evidence that senolytic approaches may be utilized as novel anti-cancer therapeutics.

Senolysis is clearly a growing and exciting field, but the excitement over its therapeutic potential at the same time needs caution as very little is known about how it works. In particular, it is unclear how senescent cells confer resistance to apoptosis and how is this overcome by senolytic agents? Is the effect of senolytics dependent on the mode of induction of senescence? Do different agents kill senescent cells by the same or distinct mechanisms? Also, what are the consequences of eliminating OIS-cells in tumours? What effect does the killing of senescent cells have on the immune response/tumour microenvironment? The mechanistic insights into these aspects will accelerate developing therapeutics to further benefit human health in aging, aging-related diseases, and cancer.

1.1.7 Concluding remarks

Cellular senescence was initially believed to be irreversible. But it is increasingly recognized that it is a highly complicated process contributing to both normal development and pathological states. In this section, some major progress in characterising key senescence biomarkers and defining the biological changes and consequences of OIS has been reviewed. However, there are a number of important questions remain to be answered. How do different oncogenic stimuli induce senescence? What are the mechanisms of disengaging senescent brake? The versatility of high-throughput screening approaches, omics-based approaches, and newly developed *in vivo* models will continue to unravel the answers to these questions. In the next section, we will provide more insights into metabolic reprogramming, a hallmark of cellular senescence, in OIS and other types of cellular senescence.

1.2 Metabolic reprogramming in cellular senescence

Apart from the key features described above in OIS, cellular senescence is also characterized by substantial metabolic alterations, which is the research area I am particularly interested in. In this section, I will review the role of altered metabolism, specifically energy metabolism, oxidative stress, and anabolism, in the establishment and maintenance of cellular senescence. Overall, the up-regulation of these metabolic activities were evidenced during the OIS program (Fig. 1.2).

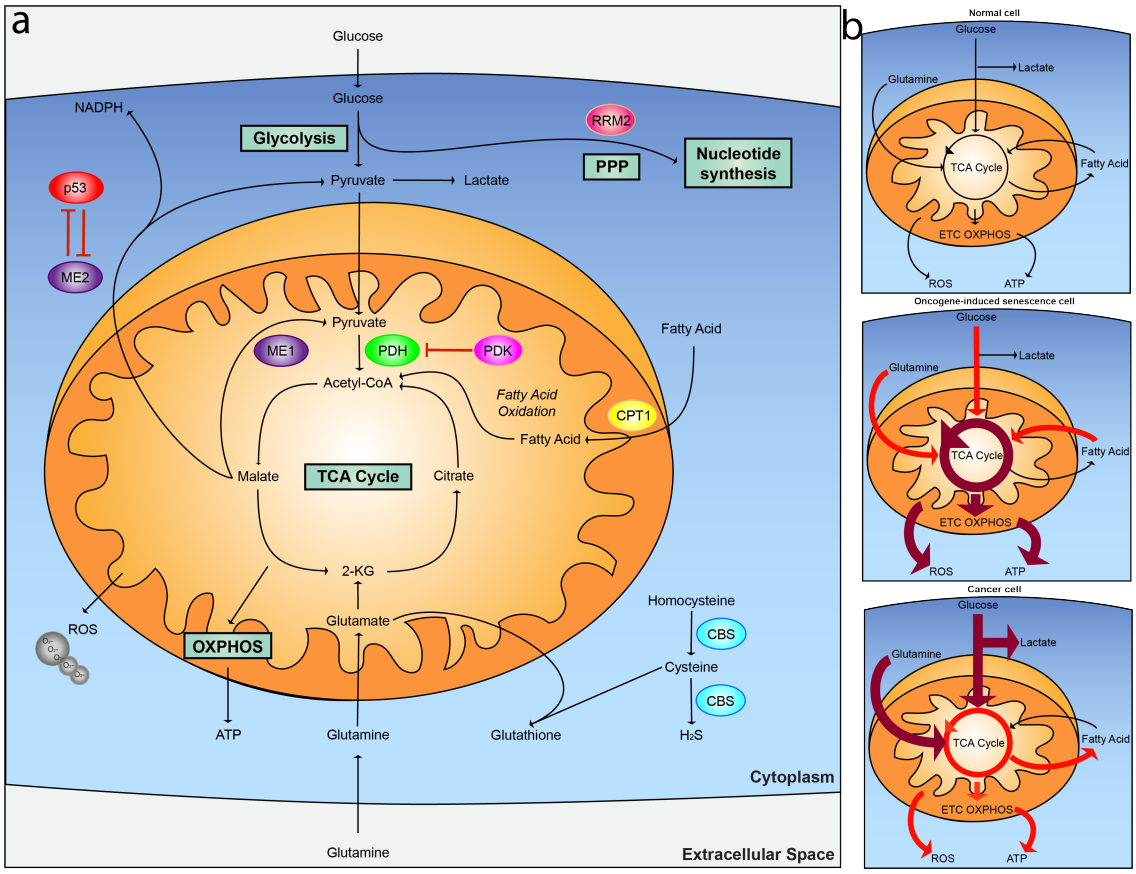


Figure 1.2 Metabolic pathways reprogrammed in OIS and cancer.

(Figure reused from Zhu & Blake et al., 2020, Mech Ageing Dev. doi: 10.1016/j.mad.2020.111229. Inclusion of figures in a thesis is permitted by Elsevier)

(a) Schematic representing the cellular metabolic pathways. The mitochondria utilise carbon sources derived from glycolysis, and it serves as the main cellular energy metabolism organelle through the TCA cycle and OXPHOS to provide ATP. Several enzymes involved in metabolism have been shown to regulate OIS, such as CPT1 involved in the fatty acid oxidation, RRM2 involved in the PPP and nucleotide synthesis, ME1/2 involved in the NADPH metabolism, PDK/PDH involved in the TCA cycle, and CBS involved in the transsulfuration pathway. (b) Normal, OIS and cancer cells exhibit distinct metabolic reprogramming. The global metabolism is hyperactivated in both OIS and cancer cells. Hyperactivated TCA cycle and OXPHOS generate sufficient ATP to support SASP factor production, and mitochondria-derived ROS is enhanced as a result of mitochondria dysfunction in OIS; while the increased energy demand for cancer cell proliferation is satisfied through elevated glutamine and glucose metabolism.

1.2.1 Energy metabolism in senescence

The energy generation is required for growth and the maintenance of cellular functions. In eukaryotic organisms, adenosine triphosphate (ATP), a compound with high potential energy is the main carrier of chemical energy. Glucose, fatty acids and amino acids function as the fuels to drive ATP synthesis. Over a hundred ATP molecules are synthesized from the completed breakdown of one molecule of fatty acid, and almost forty ATP molecules result from amino acid and glucose oxidation [169]. The enzymes and the physical environment necessary for the metabolism of these molecules mainly reside within mitochondria, leading to a common designation as the "powerhouse of the cell". The process of breaking down these fuels via sequential oxidation-reduction reactions by the mitochondria gives rise to ATP synthesis is termed oxidative phosphorylation (OXPHOS). Comparatively, Glycolysis is a series of enzyme-catalysed sequential metabolic reactions that converts glucose into pyruvate. Although both OXPHOS and glycolysis are the major cellular metabolic pathways to produce energy, OXPHOS involves complete combustion of glucose to carbon dioxide and water, yielding approximately 17 times as much useful energy as does glycolysis. Owing to its high energy yield, mitochondrial oxidative phosphorylation is responsible for supplying over 95% of the total ATP in eukaryotic cells. In addition to energy metabolism, mitochondria play a critical role in maintaining metabolic intermediates, calcium balance, redox balance, beta-oxidation and apoptotic signalling (Fig. 1.2a). To adapt cellular metabolic demands and maintain mitochondrial quality control, mitochondria also crosstalk with the nucleus via retrograde signalling to regulate gene expression [170]. Senescent cells exhibit up-regulated glycolysis [89] and mitochondrial deregulation including mitochondrial DNA (mtDNA) mutation, structural disorientation and impaired function [171] [172]. Therefore, alterations of energy metabolism centred at mitochondria may contribute significantly to metabolic reprogramming under different cellular responses including senescence [173] [174].

1.2.1.1 Dysregulated glycolysis in cellular senescence

Early studies showed the replicative senescent human diploid fibroblasts (HDFs) exhibited an elevated glucose uptake and consumption rate [175]. Goldstein et al.

further identified an elevated lactate production in the senescent progeria cells using ^{14}C-isotope labelled pyruvate and glutamate [176] possibly due to increased energy demand and insufficient OXPHOS during senescence. Enhanced glycolysis has been later reported in OIS [89] (Fig. 1.2b), stress-induced senescence [95] [177] [178] and replicative senescence [179] [180]. Paradoxically, activation of ATM in response to replication stress inhibits the pentose phosphate pathway, a process for the production of sugar bases of all nucleotides while ATM inactivation leads to senescence bypass by increase of PPP activity for nucleotide biosynthesis [181] (Fig 1.2), suggesting a down-regulated PPP during OIS mediated by ATM signalling. Together, elevated glycolysis and suppressed PPP in different types of senescence maximise energy production (Fig. 1.2).

Elevated glycolysis observed in different types of cellular senescence is associated with activation of the key signalling pathways. During OIS, Retinoblastoma (Rb) is responsible for transcriptional upregulation of glycolytic genes, whereas elevated glycolysis is abolished in Rb depleted oncogene-induced senescent human fibroblasts [180]. Unlike OIS, in stress-induced senescence triggered by irradiation, AMPK and NF-kB signalling pathways are activated to stimulate glycolysis [180] and consequently transcriptionally upregulates lactate dehydrogenase A and monocarboxylate transporter 1 [177]. Furthermore, upregulated glycolysis and lactate production can activate NF-kB signalling and reinforce SASP production, thus forming a positive feedback loop. Moreover, extracellular lactate secreted from senescent cells contributes to the formation of the anti-inflammatory microenvironment and inhibits immune surveillance, thus promoting wound healing and tumourigenesis [182] [183].

1.2.1.2 Mitochondrial deregulation in cellular senescence

Senescent cells exhibit mitochondrial deregulation including mitochondrial DNA (mtDNA) mutation, structural disorientation and impaired function [171] [172]. Porter et al. reported that in human skeletal muscle mitochondrial OXPHOS capacity was gradually impaired with chronological aging, leading to a reduced ATP production [184]. In contrast to declined mitochondrial OXPHOS capacity with aging, OIS also harnesses elevated pyruvate oxidation, TCA cycle and mitochondrial respiration [185, 186] (Fig. 1.2b). Kamei et al. reported in replicative senescent budding yeast, the metabolic

enzymes involved in glycolysis and TCA cycle were transcriptionally upregulated in accompany with an accumulation of pyruvate and TCA cycle intermediates [187]. Pyruvate dehydrogenase (PDH), a mitochondrial gatekeeper enzyme, was reported to play a crucial role In $BRAF^{V600E}$-induced senescence [185]. PDH hyperactivation by inhibition of PDH-negative regulator dehydrogenase kinase 1 (PDK1) promotes the conversion of pyruvate to acetyl-CoA, the entry substrate for the TCA cycle and enhances mitochondrial respiration and oxidative stress while PDH inhibition alleviates $BRAF^{V600E}$ -induced senescence. Alternatively, PDH can be activated by Pyruvate Dehydrogenase Phosphatase Catalytic Subunit 2 (PDP2), the PDH-activating enzyme, through the binding to its promoter region in OIS cells [180]. In addition, fatty acid oxidation also contributes to mitochondrial hyperactivation in OIS cells [186] (Fig. 1.2a). In RIS, pharmaceutical inhibition of fatty acid oxidation suppressed mitochondrial respiratory activity, and compromises cytokine secretion. These studies indicated up-regulated mitochondrial activity during senescence may be attributed to the increased energy demand due to SASP secretion in senescent cells.

Not only mitochondrial function is compromised, mitochondrial dynamics is also changed during cellular senescence [188]. Under normal conditions, mitochondria continually undergo fission and fusion events to maintain the quality of mtDNA and stimulate the selective degradation of dysfunctional mitochondria by autophagy, termed mitophagy [189]. Altered mitochondrial morphology, mtDNA copy number, and mitochondrial mass gain have been observed in OIS [89]. Furthermore, reduced mitochondrial fission has been detected in stress-induced and replicative senescence. The dynamin-related protein 1 (Drp1) and mitochondria fission protein 1 (Fis-1) were both downregulated in replicative senescent Human Umbilical Vein Endothelial Cells (HUVECs), and subsequently led to mitochondrial elongation and increased ROS accumulation [190]. Inhibition of mitochondrial fission through experimental approaches induces cellular senescence. For example, treatment with deferoxamine in HDFs leads to elongated mitochondrial, elevated ROS, dysregulated mitochondria, and cellular senescence [191]. Transcriptional silencing of Fis-1 [192] or mitochondrial E3 ubiquitin ligase March 5 [193] also reduced mitochondrial fission, resulting in senescence. In addition to impaired fission event, mitochondrial fusion can be triggered

upon stress stimuli to counteract cellular stresses via enhancing the ATP synthase activity [194] [195]. Mitochondrial dynamic alteration through fusion has been linked to increased OXPHOS, ATP production and fatty acid oxidation in dormant memory T-cells, and such metabolic reprogramming drives memory T-cell activation [196]. Mitochondrial fusion promotes senescent cell metabolic rewiring, driving SASP secretion and activate anti-apoptotic signalling in senescent cells [190] [197] [198]. Taken together, alterations of mitochondrial dynamics such as fission and fusion events have been shown to be crucial for mediating metabolic reprogramming during replicative and stress-induced senescence, but its role in OIS remains unknown.

Mitochondrial dysfunction during senescence leads to ROS overproduction (Fig. 1.2), which causes macromolecular damage and induction of a positive feedback loop that reinforces senescence. Ogrunc et al. demonstrated that ROS overproduction is essential for stimulating hyperproliferation and DDR during RIS [199]. However, whether mitochondrial dysfunction was associated with RIS and responsible for ROS overproduction remains unclear. Treatment of Electron Transport Chain (ETC) inhibitor, antimycin A, elevates mitochondrial-derived ROS and leads to p16, p21 and p27 upregulation [200]. In addition, human fibroblasts treated with carbonyl cyanide p-trifluoromethoxyphenylhydrazone (FCCP), which uncouples oxidative phosphorylation, exhibit significantly increased ROS, DNA damage, and senesce within 12 days [201]. Furthermore, ROS can cause mitochondrial dysfunction. Early in 1972, Harman et al. suggested that mitochondrial dysfunction was a secondary effect resulted from mitochondrial Reactive Oxygen Species (ROS) accumulation, and ROS was the primary driver of cellular senescence [202] (Fig. 1.2a). Later studies supported Harman's theory by showing that superoxide anion generated from mitochondria Complex I and III caused pathological disturbance [203] [204], and mitochondrial oxidative stress led to cellular senescence [205] [206]. The first *in vivo* mouse model used to study oxidative stress-induced mitochondrial dysfunction in aging was established from Schriner group by genetically overexpressing a ROS scavenging enzyme called mitochondrial-targeted catalase (mCAT) in mouse. They demonstrated that mCAT mice have lowered mitochondrial oxidative stress, damage, mtDNA mutation and prolonged lifespan compared with control mice [207]. Phenotypically, mCAT mice exhibit decreased

susceptibility for age-related diseases such as cardiac disease, naturally-occurring lung cancer and ischemic myopathy induced by high-fat diet [208] [209] [210] [211]. mCAT overexpression in heart and skeletal muscle tissues prevented mtDNA mutation and deletion, protects mitochondria from oxidative stress, alleviates p16 induction and cardiomyopathy [212] [213] [214]. Conclusively, these findings demonstrate that ROS induces mitochondrial dysfunction and contributes to cellular senescence and age-related pathologies *in vivo*. However, the relevance of mitochondrial dysfunction during the AIS program remains poorly understood.

The mechanistic involvement of AMP-activated protein kinase (AMPK) and NAD+/NADH balance are proposed as key metabolic switches for modulating senescence. A rapid increase in energy demand is required for senescence establishment due to its phenotypical changes such as SASP secretion [95]. Therefore, ATP level decrease, AMP/ATP ratio increase may activate a central regulator of cellular and organismal metabolism, AMP-activated protein kinase (AMPK) [215] [216]. AMPK senses and adapts cellular energetic stress through activating catabolic pathways and mitochondrial biogenesis such as fatty acid oxidation and autophagy [217]. Acute activation of the AMPK pathway can activate autophagy and NAD^+ synthesis, providing resistance to hydrogen peroxide-induced cellular senescence [218]. In contrast, chronic activation of AMPK signalling, experimentally achieved through treatment with exogenous AMP [219] or oligomycin [200], leads to p53-dependent cell cycle arrest [220]. Likewise, the downregulation of mitochondrial malic enzyme activates p53 through AMPK-mediated signalling in a positive feedback manner, enhancing p53 activation and reinforcing senescence [221] (Fig 1.2). Moreover, the perturbed NAD^+/NADH ratio has also been shown to activate AMPK signalling pathway and triggers senescence. Restoration of NAD^+ level and NAD+/NADH ratio, abrogates senescence in response to mitochondrial challenges [222]. NAD+/NADH ratio perturbation has been also found in several age-related disease models, and restoring NAD+/NADH balance showed beneficial effects in such mouse models [223]. Recently, Nacarelli et al. demonstrated the rate-limiting enzyme of the NAD^+ salvage pathway, nicotinamide phosphoribosyltransferase (NAMPT), controls the pro-inflammatory SASP. More specifically, the NAMPT-NAD^+ signalling axis increases glycolysis and mitochondrial respiration, and thus suppresses

AMPK and p53 to enhance NF-kB activity [224]. Therefore, AMPK pathway activation and NAD^+/NADH ratio imbalance as the consequence of mitochondrial dysregulation may mechanistically reinforce senescence.

Conclusively, elevated glycolysis and mitochondrial OXPHOS are the two key metabolic alterations associated with cellular senescence, and support other effectors of senescence such as the SASP. The deregulation of mitochondrial function and dynamics, increased ROS production, NAD+/NADH ratio and AMPK signalling activation contribute to the establishment and maintenance of cellular senescence.

1.2.2 Reactive oxygen species-induced signalling in senescence

As reviewed above, the elevated ROS production contributes to mitochondrial dysfunction. In this section, we will discuss further about the contribution of ROS including its highly reactive chemical property, potential damages to DNA, lipids, proteins, and retrograde signalling in cellular senescence establishment and maintenance.

Reactive oxygen species (ROS) including the superoxide anion (O2−), hydrogen peroxide (H_2O_2), and hydroxyl radicals (OH), are produced from aerobic metabolism. The production and removal of ROS are tightly controlled to maintain the intracellular homeostasis. However, such equilibrium may be disrupted under certain conditions and results in the accumulation of ROS. Consequently, cells experience oxidative stress which can cause damage to biomolecules such as lipids, proteins and DNA.

ROS causes oxidative nuclear and mitochondrial DNA damage. Consequently, deoxyribose oxidation, strand breakage, removal of nucleotides, a variety of modifications in the organic bases of the nucleotides, and DNA-protein crosslinks may occur. Both the sugar and base moieties of DNA are susceptible to oxidation by ROS. Oxidative attack to DNA bases generally involves hydroxyl radical addition to double bonds, while sugar damage mainly results from hydrogen abstraction from deoxyribose [225]. ROS contributes to cellular senescence induction. In 1999, Lee et al. first demonstrated that without elevation of ROS production RAS^{G12V} was unable to initiate

OIS [226]. A later study demonstrated that ROS overproduction is essential for stimulating hyperproliferation and DDR during RIS [199]. Together, these findings highlighted DNA damage caused by elevated ROS is essential for RIS establishment. However, given that AIS does not exhibit DDR, the relevance of ROS with AIS remains unclear. Comparing to nuclear DNA, mitochondrial DNA is more susceptible to ROS damage due to the lack of protective protein, histones, and the close location to the ROS producing systems [227]. Accumulation of mitochondria-derived ROS causes direct damage to mitochondria which is exacerbated by the impaired autophagy in senescence. Studies have linked mitochondria-derived ROS with DNA Damage Response (DDR). Under normal conditions, ROS is required at a physiological level to maintain intracellular redox balance, and it is consistently generated through OXPHOS. For example, nuclear factor erythroid 2-like2 (NRE2L2), which is a basic leucine protein, is activated in the presence of ROS. NRE2L2 gene relates to a crucial pathway to control the expression of genes encoding antioxidant and mitochondrial biogenesis proteins [228] [229]. Studies have shown the activation of the NRE2L2-related pathway protects cells against stresses and delays replicative [230] and stress-induced [231] [232] senescence onset.

Lipid peroxidation is often associated with oxidative stress and it can lead to further damage through the production of lipid-derived radicals. The production of Malondialdehyde (MDA) as through lipid peroxidation can cause cell membrane damage. Thus the level of lipid peroxidation has been widely used as an indicator of ROS-mediated damage to cell membranes [233]. Chemically, hydroxyl radical (HO•) and hydroperoxyl ($HO•_2$) are the two main types of ROS that can cause damage to lipids. They attack the lipid molecules at the unsaturated bond between two carbon atoms thus the polyunsaturated fatty acids present in membrane phospholipids are particularly vulnerable [234]. The peroxidation of polyunsaturated fatty acid by ROS is thought to lead to chain breakage and the compromised cell membrane integrity.

In parallel, oxidative stress may cause damage to proteins in a variety of ways. For example, ROS can directly modify protein activity through nitrosylation, carbonylation, disulphide bond formation, and glutathionylation. Tissues injured by oxidative stress

generally contain increased concentrations of carbonylated proteins which is a widely used marker of protein oxidation [235]. The amino acids in a peptide differ in their susceptibility to attack by ROS. For example, thiol groups and sulphur-containing amino acids are very susceptible sites for attack by ROS. Furthermore, oxidation of iron-sulphur centres by superoxide anion is irreversible and leads to enzyme inactivation [236]. It has also been suggested that the ROS-damaged proteins are more vulnerable to ubiquitination and subsequent protein degradation [237]. Thus, the oxidative stress resulting from mitochondrial dysfunction may promote protein oxidation and misfolding, which is intimately linked to upregulated Unfolded Protein Response (UPR) and autophagy in senescent cells [238]. However, no direct evidence of ROS-mediated protein damage has been linked to OIS.

Apart from the potential damage caused by ROS during cellular senescence, ROS also functions as a secondary messenger to stabilize cell cycle arrest upon genomic instability. One positive feedback loop is reported in OIS between p53/Rb and DDR. Mitochondrial dysfunction and ROS production in response to oncogenic RAS is p53/Rb tumour suppression pathway-dependent [89]. Several studies have suggested p53 plays a crucial role in pro-oxidant signalling. p53 is required for both transcriptional and functional deactivation of one essential antioxidant enzyme, named Mitochondrial manganese superoxide dismutase (MnSOD) [239] [240]. Moreover, p53 transcriptionally represses $NAD(P)^+$-dependent mitochondrial malic enzyme, which is required for antioxidant defences. Although mitochondrial-derived ROS may not exert direct damage to nuclear DNA, studies have shown a transcriptional regulation of cellular ROS level through activating other ROS producing mechanisms such as NAD(P)H oxidase pathway [241] [242]. Similarly, in replicative senescence and stress-induced senescence triggered by irradiation, DNA Damage Response (DDR) and p21 pathways are activated to induce mitochondrial dysfunction through GADD45-MAPK14(p38MAPK)-GRB2-TGFBR2-TGFbeta signalling, which subsequently enhanced ROS production. Oxidative stress and DDR forms a positive feedback loop for senescence maintenance [243]. Specifically, ataxia-telangiectasia mutated (ATM) protein kinase, which is one of the most important regulators involved in DDR, activates AKT/mTORC1 signalling to promote mitochondrial

dysfunction via PGC-1beta. Pharmaceutical inhibition of mTORC1 or PGC-1beta deletion abrogates oncogene-induced, stress-induced senescence in mouse liver [244].

In conclusion, accumulation of cellular oxidative stress may cause damage to DNA, lipids and proteins, thereby contributing to DNA damage response, membrane integrity and protein misfolding, respectively. Whether this mechanism contributes to OIS induction remains to be determined, elevated oxidative stress has been observed as a secondary messenger to re-enforce OIS and other types of cellular senescence.

1.2.3 Anabolic reprogramming in senescence

Despite the fact that senescence cells exhibited up-regulated catabolic activities such as glycolysis and OXPHOS to support the elevated energy demand, enhanced anabolism was also observed during OIS and other types of cellular senescence. Overall, a simultaneous up-regulation of metabolism and anabolism suggests a high turnover rate of intracellular organelles during the senescence program.

1.2.3.1 Glycogenesis in cellular senescence

In contrast to glycolysis which breaks down glucose, glycogenesis is the process of glycogen synthesis where glucose molecules are added to chains of glycogen for storage. Glycogen accumulation has been detected in different types of senescence and age-related disease models, including replicative senescent primary human fibroblasts [245], myelinated axons of diabetic mice model [246], and cerebral cortex of chronologically aged humans [247]. Mechanistically, glycogenesis is mainly controlled by glycogen synthase (GS) which can be activated through its upstream regulators such as glycogen synthase kinase 3 (GSK3) and AKT [245], or AMPK [248]. However, the function of elevated glycogenesis in senescence remains unclear and has been suggested to be the downstream effector of PI3K/AKT/mTORC1 signalling [249].

1.2.3.2 Lipogenesis in cellular senescence

Enhanced lipid biosynthesis, termed lipogenesis, was reported during cellular senescence to support the elevated demand of organelle biosynthesis, such as lysosomes, mitochondria, Endoplasmic Reticulum (ER) and plasma membrane. Quijano

et al. characterised the changes of metabolome during OIS through LC/MS-based metabolomics and revealed the distinct lipid metabolism exhibited by OIS and replicative senescence cells with certain long-chain free fatty acids (FFA) showing more than 5-fold increase in RIS. Furthermore, hyperactivated lipogenesis in senescent cells may cause accumulation of intracellular lipid droplets, which is linked to age-related diseases such as diabetes, CVD [250] and steatosis [251]. Ogrodnik et al. demonstrated that lipid accumulation in mouse live tissues leads to cellular senescence and steatosis and senolytic therapeutics eliminates senescent hepatocytes and reduces overall hepatic steatosis [251]. More recently, they also reported that the accumulation of lipid droplets in periventricular glia of obese mice induced glial cell senescence and elimination of senescent cells using senolytic compounds restored neurogenesis and alleviated anxiety in the obesity mouse model [252].

Mechanistically, sterol regulatory element-binding protein 1 (SREBP1), a master regulator of lipogenesis, is the key molecule involved in increased lipogenesis downstream of PI3K/AKT/mTORC and AMPK signalling. mTOR signalling activates SREBP1, while AMPK negatively regulates SREBP1 [253] [217]. SREBP1 transcriptionally governs a few keys enzymes involved in lipogenesis, including ATP citrate lyase (ACL), acetyl-CoA carboxylase (ACC) and fatty acid synthase (FAS) [254]. Thus, the activity of SREBP1 determines the overall cellular lipogenic state. Transcriptional overexpression of SREBP1 in HDFs is sufficient to enhance lipogenesis resulting in membranous lipid accumulation, increase of cell mass, and senescence induction. Therefore, an imbalance between lipogenesis mediated by SREBP1 signalling and cellular growth are involved in senescence initiation.

1.2.3.3 protein synthesis in cellular senescence

Deregulated protein homeostasis is one of the key features of senescence. Both hyperactivated de novo protein synthesis and impaired protein degradation contribute to an imbalance of protein homeostasis during cellular senescence. The increase of protein synthesis in senescent cells is the downstream effect of the PI3K/AKT/mTOR signalling pathway. It has been well established that PI3K/AKT/mTORC stimulate translation machinery through activation of several elongation factors (e.g. eIF4B, eIF4E,

eEF2 [255]. Moreover, activation of glycogen synthase kinase (GSK)-3, which positively regulates protein synthesis, was observed in replicative senescence [256]. It has been shown that GSK-3β phosphorylated and inactivated 4E-BP1, thereby increasing eIF4E-dependent protein synthesis [257].

Protein homeostasis is also maintained through chaperone-mediated protein folding, proteasome-mediated degradation and autophagy-mediated recycling. As discussed above, ROS accumulation in senescent cells causes oxidative damage in protein. This proteotoxicity is irreversible and the damaged proteins are required to be eliminated to maintain homeostasis. However, impaired proteasome function and autophagy cause accumulation of damaged proteins in senescent cells. Bussian et al. demonstrate that the presence of senescent astrocytes and microglia cells in a neurodegenerative disease mouse model led to tau protein accumulation, which is the subunit protein of the neurofibrillary tangles that commonly used as the hallmark of Alzheimer disease (AD) [258]. Selective elimination of senescent cells alleviates tau protein aggregation, reduces neurons degeneration and improves cognitive function.

1.2.3.4 Nucleotide metabolism in cellular senescence

Nucleotide metabolism and imbalances in dNTP pools have long been known to play a role in a variety of human pathologies [259]. The first study by Arid et al. reported that the replication stress during RIS was due to a decrease of dNTP levels as the result of transcriptional suppression of RRM2, a rate-limiting enzyme for the conversion of rNDP/rNTP to dNDPs/dNTPs [260]. Recently, the mechanism by which RRM2 suppression leads to a decreased dNTP pool during OIS has been uncovered using LC/MS-based metabolomics, where pharmacological and genetic inhibition of RRM2 decreased metabolic flux from glucose into nucleotide synthesis [261] (Fig. 1.2). Consistent with this finding, the decrease of thymidylate synthase and the large subunit RRM1 were also detected during either RAS or c-MYC-induced senescence which consequently caused an impairment of global dNTP metabolism [262] [263]. Moreover, one study reported that p16 suppression during OIS mediates nucleotide metabolic reprogramming through the mTORC1 signalling pathway, resulting in OIS bypass. Mechanistically, transcriptional inhibition of p16 leads to the activation of mTORC1

signalling and in turn the up-regulation of ribose-5-phosphate isomerase A (RPIA), a pentose phosphate pathway enzyme. In fact, nucleotide deficiency was suggested to promote genomic instability in early stages of tumourigenesis [264]. Suppression of RRM2 gene transcription is mediated through the replacement of E2F1 transcriptional activator by E2F7 transcriptional repressor at its promoter region [260]. Inhibition of RRM2 activates p53 andp53 activation can in turn, directly enhance E2F7 expression [265]. Consequently, the suppression of nucleotide metabolism is reinforced during OIS. Overall, the downregulation of nucleotide metabolism contributes to senescence initiation through replication stress and genomic instability.

1.2.4 Concluding remarks

Metabolic reprogramming contributes to senescence induction and maintenance. Significant progress has been made in characterizing this metabolic switch. Mitochondrial deregulation, enhanced oxidative stress and impaired anabolism are the key metabolic features in senescence and age-related diseases (Fig. 1.2).

The research from our lab has revealed novel mechanistic insights into AIS. Using a whole protein-coding genome RNAi screen, we identified a number of essential regulators of AIS. Importantly, more than 10% of the identified candidates are metabolism-associated, including a key enzyme involved in the transsulfuration pathway, Cystathionine β-Synthase (CBS) [121]. Characterization of the role of CBS in AIS and cancer pathogenesis forms a major focus of my research.

Cystathionine-β-synthase (CBS) is the first enzyme involved in the transsulfuration pathway, and it converts homocysteine (Hcy) to cystathionine. CBS, acting mainly through control of Hcy, H_2S and GSH metabolism exerts diverse biological functions including contributing to the control of mitochondrial bioenergetics, redox homeostasis, DNA methylation and protein modification [266]. Deregulation of CBS and the associated alterations in Hcy and/or H_2S levels leads to a wide range of pathological disturbances in the cardiovascular, immune, and central nervous systems and contributes to disease development, such as CBS-deficient homocystinuria (CBSDH)

[267]. Furthermore, numerous studies suggest CBS activity and the transsulfuration pathway play important but complex roles in cancer biology, and it appears that CBS role in cancer is tumour-type specific. I have reviewed the current understanding of the physiological roles of CBS in the attached manuscript (Zhu et al Biomed Res Int. 2018. doi: 10.1155/2018/3205125)

1.3 Cystathionine β-Synthase in Physiology and Cancer

Appendix 1

Inclusion of the manuscript in a thesis is permitted by Hindawi.

1.4 Hypothesis and aims

The PI3K/AKT/mTORC1 signalling network is essential for homeostatic control of cell growth, proliferation, and survival. Molecular aberrations in the PI3K/AKT/mTORC1 signalling pathway underpin a large proportion of oncogene-driven cancers. In fact, 38% of solid tumours across 19784 consecutive tumour samples and more than 40 cancer types exhibit aberrant signalling through this pathway [268], indicating it is a driver of many sporadic human cancers. Paradoxically, PI3K/AKT/mTORC1 hyperactivation causes a senescence-like phenotype in non-transformed cells, which acts as a protective brake against tumour initiation [121]. While most OIS studies have focused on RAS/MAPK-induced senescence, little is known about the mechanisms regulating AIS and its potential tumour-suppressive function. Understanding the molecular requirements for PI3K/AKT-induced senescence and determining their pathway specificity will be essential to identify which contexts they can be manipulated to target cancer.

Metabolic reprogramming has been demonstrated as a hallmark in OIS. It is essential for OIS establishment and maintenance. AIS cells exhibit a rewired metabolic phenotype to maximize energy production. Through a whole protein-coding genome RNAi screen we identified a number of metabolic genes as essential regulators of AIS [121]. CBS was the top-ranked hit. We hypothesize that CBS is required for AIS maintenance and that interfering with CBS-related metabolic reprogramming may cause AIS escape and promote tumorigenesis. To gain more insight into the metabolic dependency of AIS, we will characterize the role of CBS, an enzyme involved in transsulfuration and transmethylation metabolic pathways.

To address these hypotheses, I have formulated three specific research aims:

AIM1: To define the transcriptional and metabolic profiles of AIS.

AIM2: To characterise the role of CBS in AIS maintenance.

AIM3: To evaluate the potential role of CBS as a tumour suppressor in gastric cancer.

CHAPTER 2 Methods and Materials

2.1 Mammalian cell culture

Tissue culture was carried out in a sterile condition and cells were incubated at 37°C, 5% v/v CO_2. Cell passage was performed every third or fourth day, depending on the growth rates, by washing with PBS (MgCl2/CaCl2-/-), dissociating with 0.25% (w/v) Trypsin-EDTA (Gibco™-25200056) and resuspending in defined growth media. Cell counts were determined using the Coulter Counter Z2 (Beckman-Coulter-383550). For short-term or long-term storage, cells were cryopreserved at -80°C or -196°C, respectively, using recommended freeze medium (e.g. Complete growth medium supplemented with 5% (v/v) DMSO.) Mycoplasma contamination detection in cell culture was routinely performed by Genotyping laboratory at PMCC.

BJ TERT-immortalized human foreskin fibroblasts (BJ-T) were a gift from Robert Weinberg (Massachusetts Institute of Technology, USA) [269]. Primary IMR-90 lung fibroblasts originating from the American Type Culture Centre (ATCC CCL-186) were obtained from the Garvan Institute of Medical Research, Sydney, Australia. Human embryonic kidney (HEK293T) cells were purchased from the ATCC (ATCC-CRL-3216). Human gastric cancer cell lines, AGS (ATCC CRL-1739), Hs 746T (ATCC HTB-135), KATO III (ATCC HTB-103), NCI-N87 (ATCC CRL-5822), SNU1 (ATCC CRL-5971) and SNU5 (ATCC CRL-5973) originating from the American Type Culture Centre (Table 2.1), and were generous gifts from Dr. Karen Sheppard (Peter MacCallum Cancer Centre, Australia). The human fetal gastric epithelial cell line GES-1, which is SV40-immortalized, was established by Ye et al. [270] and was provided by Dr. Caiyun Fu (Zhejiang Sci-Tech University, China). All cells were tested for mycoplasma contamination prior to experimentation and intermittently tested thereafter by PCR. BJ-TERT cells were cultured in Dulbecco's Modified Eagle's Medium (DMEM) (Gibco™ #11965084) + 20 mM HEPES, 17% Medium 199 (Gibco™ #11150067), 15% fetal bovine serum (FBS), and 1% GlutaMAX™ L-alanyl-L-glutamine dipeptide (Gibco™ #35050061). IMR-90 cells were cultured in Eagle's Minimum Essential Medium (EMEM) supplemented with 10% FBS, 5 mM sodium pyruvate (Gibco™, #11360070), 1% non-essential amino acids (Gibco™, #11140050), and 1% GlutaMAX™. HEK-293T, GES-1, Hs 746T, cells were cultured in DMEM + 20 mM HEPES,

10% FBS, and 1% GlutaMAX™. AGS cells were cultured in Kaighn's Modification of Ham's F-12 Medium (F-12K) (ATCC® 30-2004™) supplemented with 10% FBS and 1% GlutaMAX™. KATO III and SNU-5 cells were cultured in Iscove's Modified Dulbecco's Medium (IMDM) supplemented with 20% FBS and 1% GlutaMAX™. NCI-N87 and SNU-1 cells were cultured in RPMI-1640 Medium supplemented with 10% FBS and 1% GlutaMAX™. All cell lines were maintained at 37°C with 5% CO2 except for IMR-90 (3% O2) in a humidified incubator. Cell numbers were determined using a Z2 Coulter Counter (Beckman Coulter).

2.2 Pharmacological compounds

Aminooxyacetic acid (AOAA) (C13408), GYY4137 (SML0100), L-Homocysteine (69453), L-Cysteine (C7352), S-adenosyl-L-methionine (SAM) (A7007) were purchased from Sigma-Aldrich. Azacitidine (Celgene-VIDAZA®) was a kind gift from Dr. Shatha Abuhammad from PMCC.

2.3 Plasmids cloning & amplification

pBABE-puro was a gift from Morgenstern, Land & Weinberg (Addgene plasmid-1764) [271]. pBABE-puro-myr-AKT1 was generated by the Pearson laboratory described previously [34] and pBABE-puro-HRAS^{G12V} was generously donated by Dr. Patrick Humbert (Peter MacCallum Cancer Centre, Australia). pCW57.1-4EBP1_4xAla was deposited by David Sabatani (Addgene-38240) and HA-myrAKT1 was directly subcloned into this vector to generate pCW57.1-myrAKT1. The REBIR construct, a modified doxycycline-inducible mirE small hairpin RNA (shRNA) expression version of TRMPVIR [272], was a gift from Sang-Kyu Kim (Peter MacCallum Cancer Centre, Australia) by substituting Venus with enhanced blue fluorescent protein (EBFP2). The Dharmacon™ GIPZ lentiviral shRNAs targeting human genes using 4-5 multiple shRNA constructs were obtained from Horizon Discovery, UK and were tested for functional knockdown efficacy in BJ-TERT cells, and the two best shRNA hairpins were subcloned into the REBIR construct by Dr. Keefe Chan and Dr. Jian Kang (Table 2.2).

The cloning vector pBSK(+) containing the cDNA encoding human CBS isoform 1 was synthesized and purchase from Biomatik company (Biomatik Cooperation, Cambridge, Canada). To generate an inducible CBS overexpression construct, CBS cDNA was

subcloned into REBIR plasmid in which the dsRed2/mirE cassette has been removed and EBFP2 was replaced with the puromycin resistance gene. The resulting plasmid was designated pRT3-puro-CBS. The single mutation p. I278T was introduced into the pRT3-puro-CBS vector by site-directed mutagenesis via primer extension involving incorporating mutagenic primers in nested PCRs before combining them in the final product. The primers used for site-directed mutagenesis were: AGCTTGCGTTGGATCCATGCC (CBS 5' forward), TACCCGGTAGAATTACGCGTCTACT (CBS 3' reverse), AGAATCA**C**CGGAGTGGACCCAG (CBS I278T, forward) and CTGGGTCCACTCCG**G**TGATTCT (CBS I278T, reverse). The resulting plasmid was designated pRT3-puro-CBS^{I278T}. The sequencing was performed in Australian Genome Research Facility.

The pRDF envelope plasmid was from Mary Collins [273] and the Moloney murine leukaemia virus gag-pol expression vector pEQ-PAM3-E was from Elio Vanin [274]. pMDL/pRRE (Addgene plasmid-12251), the lentiviral gag-pol expression vector and pRSVREV (Addgene plasmid-12251), the lentiviral packaging plasmid were deposited by Didier Trono [275]. The lentiviral envelope protein vector pCMV-VSV-G was from Robert Weinberg (Addgene plasmid-8454) [276]. All plasmids contained an ampicillin resistance cassette under a bacterial promoter for selection in bacterial culture.

TOP10F Escherichia coli (Invitrogen-C303003) chemically-competent cells were transformed with the plasmid DNA using the heat shock method [277]. Approximately 100ng of plasmid DNA was added to 50µl bacterial stock and incubated on ice for 1min. Plasmid uptake was achieved by heat shock at 42°C for 1min, then recovered on ice for 5min. The 50µl culture was propagated on Luria broth (LB) agar plates containing 75µg/ml ampicillin (Sigma-A0166) overnight at 37°C. Single colonies were picked and further propagated in 400mL LB Broth containing 75µg/ml ampicillin overnight. 1ml of culture was combined with 1ml 100% (v/v) glycerol (Sigma-G5516) and preserved at -80°C for later use. Plasmid DNA was purified using the NucleoBond Xtra Maxi kit (Macherey-Nagel-740414) according to the manufacturer's protocol and plasmid concentration and purity were determined using the NanoDrop ND-1000.

2.4 Plasmid transfection, virus concentration & transduction

Crude viral media was produced by HEK-293T cells transfected with retroviral or lentiviral constructs. Cells were seeded 24 hours prior to transfection in tissue culture flasks at 80%-90% confluency. For retroviral constructs, the transfection reagent master mixes were prepared by combining equal mass of plasmid DNA vectors, pEQ-PAM3-E, and RD114 envelope plasmid as previously described [278]. For the lentiviral transfection, plasmid DNA vectors were combined with pMDL, pRSV-REV and pCMV-VSV-G packaging plasmids. (3:1:1:1 mass ratio). Plasmid mixtures were combined with polyethylenimine (PEI, 1mg/ml stock at 5ul per ug plasmid), a cationic polymer for gene delivery [279]. The Mixtures were vortexed briefly and incubated at RT for 25min before adding to the media in a dropwise manner. The culture media refreshed with complete media at 24h post-transfection. At 48 and 54h post-transfection, the culture media containing viral particles was collected and passed through a 0.4µm filter. Virus-containing media were either concentrated and applied to target cells or stored at -80°C for later use.

Ultracentrifuge tubes were sterilized overnight under UV one day prior to virus concentration. On the concentration day, ultracentrifuge tubes were filled with 25mL virus-containing media to top. The tubes were weighed and balanced (all need to be within 0.1 g) prior to ultracentrifuge spin in 70Ti rotor (Beckman-337922) at 25000g for 2h at 4°C (BECKMAN-OPTIMA L-100XP). Supernatants were discarded into 1% w/v Virkon™ S solution (LANXESS Energizing Chemistry) for disinfection. Ultracentrifugation was repeated twice and tubes were inverted to drain excess supernatant on paper soaked in 1% w/v Virkon™ S for 15 min. Pellets were carefully resuspended in 400µL DMEM. Concentrated virus was stored at -80°C until further use.

Cells were seeded 24 hours before virus infection at 60-70% confluency. The virus-containing media (12.5mL/1E6 cells) was added with 4µg/ml polybrene (MPBio-TR-1003-G). 8 hours later, the second virus hit was performed. 48 hours after first virus hit, media was removed and replaced with complete media containing the defined antibiotics (e.g. 1µg/ml puromycin (Sigma-P7255)) to select for successfully transduced

cells. Cell lines without antibiotic resistance marker were selected by cell sorting based on the presence of fluorescent marker.

2.4.1 CRISPR/Cas-9 gene deletion of PTEN

Lentiviral particle of Cas9 (with mCherry) and sgRNA (with GFP) expression was produced as described above. The PTEN sgRNA was designed using software provided at crispr.mit.edu (Table 2.3). Cells were infected at 0.5 MOI with Cas9-expressing lentivirus. mCherry+ cells were sorted (BD FACSAria III flow cytometer), and subsequently re-infected with lentiviruses expressing sgRNA. The mCherry+/GFP+ cells were sorted and collected. Western blotting was performed to determine gene deletion efficiency.

2.5 Fluorescence-activated cell sorting

Cells were trypsinized and resuspended in complete media. 100µl of resuspension was counted using Coulter Counter Z2. Cells were then centrifuged at 400g for 5mins at RT. Cell pellet was washed once in PBS prior to resuspension in FACS sorting solution (PBS+2% v/v FBS+5mM EDTA) at 10^7 cells/ml. FACS was performed on BD FACSAria Fusion with the help of Ralph Rossi, Viki Milovac and Sophie Curcio from PMCC Flow cytometry core. For BEBIR-shRNA cell lines, the BFP positive cells were sorted first and then expanded. Cells were treated with 1µg/ml doxycycline for 48 hours before being sorted for cells with both dsRED and BFP fluorescence. The sorted cells were expanded in the culture medium without doxycycline before the third time sorting for BFP/dsRED positivity.

2.6 siRNA transfection of BJ-TERT and IMR-90 fibroblasts

Gene-specific siRNAs including CBS (L-008617-00), CTNS (L-019914-00), GGH (L-007616-01), SLC7A6 (L-005883-00), SLC20A1 (L-007432-02), SLC22A11 (L-007445-00), SLC25A13 (L-007472-00), TP53 (L-003329-00) and MYC (L-003282-02) and On-Target Plus Non-Targeting siRNA control (D-001810-01) were purchased from Horizon Discovery. siRNA transfection was performed by reverse transfection in 96-well plates where cells were seeded onto plates containing transfection reagents and siRNA mixture. Reserve transfection was performed in 96-well black polystyrene clear flat-bottomed plates (Corning-3603). 0.1 µL (For BJ-TERT) or 0.4 µL (For IMR-90) Dharmafect 1 (Dharmacon-

T-2001-01) and 20nM ON-TARGETplus SMARTPool siRNA (Dharmacon) per well were mixed and dispensed into each well. 4,000 BJ-TERT or 12,000 IMR-90 cells in a total volume of 100 µL or 200 µL per well was then added. The negative controls including cell suspension only (no Dharmafect, no siRNA) or Dharmafect only control (no siRNA) were also prepared. The fresh complete medium was replaced at 24 hours post-transfection. Cells were cultured for another 4 days before functional analysis.

2.7 Gene expression analysis

2.7.1 RNA extraction

RNA isolation and purification were performed using the ISOLATE-II kit (Bioline-52073) according to the manufacturer's protocol. Briefly, cells were lysed on ice in lysis buffer containing 40nM DTT (SigmaAldrich-D0632). cell lysates were mixed with equal volume of 70% v/v Ethanol and loaded into the RNA-binding columns. The columns were washed with wash buffers. The purified RNA was then eluted in RNase-free H_2O and was quantified using a NanoDrop ND-1000 spectrophotometer.

For RNA products with low purity (the ratio of absorbance at 260nm and 280nm less than 1.8), Ethanol purification was performed. 20µg glycogen (Roche-10901393001) was added to RNA elute followed by 0.1 volume of 3M Sodium Acetate (SigmaAldrich-W302406) and mixed well. 2.5 volume of 100% v/v Ethanol was added and vortexed to mix thoroughly. RNA was precipitated at -80°C overnight. On the next day, samples were centrifuged at 20,000g for 15mins at 4°C. The pellets were washed with 750µL of 70% v/v ice-cold ethanol. After centrifugation, ethanol was then carefully removed without disturbing the precipitates. RNA pellets were air-dried for 15mins at RT and resuspended in 30µL RNase-free H_2O.

2.7.2 Quantitative Real-Time Polymerase Chain Reaction (qRT-PCR)

200ng of purified RNA was treated with DNase (Promega M6101) at 37°C for 15min followed by heat inactivation of DNase at 70°C for 15min. Complimentary-DNA (cDNA) synthesis by reverse transcription was performed using SuperScript™ III First-Strand Synthesis System (Invitrogen-18080051) per manufacturer's instruction under the following conditions: initial incubation at 37°C for 5min, reverse transcription at 47°C for 2 hours and reaction deactivation at 70°C for 15min. A negative control (H_2O only) and

a gDNA control (reaction minus SuperScript-III) were prepared for each primer set. Final contents were diluted in 100µl RNAse-free H2O and stored at -20°C.

qRT-PCR reactions were performed using the StepOne Plus Real-Time PCR system (Applied Biosystems-4376600) with a +0.7°C melt-curve increment. Reactions were performed in triplicate using MicroAmp Optical 96-well plates (Applied Biosystems-N8010560) using 40% v/v cDNA sample, 50% v/v Fast SYBR green Master Mix (Applied Biosystems-4385612) and 0.1µM forward and reverse primers (Table 2.5). As equal RNA was used for cDNA synthesis, changes in target gene expression were normalized to the non-POU domain-containing octamer-binding protein (NONO) housekeeping gene. Fold changes in gene expression were determined by $2^{(\Delta\Delta Ct)}$ [280]. The minus SuperScript-III and H_2O-only controls determine if gDNA contamination or primer dimer formation occurred respectively.

2.7.3 Methylation-specific PCR (MSP)

Cells were seeded 48 hours prior to genomic DNA (gDNA) extraction. Cells were trypsinized and counted. Genomic DNA was extracted using NucleoSpin® Tissue Kit (Macherey-Nagel-740952) according to manufacturer's protocol. Briefly, 10^7 cells were resuspended in lysis buffer with presence of 1.35mg/mL Proteinase K (Roche-RPROTKSOL-RO). Cell lysate was applied to DNA-binding column after adjusting binding conditions with ethanol. Column was washed and dried using buffers provided in the kit prior to elution.

DNA bisulphite modification was performed for gDNA prior to MSP using EZ DNA methylation kit (Zymo Research-D5001) according to manufacturer's protocol. 500ng gDNA was incubated with CT conversion reagent overnight at 50°C in dark, to allow non-methylated Cytosine (C) residue to be converted to Uracil (U). gDNA was applied to DNA-binding column and desulphonated for 15mins at RT. Columns were then washed and gDNA was eluted in 10 µl M-Elution buffer.

In the study of CBS promoter region MSP, PCR condition and primer sequence were adapted from Zhao and colleagues [281]. PCR amplification reaction mixture was prepared in 100 µl aliquots containing 2 µl of bisulphite converted gDNA, 200 µM dNTPs (Roche-DNTPM-RO), 1 mM Primer (Table 2.5), 1.5mM $MgCl_2$, 50mM KCl, 10mM Tris-HCl pH8.3 and 1.25unit GoTaq® DNA Polymerase (Promega-M3001). PCR amplification

reaction was performed in the T100 thermal-cycler under the following conditions: initial denaturation at 95°C for 10min, followed by 35 cycles (94°C for 30s, 55°C for 30s and 72°C for 30s) and reaction deactivation at 70°C for 15min.

2.8 Protein extraction & Western blotting

Cells seeded in 10cm petri-dish were lysed on ice using western solubilization buffer (0.5mM EDTA, 20mM HEPES, 2% w/v SDS, pH 7.9). Samples were boiled at at 95°C for 10mins and DNA were sheared using 26-gauge needle.

Protein concentration was determined using the detergent-compatible protein assay kit (BioRAD-500-0112) according to the manufacturer's instructions. Protein concentration was calculated based on protein concentration standard curve (R^2 >0.95). Protein levels were equalised and resuspended in 6x sample loading buffer (375 mM Tris-HCl, 9% w/v SDS, 50% v/v Glycerol, 0.03% v/v Bromophenol blue). Protein samples were loaded in a Mini-PROTEAN TGX™ Precast gel and separated by SDS-PAGE using Tris-glycine-SDS running buffer (25mM Tris, 192mM glycine, 0.1% w/v SDS, pH 8.7). The PageRuler plus protein ladder (Thermoscientific-26619) was used as a molecular weight marker. Protein was either wet- or semi-dry-transferred to Immobilon-PVDF membranes (Millipore-OPVH00010). Wet-transfers were performed in 25mM Tris, 192mM glycine, 15% v/v Methanol Buffer at 4°C at constant voltage 120V for 1h; Semi-dry transfers were performed in 48mM Tris, 39mM glycine, 0.375% w/v SDS, 20% v/v Methanol Buffer at room temperature using Trans-Blot® Turbo™ Transfer System (Bio-rad 170-4155) per manufacturer's instruction. Membranes were blocked in TBS buffer (Sigma-T5912) containing 0.1% v/v Tween20 (TBST) (Sigma-P2287) and 5% w/v skim milk (Diploma) for 1h at room temperature. Primary antibodies were used for overnight incubation at 4°C and washed three times with Tris-Buffered Saline, 0.1% v/v Tween® 20 Detergent (TBST) before incubation with HRP-conjugated secondary antibodies for 1h at room temperature (Table 2.4). Membranes were developed with Western-Lightning Plus ECL (Perkin-Elmer-NEL104001EA). Images were acquired using ChemiDoc imaging System (BioRAD-170-01401). Membranes were stripped and then re-probed for β-Actin as a loading control. Protein quantitation was performed using Image Lab software (V5.2, BioRAD) and expressed as fold changes after normalizing with β-Actin intensity.

2.9 Cell proliferation, clonogenic & anchorage-independent growth assays

2.9.1 Cell proliferation assay

200µL cell suspension at a defined density (2,500-5000cells/mL depending on cell size) was seeded in Flat-Bottom Clear 96-welled microplate (Greiner-655101) 24 hours prior treatment. Multiple parallel plates were prepared for fixation at different time point. Treatment started at time 0 and cells were refreshed every 48 hours unless otherwise stated. Chemicals and compounds used throughout this thesis were listed in section 2.5. After removing media carefully without lifting cells, plates were fixed (at different time point including one at time 0) by adding 100µL 100% v/v methanol for 15mins at RT. 100 ul 2N Hcl containing 0.5% (v/v) Triton X-100 was added and left at RT for 30 min. 100ul 0.1M Na2B4O7.10H2O (PH 8.5) was added and left at RT for 10min

Cells were washed using PBS. 100µL 2µg/mL Propidium Iodide (PI) (Roche-11348639001) in PBS was applied to the cells after PBS wash. The fluorescent images of cells were taken using IncuCyte (Essen BioScience). Subsequent analysis of images was performed using IncuCyte S3 Analysis Software according to manufacturer's instructions.

In addition to cell proliferation assay performed through IncuCyte platform, Sulforhodamine B (SRB) Assay was another method to measure cell proliferation by quantifying cellular protein contents. Cells were fixed by 10% w/v Trichoroacetic acid (TCA) (Merck-UN1839) in complete media at 4°C for 1 hour. Cells were washed extensively in H_2O and left to air-dry at RT. 100µL 0.4% w/v SRB (Sigma-Aldrich-23016.2) staining solution was dispensed into each well and incubated at RT for 30mins. Cells were washed by H_2O five time and then by 1% v/v Acetic Acid twice (Sigma-Aldrich-A6283). Plates were air-dried at RT. SRB was then resolubilized by adding 100µL of 10mM Tris Buffer to each well. Plates were mixed and measured using a Benchmark Microplate Reader at the optical density at 564nm.

2.9.2 Colony formation assay

Colony formation assays were performed as described previously [282]. cells were seeded in 6-well culture plates at different densities (1,250/2,500/5,000/10,000 per well). Media was refreshed every 48 hours with or without defined antibiotics or doxycycline treatment. Cells were fixed with 100% v/v methanol for 30 mins at RT at

approximately 2 weeks after initial seeding depending on different cell growth rate. Cells were then stained with 0.1% w/v crystal violet for 30 mins at RT. Plates were washed in H_2O intensively. Images were obtained using a BioRad ChemiDoc Touch gel-imaging platform. Total colony area, expressed as percentage of cell coverage per well, was determined using the ImageJ plugin ColonyArea [283].

2.9.3 Anchorage-independent growth assay

The anchorage-independent growth (AIG) assay was performed as described by Borowicz and colleagues [284]. Seeding conditions were optimised using the transformed fibroblast line BJ7, which form colonies in soft agar and tumours in SCID-mice [269]. 24 hours prior to seeding, 0.4% w/v noble agar (Difco-214220) dissolved in complete media containing 1X Antibiotic-Antimycotic (Gibco-15240062) was prepared and dispensed 1ml per well into 6-welled plate and solidified at RT for 30 mins. Cells were suspended in 0.3% w/v noble agar which was kept at 42°C water bath, to reach the final density of 10^4 cells/mL. 1mL cell mixture was dispensed into each well and solidified at RT for 15 mins. 200 ul of culture medium was added over the upper layer of agar to prevent drying and replaced twice weekly. The time required for colony formation varies for each cell line, typically around 3 weeks. Colonies were stained by adding 200µl of nitroblue tetrazolium chloride solution (Merck-11383213001) per well and incubating plates overnight at 37°C. Cell colonies were manually counted under transmitted light microscopy.

2.10 Histopathology & Immunofluorescence (IF) Staining

2.10.1 Senescence-associated β-galactosidase staining & EdU labelling

Cells were seeded in defined culture plate at least 72h before processing. 10µM EdU (Invitrogen-A10044) was added 24h prior to fixing. Cells were fixed using 2% v/v paraformaldehyde, 0.2% v/v glutaraldehyde for 5min at RT. X-Gal staining solution [285] (25% v/v citrate buffer, 5mM potassium ferrocyanide (Sigma-P3289), 5mM potassium ferricyanide (Sigma-P-8131), 150mM NaCl (MPBio-0219484801), 2mM $MgCl_2$ (Merk-536092), 5mg X-Gal (Sigma-B4252)) was filtered with 0.22µm filter and added to the plates. Cells were incubated at 37°C for 24h. Cells were permeabilized for 1min using 0.5% v/v TritonX-100 (Sigma-T8532) in PBS. EdU was fluorescently labelled with

AlexaFluor-488 using the Click-iT (Thermoscientific-C10337) reaction solution according to the manufacturer's protocol and incubated at RT for 30min in the dark. Slides were either lined with VECTASHIELD Antifade Mounting Medium with DAPI for Fluorescence (VECTOR-H-1200) and sealed with a microscope coverslip, or stained with 500ng/mL DAPI (Invitrogen-D1306) in darkness at RT for 5min. Images were obtained using a fluorescence microscope Olympus BX-61 with SPOT (5.2) image software. A minimum of 200 cells per biological replicates were counted, with DAPI used to indicate individual cells which were then compared to EdU or SAβGal positive counterparts. SAβGal was only counted as positive in the absence of EdU incorporation.

2.10.2 IF staining for cells

Cells were seeded in defined culture plates at least 48 hours before fixation. After PBS wash cells were fixed using 4% v/v paraformaldehyde in PBS for 15 min at RT.

Slides were washed with PBS and permeabilized with 0.5% Triton X-100 in PBS for 15min at RT. For 5-methylcytosine (5-mC) staining, cells were treated with 2N HCl at RT for 30min and then neutralized for 10min with 100mM Tris-HCl buffer, pH8. After PBS wash cells were blocked in BLOTTO buffer (4% w/v BSA, 0.5% v/v Triton X-100 (TX-100) (Roche-10789704001), 1% v/v goat serum in PBS) for 30 min at 37°C. 5-mC primary antibody (Table 2.6) diluted in BLOTTO at 1:400 was added on top of the slide and covered with coverslip. Slides were incubated at 4°C overnight. Slides were washed with 0.5% v/v TX-100 in PBS at RT for 5 min for three times prior to secondary antibody incubation. The Goat anti-Mouse IgG Superclonal™ recombinant secondary antibody (Table 2.6), linked with Alexa Fluor 488 or 594 was diluted at 1:400 in BLOTTO buffer. Slides were covered with coverslip and incubated at 37°C for 1 hour in humidified container in dark to avoid fluorescent fading. Slides were washed in 0.5% v/v TX-100 in PBS at RT for 5min, three times followed by a final wash in dH_2O at RT for 5min in dark. After mounting slides with VECTASHIELD Antifade Mounting Medium with DAPI, images were taken using Olympus BX61 microscope. Fluorescence intensity was quantified using CellProfiler™ software (Broad Institute, Version 2.2.0) with help from Ms Natalie Brajanovski (Pearson Laboratory PMCC).

2.11 Tissue Microarray (TMA)

Gastric cancer patient TMA was a generous gift from Dr Xi Wang, Department of Oncology, The 903rd Hospital of PLA, Hangzhou 310013, China. The tissue microarray construction has been described previously [286] [287]. TMA slide composes of 120 tumour sections and 63 normal sections from 62 individual gastric cancer patients (Table 2.7). These patients underwent gastrectomy from 2000 to 2005 in Changhai hospital, second Military Medical University, Shanghai, China. All patients have not received any anticancer therapy before surgery. The tissue samples were obtained with patient informed consent and the protocol was approved by Institutional Review Board of Second Military Medical University.

TMA slide embedded in paraffin was baked at 60°C for 1 hour before dewaxing. Slide were incubated in 100% v/v xylene for 3 mins for three cycles followed by 100% v/v ethanol for 1 min for three cycles and incubation in 70% v/v ethanol 1 min. Slides were washed in H_2O for 1 min to complete dewax/rehydration procedures. Antigen retrieval was then performed for rehydrated slides in high pH buffer (Agilent-K8004) using pressure cooker for 45 mins. Slides were then washed in 0.1% v/v TBST for 5 mins and blocked in blocking buffer (2% w/v BSA, 0.2% v/v TX-100, 1% v/v goat serum in PBS) for 1 hour at RT. Primary antibody (Table. 2.6) diluted in blocking buffer was applied on top of the slide and covered with coverslip. Slides were incubated at 4°C overnight. Slides were washed three times in 0.1% v/v TBST at RT for 5 min prior to secondary antibody incubation. The Secondary antibody, labelled with HRP (Dako-K4002) was applied to cover the samples. Incubation at RT for 30mins was performed in humidified container. Slides were washed three times in 0.1% v/v TBST at RT for 5 min. Fluorophore (Opal620: Excitation 588 nm; Emission 616 nm; Cap Colour Amber) from Opal 7-Color Manual IHC kit (PerkinElmer-NEL811001KT) were diluted in 1X Plus Amplification Diluent (PerkinElmer-FP1498) before applying to the samples. Slides were incubated for 10 mins and washed five times in 0.1% v/v TBST at RT for 5 min in dark. Cells were counterstained with DAPI and washed in PBS prior to mounting with VECTASHIELD Antifade Mounting Medium. The images were taken using VS120 Virtual Slide Microscopy (OLYMPUS-VS120-L100-W) and analysed using HALO™ Image Analysis Software (PerkinElmer-CLS141258). The same threshold settings were applied to individual patient sections.

Total number of cells expressing cytoplasm CBS (Red fluorescence) was divided by total cell number (DAPI) from each section and was shown as %Red Positive. Average cytoplasm fluorescence intensity on tumour tissue section were compared to normal tissue section from the same patient and expressed as fold change relative to normal control.

2.12 Intracellular H_2S production measurement

Intracellular H_2S was measured using 7-Azido-4-Methylcoumarin (AzMC) fluorescent dye [288]. Protocol was adapted from Szabo Laboratory with minor modifications [289]. Cells were seeded in 10cm plate at 80% confluency with equal cell number 24 hours before harvest. One extra plate was prepared for cell number counting. On harvesting day, AzMC reaction master mix consisted of 200mM Tris-HCl pH8, 20mM L-Cysteine (SigmaAldrich-30089), 1mM L-Homocysteine (SigmaAldrich-69453), 100µM Pyridoxal 5'-phosphate hydrate (SigmaAldrich-P9255), 20mM AzMC (SigmaAldrich-802409) in H_2O was prepared and kept on ice. Serial dilution of Na_2S (SigmaAldrich-407410) in H_2O was prepared for generating H_2S concentration standard curve (0, 2.5, 5, 10, 20, 25, 50µM). Cells were washed with cool PBS twice and lifted mechanically using rubber cell lifters in 1mL PBS on ice. Samples were centrifuged at 700g for 10mins at 4°C and the supernatant was discarded without disturbing cell pellets. Cell pellet was then resuspended in 100µl cell lysis buffer (50mM Tris-HCl pH8, 150mM NaCl, 1% v/v IGEPAL® CA-630(SigmaAldrich-I3021), 1% v/v Triton-X100) and kept on ice for 1 hour. Samples were then centrifuged at 20,000g for 10mins at 4°C. Supernatants (100µl) were transferred to new eppendorf tubes and mixed with 100µl AzMC reaction master mix. Samples were briefly vortexed and incubated at 37°C in dark for 2 hours. Reaction mixtures were transferred into 96-well black clear flat bottom microplate (Sigma-CLS3603). Plate was read at 340nm excitation and 445nm emission wavelength using Cytation™3 Cell imaging multi-mode reader (BioTek). Fluorescence intensity was normalised with cell number and Intracellular H_2S production was determined based on H_2S standard curve. Statistical analyses were performed using Student's t-test.

2.13 Glutathione (GSH) detection assay

GSH detection assay was performed using Glutathione Assay Kit (Cayman Chemical-703002) according to manufacturer's protocol. Briefly, cells were seeded 24 hours before harvesting in 10cm plate at 80% Confluency with equal cell number. One extra plate was prepared for cell number counting after cell harvesting. On harvesting day, cells were washed twice with PBS and lifted using rubber scraper in 1mL PBS on ice. Samples were centrifuged in eppendorf tubes at 400g for 5mins at 4°C. Supernatants were discarded and cell pellets were resuspended in 100µl MES buffer (50mM MES, 1mM EDTA, pH6). Samples were then lysed using freeze-thaw method in LN_2. Supernatants (100 µl) were collected without disturbing pellet after centrifugation at 12,000 g for 15 min at 4°C. 100µl of 2.5M metaphosphoric (MPA, SigmaAldrich-239275) was added to samples for deproteination. Samples were then vortexed and kept at RT for 5mins prior to centrifugation at 3,000g for 2mins. The supernatants were collected and added 10µl of 4M triethanolamine (TEAM, SigmaAldrich-T58300). The deproteinated and neutralized supernatants were used for the determination of the amount of total GSH by incubating with the assay reagents (provided from the kit) in a 96-well plate. After 25 min incubation in dark, the absorbance at 405 nm was measured using a Benchmark Microplate Reader. Data were normalised with cell number and GSH standard curve. Statistical analyses were performed using Student's t test.

2.14 Metabolomics

2.14.1 Gas chromatography-mass spectrometry (GC/MS) based Metabolomics

GC/MS based metabolomics was performed in collaboration with Metabolomics Australia. Cells were seeded in 6-welled plates at 5,000/well four days prior to harvest. On the harvesting day, after wash with prewarmed Saline at 37°C, 1mL of liquid nitrogen was immediately poured into each well. After LN_2 was boiled off, metabolite samples were harvested using ice-cold methanol:chloroform:scyllo-inositol (MeOH:$CHCl_3$ 9:1 v/v, and 3µM scyllo-inositol as internal standard)(Sigma-Aldrich-C2432/I8132) solution. Metabolites were collected using cell lifters and transferred to eppendorf tubes. Samples were then centrifuged at 4°C for 3mins at 16,100g to create an upper aqueous

(MeOH) and lower organic layers (CHCl3). Supernatants were transferred to new eppendorf tubes for LN_2 snap-freezing.

For GC-MS analysis, 300µl of the aqueous phase was evaporated to dryness using vacuum centrifuge at 4°C. Samples were derivatized with 25µl 3% w/v methoxyamine in pyridine (Sigma-Aldrich-226904/270970) for 60 min at 50°C with mixing at 900 rpm, followed by trimethylsilylation with 25µl BSTFA + 1 % TMCS (Thermo Scientific-38831) for 60 min at 50°C with mixing at 900 rpm. The derivatized sample (1µl) was analysed using Shimadzu GC/MS-TQ8040 system. Metabolites were normalised based on pooled metabolite peak area median and identified based on GC retention time and mass spectra as compared with authentic standards and in conjunction with MSD ChemStation Data Analysis Application (Agilent) using in-house and Wiley metabolite libraries.

Statistical analyses were performed using Student's t test. Metabolites were considered to be significant if their adjusted p-values after Benjamini & Hochberg correction were less than 0.05. Further data analysis and enrichment analysis were performed through MetaboAnalyst 4.0 [290].

2.14.2 Thiol derivatization & detection using Liquid chromatography-mass spectrometry (LC/MS) based Metabolomics

LC/MS-based metabolomics was performed in collaboration with Dr. Darren Creek and Dr. Dovile Anderson in Monash Institute of Pharmaceutical Sciences. Thiol derivatization using N-Ethylmaleimide (NEM) and LC/MS based detection were described previously [291] and optimized. Briefly, 50,000 cells were seeded in 6-welled plates four days before harvest. Cells were washed with ice-cold Saline at 4°C. Metabolite samples were harvested using ice-cold extraction buffer containing 5 mM NEM (Sigma-Aldrich-E3876) in 80% v/v methanol and 20% v/v 10mM ammonium formate (Sigma-Aldrich-516961) at pH 7. Final concentration of 2 µM L-Valine-13C5,15N (Sigma-Aldrich-600148), D-Sorbitol-13C6 (Sigma-Aldrich-605514) and L-Leucine-13C6 (Sigma-Aldrich-605239) were used in the extraction buffer as internal standards. Metabolites were collected using cell lifters and transferred to eppendorf tubes. Samples were mixed at 4°C on vortex mixer for at 1 hour at 1,000 rpm before centrifugation at 20,000 g for 10 mins at 4°C. Supernatants were stored on ice and processed as per described previously [291] at The

Monash Institute of Pharmaceutical Sciences Australia. Peak intensities were normalized against internal standards and cell numbers, and the statistical analyses were carried out using one-way ANOVA.

2.15 RNA-sequencing and analysis

Poly-A selective RNA-seq libraries were prepared using the TruSeq RNA sample preparation kit (Illumina®) and sequenced on Illumina® NextSeq 500. The quality of the generated 50 bp paired-end reads from BJ-TERT cells was assessed with TapeStation System (Agilent-G2991AA). Tophat2 (version 2.0.13)/Bowtie2 (version 2.2.3.0) or HISAT2 (version 2.0.4) for the 75 bp single reads, which were used for alignment to the genome (hg19/GRCh37). Cutadapt (version 1.7.1 with Python 2.7.8) was used for adapter and quality trimming. Picard 1.125 was used to generate BAM indices and to calculate insert size. Samtools 0.1.18 was used to sort and merge. Reads were counted using feature counts (version1.6.2) in Galaxy. The differential expression of genes was then calculated utilizing the DESeq2 package v1.24.0 and plotted in R. Absolute gene expression was defined determining RPKM. Gene set enrichment analysis (GSEA) of a preranked list $\log_2FC \times -\log_{10}$(p-value) with average raw counts ≥20 from three biological replicates from at least one sample set was performed according to the Hallmark gene set from the molecular signatures database MSigDBv6.1 (Broad Institute). Heatmaps were generated using Morpheus (Broad Institute).

2.16 Mouse xenograft model establishment

Female NSG mice aged between 8-10 weeks were used for establishing AGS gastric cancer xenograft model. Mice were randomized into three groups of six mice. AGS gastric cancer cell line was transduced by retrovirus carrying either RT3-CBS-puro or RT3-CBS^{I278T}-puro constructs. Virus production and antibiotic selection were described in section 2.4. On Implantation day, matrigel (Gibco-A1413201) was removed from freezer and placed on ice to thaw. Cells were washed, trypsinized and collected into 50mL sterile tubes. Cells were then centrifuged at 400g for 3 mins at 4°C. Media was removed and cell pellet was resuspended with PBS. Cell suspension stained with trypan blue was counted using and haemocytometer. Cell concentration was adjusted to 1E8

cells /mL in PBS. Cell suspension was mixed on ice with equal volume of matrigel using pre-cooled 1mL-pipettes (Gilson-F110122).

Mice were anaesthetized using isoflurane. 5E6 cells in 100µl PBS-Matrigel mixture was injected to mice right flank, using pre-cooled 0.3mL insulin syringes (BD-230-4533). Mice in Group 1 and 2 were implanted with AGS-RT3-CBS-puro cells, and Group 3 mice was injected with RT3-CBS^{I278T}-puro cells. The syringe was only filled for one injection at a time and cells were mixed by inversion between each use. When all tumours appear to be measurable (approximately > 4mm x 4mm at one-week post-implantation), each mouse was numbered by making ear clips. Mice were weighed and tumours were measured three times weekly using an electronic calliper (Sidchrome-SCMT26115). Once tumours reached an average volume of 100mm^3 calculated by $V = (W^2 \times L)/2$, mice in group 2 and group 3 were administered with doxycycline both in the drinking water (0.2% Doxycycline hyclate (Sigma-Aldrich-D9891), 2% w/v sucrose (Sigma-Aldrich-S8501)) and 600mg Doxycycline/kg food (SpecialtyFeeds-SF08). Mice were sacrificed once tumours reached 1200mm^3, and tumours were half snap-frozen and half fixed in formalin for further analysis.

2.17 Chapter 2 Tables

Table 2.1 Gastric cancer cell lines

	tissue	morphology	growth properties	doubling time	tumorigneic	medium (ATCC)	oncogenes
AGS	gastric adenocarcinoma	epithelial	adherent	20 hours	BALB/c	DMEM+10%FBS	Unknown
Hs746T	derived from metastatic site: left leg	epithelial	adherent	47 hours	yes	DMEM+10%FBS	Unknown
SNU-5	derived from metastatic site: ascites	epithelial	clusters in suspension	34 hours	colony formation efficiency 27%	IMDM+20%FBS	myc+erbB2+
NCI-SNU-1	derived from metastatic site: ascites	epithelial	clusters in suspension	26 hours	colony formation efficiency 1.9%	RPMI+10%FBS	myc+erbB2+
NCI-N87	deirved from metastatic site liver	epithelial	adhernet	47 hours	yes	RPMI+10%FBS	myc+erbB2+
KATOIII	metastatic sites: pleural effusion, supraclavicular and axillary LNs and Douglas' cul-de-sac	spherical with attached epithelial cells	mixed suspension and adhernet cells	36 hours	not tunorigenic in nude mice	IMDM+1.5 g/L sodium bicarbonate +20%FBS	Unknown

Table 2.2 shRNA primers and sequences for cloning inducible knockdown constructs.

Library	Vendor Reagent ID	Gene Name	Entrez Gene ID	Entrez Gene Symbol	Genbank Accession Numbers	Sequence	Species
RHS6046 Human v3 shRNA drug targets	V3LHS_363334	cystathionine-beta-synthase	875	CBS, HIP4	NM_001178009	CGACTCAGTGCGGAACTAC	Homo sapiens
RHS6046 Human v3 shRNA drug targets	V3LHS_363331	cystathionine-beta-synthase	875	CBS, HIP4	NM_001178009	CAGACGGAGCAGACAACCT	Homo sapiens
Common primers for mir30 shRNA amplification							
mir30 XhoI fwd	CAGAAGGCTCGAGAAGGTATATTGCTGTTGACAGTGAGCG						
mir30 EcoRI rev	CTAAAGTAGCCCCTTGAATTCCGAGGCAGTAGGCA						

Table 2.3 PTEN sgRNA sequence used for CRISPR knockout

Gene	Ensembl ID	Sequence	Guide with flanking sequence (10bp before and after the guide + PAM)	Chromosome	PAM position in chromosome	On-target efficiency	Exon	Targets last exon	10bp off-target match	Off-target score
PTEN	ENSG00000171862.5	AGCTGGCAGACCACAAACTG	CTTCACCTTTAGCTGGCAGACCACAAACTGAGGAGGATCTGCA	10	89717771	0.753703	7	FALSE	FALSE	0

Table 2.4 Antibodies used for Western immunoblotting

Primary antibodies			
Protein/Target	Molecular Weight(kDa)	Primary Antibody Details	Dilution Factor
β-Actin	42	Mouse; MPBio-691001	1:10,000
pan-AKT	60	Rabbit; Cell Signalling 4691	1:1,000
phospho-AKT (S473)	60	Rabbit; Cell Signalling-4058	1:2,000
ERK1/2	42-44	Rabbit; Cell Signalling-9102	1:1,000
phospho-ERK1/2 (T202/Y204)	42-44	Rabbit; Cell Signalling-9101	1:1,000
Hemagglutinin (myr-AKT1)	60	Mouse; Pearson Lab 12CA5	1:2,000
H-RAS (C-20)	21	Rabbit; SantaCruz-520	1:500
N-RAS (F155)	21	Mouse; SantaCruz-31	1:500
p53	53	Mouse; Pearson Lab	1:1,000
p53 (D0-1)	53	Mouse; SantaCruz-126	1:2,000
p21 (C-19)	21	Rabbit; Cell Signalling-2947	1:500
p16	16	Rabbit; PharMingen-554230	1:1,000
p16 (C-20)	16	Rabbit; SantaCruz-468	1:500
PRAS40	40	Rabbit; Cell Signalling-2610	1:1,000
phospho-PRAS40 (T246)	40	Rabbit; Cell Signalling-2997	1:1,000
Rb	110	Mouse; Cell Signalling-9309	
phospho-Rb (Ser807/811)	110	Rabbit; Cell Signalling-9308	1:1,000
IGF-I Receptor β (111A9)	95	Rabbit; Cell Signalling-3018	1:2,000
Phospho-IGF-I Receptor β (Tyr1135) (DA7A8)	95	Rabbit; Cell Signalling-3918	1:2,000
NF1	250	Rabbit; SantaCruz-67	1:500
phospho-AMPKα (T172)	62	Rabbit; Cell Signalling-2535	1:1,000
CBS	61	Rabbit; Proteintech-14787-1-AP	1:2,500
CBS (B-4)	61	Mouse; SantaCruz-133154	1:500
S6 Ribosomal Protein (5G10)	32	Rabbit; Cell Signalling-2217	1:1,000

Phospho-S6 Ribosomal Protein (Ser235/236) (2F9)	32	Rabbit; Cell Signalling-4856	1:1,000
PTEN (138G6)	54	Rabbit; Cell Signalling-9559	1:1,000
FADD (H-181)	27	Rabbit; SantaCruz-5559	1:500
SLC7A11 (D2M7A)	35	Rabbit; Cell Signalling-12691	1:1,000
FLAG		Mouse; Merck-F3165	1:1,000
Secondary antibodies			
Goat-α-Rabbit-HRP-conjugate IgG		BioRAD-170-6515	1:2,000
Goat-α-Mouse-HRP-conjugate IgG		BioRAD-172-1011	1:2,000

Table 2.5 Primers used for qRT-PCR.

Gene	Direction	Sequence (5'-3')	Tm (oC)
NONO	Forward	CATCAAGGAGGCTCGTGAGA	58.4
	Reverse	TGGTTGTGCAGCTCTTCCAT	59.3
GAPDH	Forward	GGACTCATGACCACAGTCCATGCC	64.6
	Reverse	ATGACCTTGCCCACAGCCTTGG	64.9
Tp53	Forward	AAGAAACCACTGGATGGAGAA	56.3
	Reverse	CAGCTCTCGGAACATCTCGAA	58.9
CBS	Forward	TGAGATTGTGAGGACGCCCAC	61.7
	Reverse	TCACACTGCTGCAGGATCTC	59
CSE	Forward	CAGCAATTACACCAGAAACCAAG	57.5
	Reverse	CAGCCTTCAATGTCAATCACC	56.6
3-MST	Forward	CTACGAGGACATCAAGGAGAAC	57
	Reverse	GTTCACGGTACCTGGGATG	56.6
MTR	Forward	ATGGAGCTGCTATGGTGGTC	58.9
	Reverse	CCCTGGTAAGGGTCCTCTTC	58.2
ULBP1	Forward	CAAGTGGAGAATTTAATACCCATTGAG	57.8
	Reverse	TGTTGTTTGAGTCAAAGAGGA	54.5
ULBP2	Forward	CAGAGCAACTGCGTGACATT	58.1
	Reverse	GGCCACAACCTTGTCATTCT	57.7
ULBP3	Forward	CCTGATGCACAGGAAGAAGAG	57.5
	Reverse	TATGGCTTTGGGTTGAGCTAAG	57.7
ULBP5	Forward	TGGCCGACCCTCACTCTCT	61.8
	Reverse	CCGTGGTCCAGGTCTGAACT	60.8
CXCL1	Forward	AGTCATAGCCACACTCAAGAATGG	60
	Reverse	GATGCAGGATTGAGGCAAG	55.4
CXCL10	Forward	CCAGAATCGAAGGCCATCAA	57.2
	Reverse	CATTTCCTTGCTAACTGCTTTCAG	57.9
IL-1a	Forward	ACTGCCCAAGATGAAGACCA	58.4
	Reverse	CCGTGAGTTTCCCAGAAGAA	56.7
IL-1b	Forward	GGAGATTCGTAGCTGGATGC	57.2
	Reverse	GAGCTCGCCAGTGAAATGAT	57.4
IL-6	Forward	AGTGAGGAACAAGCCAGAGC	59.2
	Reverse	CATTTGTGGTTGGGTCAGG	55.5
IL-8	Forward	GTCTGCTAGCCAGGATCCAC	59.1
	Reverse	GCTTCCACATGTCCTCACAA	57.3
CCL2	Forward	GTTGGCTCAGCCAGATGCA	59.9
	Reverse	AGCCTACTCATTGGGATCATCTTG	59.6
MICA	Forward	CCTTGGCCATGAACGTCAGG	60.5
	Reverse	CCCTCTGAGACCTCGCTGCA	63.1

IGF-1	Forward	ACCGAGGGGCTTTTACTTCA	58.4
	Reverse	TGGCTCACCTTTCCTTCTCC	58.7
IGFBP3	Forward	CAGGCAGCCTAAGCACCTAC	59.6
	Reverse	AGCTCTGCTTTCTGCCTTTG	57.9
NRF2	Forward	CTTGGCCTCAGTGATTCTGAAGTG	60.8
	Reverse	CCTGAGATGGTGACAAGGGTTGTA	61.5
NQO1	Forward	CAGCTCACCGAGAGCCTAGT	60.3
	Reverse	GAGTGAGCCAGTACGATCAGTG	59.5
HMOX1	Forward	GGGTGATAGAAGAGGCCAAGA	58.3
	Reverse	AGCTCCTGCAACTCCTCAAA	58.7
PRDX1	Forward	CACTGACAAACATGGGGAAGT	57.7
	Reverse	TTTGCTCTTTTGGACATCAGG	55.9
SLC3A2	Forward	AGCATCCGTGTCATTCTG	53.7
	Reverse	GAGCATCCTTCACCTTGG	54.1
SLC7A11	Forward	AGGCTTCTCATGTGGCTGAT	58.5
	Reverse	AGAATTGAGAGCACGATGCA	56.8
KEAP1	Forward	GGGAGGTGGCCAAGCAAGAGG	64.8
	Reverse	TCACCTGCGTGGGCTTGTGCAG	67.3
OSGIN1	Forward	CTGCCTGTCAGGTCCGCTGC	65
	Reverse	GCGTGCTCCTTCCGGTGCTT	65
CBS(MSP)	Forward	CAGAGGATAAGGAAGCCAAG	57.9
	Reverse	TCCCAATCTTGTTGATTCTGAC	58.8
CBS-methylated	Forward	CGAGATATTGGTCGGCGTC	60.5
	Reverse	CCCCGACTACGACGAAACG	62.8
CBS-unmethylated	Forward	TTATGAGATATTGGTTGGTGTT	55.7
	Reverse	TACCCCAACTACAACAAAACA	58

Table 2.6 Antibodies used for IF staining

Primary antibodies		
Protein/Target	Primary Antibody Details	Dilution Factor
5-methylcytosine (33D3)	Mouse; abcam-10805	1:400
CBS	Rabbit; Proteintech-14787-1-AP	1:200
phospho-AKT (S473)	Rabbit; Cell Signalling-4058	1:200
Secondary antibodies		
Goat Anti-Mouse IgG H&L (Alexa Fluor® 488)	abcam-150113	1:1,000
HRP Labelled Polymer Anti-Mouse	Dako EnVision+ System-K4001	undiluted
HRP Labelled Polymer Anti-Rabbit	Dako EnVision+ System-K4003	undiluted

Table 2.7 TMA sample slide layout.

									Total	Normal: A or B		Cancer: C afterwards		62 patient				
										63		120						
	0316276A	0316199A	0316199A	0316199C	0316198A	0316198C	0316198C	0316163B	0316163C	0316163C	0316163D	0316163E	0312665B	0312665C	0312665D	0312664A	0312664C	0312664C
	0315911B	0315911C	0315911C	0315980B	0315980C	0315980C	0315981B	0315981C	0315981C	0316070A	0316070C	0316070C	0313942C	0313951A	0313951C	0312663A	0312663C	0312663C
	0315809A	0315809C	0315725B	0315725C	0315725C	0315726A	0315726C	0315726C	0315726J	0315722B	0315722D	0315722D	0313942B	0313942C	0313941A	0313941C	0313941C	0313940C
	0315594B	0315594C	0315605A	0315605C	0315605C	0315605D	0315617B	0315617C	0315721B	0315721C	0315722E	0315722G	0313867H	0313868A	0313868C	0313868C	0313940B	0313940C
	0315594C	0315440B	0315440C	0315440C	0315441B	0315441C	0315441C	0315422A	0315422C	0315422C	0315324A	0315324C	0313867A	0313867C	0313867C	0313866A	0313866C	0313739C
	0315147A	0315147C	0315233A	0315233C	0315233C	0313251A	0313251C	0315251C	0315254B	0315254C	0315254C	0315324C	0313584C	0313584H	0313636B	0313636C	0313636C	0313739A
	0315066B	0315066C	0315066C	0315010B	0315010C	0315010C	0315010D	0315010J	0314910A	0314910C	0314910C	0314827C	0313584B	0313584C	0313580B	0313580C	0313580C	0313243C
	0314647A	0314647C	0314120B	0314120C	0314120G	0314813A	0314813C	0314813C	0314825B	0314825C	0314827A	0314827C	0314952B	0314952C	0314952H	0314952G	0313243A	0313243C
	0313242B	0313242C	0313242C	0313241B	0313241C	0313122A	0313122C	0313122C	0313103A	0313103C	0313103C	0313091C	0314547B	0314547C	0314547C	0314546B	0314546C	0314546C
0312742C	0312742B	0312742C	0312862B	0312862C	0312862C	0313087B	0313087C	0313087C	0313090B	0313090C	0313091A	0313091C	0314405B	0314405C	0314405C	0314462B	0314462C	0314462C
														0314383A	0314383C			

CHAPTER 3 The transcriptional and metabolic profiling of AKT-induced senescence

3.1 Preface

This chapter aims to characterise the transcriptomic and metabolic profiles of AKT-induced senescence (AIS) to identify the molecular signatures and metabolic phenotypes of AIS and provide more mechanistic insight into AIS establishment and maintenance.

Publication arising from this chapter:

Chan KT, Blake S, Zhu H, Kang J, Trigos AS, Madhamshettiwar PB, Diesch J, Paavolainen L, Horvath P, Hannan RD, George AJ, Sanij E, Hannan KM, Simpson KJ, and Pearson RB. A functional genetic screen defines the AKT-induced senescence signalling network, Cell Death and Differentiation, 2019.

3.2 Introduction

The PI3K/AKT/mTORC1 signalling pathway is critical for regulating cellular growth and proliferation [292]. Aberrant activation of this signalling network drives the pathogenesis in many sporadic human cancers. Specifically, phosphatase and tensin homologue (PTEN) loss is the most commonly observed aberration in the PI3K/AKT/mTORC1 signalling pathway and is detected in 30% of all tumour samples analysed using immunohistochemistry [268]. The second most common genetic aberration in the pathway is the phosphatidylinositol-4,5-bisphosphate 3-kinase catalytic subunit alpha (PIK3CA) activating hotspot mutations, including E545K in the helical domain and H1047R in the kinase domain, which are found in 13% of tumours [268]. Moreover, PTEN inactivating mutations (6%) and AKT1 mutations (1%) also contribute to tumour malignancy [268]. Furthermore, the prevalence of PI3K/AKT/mTORC1 signalling pathway alterations has been suggested to be tumour-specific. PTEN loss is observed in 57% of hepatocellular, 48% of colorectal, 36% of gastric, 52% of prostate and 49% of endometrial cancer, where a high prevalence of PIK3CA mutations is shown in 37% of endometrial, 31% of breast, 29% of cervical, and 27% of anal cancers. In addition, an AKT E17K mutation is observed in 1.4-8% of breast, colorectal and ovarian cancers, resulting in pathological cytoplasmic membrane

localization and constitutive activation [293]. Overall, at least one aberration in the PI3K/AKT/mTORC1 signalling pathway is found in approximately 70% of endometrial cancers and at least 50% of breast, prostate, anal, hepatocellular, colorectal and cervical cancers, highlighting the importance of this pathway as a key cancer driver.

Paradoxically, hyperactivation of oncogenic pathways such as RAS/ERK or PI3K/AKT/mTORC1 can lead to cellular senescence in normal cells, termed oncogene-induced senescence (OIS). OIS is a potent tumour suppressive mechanism [22]. While RAS-induced senescence (RIS) has been extensively characterized, the understanding of mechanisms controlling AKT-induced senescence (AIS) and how it is subverted in cancer is still limited. We and others have demonstrated that hyperactivation of the PI3K/AKT/mTORC1 signalling pathway by PIK3CA mutants (E545K or H1047R), PTEN knockdown, or constitutively active AKT isoforms (AKT1, AKT2 or AKT3) caused senescence in normal cells [34] [20]. AIS exhibits several senescence hallmarks including cell cycle arrest, increased SA-βGal activity and a senescence-associated secretory phenotype (SASP). Distinct from RIS, AIS does not display p16 upregulation, a DNA Damage Response (DDR) or senescence-associated heterochromatin foci (SAHF). Instead, upregulation of p53/p21 is observed in AIS cells, and the elevated p53 expression is attributed to increased mTORC1-dependent translation and Murine Double Minute 2 (MDM2)-dependent stabilization [34] [20]. Furthermore, cellular senescence induced by PTEN depletion has been detected in murine models of prostate cancer and acts as a critical brake against tumourigenesis [20] [21].

In this chapter, we will compare the molecular landscape of AIS with that of RIS to identify unique and shared molecular signatures and metabolic phenotypes in these two types of OIS, thus providing in-depth mechanistic insights into AIS establishment and maintenance.

3.3 Results

3.3.1 Human skin fibroblasts (BJ-T cells) with hyperactivation of AKT and RAS develop senescence with distinct kinetics

Telomerase reverse transcriptase (hTERT)-immortalised human skin fibroblasts (BJ-T) have been widely utilised as a non-transformed cell model for OIS research. The

expression of hTERT has been shown to prevent replicative senescence but not OIS [30]. We generated BJ-T cells constitutively expressing myr-AKT1 or $HRAS^{G12V}$ by retrovirus transduction of pBabe- myr-AKT1 or $HRAS^{G12V}$ which we have shown to induce approximately 70-80% senescence in BJ-T cells [34]. To ensure a transduction efficacy that could be reproduced in multiple experiments, the virus-containing medium harvested from HEK293T cells was concentrated before virus transduction into BJ-T cells. Using this approach, we consistently observed approximately 70% of SA-βGal-positive cells (Fig. 3.1.1a) and 10% of EdU-positive cells (Fig. 3.1.1b) by day 14 post-transduction of myr-AKT1. Constitutive activation of $HRAS^{G12V}$ in BJ-T cells induced senescence to a similar extent as AIS (Fig. 3.1.1a-b). We then used these conditions to characterize the transcriptional and metabolic alterations during OIS.

To confirm the activation of signalling pathways downstream of AKT/RAS activation we performed western immunoblotting at Day 14 post-transduction (Fig. 3.1.1c), a time point with equivalent senescence induction. Overexpression of myr-AKT1 resulted in increased phosphorylation levels of AKT and proline-rich Akt substrate of 40 kDa (PRAS40), indicating hyperactivation of AKT signalling as expected. AIS cells exhibited elevated expression of p53 and p21, consistent with our previous finding that AIS depends on the p53/p21 tumour suppressive network [34]. Hyperactivation of $HRAS^{G12V}$-induced the ERK signalling pathway, as illustrated by increased phosphorylation of Erk1/2. Significant elevation of p16 was observed in RIS cells but not AIS, consistent with distinct tumour suppressive networks being activated during AIS and RIS [34]. Furthermore, the expression levels of several senescence-associated proteins were examined. The total Retinoblastoma (Rb), a key regulator of the G1/S phase transition, and its inhibitory phosphorylation at serine 807/811 were suppressed in both AIS and RIS cells [294]. Similar changes were also observed in the expression levels of Cyclin A [8], which mediates S to G2/M phase transition and Lamin B1 [295] which regulates chromatin changes during OIS. These results are consistent with the exit from the cell cycle upon oncogenic RAS or AKT stimulation. Compared with RIS, AIS cells display overlapping phenotypes controlled by distinct regulatory networks.

The distinct but overlapping phenotypes of AIS and RIS prompted us to further understand AIS, as this could provide valuable insight into how to better treat cancers

driven by specific oncogenes. We therefore performed RNA-seq analysis (Fig. 3.1.2a-b) to (1) identify the molecular signatures required for AIS initiation and (2) characterize the changes in molecular signatures during the transition from AIS initiation to maintenance.

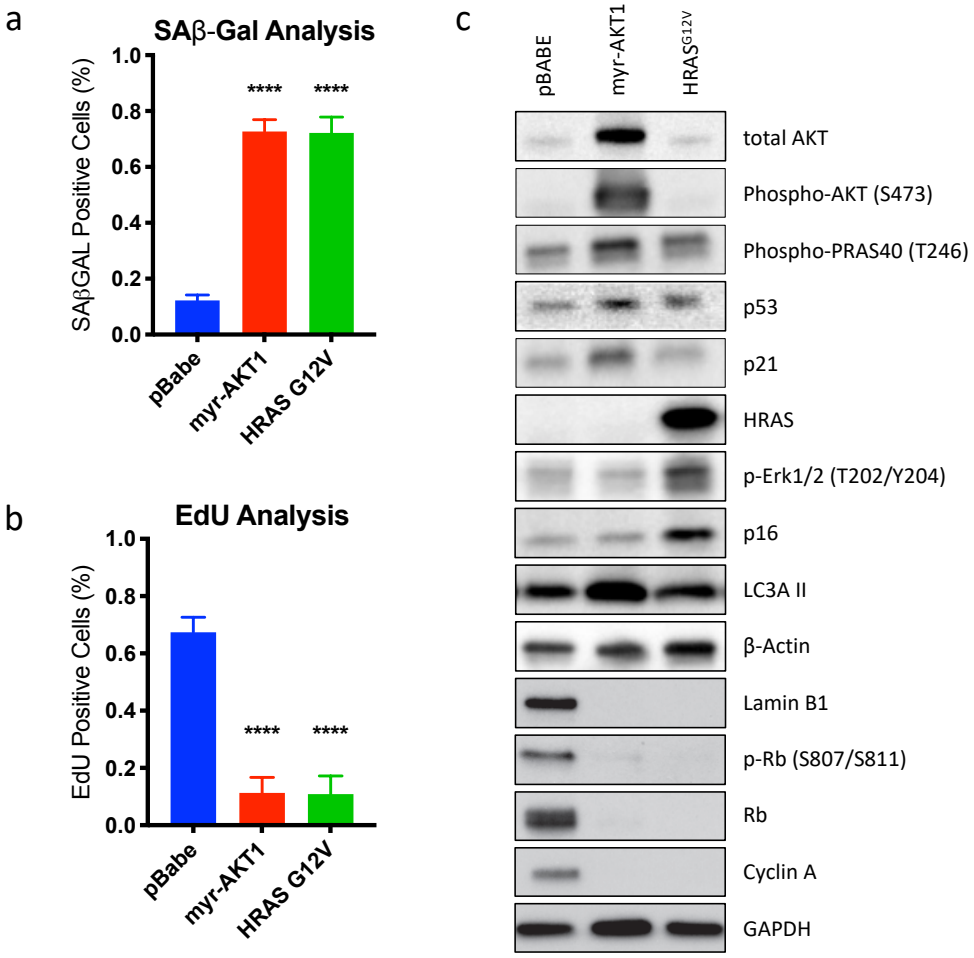


Figure 3.1.1 Hyperactivation of AKT and RAS in BJ-T cells developed senescence.

(a-b) BJ-T cells were transduced with pBabe empty vector control, myrAKT1 or $HRAS^{G12V}$ and characterised at day 14 post-transduction by (a) SA-βGal activity, (b) EdU staining and (c) western blotting. Actin and GAPDH were used as the loading controls. Data are expressed as mean ± SEM. n = 3 experiments. *P < 0.05; **P < 0.01; ***P < 0.001 ****P < 0.0001 by one-way ANOVA as compared with normal proliferating cells.

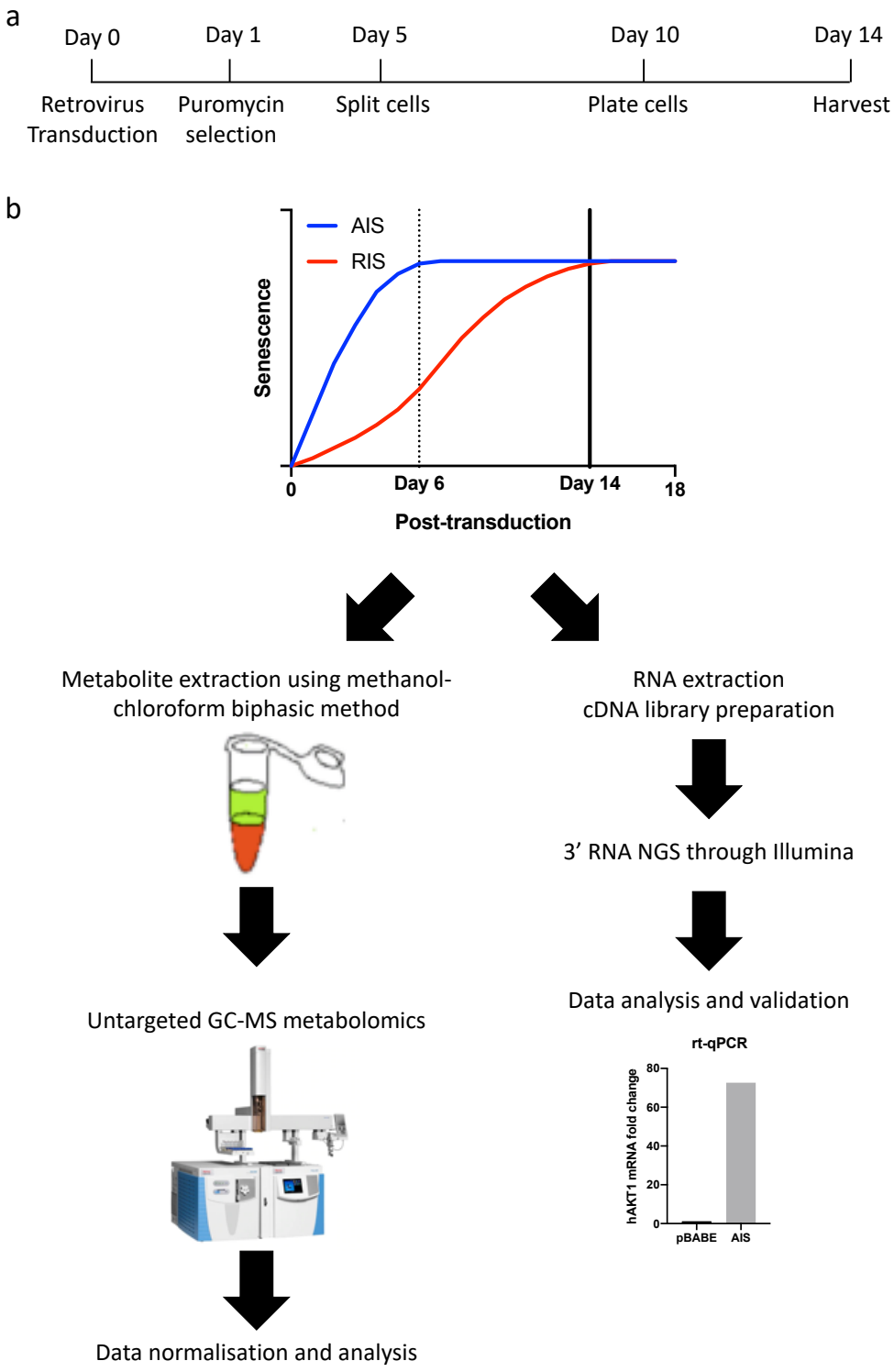


Figure 3.1.2 Schematic diagram of the methodology and timeline for RNA-seq and untargeted GC/MS metabolomics.

(a) BJ-T cells were transduced with either pBABE empty vector, myr-AKT1 or $HRAS^{G12V}$. RNA and metabolites were harvested at the indicated time points. (b) After the cDNA library preparation, 3'RNA-seq was performed. The metabolites extracted using methanol and chloroform biphasic method were analysed by GC/MS. Each individual metabolite was identified based on retention time, and the peak intensity of metabolite was used for comparative analysis after normalisation. n=3 biological replicates for 3' RNA-seq, and 6 biological replicates were used for metabolomics.

3.3.2 Transcriptomic analysis identified the key molecular signatures of AIS

To identify the molecular signatures required for AIS establishment, we investigated the optimal time points for when (1) a robust induction of senescence could be observed and (2) both AIS and RIS exhibited senescence at a comparable extent. We chose day 6 post-transduction of myr-AKT1 as the time point to perform an RNA-seq analysis in AIS cells, when senescence was robustly established as shown in our previous study [34]. The samples were harvested by Dr Keefe Chan in our lab and sent for a paired-end RNA-seq. In contrast, the establishment of RIS occurs at a later stage following a hyperproliferation phase [34]. We therefore measured the transcriptomic changes in RIS on Day 14 post-transduction when RIS firmly established (Fig. 3.1.1a-b). We utilised adjusted p-value < 0.05 and absolute Log_2 Fold Change > 0.5 as the cut-offs to identify the differentially regulated genes (Fig. 3.2a). 1653 up-regulated and 1899 down-regulated genes were identified on Day 6 for AIS, and 1248 up-regulated and 1647 down-regulated genes on Day 14 for RIS. There were 287 up-regulated and 454 down-regulated genes shared by AIS and RIS (Fig. 3.2b). In addition, the volcano plot generated based on Log_2 Fold change versus $-log_{10}$ p-value from the differential expression analysis demonstrated the significantly up- or down-regulated genes and highlighted the top ten altered genes during AIS (Fig. 3.2c) and RIS (Fig. 3.2d).

To identify the significant pathways altered during AIS and RIS, we performed Gene Set Enrichment Analysis (GSEA) using the molecular signature database (MSigDB) hallmark gene sets. The gene sets with normalised p-value < 0.05 were considered as significantly regulated, and were ranked based on normalised enrichment score (NES). Overall, 22 pathways were significantly up-regulated and 8 pathways were significantly down-regulated during AIS (Fig. 3.2e). AIS and RIS shared 9 up-regulated molecular signatures including KRAS signalling, inflammatory response, TNF-alpha signalling via NF-kB, unfolded protein response, coagulation, oxidative phosphorylation, mTORC1 signalling, complement and hypoxia. Furthermore, the down-regulation of early and late estrogen response were identified in both types of OIS.

In addition to the shared signatures, we also identified the specific genetic alterations in each type of OIS. Consistent with the previous findings that AIS is p53/p21-dependent [34], the p53 pathway was identified as the most significantly enriched gene set and was

not detected in RIS. Furthermore, the up-regulation of IFN-alpha, TNF-alpha, inflammatory response, IFN-gamma and protein secretion during AIS was consistent with a SASP. Conversely, downregulation of the genes targeted by E2F and involved in G2M checkpoint in AIS cells indicated the exit of the cell cycle. In contrast, 16 pathways were identified being up-regulated during RIS and 11 pathways were down-regulated (Fig. 3.2f). While genes targeted by Myc were identified as most significantly enriched, RAS signalling was one of the top up-regulated gene sets in RIS consistent with the oncogenic hyperactivation induced by $HRAS^{G12V}$. Similar to AIS, GSEA indicated the presence of SASP in RIS cells by showing the upregulation of inflammatory response, IL-2/STAT5, TNA-alpha and IL-6/JAK/STAT signalling pathways. In addition, the DNA repair pathway was significantly up-regulated during RIS, consistent with the RIS-specific DNA damage response resulting from replication stress during the hyper-proliferation phase. Interestingly, different from AIS showing upregulation of the IFN-alpha signature, this signature was downregulated during RIS, suggesting the distinct SASP secretion profile by RIS and AIS. Overall, significant transcriptional changes are associated with OIS in non-transformed cells. The common gene signatures shared by both AIS and RIS represent the senescence hallmarks and the molecular signatures that are unique for AIS or RIS and are associated with the distinct molecular mechanisms underpinning each type of OIS.

a

	Up	Flat	Down
Day 6 AIS	1653	25091	1899
Day 14 AIS	180	23481	128
Day 14 RIS	1248	20894	1647

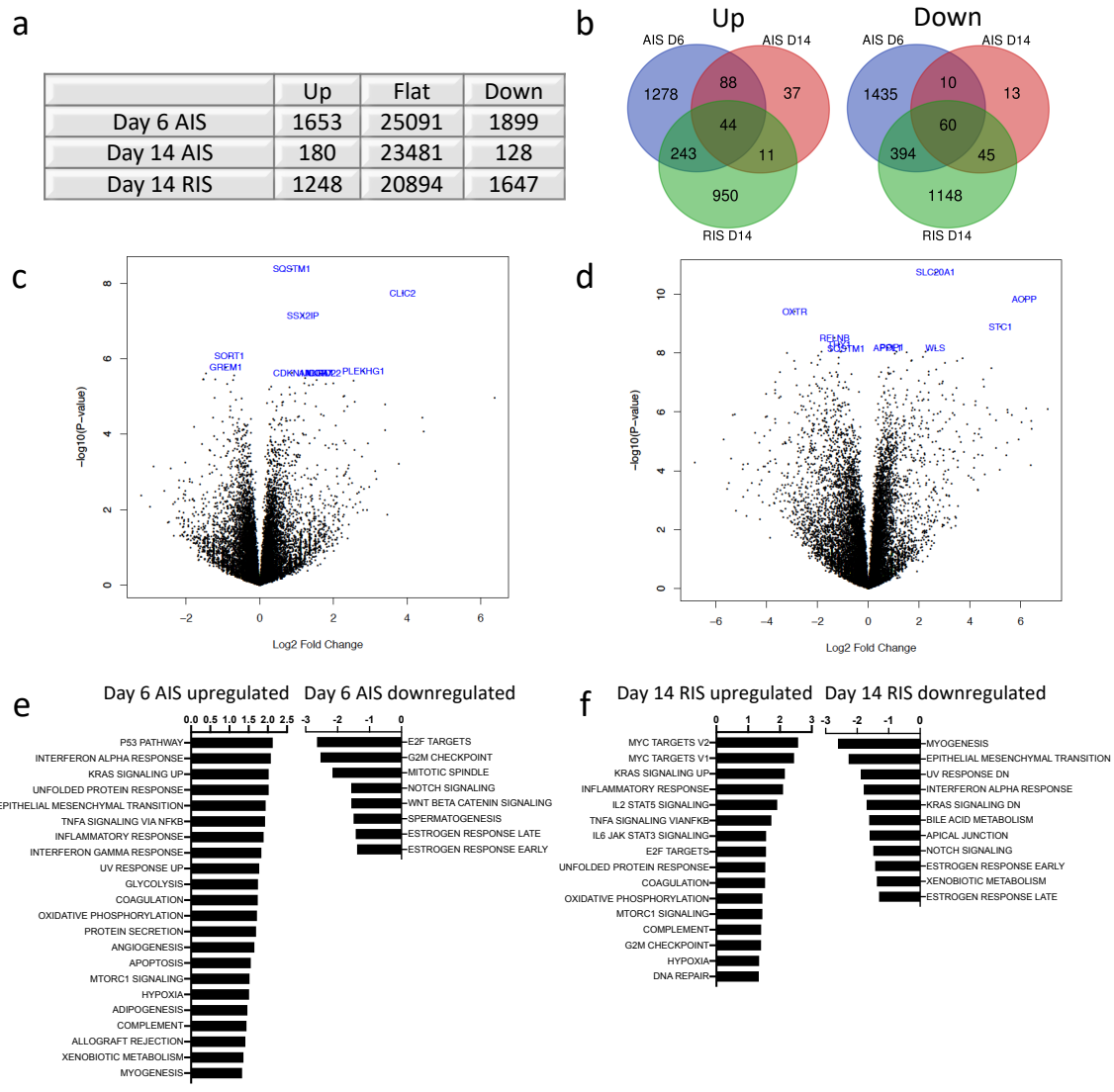


Figure 3.2 The transcriptomic profiling identify molecular signatures of AIS and RIS establishment.

Analysis of RNAseq data of AKT-induced senescence (AIS) or RAS-induced senescence (RIS) vs proliferating cells showing the differentially expressed genes in Day 6 AIS, Day 14 AIS and Day 14 RIS. (a) Significantly up or down-regulated genes based on adjusted p-value < 0.05 and absolute $\log_2$Fold Change > 0.5. (b) Venn diagram Volcano plots of (c) Day 6 AIS and (d) Day 14 RIS. (e-f) Gene set enrichment analysis using the Molecular Signature database hallmark gene sets showing normalized enrichment score (NES) for significantly upregulated and downregulated gene sets on (e) Day 6 AIS and (f) Day 14 RIS compared to proliferating cells. cDNA library preparation and RNA sequencing were performed with assistance of by the Molecular Genomics Core Facility (PMCC, Australia). RNA samples were prepared and validated by me. Bioinformatics analysis was performed with the assistance of Dr. Anna Trigos and Dr. Maria Doyle (PMCC, Australia).

3.3.3 The dynamic transcriptomic changes during AIS

While the senescence phenotype is stably maintained in AIS cells, whether the molecular signatures in AIS are sustained during the transition from initiation to maintenance is still unknown. We therefore compared the transcriptomic profile of AIS cells at day 6 and day 14 to compare the transcriptional re-wiring during AIS and gain more insight into the molecular requirements for AIS maintenance. D6 or D14 AIS cells were compared with D6 or D14 proliferating controls respectively. Strikingly, only 180 up-regulated and 128 down-regulated genes were identified in Day 14 AIS cells (Fig. 3.3), compared to 1653 up-regulated and 1248 downregulated genes identified in Day 6 AIS cells (Fig. 3.2a). Among the significantly altered genes in Day 14 AIS cells, 73% (132/180) of up-regulated genes and 55% (70/128) of down-regulated genes overlapped with Day 6 AIS (Fig. 3.2b). The results suggest that transcriptional regulation occurs early during senescence induction driven by AKT hyperactivation and less than 10% of alterations are required for senescence maintenance.

Comparing the significantly regulated gene sets identified by GSEA on day 14 AIS with those on day 6 AIS provided more insight into the transcriptional regulation of AIS establishment and maintenance. Within the down-regulated gene sets, G2M checkpoint, E2F target and mitotic spindle were shown in both day 6 and day 14 AIS cells, indicating the persistent cell cycle arrest during AIS while within the up-regulated gene sets, 12 gene sets were shown in both Day 6 (Fig. 3.2e) and Day 14 AIS (Fig. 3.3), such as p53 pathway, mTORC1 signalling, unfolded protein response and glycolysis, suggesting they are required for both AIS initiation and maintenance. In contrast, downregulation of gene sets involved in NOTCH, WNT/beta-Catenin, and estrogen response and upregulation of gene sets involved in OXPHOS, protein secretion and hypoxia were uniquely exhibited in day 6 AIS cells but not in day 14 AIS cells, indicating alterations in these molecular pathways or biological processes are specifically required for senescence induction.

Overall, the comparison of gene signatures of AIS at the early- and late stage revealed the transcriptional alterations from AIS initiation to maintenance. In general, the global transcriptional profile is rapidly and extensively changed at the time of AIS onset. Once the senescence program establishes, the transcriptional changes gradually diminish via

complex regulatory mechanisms or feedback loops. Meanwhile, post-transcriptional regulation may be the major mechanism responsible for maintaining the senescence program, which could be investigated through tandem mass spectrometry [296].

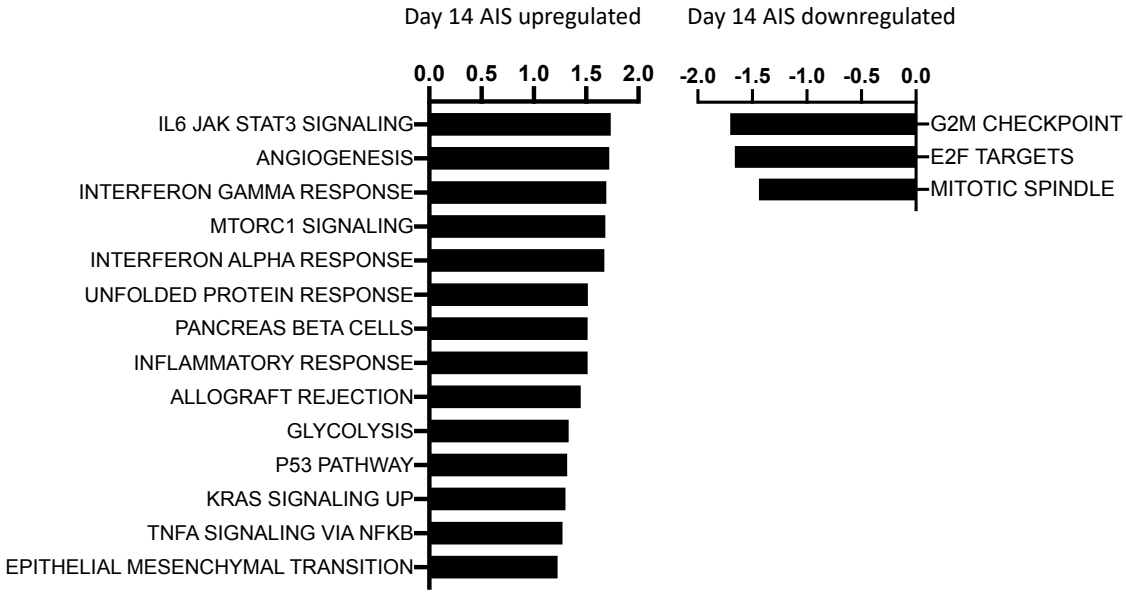


Figure 3.3 The transcriptomic profiling identifies molecular signatures of AIS maintenance.

Gene set enrichment analysis using Molecular signature database hallmark gene sets showing normalized enrichment score (NES) for significantly upregulated and downregulated gene sets on Day 14 AIS compared to proliferating cells.

3.3.4 Metabolic reprogramming during OIS

The transcriptomic profiling data revealed that the upregulated metabolic processes, such as glycolysis and OXPHOS, were enriched in both AIS and RIS cells and sustained from AIS initiation to maintenance, which provided strong support for the critical role of metabolic alterations in OIS (reviewed in Chapter 1.2.1). To characterize the metabolic reprogramming in AIS we use metabolomics analysis to assess the global metabolic profile of AIS compared with that of RIS and normal proliferating cells. Considering that it is more possible to detect significant metabolic changes at a relatively later time point to assess the metabolic alterations required for AIS maintenance, we performed the metabolomic analysis at day 14 post-transduction (Fig. 3.1.2). The metabolites from BJ-T human skin fibroblasts overexpressing either myr-AKT1 (AIS), $HRAS^{G12V}$ (RIS) or pBABE control (proliferating) cells were extracted for GC/MS-based untargeted metabolomic analysis (Methods described in Chapter 2.14.1). The heatmap and hierarchical clustering of the metabolome separated AIS and RIS cells from normal proliferating cells, indicating substantial metabolic rewiring driven by oncogenic activation, consistent with our transcriptome analysis. However, AIS and RIS cells clustered together suggesting similar metabolic profiles in AIS and RIS (Fig. 3.4.1a), consistent with the principal component analysis (PCA) (Fig. 3.4.1b).

To further interrogate the specific metabolic alterations associated with OIS, we analysed the change of each metabolite in AIS or RIS cells comparing with pBABE control cells. 25 significantly regulated metabolites were identified in AIS cells (Table 3.1) and 35 metabolites in RIS cells (Table 3.2) with p-value < 0.05 and absolute Log_2 Fold Change > 0.5 as the cut-off values. These metabolites were analysed by metabolite set enrichment analysis (MSEA) using the Small Molecule Pathway Database (SMPDB) through MetaboAnalyst [290]. The metabolic pathways with FDR < 0.05 were considered as significantly regulated (Table 3.3 and 3.4). Overall, similar metabolic pathways were enriched in both AIS and RIS cells (Fig. 3.4.1c and Fig. 3.4.1d) with the Warburg effect ranked as the top metabolic signature in both AIS and RIS.

The Warburg effect is associated with intracellular energy synthesis and involved in the changes of glucose and glutamine metabolism, tricarboxylic acid (TCA) cycle and oxidative phosphorylation [297] [298]. To analyse how energy production was

perturbed in AIS and RIS, the key metabolic and genetic alterations identified from the metabolomic and transcriptomic analysis, respectively, were annotated in a metabolic map illustrating glycolysis, glutamine metabolism and tricarboxylic acid (TCA) cycle. The significant changes on the metabolites and genes from AIS (Fig. 3.4.2a) or RIS (Fig. 3.4.2b) compared to pBABE (adjusted p-value < 0.05, absolute $Log_2FC > 0.5$) were highlighted in red arrows. The metabolomic data indicated the up-regulation of TCA cycle function during both AIS and RIS, evidenced by five significantly elevated mitochondria-related metabolites (citrate, α-ketoglutarate, fumarate, malate, glutamine and glutamate). Surprisingly, the gene expression analysis did not identify the expression levels of enzymes involved in TCA cycle were significantly changed. This may be due to limitations in the sensitivity and analysis of the transcriptomic data. Nevertheless, it also suggested that the post-transcriptional mechanisms are potentially involved in regulation of the TCA cycle hyperactivation, which is consistent with the previous findings in cancer cells showing both post-transcriptional and post-translational modifications (PTMs) orchestrate the tightly controlled regulation of metabolic adaptations [299]. Besides the TCA cycle, several key metabolites in glycolysis and glutamine metabolism were also elevated in both AIS and RIS cells, including glyceraldehyde 3-phosphate (G3P), glutamine, and glutamate. The transcriptomic analysis uncovered the expression of glycolysis related genes including hexokinase 2 (HK2), alpha-enolase (ENO1) and Solute Carrier Family 16 Member 1 (SLC16A1) were upregulated in RIS cells whereas no glutamine metabolism-related genes was found differently regulated. In contrast, the AIS cells showed increased expression of Isocitrate dehydrogenase 1 (IDH1) but no change in expression of glycolysis-related genes. These results suggested that the similar metabolic phenotype in AIS and RIS may be achieved through distinct transcriptional regulation. It is noted that while the down-regulation of gene expression in the Pentose Phosphate Pathway (PPP) was specifically observed in RIS cells, no significant changes in the levels of PPP metabolites were observed. It is possible that the sensitivity of the GC-MS is insufficient to detect functional changes in metabolite levels. The potential alteration in PPP activity is consistent with previous findings showing that insufficient activities of PPP and nucleotide synthesis [260] [300] [26] [262] result in dNTP deficiency and subsequently triggers DNA damage in RIS [262] [301]. The integration of transcriptomic and metabolomic data analyses thus provided important insight into the

metabolic reprogramming during OIS and demonstrated AIS and RIS cells exhibited a hyperactive metabolic phenotype with increased glycolysis and glutamine metabolism together with an enhanced TCA cycle. Further experiments are required to dissect the molecular mechanisms underpinning metabolic rewiring that are likely to be mediated by both transcriptional and post-transcriptional regulation.

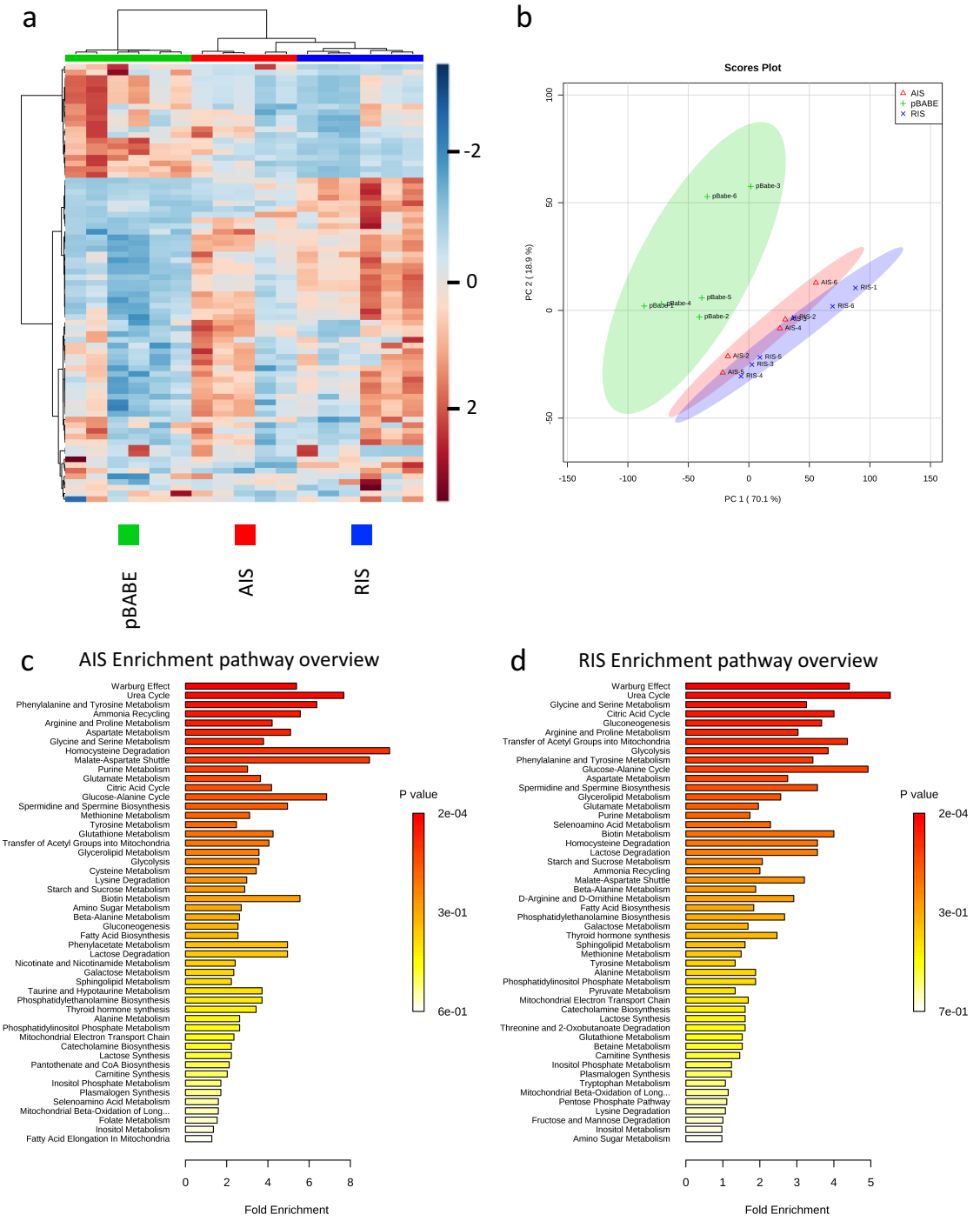


Figure 3.4.1 Metabolic profiling identifies metabolic reprogramming in AIS and RIS.

Through global untargeted GC/MS metabolomics, the peak intensity of all metabolites identified was analysed by MetaboAnalyst 4.0 after a median normalisation. (a) Heatmap and hierarchical clustering of the top 50 significant metabolites based on adjusted p-value in the proliferating (pBabe), AIS or RIS cells. (b) The principal component analysis. The metabolites significantly regulated in AIS or RIS compared with pBABE proliferating control were selected for Metabolite Set Enrichment Analysis (MSEA) based on BH-adjusted p-value < 0.05 and absolute $\log_2$Fold Change > 0.5. (c) AIS and (d) RIS enrichment pathway overview. Note: The sample AIS-1 was excluded due to a technical issue in sample processing independent of sample quality. Metabolite preparation and GC/MS were performed with assistance of Metabolomics

Australia. Metabolite samples were prepared and validated by me. Data analysis was performed with the assistance of Dr. David de Souza from Metabolomics Australia.

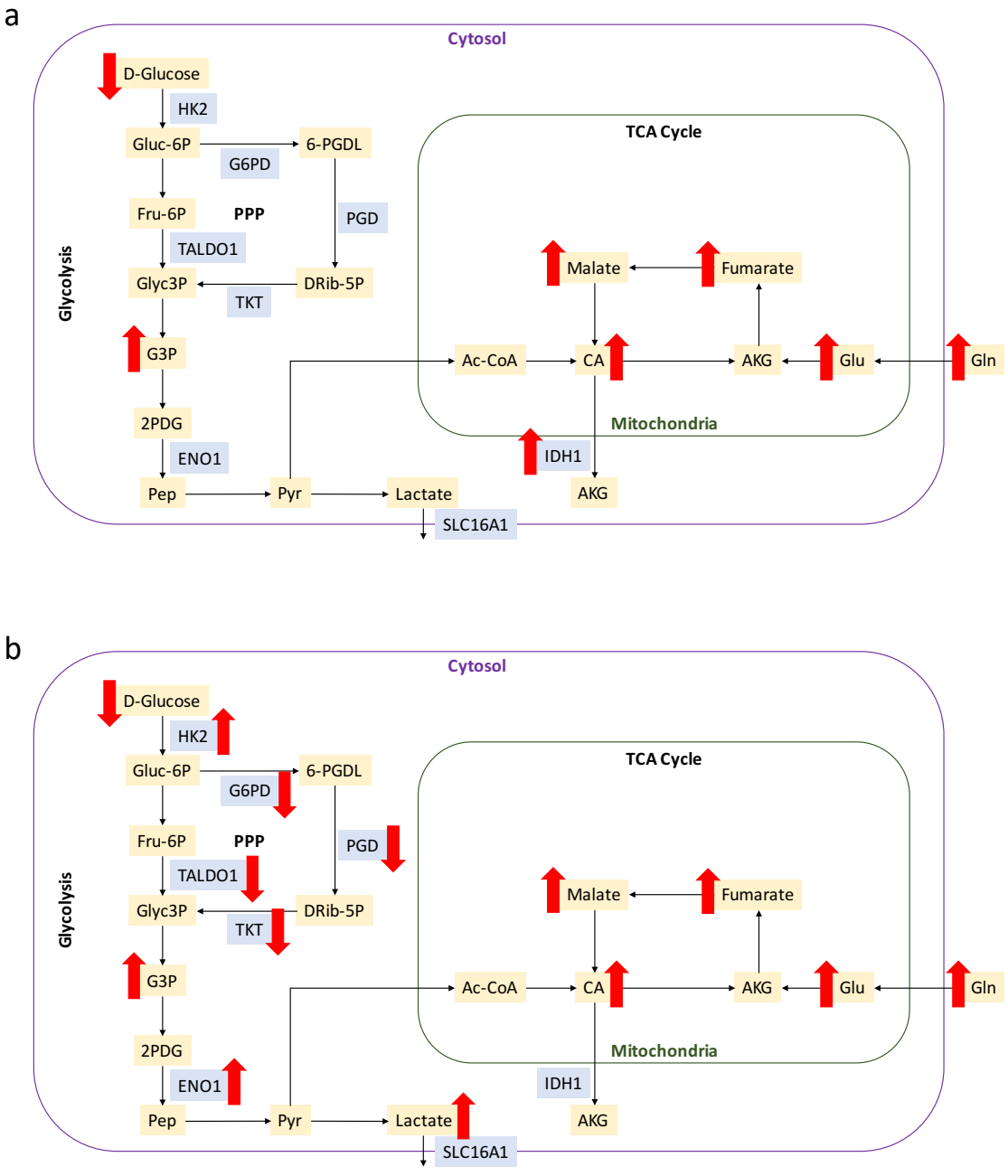


Figure 3.4.2 Transcriptional and metabolic alterations in energetic biosynthesis during AIS and RIS.

The significantly regulated genes and metabolites in (a) Day 6 AIS and (b) Day 14 RIS comparing to the proliferating control were identified based on adjusted p-value<0.05, absolute Log_2FC > 0.5 and highlighted in the map illustrating energy production through glycolysis, glutamine metabolism and TCA cycle. Yellow and blue boxes represent metabolites and genes, respectively. Red arrows indicate statistically significant up- or down-regulation.

3.3.5 Mitochondrial hyperactivation and oxidative stress in AIS cells

Mitochondrial dysfunction occurs during senescence (reviewed in Chapter 1.2.1). The transcriptomic analysis of AIS and RIS cells identified an upregulated oxidative phosphorylation gene signature and the metabolomic analysis revealed activated TCA cycle in both AIS and RIS, suggesting enhanced mitochondrial activity during OIS. To assess the status of mitochondrial respiration and ATP biosynthesis in OIS, we performed a Seahorse XF mitochondrial stress test to directly evaluate the oxidative phosphorylation and glycolysis in AIS and RIS cells at day 14 post-transduction (Fig. 3.5a).

Overall, both AIS and RIS cells exhibited significantly elevated mitochondrial respiration (Fig. 3.5b). The basal oxygen consumption rate (OCR) was dramatically upregulated in AIS and RIS cells, together with significantly increased ATP production (Fig. 3.5c-d). Moreover, proton leakage was measured upon the treatment of oligomycin which suppresses the ATP-linked mitochondrial respiration. The increased proton leak in AIS and RIS suggested OXPHOS through ETC reaction was enhanced during OIS (Fig. 3.5e). The full mitochondrial respiration potential was then stimulated by the disruption of the inner membrane gradient through the treatment of carbonyl cyanide-p-trifluoromethoxyphenyl-hydrazon (FCCP). Similarly, the maximal respiratory capacity indicated by maximal OCR was significantly elevated in both AIS and RIS cells (Fig. 3.5f). Lastly, mitochondrial respiration can be completely shut down by adding the inhibitor of Complex III, Antimycin. The oxygen consumed after adding antimycin A is independent of mitochondrial activity, thus termed non-mitochondrial OCR. The non-mitochondrial OCR and reserve capacity in AIS and RIS cells were also significantly increased (Fig. 3.5g-h). These results further emphasise the mitochondrial hyperactivity that characterises OIS cells. Despite mitochondrial respiration and energetic biosynthesis being elevated in both AIS and RIS cells at day 14 post-transduction, RIS cells exhibited significantly elevated mitochondrial function, evidenced by higher basal OCR, ATP production, proton leak and maximal respiration than AIS cells. However, further investigation is required to assess the biological relevance of the differences in mitochondrial function between cells undergoing AIS and RIS. Furthermore, we analysed the extracellular acidification rate (ECAR) to measure glycolysis and lactate production

(Fig. 3.5i). The significantly upregulated ECAR suggested enhanced glycolysis and lactate production in both AIS and RIS cells.

As mitochondria are the major intracellular sources of ROS production and mitochondrial dysfunction can disrupt mitochondrial redox homeostasis [9], we therefore measured the mitochondrial superoxide level using MitoSOX and cytosolic ROS level using DCFH-DA by flow cytometric analysis. We demonstrated the elevated cytosolic and mitochondrial ROS levels in AIS cells (Fig. 3.5j-k). ROS accumulation results in oxidative stress which causes macromolecular damages including proteins, DNA and lipids [302] and contributes to AIS maintenance. In Chapter 4, we will further investigate the impact of the changes in ROS in AIS.

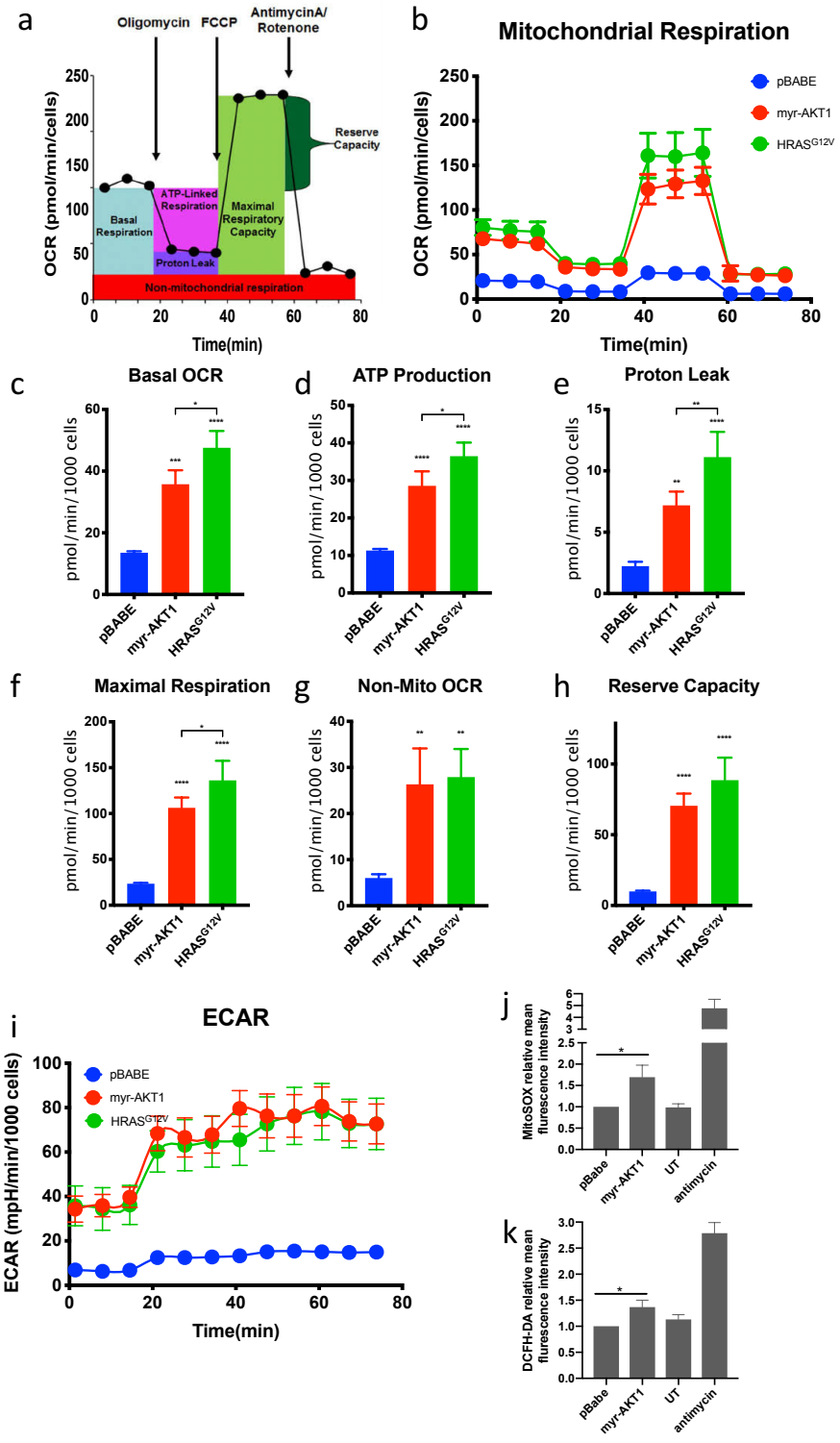


Figure 3.5 mitochondrial activity and reactive oxygen species accumulation in AIS and RIS cells.

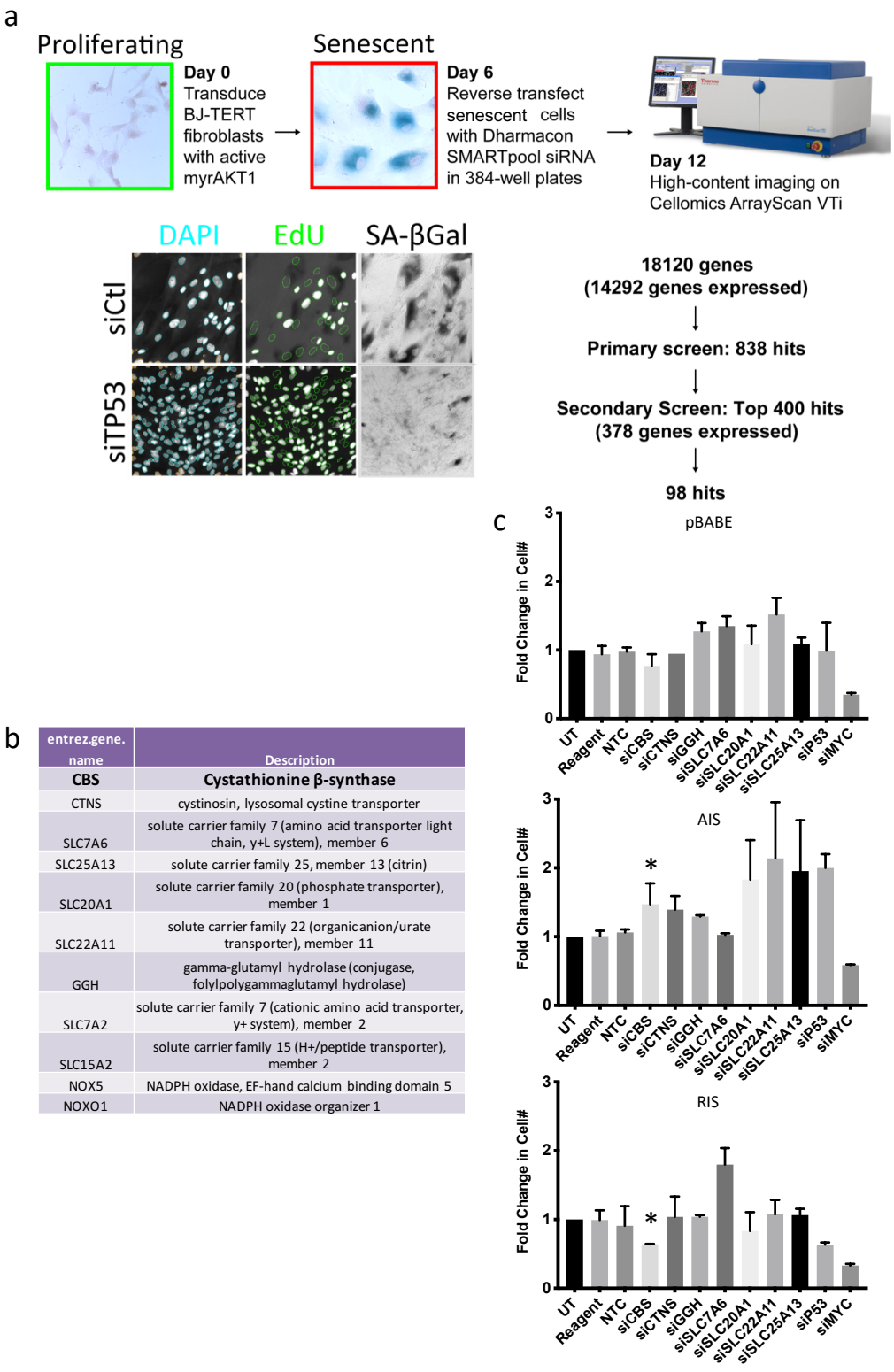
(a) The mitochondrial activity of the proliferating (pBabe), AIS and RIS cells at 14 days post-transduction were assessed by the seahorse XF mitochondrial stress test. (b) The mitochondrial respiration was assessed by oxygen consumption rate (OCR). (c) basal OCR, (d) ATP production, (e) Proton Leak, (f) Maximal respiration, (g) non-mitochondrial OCR and (h) Reserve capacity. (i) Extracellular acidification rate. (j) Mitochondrial superoxide production using MitoSOX and (k) cytosolic ROS by DCFH-DA by flow cytometric analysis. Data are expressed as mean ± SEM. n = 3 experiments. *P < 0.05; **P < 0.01; ***P < 0.001 ****P < 0.0001 by one-way ANOVA as compared with normal proliferating cells.

3.3.6 A genome-wide RNAi screen identifies novel mediators of AIS

To provide further mechanistic insight into the regulation of AIS, Dr Keefe Chan in our group performed a genome-wide RNAi screen (Fig. 3.6a) to determine the essential regulators of AIS [118]. Briefly, BJ-T cells were transduced with myrAKT1 to induce senescence and AIS cells at day 6 were reverse transfected with the siGENOME® SMARTpool library to individually knockdown 18,120 genes. At day 12 post-transduction (6 days post-siRNA transfection), the senescence-associated markers including SA-βGal, EdU incorporation and cell number were examined using high-throughput imaging [118]. The primary screen identified 838 hits and the top 400 hits proceeded to the secondary screen. 98 genes were identified as AIS regulators from the secondary screen. Further testing on the specificity of hits for AIS vs. RIS may have implications for manipulating senescence in different oncogenic contexts. We demonstrated that NF-κB signalling regulated SASP in both AIS and RIS cells. More importantly, we identified neurofibromin 1 (NF1) as a specific AIS mediator. Our study reveals the key mechanisms of tumour suppression by AIS and provides the opportunities to identify putative AIS regulators which can be harnessed for pro-senescence therapy for PI3K/AKT/mTORC1-driven cancers [121].

To better understand the specific metabolic alterations that are important for the maintenance of AIS, we further analysed data of this RNAi screen. Strikingly, within 98 genes identified from the secondary screen, 11 hits (10%) were associated with cellular metabolism (Fig. 3.6b). Cell proliferation assays were performed to validate nine metabolism-associated genes (Fig. 3.6c). Knockdown of p53, a known AIS regulator, significantly increased AIS cell proliferation but not RIS or the proliferating cell control. In contrast, loss of myc, a growth promoting gene, significantly impaired the proliferation of all cell types. Interestingly, knockdown of CBS gene expression increased cell number of AIS cells but decreased cell number of RIS cells, suggesting it may play a distinct regulatory role during AIS and RIS. CBS converts homocysteine (Hcy), a key metabolite in the transmethylation pathway, to cystathionine which is subsequently hydrolysed by cystathionine gamma-lyase (CTH) to form cysteine, the crucial precursor for glutathione (GSH) production. CBS also catalyses the production of H_2S which modulates mitochondrial functions and cellular bioenergetics in a concentration-

dependent manner (reviewed in Chapter 1.3). Therefore, CBS acts as a hub for coordinating the transsulfuration and transmethylation pathways. Given that AIS is associated with metabolic changes and CBS is a key metabolic hit in the screen, we therefore focused on testing the hypothesis that CBS is responsible for these metabolic changes in chapter 4.



entrez.gene. name	Description
CBS	**Cystathionine β-synthase**
CTNS	cystinosin, lysosomal cystine transporter
SLC7A6	solute carrier family 7 (amino acid transporter light chain, y+L system), member 6
SLC25A13	solute carrier family 25, member 13 (citrin)
SLC20A1	solute carrier family 20 (phosphate transporter), member 1
SLC22A11	solute carrier family 22 (organic anion/urate transporter), member 11
GGH	gamma-glutamyl hydrolase (conjugase, folylpolygammaglutamyl hydrolase)
SLC7A2	solute carrier family 7 (cationic amino acid transporter, y+ system), member 2
SLC15A2	solute carrier family 15 (H+/peptide transporter), member 2
NOX5	NADPH oxidase, EF-hand calcium binding domain 5
NOXO1	NADPH oxidase organizer 1

Figure 3.6 A high-throughput genome-wide RNAi screen identifies essential regulators of AIS.

(a) Schematic diagram showing the workflow for the Genome-wide RNAi screen. BJ-T fibroblasts were transduced with myr-AKT1 and reverse transfected with SMARTpool siRNAs at day 6. Cell number, EdU and SA-βGal were utilised to assess senescence. (b) Gene candidates identified through the screen that are associated with cellular metabolism. (c) BJ-T fibroblasts were transduced with pBabe, myr-AKT1 and $HRAS^{G12V}$ and reverse transfected with siRNAs on day 6 and cell number was measured by IncuCyte after

PI staining on day 12. Data are expressed as mean ± SEM. n = 3 experiments. *P < 0.05 by student's t-test as compared with NTC control cells. Genome-wide RNAi screen and data analysis were performed by Dr. Keefe Chan.

3.4 Discussion

While aberrant activation of PI3K/AKT/mTORC1 signalling drives tumour formation and progression, hyperactivation of this signalling pathway in non-transformed cells results in cellular senescence, which is a potent tumour-suppressive mechanism that must be overcome for tumour initiation and progression. Understanding the molecular mechanisms underpinning AIS cells and how they are subverted in cancer will provide opportunities to identify therapeutic strategies for targeting PI3K/AKT/mTORC1-driven cancers. In this chapter, we delineated the molecular landscape of AIS by characterising the transcriptome and metabolome to provide mechanistic insights into AIS establishment and maintenance. We demonstrated that (1) compared to normal proliferating cells, AIS and RIS cells exhibited distinct transcriptomes and metabolomes, supporting the concept that transcriptional and metabolic reprogramming is a key feature of OIS. (2) The common molecular signatures in both AIS and RIS cells represent the hallmarks of senescence and the molecular signatures that are unique for AIS or RIS are associated with the distinct molecular mechanisms underpinning these two types of OIS. The early and late molecular response to AKT hyperactivation revealed the dynamic changes of the transcriptome during AIS initiation and maintenance. (3) Despite some differences in the intricate mechanisms of AIS and RIS, it is clear that OIS is characterised by a highly active metabolic status with enhanced glycolysis, TCA cycle and oxidative phosphorylation to maximize energy production.

3.4.1 The hallmarks of senescence shared by AIS and RIS

The GSEA identified the key senescence hallmarks including cell cycle arrest, SASP and elevated glycolysis and oxidative phosphorylation in both AIS and RIS (Fig. 3.7). Along with these well-established senescence hallmarks, our data also revealed several molecular signatures presented by both types of OIS.

(1) GSEA data showed that unfolded protein response (UPR) was significantly enhanced in both RIS and AIS. The data for RIS is consistent with the previous findings by other groups that UPR was a component of senescence induced by various stresses including RAS hyperactivation [303]. In contrast, the role of PI3K/AKT signalling in regulating the UPR and endoplasmic reticulum (ER) stress

response is controversial. AKT signalling has been reported to play a critical role in cell survival by protecting from ER stress-induced cell death signalling [304]. However, a study from the Colman-Lerner lab reported one of the essential UPR and ER stress transducers, PKR-like ER kinase (PERK) was an AKT substrate and AKT-mediated activation of PERK/eIF2α was detected in certain conditions, such as hypoxia[305]. Recently, hyperactivation of SASP in chemotherapy-induced senescent cells was reported to be associated with proteotoxic stress and contributed to the activation of the endoplasmic reticulum stress-UPR-autophagy cascade [306]. Consistent with this finding, our gene set enrichment analysis implicated UPR as a key component for AIS establishment. Moreover, consistent with degradation of ER-associated misfolded proteins through increased autophagy in AIS, expression of the microtubule-associated protein light chain 3 (LC3) that is correlated with the number of autophagosomes [307], was strongly induced in AIS cells, suggesting increased autophagy associated with PI3K/AKT/mTOCR1-driven senescence (Fig 3.1.1c). Further evaluation using immunofluorescence staining of LC3 will be required to confirm the change in autophagy. High levels of protein synthesis and secretion in senescent cells have been thought to overwhelm the cellular capacity of protein processing and transport, leading to high proteotoxic stress and autophagy. We therefore hypothesise that targeting autophagy may enhance proteotoxic stress and lead to ER-related death in AIS cells, a hypothesis that could be further tested by depleting the critical protein in the formation of autophagosome Beclin-1 [308].

(2) GSEA identified a significantly upregulated hypoxia response in both types of OIS. Interestingly, several groups have demonstrated that activation of hypoxia signalling in RIS cells and further activation leads to senescence escape and contributes to tumourigenesis [309] [310] [311] [312]. Conversely, the knockdown of Hypoxia Inducible Factor-1α (HIF-1α) expression in RIS fibroblasts induced apoptotic cells death [313]. Activation of hypoxia signalling has been considered as a response to oxidative stress. Consistently, the metabolomic analysis and the Seahorse mitochondrial function assay demonstrated mitochondrial hyperactivation in OIS cells and consequently ROS production.

This oxidative stress induces oxidative damages to DNA, proteins and lipids, resulting in the proliferative arrest. We thus hypothesise that activation of hypoxia signalling in OIS cell may protect from oxidative stress-induced cell death and prime oncogene-activated cells for senescence escape and tumourigenesis. In chapter 4 we explore how AIS cells maintain intracellular redox balance to facilitate cell survival.

(3) Suppression of NOTCH signalling was observed in both types of OIS. The NOTCH signalling has a key role in cell differentiation and stem cell state [314], and has been linked to tumourigenesis through either oncogenic or tumour-suppressive functionality [315]. Activation of NOTCH signalling in RIS cells suppressed Senescence Associated Heterochromatic Foci and increased chromatin accessibility [81]. Interestingly, NOTCH signalling can induce a type of senescence, NOTCH-induced senescence (NIS) where cells have distinct secretome from RIS cells [316]. Recently, NOTCH signalling was reported to induce NIS in adjacent cells (secondary senescence) [81] [317]. However, our transcriptomic analysis suggested the suppression of NOTCH signalling in both AIS and RIS cells. To determine its role in OIS establishment, we will need to investigate whether activation of NOTCH signalling in OIS cells delays senescence and causes SASP or chromatin structural or other phenotypic changes.

The GSEA also identified several signalling pathways related to the inflammatory responses being up-regulated in both AIS and RIS, strongly supporting the induction of the SASP as a hallmark of OIS. However, AIS and RIS appear to have distinct SASP profiles, where the up-regulation of IFN-gamma response is AIS-specific and the increases of IL-2 and IL-6 downstream signalling are RIS-specific. Moreover, the IFN-alpha response was stimulated during AIS but suppressed during RIS, consistent with the study indicating p38 activation in RIS cells negatively regulates interferon signalling [47]. These findings suggested that the senescence phenotypes vary depend on the oncogenic stimulus. Further characterization of SASP profile by cytokine array or mass spectrometry will reveal the distinct secretory profiles driven by AKT and RAS. The SASP is a key non-autonomous feature of senescence and senescent cells interact with the microenvironment via SASP (reviewed in Chapter 1.1.2). The SASP either plays a

protective role by promoting immune surveillance or promotes inflammation and tumourigenesis. Whether the distinct secretory factors from AIS and RIS affect the senescence-associated immune response and subsequently impact oncogene-driven tumourigenesis remains to be determined and will be an important focus of ongoing studies.

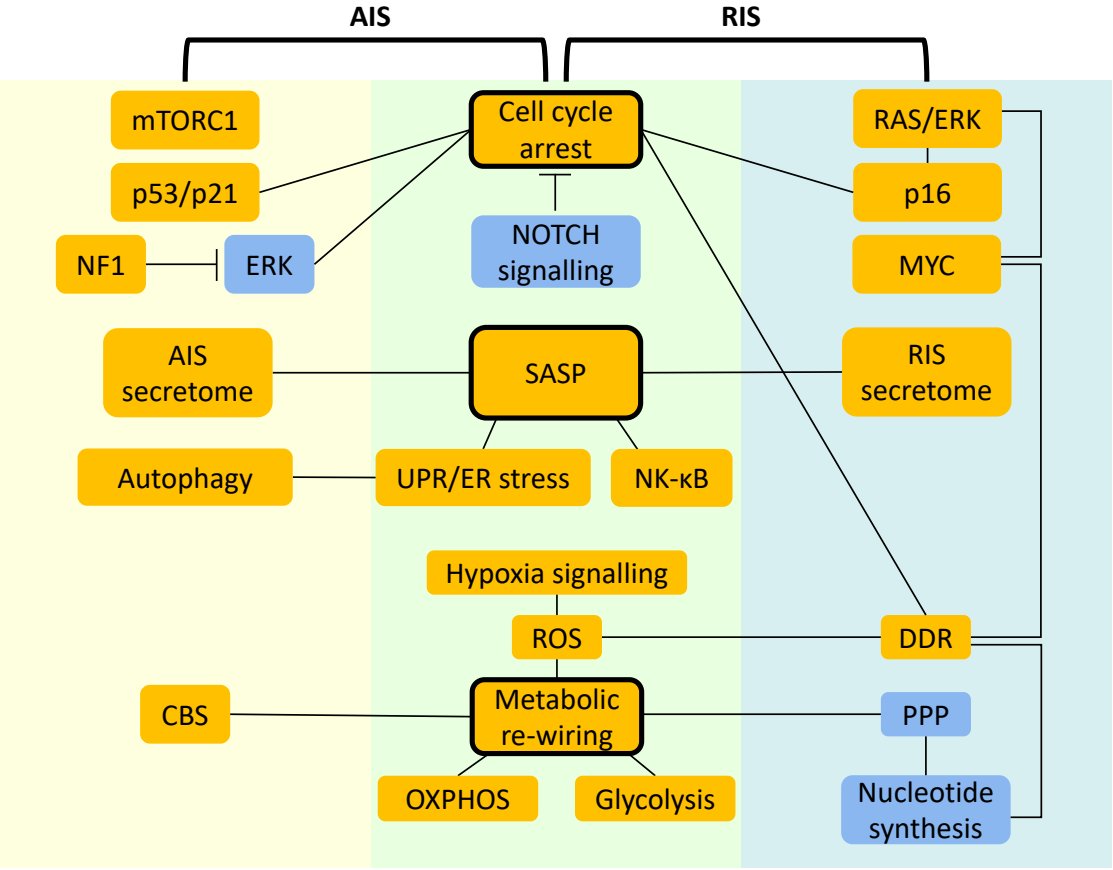


Figure 3.7 Common and unique features of AIS and RIS.

Data analysis of the transcriptional and metabolic profiling, as well as the whole genome RNAi functional screen, identify common and unique features of AIS and RIS. The orange or blue colour indicates up- or down-regulation respectively.

3.4.2 The distinct molecular mechanisms underpinning AIS and RIS

The transcriptomic analysis not only revealed the common signatures shared by AIS and RIS, but also demonstrated the distinct molecular mechanisms underpinning AIS and RIS which are consistent with our previous findings [34] (Fig 3.7). The RNA-seq data confirmed activation of p53 pathway and increase of transcription of p21, a main downstream target of p53, highlighting the dependency of AIS on p53/p21 axis [34]. In contrast, there was an increase of mRNA expression of Cyclin-Dependent Kinase Inhibitor 2A (*CDKN2A*) in RIS cells, consistent with its dependency on p16 activation [318] [319]. As expected, the up-regulation of the DDR gene set was specifically identified during RIS, supporting the DNA damage via hyperproliferation-induced replication stress contributes to RIS [320].

The RNA-seq data also confirmed the activation of oncogenic signalling in OIS cells. GSEA demonstrated upregulation of PI3K/AKT/mTORC1 or RAS pathway in AIS or RIS cells, respectively. Interestingly, we recently uncovered NF-1-mediated suppression of ERK signalling was required for AIS maintenance and depletion of NF-1 restored ERK signalling activity and led to AIS escape but had no effect on RIS, suggesting a specific regulatory role of NF1-ERK signalling in engagement of AIS brake and cooperation of PI3K/AKT/mTORC1 signalling and RAS/ERK signalling can evade this barrier and initiate tumourigenesis [121]. While the antagonism of these two oncogenic pathways was not observed in RIS cells, GSEA suggested specific activation of MYC signalling in RIS cells. It is well known that RAS can activate MYC either though activation of downstream ERK signalling, leading to MYC phosphorylation at Ser 62 [321] or inhibition of glycogen synthase-3 (GSK-3), resulting in MYC phosphorylation at Thr58 [322]. Phosphorylation of MYC subsequently stabilizes MYC protein and increases MYC protein expression [323]. As another classic oncogene, MYC hyperactivation induces apoptosis by stabilization of p53 via induction of Arf [324] or by suppressing anti-apoptotic genes such as BCL2 and $BCLX_L$ [325]. Activation of both MYC and RAS has been shown to induce oncogenic transformation in primary rodent cells by Weinberg and colleagues more than thirty years ago [326]. Later studies found this cooperation was based on blocking MYC-induced apoptosis by RAS and abrogating RAS-induced senescence by MYC, thus overcoming the barriers and paving the way to transformation and tumour initiation

[327]. However, a recent study reported that the cooperativity of RAS and MYC did not occur in human cells and instead, activation of MYC together with RAS in human fibroblasts induced DNA damage [328], in support of our finding of upregulation of MYC signalling in RIS cells. To further define the role of MYC in RIS and transformation, we need to assess the cellular and molecular responses by modulating MYC signalling activity, for example using BET inhibitors [329].

Collectively, our transcriptomic analysis suggested that depending on the oncogenic stimulus by RAS/ERK and PI3K/AKT/mTORC1, senescence can be triggered through distinct and overlapping mechanisms which establish the key effector programs involved in cell cycle arrest, SASP, mitochondrial dysfunction and macromolecular damages to maintain the senescence state.

The RNA-seq data analysis of early and late molecular response to AKT hyperactivation revealed the dynamic changes of transcriptome during AIS initiation and maintenance. Such transcriptional fluctuation from early to late stage of AIS may be associated with the feedback loops or negative regulation by sustained activation of AKT signalling. It is noted that the molecular signatures involved in p53 pathway, mTORC1 signalling, inflammatory response, TNF-alpha signalling via NF-kB and glycolysis were enriched in both early and late stage of AIS, suggesting they play a critical role of both AIS initiation and maintenance and impairing these signalling pathways or processes may disrupt senescence program and cause senescence bypass or escape. Indeed, those genes identified from the RNAi screen were enriched in the inflammatory response and TNF-alpha signalling via NF-kB pathways (Table 3.5), further supporting SASP is required for AIS maintenance.

This dynamic transcriptional alteration is also potentially associated with the change of senescent cell populations. In addition to the cell-autonomous genetic changes, cellular senescence can be regulated by a non-cell autonomous mechanism via interactions with the adjacent cells and the cellular microenvironment. The terms ‘secondary senescence’ describes the spreading of senescence to the adjacent normal cells through cellular interaction, SASP and exosome secreted by senescent cells [14] [43]. Apart from the traditional method of analysing gene expression in the bulk population, single-cell RNA sequencing (scRNA-seq) allows analysis of the transcriptome at an individual cell level.

Using scRNA-seq analysis Teo *et al*. illustrated a functional diversification between primary and secondary senescence induced by RAS hyperactivation and identified suppression of SASP and increased fibrillary collagens in the secondary senescent cells compared to the primary ones [317]. It will be important to take a similar approach to investigating AIS to reveal its senescent cell sub-population diversity. Therefore, OIS is a spatiotemporal-regulated cell state composed of different sub-populations with diverse transcriptional, biochemical and morphological alterations. Understanding this dynamic nature of OIS in the context of cancer will uncover new therapeutic possibilities to target cancer.

3.4.3 AIS and RIS exhibit similar metabolic phenotypes

These results from transcriptomic and metabolic profiling, as well as seahorse mitochondrial function assay, delineate a hyperactive metabolic phenotype in OIS cells with maximization of energy production through enhanced glucose and glutamine utilisation, TCA cycle and oxidative phosphorylation. As illustrated in Fig. 1.2, the bioenergetics is related to glucose and glutamine metabolism, TCA cycle and oxidative phosphorylation. This increased energy production during OIS is proposed to support the energy-consuming processes such as SASP and autophagy and therefore is considered to be critical for senescence induction and maintenance (reviewed in Chapter 1.2.1).

RNA-seq data analysis and the functional seahorse assay indicated upregulated glycolysis in both AIS and RIS. Interestingly, the change of glycolysis pathway in metabolomics analysis was not statistically significant ($p > 0.05$, Table 3.3 and 3.4). This may be due to limitations in the sensitivity of our GC/MS analysis in detecting levels of rate-limiting metabolites that are important as indicators of the pathway activity. The steady-state metabolomic analysis can only provide a snapshot of the cellular metabolic state at one particular time point and cannot measure the dynamic flux through the pathway. For example, the abundance of pyruvate was not significantly changed in either AIS or RIS. This is possibly attributed to the accelerated glycolysis which produces pyruvate at a high rate and simultaneously the hyperactivated TCA cycle which consumes pyruvate at an equally high rate, thus leading to a high turnover rate while

the pool size of pyruvate remained unchanged. To further define the changes in glycolysis, we will need to perform stable isotope labelling to measure glycolytic flux [330].

Interestingly, RNA-seq analysis did not identify elevated mRNA expression of the metabolic enzymes involved in glycolysis and TCA cycle in OIS cells compared to the proliferating cells (Fig 3.4.2), suggesting that post-transcriptional regulation may drive metabolic re-wiring in OIS. Recent findings have described the post-translational modifications such as protein phosphorylation [331], O-GlcNAcylation [332] and Lysine acylation [333] that affect mitochondrial enzyme function. Further studies of the regulation of metabolic reprogramming via translational and the post-translational modification using tandem mass spectrometry may provide more mechanic insight of metabolic reprogramming in OIS [296].

While the metabolomics data analysis revealed the similar metabolic profile in AIS and RIS, identification of specific metabolic alterations in each type of OIS will provide an understanding of how each oncogenic pathway drives senescence and thus help develop appropriate strategies to selectively target oncogene-driven cancers (Fig 3.7). The analysis of differential gene expression in RIS uncovered the mRNA expression levels of four enzymes involved in the pentose phosphate pathway (PPP) including glucose-6-phosphate dehydrogenase (G6PD), phosphogluconate dehydrogenase (PGD), transketolase (TKT) and transaldolase 1 (TALDO1) were significantly downregulated. Insufficient PPP activity and nucleotide synthesis [260] [300] [26] [262] during RIS has been reported to lead to dNTP deficiency and subsequently trigger DNA damage and replication stress [262] [301]. These metabolic vulnerabilities lead to the hypothesis of which RAS-driven cancers may be more susceptible to DNA damage targeting drugs. Different from RIS, the activity of PPP was unaffected in AIS. This is consistent with our previous finding showing lack of replication stress and DNA damage response in AIS [34]. However, it is noted that GC-MS metabolomics may have serious retention and selectivity issues for highly polar compounds such as nucleotides [334]. Therefore, to further assess the metabolic alteration in nucleotide synthesis and nucleotide levels, future studies will utilise ion-pair liquid chromatography-electrospray ionization mass spectrometry (IP-LC-ESI-MS) [335].

To further investigate the specific metabolic alterations that are important for the maintenance of AIS, we analysed the data of a genome-wide RNAi screen to overcome AIS-induced cell cycle arrest in human fibroblasts. Two genes belonging to the NADPH oxidase (NOX) enzyme family which is involved in superoxide production, NADPH oxidase organizer 1 (NOXO1) and NADPH oxidase 5 (NOX5) were identified as high confidence hits. This is consistent with our finding that NOXO1 was significantly up-regulated during AIS (FC > 2, adjusted-p < 0.0001). Loss of NOXO1 or NOX5 during AIS leads to AIS escape, suggesting ROS production is essential for AIS maintenance. We thus hypothesize that oxidative stress induced by hyperactivated AKT signalling maintains the senescence phenotype and release of oxidative stress could overcome the senescence barrier, and will test this hypothesis in chapter 4. More importantly, we found that loss of CBS increased the cell number of AIS cells but decreased cell number of RIS cells, suggesting a specific dependence of CBS-associated metabolism on AIS maintenance, which we will thoroughly explore in chapter 4 to unravel the unique metabolic rewiring in AIS.

Taken together, in this chapter we established AIS and RIS in human fibroblasts and characterized the morphological, transcriptional and metabolic changes during senescence establishment and maintenance (Fig. 3.7). We identified the common molecular signatures of these two types of OIS which revealed the hallmarks of OIS, as well as the dynamic changes of transcriptome during AIS initiation and maintenance. More importantly, combining the results from transcriptional and metabolic profiling as well as the whole genome RNAi functional screen, we revealed the profound metabolic re-wiring in AIS, supporting the concept that metabolic reprogramming drives AIS and contributes to senescence escape and tumourigenesis. Therefore, in the next chapter, we will provide more mechanistic insights into the metabolic reprogramming in AIS maintenance and explore the possibility of harnessing these metabolic vulnerabilities to treat cancer.

3.5 Chapter 3 Tables

Table 3.1 Differential metabolite analysis of pBABE with AIS

	t-statistic	p-value	BH Adjusted p-value	log2 fold change	standard error
L.Serine.Pk1	6.958472	#######	0.002693	1.2403947	0.178257
L.Aspartic.acid	-6.77567	#######	0.002693	-0.75815	0.111893
L.Malic.acid	-6.652114	0.0001	0.002693	-0.770413	0.115815
Citric.acid	-6.271724	0.0001	0.002693	-0.714095	0.113859
L.Tryptophan.Pk2	-8.627273	0.0002	0.002693	-0.451172	0.052296
Glutamate	-6.134613	0.0002	0.002693	-0.969718	0.158073
Fumaric.acid	-5.398266	0.0005	0.00526765	-0.569067	0.105417
L.Proline.Pk1	-6.23561	0.0007	0.00683284	-1.095639	0.175707
L.Tyrosine.Pk2	-5.360041	0.0009	0.00811581	-1.145017	0.213621
Cysteine	-4.807465	0.0013	0.00876474	-0.64465	0.134094
D.Glucose.Pk1	4.873948	0.0013	0.00876474	0.5261451	0.10795
Hexadecanoic.acid	4.893643	0.0014	0.00876474	0.6682229	0.136549
D.Talose.Pk1	4.638	0.0018	0.01031576	0.5207897	0.112288
D.Gluconic.Acid.Delta.Lactone	4.552739	0.002	0.01031576	0.490746	0.107791
Hypoxanthine	-4.810248	0.0021	0.01031576	-1.931901	0.401622
D.Glucose.Pk2	4.410037	0.0023	0.01031576	0.5049861	0.114508
Glutamine	-4.570756	0.0024	0.01031576	-1.971814	0.431398
L.Phenylalanine.Pk2	-4.20187	0.0024	0.01031576	-0.682696	0.162474
D.Talose.Pk2	4.305783	0.0027	0.01113365	0.5006086	0.116264
scyllo.Inositol	4.03284	0.003	0.01141918	0.4740291	0.117542
Glyceric.acid	-4.102333	0.0033	0.01200161	-0.471765	0.114999
L.Serine.Pk2	-3.835254	0.0043	0.01432138	-0.687076	0.179147
Benzoic.Acid	4.197245	0.0043	0.01432138	0.501409	0.119461
L.Ornithine	-4.010912	0.0051	0.01638715	-0.706361	0.17611
Isocitric.Acid	-3.476828	0.007	0.0216178	-0.523726	0.150633
L.Lysine.Pk3	-3.444371	0.0076	0.02260193	-0.737918	0.214239
Tetradecanoic.acid	3.252846	0.01	0.02839182	0.5602457	0.172233
D.Maltose.Pk3	-3.125499	0.0122	0.03176534	-0.397265	0.127105
Ribitol	3.122236	0.0123	0.03176534	0.3566003	0.114213
D.....3.Phosphoglyceric.acid	-3.135145	0.0124	0.03176534	-0.608867	0.194207
myo.Inositol	3.41961	0.0139	0.03447434	0.5849076	0.171045
Proline..trans.4.hydroxyl.L..	-2.875068	0.0189	0.04547332	-0.396611	0.137948
Octadecanoic.acid	3.095428	0.0205	0.04790883	0.5575424	0.180118
Putrescine	2.73429	0.0232	0.05249575	0.5611991	0.205245
L.Alanine	-2.734979	0.0248	0.05453461	-0.445975	0.163063
D.Erythrose	2.625668	0.028	0.0590141	0.3170571	0.120753
D.Gluconic.Acid	-2.624824	0.0284	0.0590141	-0.37864	0.144254
L.Methionine	-2.712259	0.0305	0.06187318	-0.396607	0.146228
Cholesterol	-2.545473	0.0327	0.06446576	-0.265193	0.104182
D.Maltose.Pk1	2.525094	0.0453	0.08723368	0.9096538	0.360246
L.Valine	-2.285486	0.0486	0.08934318	-0.313637	0.13723
Lactic.Acid	-2.278694	0.0487	0.08934318	-0.249702	0.109581
Urea	-2.260023	0.0502	0.08994576	-0.412125	0.182354

D.Myo.Inositol.1.phosphate	-2.11178	0.0639	0.11179928	-0.262778	0.124435
L.Tyrosine.Pk1	-2.129832	0.0684	0.11656497	-0.263505	0.123721
L.Isoleucine	-2.077254	0.0696	0.11656497	-0.304699	0.146684
Fructose.6.phosphate	-1.96176	0.0834	0.13658749	-0.446814	0.227762
Pyroglutamic.acid	-1.813349	0.1032	0.16437401	-0.198387	0.109404
Glucose.6.phosphate.Pk2	-1.812824	0.1046	0.16437401	-0.385681	0.212751
beta.Alanine	1.880894	0.1109	0.17072634	0.3546113	0.188533
D.Glucosamine	1.689415	0.1282	0.19350503	0.2249949	0.133179
L.Threonine.Pk2	-1.641954	0.1377	0.20385987	-0.261686	0.159374
Oxalic.acid	1.622034	0.1423	0.20673646	0.4178783	0.257626
Glucose.6.phosphate.Pk1	-1.583568	0.1494	0.21304668	-0.337532	0.213146
D.Ribose	1.461139	0.1781	0.2470248	0.1029054	0.070428
Glycine.Pk1	-1.514849	0.1797	0.2470248	-0.362235	0.239123
D.Fructose.Pk2	1.435509	0.1864	0.2517694	0.1643218	0.114469
DL.Lactic.acid	-1.418689	0.1913	0.25392478	-0.217085	0.153018
D.Fructose.Pk1	1.339117	0.2138	0.27905405	0.1581397	0.118093
D.Maltose.Pk2	-1.347001	0.2212	0.28389307	-0.181916	0.135052
D.Xylose	-1.318006	0.237	0.29910218	-0.397315	0.301451
Sucrose	-1.248753	0.2461	0.30560633	-0.406252	0.325326
L.Lysine.Pk2	-1.105651	0.2983	0.36452884	-0.169566	0.153363
L.Leucine	-0.965039	0.3619	0.43541506	-0.2515	0.260612
L.Threonine.Pk1	0.91079	0.3933	0.46591175	0.2779002	0.30512
Glycerol.2.phosphate	0.592455	0.5716	0.66687266	0.1740059	0.293703
Glycine.Pk2	0.556603	0.5918	0.68010029	0.1593564	0.286302
Pyridoxine	-0.530234	0.6131	0.69423357	-0.05961	0.112421
meso.Erythritol	-0.454832	0.6603	0.7368121	-0.0505	0.111029
Adenine	-0.442513	0.6703	0.73728486	-0.276847	0.625623
gamma.Aminobutyric.acid..GABA.	-0.383395	0.7106	0.7706271	-0.054281	0.14158
Uridine	0.337047	0.7443	0.79598259	0.0854169	0.253427
Mannitol	0.274974	0.7896	0.82403061	0.0547459	0.199095
Succinc.acid	-0.250727	0.8102	0.82403061	-0.01809	0.072152
GSH	-0.248069	0.8107	0.82403061	-0.105247	0.424264
Sorbitol	0.24333	0.8133	0.82403061	0.0468756	0.192642
L.Phenylalanine.Pk1	-0.051787	0.9598	0.95983013	-0.009559	0.184591

Table 3.2 Differential metabolite analysis of pBABE with RIS

	t-statistic	p-value	BH Adjusted p-value	fold change	standard error
Citric.acid.Results	-11.212	5.57E-07	3.57E-05	-1.32702	0.11836
Benzoic.Acid.Results	10.94597	9.91E-07	3.57E-05	0.805698	0.07361
L.Tyrosine.Pk2.Results	-10.1622	2.34E-06	5.16E-05	-2.0557	0.20229
L.Malic.acid.Results	-9.8916	2.87E-06	5.16E-05	-1.0969	0.11089
Hexadecanoic.acid.Results	8.567917	7.18E-06	9.75E-05	1.036204	0.12094
Isocitric.Acid.Results	-8.41828	9.27E-06	9.75E-05	-1.13237	0.13451
L.Ornithine.Results	-8.20991	9.51E-06	9.75E-05	-1.91715	0.23352
L.Lysine.Pk3.Results	-8.22622	1.08E-05	9.75E-05	-1.8673	0.22699
Fumaric.acid.Results	-7.92919	1.27E-05	0.00010186	-0.8822	0.11126
L.Aspartic.acid.Results	-7.7885	1.62E-05	0.00011671	-0.8698	0.11168
Hypoxanthine.Results	-7.62248	2.01E-05	0.0001314	-2.52618	0.33141
Octadecanoic.acid.Results	7.316978	3.53E-05	0.00021205	0.977804	0.13363
L.Serine.Pk1.Results	7.099591	4.05E-05	0.00022445	1.455708	0.20504
L.Lysine.Pk2.Results	-7.05	4.68E-05	0.00024059	-0.94099	0.13347
Lactic.Acid.Results	-6.75826	5.06E-05	0.0002429	-0.71369	0.1056
scyllo.Inositol.Results	6.499229	6.96E-05	0.0003132	0.752009	0.11571
L.Methionine.Results	-5.58295	0.00024	0.00101085	-0.62031	0.11111
myo.Inositol.Results	5.642433	0.00025	0.00101085	0.680162	0.12054
D.....3.Phosphoglyceric.acid.Results	-5.85226	0.00033	0.00123898	-0.90039	0.15385
L.Serine.Pk2.Results	-5.89228	0.00037	0.00123898	-0.95674	0.16237
L.Proline.Pk1.Results	-6.17688	0.00038	0.00123898	-1.12126	0.18152
Proline..trans.4.hydroxyl.L..Results	-5.3229	0.00038	0.00123898	-0.65257	0.1226
beta.Alanine.Results	-4.81999	0.00076	0.00238587	-0.55504	0.11515
L.Threonine.Pk1.Results	5.327701	0.00096	0.00288603	0.975052	0.18302
D.Gluconic.Acid.Results	-4.89437	0.00106	0.00295013	-0.64825	0.13245
L.Threonine.Pk2.Results	-4.64252	0.00107	0.00295013	-0.57566	0.124
Tetradecanoic.acid.Results	4.852982	0.00113	0.00300154	0.710243	0.14635
L.Phenylalanine.Pk2.Results	-4.78153	0.00151	0.0038912	-0.71783	0.15013
Adenine.Results	-5.46622	0.0018	0.00446469	-2.12109	0.38804
L.Alanine.Results	-4.15542	0.00223	0.00535287	-0.70582	0.16986
D.Glucose.Pk1.Results	4.035383	0.00243	0.00564285	0.516552	0.12801
D.Gluconic.Acid.Delta.Lactone.Results	3.947429	0.0028	0.00629376	0.504121	0.12771
Urea.Results	-4.04448	0.00307	0.00670794	-0.64434	0.15931
D.Talose.Pk1.Results	3.834254	0.00335	0.00708384	0.508067	0.13251
DL.Lactic.acid.Results	-3.87044	0.00352	0.00724742	-0.47335	0.1223
L.Tryptophan.Pk2.Results	-5.05439	0.00365	0.00730184	-0.5751	0.11378
L.Tyrosine.Pk1.Results	-3.61391	0.00482	0.0092023	-0.35168	0.09731
L.Valine.Results	-3.64317	0.00486	0.0092023	-0.49845	0.13682
D.Glucose.Pk2.Results	3.256585	0.00882	0.01629073	0.447273	0.13734
D.Maltose.Pk3.Results	-3.17149	0.01032	0.01857742	-0.42207	0.13308
Pyroglutamic.acid.Results	-3.10137	0.01131	0.01985899	-0.33411	0.10773
D.Talose.Pk2.Results	3.035236	0.01297	0.02223661	0.438529	0.14448
Pyridoxine.Results	-2.82546	0.02228	0.03731403	-0.28705	0.1016

Table 3.3 AIS cell metabolic signatures revealed by MSEA

	total	expected	hits	Raw p	Holm p	FDR
Warburg Effect	58	1.30	7	1.56E-04	1.54E-02	1.48E-02
Urea Cycle	29	0.65	5	2.99E-04	2.93E-02	1.48E-02
Phenylalanine and Tyrosine Metabolism	28	0.63	4	2.76E-03	2.68E-01	9.12E-02
Ammonia Recycling	32	0.72	4	4.57E-03	4.39E-01	9.99E-02
Arginine and Proline Metabolism	53	1.19	5	5.05E-03	4.79E-01	9.99E-02
Aspartate Metabolism	35	0.79	4	6.36E-03	5.98E-01	1.05E-01
Glycine and Serine Metabolism	59	1.32	5	8.04E-03	7.48E-01	1.14E-01
Homocysteine Degradation	9	0.20	2	1.58E-02	1.00E+00	1.88E-01
Malate-Aspartate Shuttle	10	0.22	2	1.94E-02	1.00E+00	1.88E-01
Purine Metabolism	74	1.66	5	2.06E-02	1.00E+00	1.88E-01
Glutamate Metabolism	49	1.10	4	2.09E-02	1.00E+00	1.88E-01
Citric Acid Cycle	32	0.72	3	3.20E-02	1.00E+00	2.46E-01
Glucose-Alanine Cycle	13	0.29	2	3.23E-02	1.00E+00	2.46E-01
Spermidine and Spermine Biosynthesis	18	0.40	2	5.93E-02	1.00E+00	4.19E-01
Methionine Metabolism	43	0.96	3	6.78E-02	1.00E+00	4.43E-01
Tyrosine Metabolism	72	1.62	4	7.16E-02	1.00E+00	4.43E-01
Glutathione Metabolism	21	0.47	2	7.81E-02	1.00E+00	4.55E-01
Transfer of Acetyl Groups into Mitochondria	22	0.49	2	8.48E-02	1.00E+00	4.66E-01
Glycerolipid Metabolism	25	0.56	2	1.06E-01	1.00E+00	5.23E-01
Glycolysis	25	0.56	2	1.06E-01	1.00E+00	5.23E-01
Cysteine Metabolism	26	0.58	2	1.13E-01	1.00E+00	5.33E-01
Lysine Degradation	30	0.67	2	1.43E-01	1.00E+00	6.12E-01
Starch and Sucrose Metabolism	31	0.70	2	1.51E-01	1.00E+00	6.12E-01
Biotin Metabolism	8	0.18	1	1.67E-01	1.00E+00	6.12E-01
Amino Sugar Metabolism	33	0.74	2	1.67E-01	1.00E+00	6.12E-01
Beta-Alanine Metabolism	34	0.76	2	1.75E-01	1.00E+00	6.12E-01
Gluconeogenesis	35	0.79	2	1.84E-01	1.00E+00	6.12E-01
Fatty Acid Biosynthesis	35	0.79	2	1.84E-01	1.00E+00	6.12E-01
Phenylacetate Metabolism	9	0.20	1	1.85E-01	1.00E+00	6.12E-01
Lactose Degradation	9	0.20	1	1.85E-01	1.00E+00	6.12E-01
Nicotinate and Nicotinamide Metabolism	37	0.83	2	2.00E-01	1.00E+00	6.39E-01
Galactose Metabolism	38	0.85	2	2.08E-01	1.00E+00	6.45E-01
Sphingolipid Metabolism	40	0.90	2	2.25E-01	1.00E+00	6.76E-01
Taurine and Hypotaurine Metabolism	12	0.27	1	2.40E-01	1.00E+00	6.78E-01
Phosphatidylethanolamine Biosynthesis	12	0.27	1	2.40E-01	1.00E+00	6.78E-01
Thyroid hormone synthesis	13	0.29	1	2.57E-01	1.00E+00	7.06E-01
Alanine Metabolism	17	0.38	1	3.22E-01	1.00E+00	8.39E-01
Phosphatidylinositol Phosphate Metabolism	17	0.38	1	3.22E-01	1.00E+00	8.39E-01
Mitochondrial Electron Transport Chain	19	0.43	1	3.53E-01	1.00E+00	8.88E-01
Catecholamine Biosynthesis	20	0.45	1	3.68E-01	1.00E+00	8.88E-01
Lactose Synthesis	20	0.45	1	3.68E-01	1.00E+00	8.88E-01
Pantothenate and CoA Biosynthesis	21	0.47	1	3.82E-01	1.00E+00	9.01E-01
Carnitine Synthesis	22	0.49	1	3.96E-01	1.00E+00	9.12E-01
Inositol Phosphate Metabolism	26	0.58	1	4.50E-01	1.00E+00	9.90E-01
Plasmalogen Synthesis	26	0.58	1	4.50E-01	1.00E+00	9.90E-01
Selenoamino Acid Metabolism	28	0.63	1	4.75E-01	1.00E+00	1.00E+00
Mitochondrial Beta-Oxidation of Long Chain Saturated Fatty Acids	28	0.63	1	4.75E-01	1.00E+00	1.00E+00
Folate Metabolism	29	0.65	1	4.87E-01	1.00E+00	1.00E+00
Inositol Metabolism	33	0.74	1	5.33E-01	1.00E+00	1.00E+00
Fatty Acid Elongation In Mitochondria	35	0.79	1	5.54E-01	1.00E+00	1.00E+00
Propanoate Metabolism	42	0.94	1	6.22E-01	1.00E+00	1.00E+00
Histidine Metabolism	43	0.96	1	6.31E-01	1.00E+00	1.00E+00
Fatty acid Metabolism	43	0.96	1	6.31E-01	1.00E+00	1.00E+00
Steroid Biosynthesis	48	1.08	1	6.72E-01	1.00E+00	1.00E+00
Pyrimidine Metabolism	59	1.32	1	7.48E-01	1.00E+00	1.00E+00
Valine, Leucine and Isoleucine Degradation	60	1.35	1	7.54E-01	1.00E+00	1.00E+00
Tryptophan Metabolism	60	1.35	1	7.54E-01	1.00E+00	1.00E+00
Bile Acid Biosynthesis	65	1.46	1	7.82E-01	1.00E+00	1.00E+00
Arachidonic Acid Metabolism	69	1.55	1	8.02E-01	1.00E+00	1.00E+00

Table 3.4 RIS cell metabolic signatures revealed by MSEA

	total	expected	hits	Raw p	Holm p	FDR
Warburg Effect	58	1.81	8	2.34E-04	2.32E-02	2.32E-02
Urea Cycle	29	0.91	5	1.50E-03	1.47E-01	7.42E-02
Glycine and Serine Metabolism	59	1.84	6	7.89E-03	7.65E-01	2.60E-01
Citric Acid Cycle	32	1.00	4	1.52E-02	1.00E+00	3.49E-01
Gluconeogenesis	35	1.09	4	2.07E-02	1.00E+00	3.49E-01
Arginine and Proline Metabolism	53	1.65	5	2.12E-02	1.00E+00	3.49E-01
Transfer of Acetyl Groups into Mitochondria	22	0.69	3	2.84E-02	1.00E+00	4.02E-01
Glycolysis	25	0.78	3	3.99E-02	1.00E+00	4.93E-01
Phenylalanine and Tyrosine Metabolism	28	0.87	3	5.33E-02	1.00E+00	5.86E-01
Glucose-Alanine Cycle	13	0.41	2	5.94E-02	1.00E+00	5.89E-01
Aspartate Metabolism	35	1.09	3	9.19E-02	1.00E+00	8.27E-01
Spermidine and Spermine Biosynthesis	18	0.56	2	1.06E-01	1.00E+00	8.74E-01
Glycerolipid Metabolism	25	0.78	2	1.82E-01	1.00E+00	1.00E+00
Glutamate Metabolism	49	1.53	3	1.93E-01	1.00E+00	1.00E+00
Purine Metabolism	74	2.31	4	1.95E-01	1.00E+00	1.00E+00
Selenoamino Acid Metabolism	28	0.87	2	2.16E-01	1.00E+00	1.00E+00
Biotin Metabolism	8	0.25	1	2.25E-01	1.00E+00	1.00E+00
Homocysteine Degradation	9	0.28	1	2.49E-01	1.00E+00	1.00E+00
Lactose Degradation	9	0.28	1	2.49E-01	1.00E+00	1.00E+00
Starch and Sucrose Metabolism	31	0.97	2	2.52E-01	1.00E+00	1.00E+00
Ammonia Recycling	32	1.00	2	2.64E-01	1.00E+00	1.00E+00
Malate-Aspartate Shuttle	10	0.31	1	2.73E-01	1.00E+00	1.00E+00
Beta-Alanine Metabolism	34	1.06	2	2.87E-01	1.00E+00	1.00E+00
D-Arginine and D-Ornithine Metabolism	11	0.34	1	2.96E-01	1.00E+00	1.00E+00
Fatty Acid Biosynthesis	35	1.09	2	2.99E-01	1.00E+00	1.00E+00
Phosphatidylethanolamine Biosynthesis	12	0.38	1	3.18E-01	1.00E+00	1.00E+00
Galactose Metabolism	38	1.19	2	3.35E-01	1.00E+00	1.00E+00
Thyroid hormone synthesis	13	0.41	1	3.40E-01	1.00E+00	1.00E+00
Sphingolipid Metabolism	40	1.25	2	3.58E-01	1.00E+00	1.00E+00
Methionine Metabolism	43	1.34	2	3.92E-01	1.00E+00	1.00E+00
Tyrosine Metabolism	72	2.25	3	3.93E-01	1.00E+00	1.00E+00
Alanine Metabolism	17	0.53	1	4.19E-01	1.00E+00	1.00E+00
Phosphatidylinositol Phosphate Metabolism	17	0.53	1	4.19E-01	1.00E+00	1.00E+00
Pyruvate Metabolism	48	1.50	2	4.48E-01	1.00E+00	1.00E+00
Mitochondrial Electron Transport Chain	19	0.59	1	4.56E-01	1.00E+00	1.00E+00
Catecholamine Biosynthesis	20	0.62	1	4.73E-01	1.00E+00	1.00E+00
Lactose Synthesis	20	0.62	1	4.73E-01	1.00E+00	1.00E+00
Threonine and 2-Oxobutanoate Degradation	20	0.62	1	4.73E-01	1.00E+00	1.00E+00
Glutathione Metabolism	21	0.66	1	4.90E-01	1.00E+00	1.00E+00
Betaine Metabolism	21	0.66	1	4.90E-01	1.00E+00	1.00E+00
Carnitine Synthesis	22	0.69	1	5.06E-01	1.00E+00	1.00E+00
Inositol Phosphate Metabolism	26	0.81	1	5.66E-01	1.00E+00	1.00E+00
Plasmalogen Synthesis	26	0.81	1	5.66E-01	1.00E+00	1.00E+00
Tryptophan Metabolism	60	1.87	2	5.70E-01	1.00E+00	1.00E+00
Mitochondrial Beta-Oxidation of Long Chain Saturated Fatty Acids	28	0.87	1	5.94E-01	1.00E+00	1.00E+00
Pentose Phosphate Pathway	29	0.91	1	6.07E-01	1.00E+00	1.00E+00
Lysine Degradation	30	0.94	1	6.19E-01	1.00E+00	1.00E+00
Fructose and Mannose Degradation	32	1.00	1	6.43E-01	1.00E+00	1.00E+00
Inositol Metabolism	33	1.03	1	6.55E-01	1.00E+00	1.00E+00
Amino Sugar Metabolism	33	1.03	1	6.55E-01	1.00E+00	1.00E+00
Fatty Acid Elongation In Mitochondria	35	1.09	1	6.77E-01	1.00E+00	1.00E+00
Propanoate Metabolism	42	1.31	1	7.43E-01	1.00E+00	1.00E+00
Histidine Metabolism	43	1.34	1	7.52E-01	1.00E+00	1.00E+00
Fatty acid Metabolism	43	1.34	1	7.52E-01	1.00E+00	1.00E+00
Steroid Biosynthesis	48	1.50	1	7.90E-01	1.00E+00	1.00E+00
Pyrimidine Metabolism	59	1.84	1	8.54E-01	1.00E+00	1.00E+00
Bile Acid Biosynthesis	65	2.03	1	8.81E-01	1.00E+00	1.00E+00

Table 3.5 Gene set overlap results of RNAi screen hits with MSigDB

Collection(s):	H					
# overlaps shown:	2					
# genesets in collections:	50					
# genes in comparison (n):	97					
# genes in universe (N):	38404					
Gene Set Name	# Genes in Gene Set (K)	Description	# Genes in Overlap (k)	k/K	p-value	FDR q-value
HALLMARK_INFLAMMATORY_RESPONSE	200	Genes defining inflammatory response.	6	0.03	1.23E-05	6.17E-04
HALLMARK_TNFA_SIGNALING_VIA_NFKB	200	Genes regulated by NF-kB in response to TNF.	4	0.02	1.70E-03	4.24E-02

CHAPTER 4 CBS is an essential metabolic regulator in AKT-induced senescence and suppresses oncogenic transformation and progression

4.1 Preface

This chapter aims to explore the mechanisms underpinning AKT-induced senescence escape caused by loss of CBS, and to evaluate the potential role of CBS as a suppressor of gastric tumour formation and progression. A manuscript detailing the studies presented in this chapter is currently in preparation:

Zhu H, Chan KT, Blake S, Anderson D, Creek D, Ellis S, Cullinane C, Sanij E, Kang J and Pearson RB. CBS is an essential metabolic regulator in AKT-induced senescence and suppresses oncogenic transformation and progression. (manuscript in preparation)

4.2 Introduction

PI3K/AKT/mTORC1 signalling plays a critical role in controlling multiple biological processes including cell growth, proliferation and survival, cellular metabolism, migration and angiogenesis in response to growth factor stimulation, altered nutrient and energy status, hypoxia and various cellular stresses [292]. More importantly, genomic aberrations in the PI3K/AKT/mTORC1 signalling pathway have been observed in 38% of solid tumours across 19784 consecutive tumour samples and more than 40 cancer types, [268]. Paradoxically, hyperactivation of PI3K/AKT/mTORC1 signalling pathway causes a senescence-like phenotype in non-transformed cells, which acts as a protective brake against tumour development, suggesting that additional genetic or epigenetic changes can lead to malignant progression [34]. Deregulated metabolism is another hallmark of the senescence phenotype [336]. RAS-induced senescent (RIS) cells display an active metabolic phenotype consisting of hyperactive TCA cycle, elevated mitochondrial respiration and enhanced fatty acid oxidation [186]. The studies presented in Chapter 3, systematically characterized the metabolic phenotype of AKT-induced senescent (AIS) cells and demonstrated that AIS exhibits a similar metabolic reprogramming to RIS with increased energy production. Furthermore, we identified 98 essential regulators of AKT-induced senescence (AIS) maintenance using a whole protein-coding genome RNAi screen [121]. Among the 98 AIS regulators, over 10%

(11/98) were involved in cellular metabolism and 7 of 11 metabolic-associated candidates were validated using a cell proliferation assay (Fig 3.6c). Thus, we hypothesize that metabolic alterations contribute to AIS maintenance, and that modulating metabolism may cause senescence escape and promote tumorigenesis.

In the RNAi screen for regulators of AIS escape, out of the 11 metabolism-associated genes identified Cystathionine-β-synthase (CBS) was the top-ranked hit, displaying a robust Z-score of 2.53 in the primary screen and 2/4 siRNA duplexes confirmed in the secondary deconvolution screen. We also demonstrated that CBS has a specific regulatory role in AIS but not in RIS (Fig. 3.6c). It converts homocysteine (Hcy), a key metabolite in the transmethylation pathway, to cystathionine which is subsequently hydrolysed by cystathionine gamma-lyase (CTH) to form cysteine, the crucial precursor for glutathione (GSH) production. CBS also catalyses the production of H_2S which modulates mitochondrial functions and cellular bioenergetics in a concentration-dependent manner [337]. At low concentrations, H_2S acts as a mitochondrial electron donor to mitochondrial complex II, stimulating ATP synthesis while at high concentrations, H_2S acts as a mitochondrial poison via the inhibition of cytochrome c oxidase in mitochondrial complex IV. While CBS is mainly a cytosolic enzyme, localization in the nucleus and mitochondria has been detected [338]. Thus, CBS acts through control of Hcy, H_2S and GSH metabolism and exerts diverse biological functions including regulating mitochondrial bioenergetics, redox homeostasis, DNA methylation and post-translational modification [266]. Aberrant CBS expression/activity and the associated alterations in Hcy and/or H_2S levels contributes to a wide range of pathologies including cancer [267]. Therefore, we hypothesize that CBS aberration may contribute to PI3K/AKT-driven cancers through metabolic deregulations of H_2S production, Hcy perturbation or mitochondrial energetics.

While the PI3K/AKT pathway has been found to contribute to almost all human cancers [268], CBS plays an important but complex role in cancer biology [266]. Accumulating evidence suggests that the role of CBS in cancer initiation and progression is tumour-type specific. Although activation of CBS promotes tumour growth in colon [339] [340], ovarian [341], and breast cancer [342], the function of CBS in liver cancer and melanoma

remains poorly defined with conflicting studies reporting both tumour promoting and suppressing and inconclusive roles (Reviewed in Chapter 1.3). In contrast, evidence from glioma supports a tumour-suppressive role for CBS, where CBS knockdown decreased tumour latency in U87-MG xenografts and increased tumour volume in an orthotopic model [343]. Previous studies have demonstrated CBS deficiency in human gastric cancer cells with hypermethylation at CBS promoter region, implicating loss of CBS through epigenetic regulation in gastric cancer [281].

In this chapter, we explore the molecular mechanisms by which CBS is required for AIS maintenance and loss of CBS promotes AIS escape. The essential regulatory role of CBS in the maintenance of AIS implicates it as a putative tumour suppressor during PI3K pathway-driven tumorigenesis. TCGA data analysis indicates that 3% of gastric cancers harbour CBS deletion and a subset of these exhibit hyperactive PI3K/AKT/mTORC1 signalling (Fig. 4.1.1). We thus characterize the functional significance of CBS in gastric cancer initiation and progression. Intriguingly, whilst we find that CBS loss facilitates gastric cancer development, it also exposes a potential metabolic vulnerability that can be targeted to treat gastric cancer.

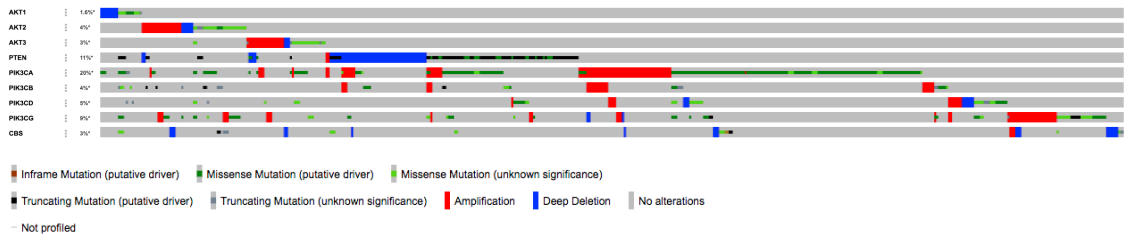


Figure 4.1.1 TCGA data analysis showing genetic aberrations in PI3K/AKT signalling and CBS in gastric cancer.

Data were acquired from 1365 patients in 6 cohorts of stomach adenocarcinoma studies where 1330 of patient samples were profiled. AKT1, AKT2, AKT3, PTEN, PIK3CA, PIK3CB, PIK3CD and PIK3CG were queried as PI3K/AKT signalling genes.

4.3 Results

4.3.1 Inhibition of CBS promotes escape from AKT-induced senescence (AIS)

To gain insight into how CBS contributes to AIS maintenance, we first measured the expression and activity of CBS in several non-transformed cells expressing hyperactivated AKT. An increase in CBS protein expression was observed in BJ-TERT human skin fibroblasts (Fig. 4.1.2a) and IMR90 human foetal lung fibroblasts (Fig. 4.1.2b) overexpressing myr-AKT1, and in BJ-TERT (Fig. 4.1.2c) and human mammary epithelial cells (HMEC; Fig. 4.1.2d) overexpressing AKT1-E17K, a clinically relevant activated mutant form of AKT. To test whether the expression of other components of the transsulfuration pathway were altered, we examined the expression levels of CTH, a key enzyme in the transsulfuration pathway and xCT, the regulatory component of the system Xc- amino acid antiporter responsible for the up-take cystine, an oxidized form of cysteine in BJ-TERT cells overexpressing myr-AKT1. We found both CTH and xCT were upregulated, suggesting that transsulfuration pathway activity is increased in AIS cells. Indeed, using a fluorescent H_2S specific probe 7-azideo-4-methylcoumarin [288], we observed that H_2S production was significantly upregulated in BJ-TERT fibroblasts upon AKT but not HRAS hyperactivation (Fig. 4.1.2e), suggesting that activation of transsulfuration pathway activity is a specific cellular response to constitutive activation of AKT.

To investigate the role of CBS in AIS maintenance, we generated BJ-TERT human skin fibroblasts expressing a doxycycline-inducible CBS shRNA and an shRNA-resistant 4-OHT-inducible estrogen receptor (ER)-tagged-CBS fusion (Fig. 4.1.2f-g). Constitutive overexpression of myr-AKT1 induced AIS, which was confirmed by a significant increase of SA-βGal positive cells and decrease of EdU positive cells (Fig. 4.1.2h-k). CBS depletion in AIS cells using two separate shRNAs targeting different regions of CBS mRNA cells significantly decreased SA-βGal activity and increased the EdU incorporation, demonstrating the critical role of CBS in AIS maintenance. Knockdown of CBS in proliferating control cells did not affect the percentage of SA-βGal and EdU positive cells. (Fig. 4.1.2h-k). To further demonstrate the on-target specificity of the knockdown, we induced CBS expression by treating with 4-OHT, which prevented senescence escape

(Fig. 4.1.2f-k). In contrast, overexpression of CBS in normal proliferating cells did not induce senescence.

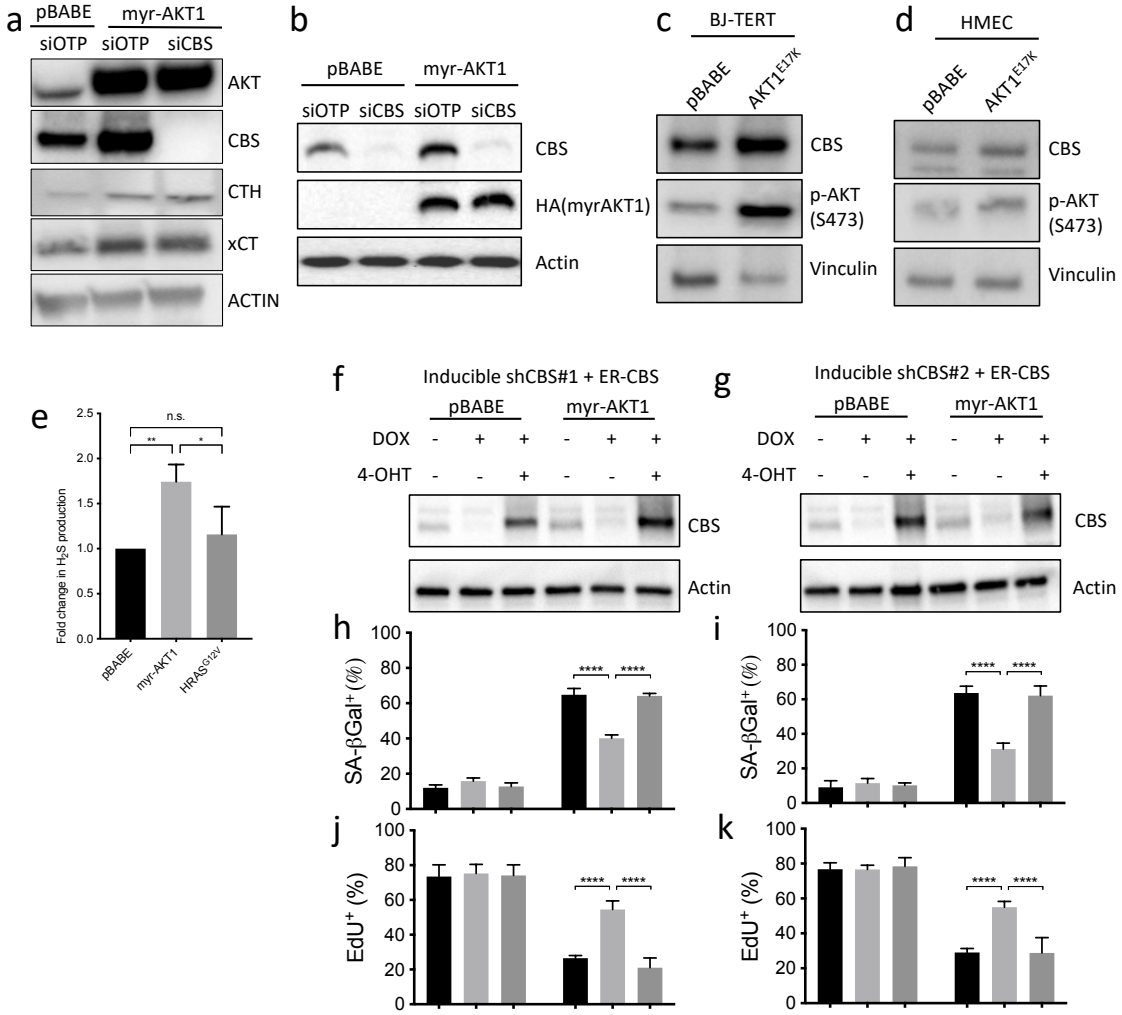


Figure 4.1.2 Inhibition of CBS promotes escape from AKT-induced senescence.

(a) BJ-TERT cells were transduced with pBabe or myrAKT1. Cells were then transfected with either CBS siRNA (siCBS) or control siRNA (siOTP) and analysed on day 5 post-transfection. Western blotting of AKT, CBS, CTH and xCT and Actin was probed as a loading control. (b) Western blotting of CBS and HA-tagged myr-AKT1 in IMR-90 control or AIS cells transfected with OTP or CBS siRNAs. Actin was probed as a loading control. (c) BJ-TERT and (d) HMEC cells were transduced with either pBabe or AKT1^{E17K} and analysed on day 14 post-transduction. Western blotting of CBS and p-AKT at S473 and Vinculin was probed as a loading control. (e) BJ-TERT cells were transduced with either pBabe, myrAKT1 or HRASG12V and analysed on day 14 post-transduction. H_2S production rate was measured by AzMC. (f-k) BJ-TERT cells with doxycycline-inducible CBS shRNA and 4-OHT-inducible CBS overexpression were transduced with pBabe or myr-AKT1 and analysed 14 days post-transduction. (f,g) Western blotting of CBS. Actin was probed as a loading control. Quantification of the percentage of cells with positive staining for (h,i) SA-βGal activity or (j,k) EdU proliferation marker incorporation. BJ-TERT cells expressing myrAKT1 were transduced with pGIPz-shCBS or control vector pGIPz-NTC.

Clonogenic assays using BJ-TERT fibroblasts expressing myr-AKT1 followed by transducing a lentiviral vector expressing CBS shRNA revealed an enhanced colony formation upon knockdown of CBS compared to the AIS control, further supporting an increase in proliferative capacity (Fig. 4.1.3a-c). To determine whether CBS knockdown-induced AIS escape occurred in other cell types, we transfected siRNA against CBS into human IMR-90 lung fibroblasts expressing myrAKT1 or a control vector (Fig. 4.1.3d-e). Similar to our findings in BJ-TERT cells, AKT1 hyperactivation also caused senescence in IMR-90 cells. CBS knockdown also caused IMR-90 cells to escape AKT-induced senescence, as demonstrated by significantly suppressed SA-βGal staining and enhanced EdU incorporation, while no significant effect on SA-βGal or EdU staining was observed in proliferating control cells.

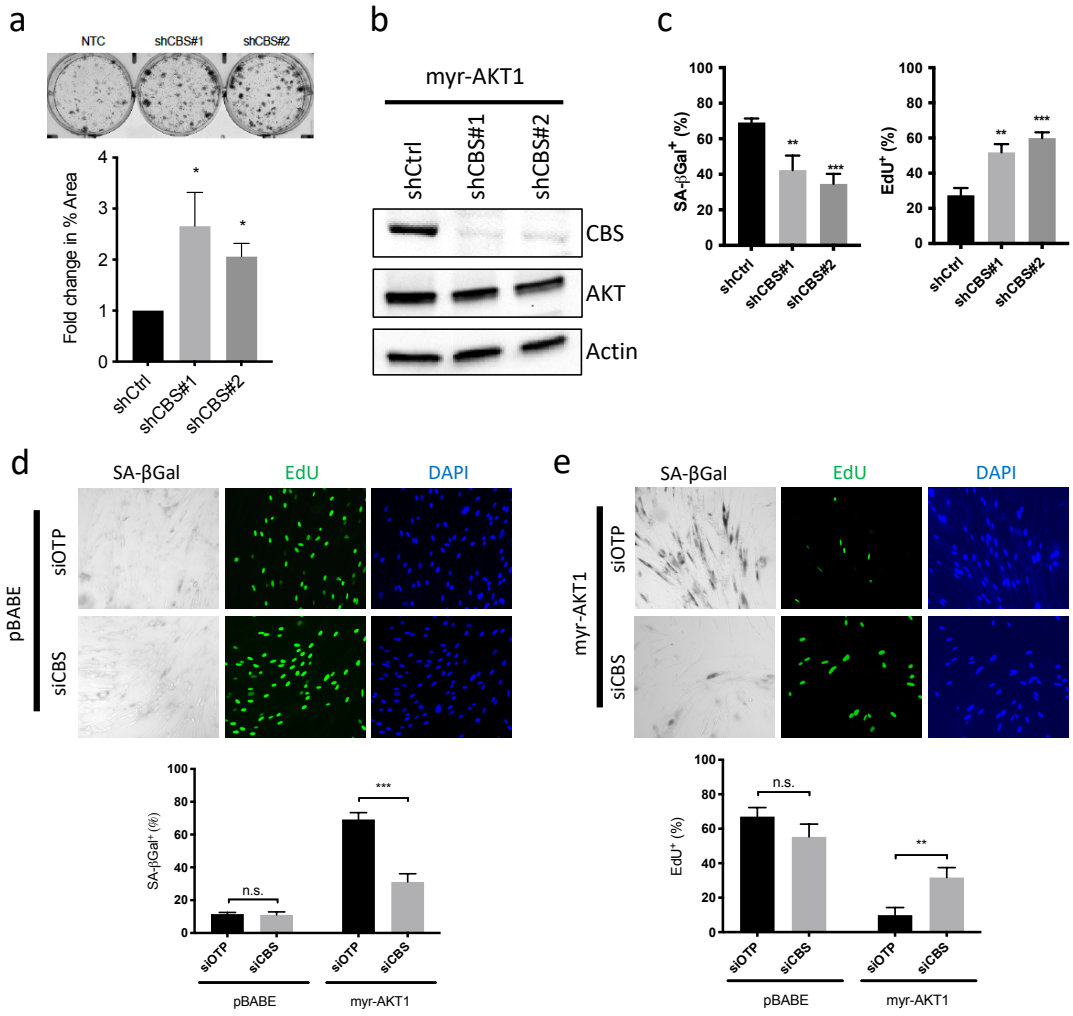


Figure 4.1.3 CBS knockdown promotes escape from AKT-induced senescence.

(a) The clonogenic growth was assessed by colony formation assays 19 d post-transduction and fold change in confluency over NTC control was quantified (b) Western blotting of CBS and total AKT. Actin was probed as a loading control. (c) SA-βGal and EdU staining quantification. IMR-90 cells were transduced with pBabe or myrAKT1. Cells were then transfected with either CBS siRNA (siCBS) or control siRNA (siOTP) and analysed on day 5 post-transfection. (d,e) Quantification of percentage of cells with positive staining for SA-βGal activity and EdU. Data are expressed as mean ± SEM. n = 3 experiments. (*) $P < 0.05$; (**) $P < 0.01$; (***) $P < 0.001$; (****) $P < 0.0001$ by one-way *ANOVA* as compared with control.

To test the impact of CBS depletion in another oncogenic context, we examined colony formation in BJ-TERT cells expressing constitutively active RAS. Different from the pro-proliferative effect of CBS depletion in AIS cells, knockdown of CBS in RIS cells, the metabolic phenotypes of which are subtly different despite similarities (Chapter 3.3.4), did not affect colony formation, suggesting a specific regulatory role of CBS in AIS but not in RIS (Fig. 4.1.4a-b).

The senescence-associated secretory phenotype (SASP) is a hallmark of senescence that distinguishes it from quiescence and terminal differentiation [344] [7]. The SASP comprises a secretome of growth factors, cytokines, and proteolytic enzymes, which are known to vary depending on the mode of senescence induction (reviewed in Chapter 1.1.2). We therefore examined whether CBS deficiency affected the SASP in AIS cells. Interestingly, knockdown of CBS did not significantly change the mRNA expression level of several key SASP-related genes which have been reported to be up-regulated in AIS cells [34] (Fig. 4.1.4c). This finding highlights the ability to separate the effects of CBS knockdown on different hallmarks, and the potential to manipulate cell cycle progression in senescent cells without changing the SASP and inflammation. Upregulation of tumour suppressor p53 and its downstream target p21 mediated the cell cycle arrest during AIS (reviewed in Chapter 1.1.1). Interestingly, depletion of CBS did not affect the activity of p53/p21 tumour suppressor axis in AIS cells. Nevertheless, the total Retinoblastoma protein (Rb) (Fig. 4.1.4d), a key regulator of the G1/S phase transition, and its inhibitory phosphorylation at serine 807/811 were markedly suppressed in AIS and partially rescued upon CBS knockdown. Similar changes were also observed in the protein expression level of cyclin A, which mediates S to G2/M phase cell cycle progression and Lamin B1 which regulates chromatin changes and gene expression during OIS (Fig. 4.1.4d). These results demonstrate CBS regulates the intrinsic cell cycle arrest associated with senescence but not the major SASP components, evidenced by the suppression of the RB pathway but non-significantly changed IL-1/6/8 signalling. Together, our findings reinforce the concept that the different aspects of senescence phenotype are interconnected and also separately controlled by distinct regulatory networks. Manipulating senescent cells by targeting specific aspects of the network may generate different phenotypes that sequentially affect other aspects of

the senescence program and modulate the interaction with the surrounding microenvironment.

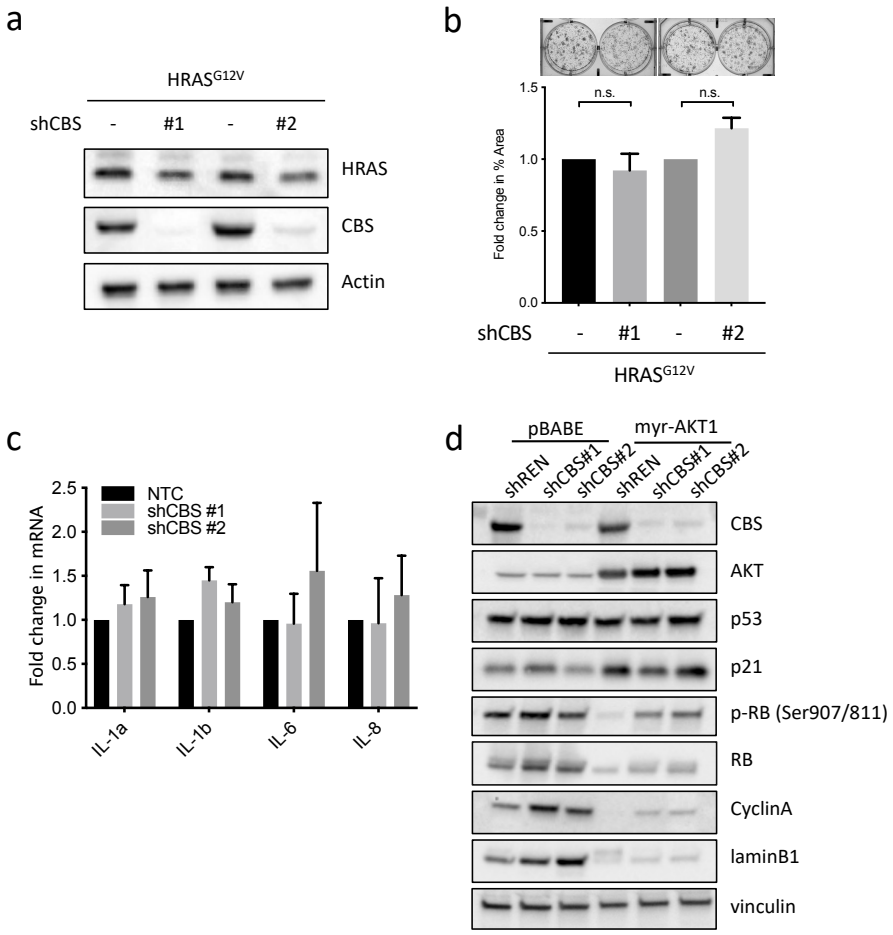


Figure 4.1.4 Characterisation of SASP and expression of key senescence markers in CBS-depleted AIS cells.

(a,b) BJ-TERT cells with doxycycline-inducible CBS shRNA were transduced with pBabe-HRAS^{G12V} and analysed on day 14 post-transduction (a) Western blotting of HRAS and CBS. Actin was probed as a loading control. (b) Clonogenic growth was assessed by colony formation assays after 19 d and fold change over the group without DOX treatment in confluency was quantified. (c) BJ-TERT cells expressing myrAKT1 were transduced with pGIPz-shCBS or control vector pGIPz-NTC. The mRNA expression levels of key SASP factors were measured on day 14 Post-transduction by qPCR. The data were normalised with Actin control and expressed as fold change over shNTC control. Data are expressed as mean ± SEM. n = 3 experiments. (d) BJ-TERT cells with doxycycline-inducible shCBS or control shREN were transduced with pBabe or myr-AKT1, treated with doxycycline (1ug/ml) on day 5 post-transduction and analysed on day 14 post-transduction. Western blotting of CBS, AKT and key senescence markers. Vinculin was probed as a loading control.

4.3.2 Upregulated transsulfuration and transmethylation pathways in AIS cells are not affected by CBS deficiency.

As reviewed in Chapter 1.3, CBS converts homocysteine to cystathionine, regulates homocysteine metabolism and contributes to H_2S and GSH biosynthesis. It is a key enzyme modulating both the transmethylation pathway and the transsulfuration pathway (Fig. 4.2.1a). Mitochondrial-localized CBS promotes production of H_2S which enhances mitochondrial electron transport and bioenergetics by donating electrons at complex II. To determine the activity of the transmethylation and transsulfuration pathways during AIS, we performed a comprehensive assessment of the thiol redox metabolome using LC/MS after thiol derivatization with N-Ethylmaleimide (NEM) [291]. Compared to control proliferating cells, AIS cells exhibited the increased abundance of hcy, methionine, SAM and SAH, indicating upregulation of transmethylation pathway activity in AIS (Fig. 4.2.1b-e). Meanwhile, cysteine levels were also increased in AIS cells, suggesting AKT activation stimulated the transsulfuration pathway (Fig. 4.2.1f). Cysteine is the limiting substrate for the synthesis of GSH, a key cellular antioxidant, and H_2S. Activation of the transsulfuration pathway can increase the synthesis of GSH and H_2S. Indeed, AIS cells exhibited a much higher level of GSH (Fig. 4.2.1g), the GSH synthesis precursor γ-Glu-Cys (Fig. 4.2.1h) and the GSH degradation product Cys-Gly (Fig. 4.2.1i) than control proliferating cells. This provides an important anti-oxidant mechanism against AKT-induced oxidative stress and preserves intracellular redox balance during AIS maintenance.

To examine whether CBS affects transmethylation and transsulfuration pathway activity during AIS, we performed LC-MS in BJ-TERT cells expressing myr-AKT1 without or with CBS depletion. Compared to AIS cells with intact CBS, an elevated hcy level in CBS-depleted cells confirmed that loss of CBS causes upstream substrate hcy accumulation (Fig. 4.2.1b). Homocysteine feeds into both the transmethylation and transsulfuration pathways. It can be metabolized either through the transmethylation pathway to generate methionine or through the transsulfuration pathway to produce cysteine. Knockdown of CBS did not significantly affect the abundance of the metabolites in the transsulfuration pathway including cysteine (Fig. 4.2.1f), GSH (Fig. 4.2.1g) and H_2S (Fig. 4.2.1j), suggesting loss of CBS does not affect the transsulfuration pathway activity in

AIS. Interestingly, the metabolites in the transmethylation pathway including methionine (Fig. 4.2.1c), SAM (Fig. 4.2.1d) and SAH (Fig. 4.2.1e) were also unaffected by CBS knockdown. Therefore, we did not detect a significant change in the metabolic activity of transsulfuration pathway and transmethylation pathway upon CBS depletion in AIS cells. Together, while increased CBS levels and transsulfuration and transmethylation pathway activity are associated with AIS, escape from senescence due to CBS deficiency is not related to these two metabolic pathways.

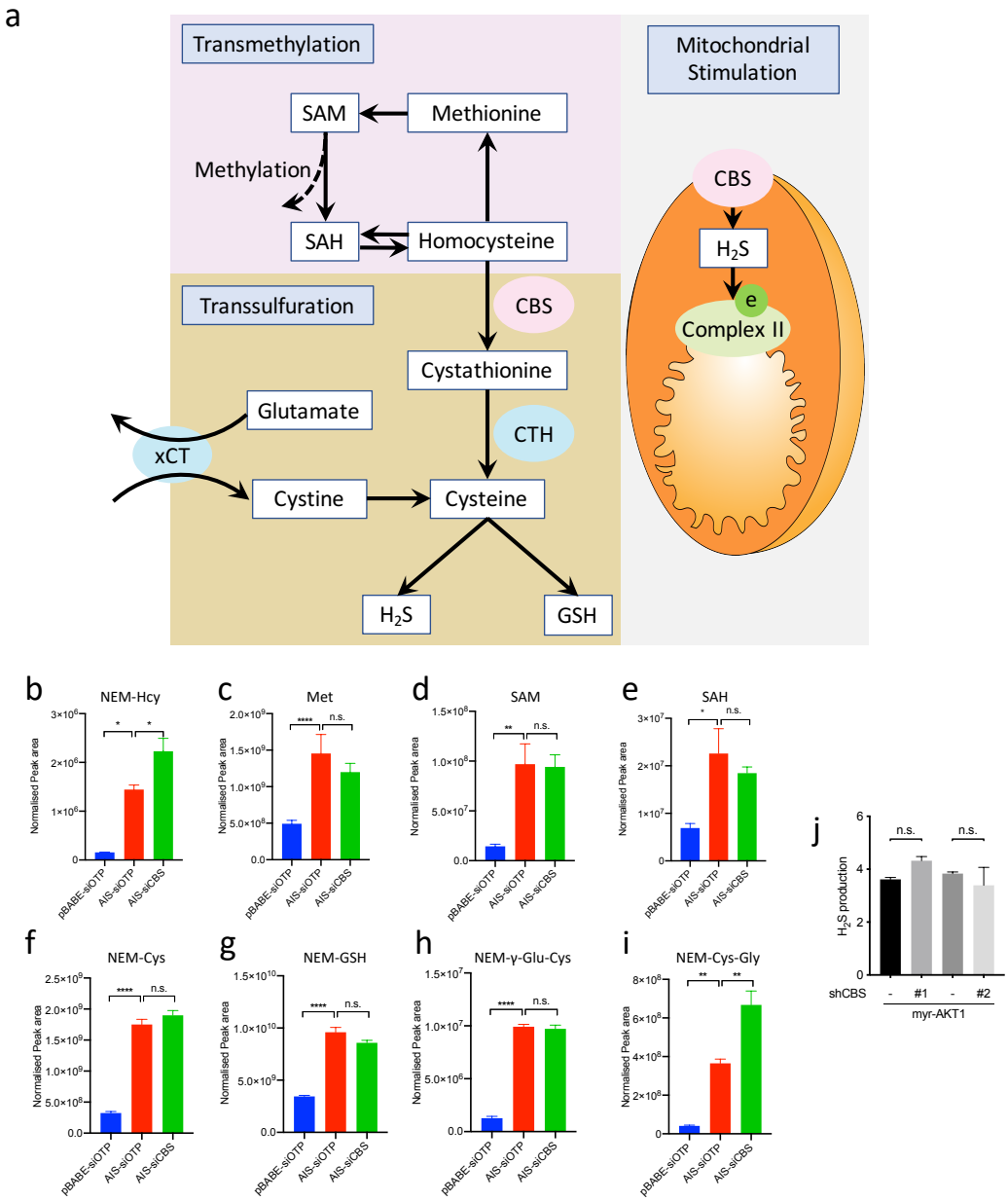


Figure 4.2.1 Upregulated transsulfuration and transmethylation pathways in AIS cells were not affected by CBS deficiency.

(a) Schematic diagram illustrating that the cytoplasmic localized CBS regulates transmethylation, transsulfuration metabolic pathways and mitochondrial localized CBS regulates electron transport chain. (b-i) BJ-TERT cells were transduced with pBabe or myrAKT1. Four days later Cells were then transfected with either CBS siRNA (siCBS) or control siRNA (siOTP) and analysed on day 6 post-transfection. The thiol redox metabolome was assessed by targeted LC/MC. The comparative levels of (b) NEM-Hcy, (c) Met, (d) SAM, (e) SAH, (f) NEM-Cys, (g) NEM-GSH, (h) NEM-γ-Glu-Cys and (i) NEM-Cys-Gly were shown, the y-axis represents normalized metabolite peak area. Data are expressed as mean ± SEM. n = 4. (j) BJ-TERT cells with doxycycline-inducible shCBS were transduced with pBabe or myr-AKT1, treated with doxycycline (1ug/ml) on day 5 post-transduction and analysed on day 14 post-transduction. H_2S production rate was measured by AzMC. Data are expressed as mean ± SEM. n = 3 experiments. (*) $P < 0.05$; (**) $P < 0.01$; (****) $P < 0.0001$ by one-way *ANOVA* as compared with control. Metabolite preparation and GC/MS were performed with assistance of Dr. Darren Creek and Ms. Dovile Anderson from Monash Institute of Pharmaceutical Sciences, Australia. Metabolite sample preparation, validation and data analysis were performed by me.

To explore whether other metabolic functions of CBS are associated with maintenance of senescence, we systematically assessed the metabolic alterations following CBS depletion using a GC/MS-based untargeted metabolomics approach. BJ-T cells transfected with empty vector (proliferating), myr-AKT1 (AIS) and myr-AKT1+shCBS (AIS escaped) displayed distinct metabolic profiles, as indicated by 3D-Principle Component Analysis (3D-PCA) and a metabolite heatmap (Fig. 4.2.2a-b). Compared to normal proliferating cells, AIS cells exhibited a hyperactive metabolic phenotype, which was detailed in Chapter 3. Consistent with the LC/MS result (Fig.4.2.1b), Hcy abundance was found to be statistically higher in CBS-depleted cells than AIS cells (Fig. 4.2.2c). Together with the pathway enrichment analysis identifying Hcy degradation as a significantly altered pathway (Fig. 4.2.2d), these results firmly support loss of CBS causes upstream substrate hcy perturbation and accumulation. Interestingly, the top pathway re-wired in CBS-depleted cells compared to AIS cells is the malate-aspartate shuttle (Fig 4.2.2d), which is the key mechanism for transporting NADH from the cytoplasm to the mitochondria in order to support oxidative phosphorylation. These data implicate that loss of CBS may alter the mitochondrial function of AIS cells. Therefore, to further explore the mechanism by which CBS depletion mediated AIS escape, we focused on investigating the metabolic rewiring of Hcy metabolism and mitochondrial function.

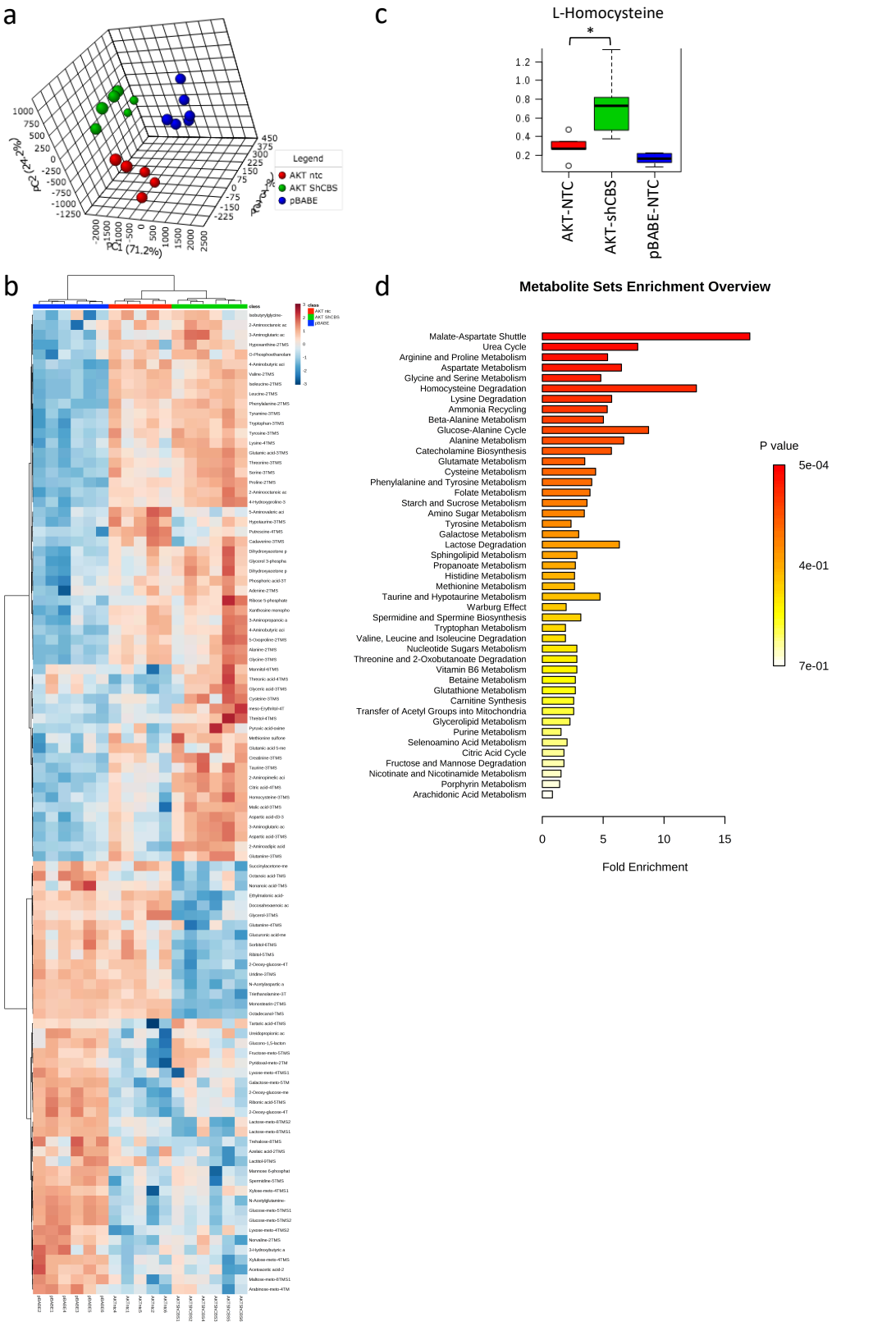


Figure 4.2.2 Depletion of CBS induced metabolic reprogramming in AIS cells.

BJ-TERT cells transduced with pBabe or myr-AKT1 were transduced with pGIPz-shCBS (AKT-shCBS) or control vector pGIPz-NTC (AKT-NTC, pBabe-NTC) on day 6 post-transduction of myr-AKT1 and the metabolic profiling was performed on day 14 post-transduction by GC/MS. N=6 in both pBabe-NTC and

AKT-shCBS groups and N=5 in AKT-NTC group. The sample AIS-1 was excluded due to a technical issue in sample processing. (a) 3D-PCA plot, x, y and z-axis represent individual principle component. (b) Heatmap of metabolites in proliferating (pBabe-NTC), AIS (AKT-NTC) and shCBS-AIS (AKT-shCBS) cells. (c) Relative level of Homocysteine after normalisation with global metabolites median. Data were expressed as mean ± SEM. (*) $P < 0.05$. (d) Metabolite Sets Enrichment Analysis for AIS-shCBS comparing with AIS cells. Metabolite preparation and GC/MS were performed with assistance of Metabolomics Australia. Metabolite samples were prepared and validated by me. Data analysis was performed with the assistance of Dr. David de Souza from Metabolomics Australia.

4.3.3 CBS depletion reduces DNA and histone methylation in AIS cells.

Extensive epigenetic changes including alterations in the chromatin landscape and DNA and histone modifications occur during OIS, which are thought to be important for maintaining a persistent senescence phenotype (reviewed in Chapter 1.1.3). Since the abundance of Hcy and the ratio of SAM: SAH affect methylation capacity [345], and Hcy accumulation exhibited by AIS cells was further up-regulated upon CBS depletion (Fig. 4.2.1b), we therefore tested whether changes in methylation occurred during AIS. 5-Methyl Cytosine (5-MC) immunofluorescent staining was performed to evaluate DNA methylation status. Overexpression of AKT reduced 5-MC staining which was further suppressed by shRNA-mediated CBS knockdown, whereas overexpression of CBS reversed these effects (Fig. 4.3a-b). In addition to the decrease in DNA methylation, CBS knockdown downregulated trimethylation of lysine 27 of Histone 3 (H3K27me3) and symmetrical dimethylation on Arginine-3 of histone H4 Histone 4 Arginine 3 (H4R3me2S) in AIS cells (Fig. 4.3c). Together, these results indicate that AIS maintenance is accompanied by reduced DNA and histone methylation.

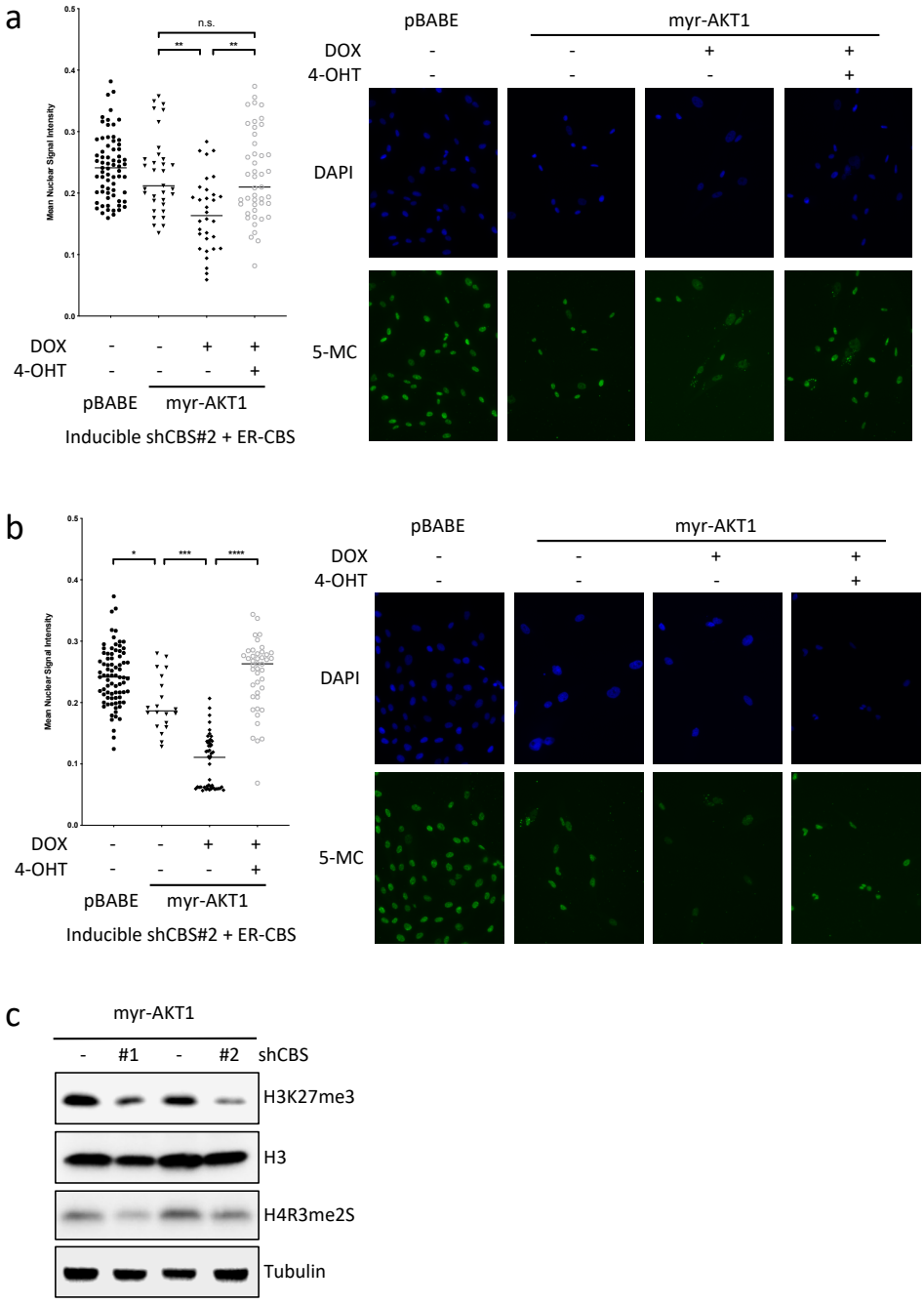


Figure 4.3 CBS-depleted AIS cells are associated with DNA and histone demethylation.

BJ-TERT cells with doxycycline-inducible CBS shRNA and 4-OHT-inducible CBS overexpression were transduced with pBabe or myr-AKT1. Five days later cells were treated with doxycycline (1ug/ml) and/or 4-OHT (20nM) and analysed 14 days post-transduction. DNA methylation in AIS cells expressing doxycycline-inducible CBS shRNA#1 (a) or CBS shRNA#2 (b) were assessed by 5-Methylcytosine (5-MC) immunofluorescent staining, DAPI (Blue); 5-MC (Green). (c) Western blotting showing H3K27me3, H3 and H4R3me2S expression. Tubulin was probed as a loading control. Experiments were performed at least 3 times. Data from one representative experiment was shown are expressed as mean ± SEM. (*) $P < 0.05$; (**) $P < 0.01$; (***) $P < 0.001$; (****) $P < 0.0001$ by one-way *ANOVA* compared with control.

4.3.4 CBS deficiency releases oxidative stress in AIS cells.

In addition to regulating the transsulfuration and transmethylation pathways, CBS also localizes in mitochondria and regulates mitochondrial function and ATP synthesis via H_2S (Fig 4.2.1a). At low concentrations, H_2S acts as a mitochondrial electron donor to mitochondrial complex II, resulting in bioenergetic stimulation [337]. At higher concentrations, H_2S acts as a mitochondrial poison via the inhibition of cytochrome c oxidase in mitochondrial complex IV [346] [347]. Mitochondrial dysfunction is a hallmark of senescence (reviewed in Chapter 1.2.1). Consistently, OIS cells exhibit mitochondrial hyperactivation which results in ROS accumulation (Fig 3.5). Moreover, we recently identified two genes involved in superoxide production, including NADPH oxidase organizer 1 (NOXO1) and NADPH oxidase 5 (NOX5) (Chapter 3.3.6), in a genome-wide RNAi screen to overcome AIS-induced cell cycle arrest in human fibroblasts [348], supporting the concept that ROS is required for AIS maintenance. We therefore evaluated the functional significance of CBS in mitochondrial dysfunction and the regulation of ROS production in AIS. Immunofluorescence staining of AIS cells using mitoTracker showed an increased intensity compared to that of proliferating cells, suggesting an increase of mitochondrial abundance in AIS cells. Although the majority of CBS localized in cytoplasm, CBS staining was detected in the vicinity of mitochondria (Fig. 4.4a). By Western blotting analysis of the cytoplasmic and mitochondrial fractions of control and AKT expressing cells, we showed CBS expression in mitochondria was increased in AIS cells (Fig. 4.4b). To specifically determine the role of CBS up-regulation in regulating mitochondrial function, we examined the oxidative phosphorylation status of AIS cells with and without CBS knockdown by measuring the oxygen consumption rate (OCR) using a Seahorse extracellular flux analyser (Fig. 4.4c-e). Hyperactivation of AKT markedly elevated OCR (Fig. 4.4d), which is consistent with upregulated mitochondrial respiration and energy production in OIS cells reported in chapter 3 (Fig. 3.5) and by other groups [186] [185]. Furthermore, siRNA-mediated CBS knockdown significantly suppressed basal OCR and ATP production (Fig. 4.4d and 4.4e), suggesting that CBS is required for enhanced oxidative phosphorylation in AIS cells and CBS deficiency reduces mitochondrial bioenergetics.

As mitochondria are the major intracellular organelle of ROS production and impaired mitochondrial function may disrupt mitochondrial redox homeostasis [349], we hypothesised that CBS deficiency-induced AIS escape could be due to the reversal of ROS-induced stress. We therefore measured mitochondrial superoxide production and cytoplasmic ROS by flow cytometric analysis using MitoSOX and H2DCFDH-DA, respectively. AKT hyperactivation promoted both mitochondrial and cytoplasmic ROS accumulation, confirming enhanced oxidative stress in AIS (Fig. 4.4f-g). Most importantly, CBS knockdown decreased ROS levels in AIS cells (Fig. 4.4f-g). Together, these results support the hypothesis that AIS is associated with increased oxidative phosphorylation and oxidative stress, and CBS loss can cause AIS escape by alleviating mitochondrial hyperactivation and ROS overproduction.

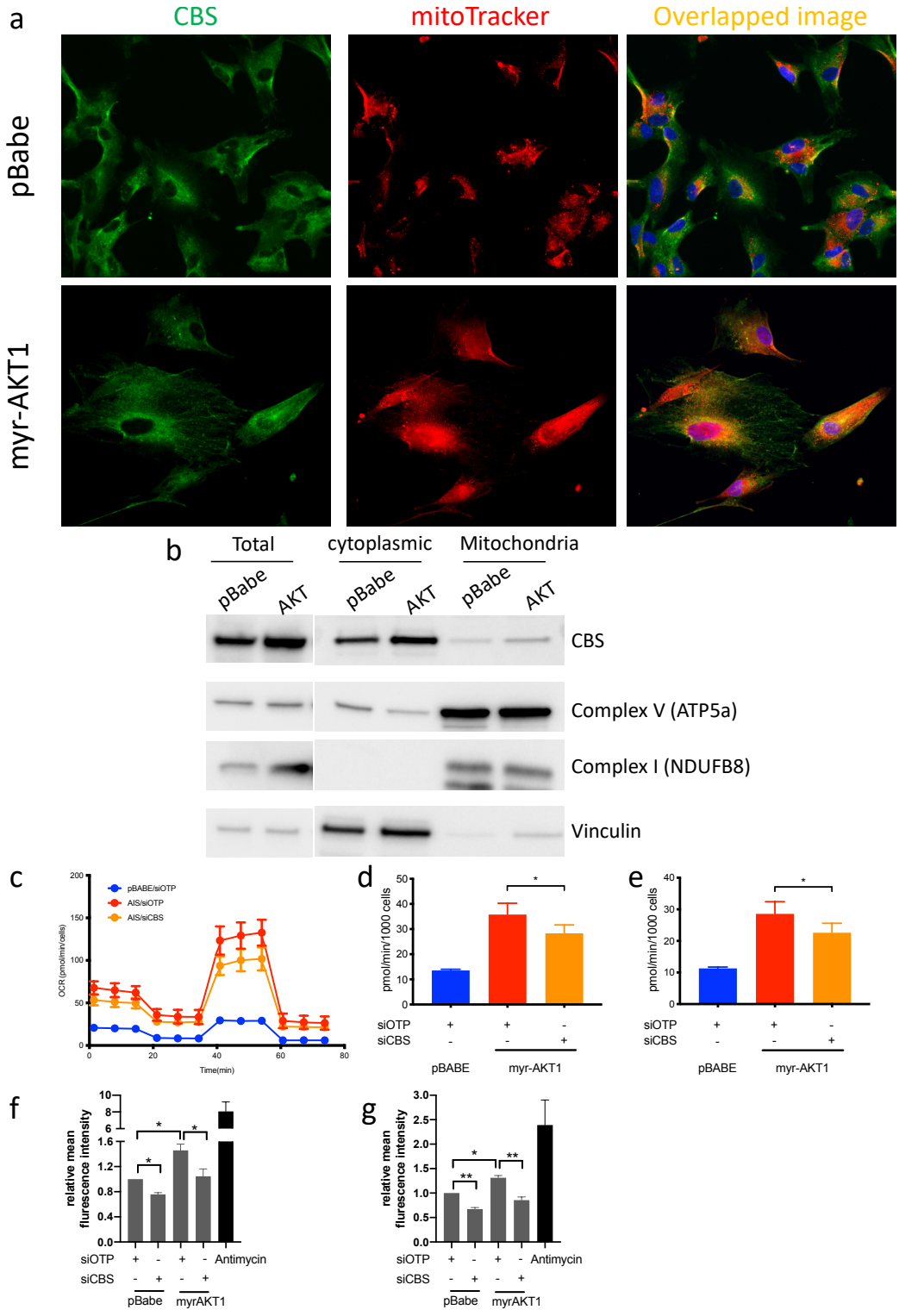


Figure 4.4 CBS deficiency reduced oxidative stress in AIS cells.

(a,b) BJ-TERT cells were transduced with pBabe or myr-AKT1 and assessed on day 10 post-transduction. (a) Immunofluorescent staining showing CBS (Green) and mitochondria (Red). (b) Western blotting showing CBS expression in total protein lysates, cytoplasm and mitochondria. ATP5a and NDUFB8 were used as the markers of mitochondria and Vinculin was a marker of cytoplasm and a loading control for total proteins. BJ-TERT cells were transduced with pBabe or myrAKT1. Four days later Cells were then

transfected with either CBS siRNA (siCBS) or control siRNA (siOTP) and analysed on day 6 post-transfection. (c) change of Oxygen Consumption Rate (OCR) with time, (d) basal OCR (e) ATP production rate was assessed using Seahorse XF96 Extracellular Flux Analyser. (f) The mitochondrial superoxide production using MitoSOX and (g) the cytoplasmic ROS using H2DCFDH-DA were measured by flow cytometric analysis. Data are expressed as mean ± SEM. n = 3 experiments. (*) $P < 0.05$; (**) $P < 0.01$ by one-way *ANOVA* as compared with control.

4.3.5 CBS deficiency induces transcriptional changes in AIS cells

We have identified alleviation of ROS-induced stress caused by CBS depletion as one possible mechanism of AIS escape. To further investigate the mechanisms of CBS-dependent maintenance, we systematically characterised the transcriptomic changes associated with CBS depletion-induced AIS escape, RNA-seq was performed on BJ-TERT cells expressing myr-AKT1 plus either CBS shRNA, TP53 shRNA or control shRNA. As we previously showed that loss of p53 restores cell cycle progression of AIS cells [34], we used shTP53 as a positive control to investigate the transcriptional regulation during AIS escape. BJ-TERT fibroblasts were transduced with myr-AKT1 or pBABE-empty vector, followed by transfection with shRNAs targeting CBS or p53 or non-targeting control. Cells were sorted at day 9 post-transduction and harvested at day 14 (Fig. 4.5.1a). Multidimensional scaling (MDS) analysis of gene signature similarity demonstrated that knockdown of CBS or TP53 in AIS cells induces distinct transcriptional alterations (Fig. 4.5.1b). This indicates that CBS loss-induced AIS escape is distinct from p53 loss-induced escape, consistent with our finding that CBS loss-induced AIS escape is p53 independent. Furthermore, differential gene expression analysis of AIS cells depleted of CBS compared with control revealed 431 genes significantly up-regulated (adjusted p-value < 0.05, $Log_2FC > 1$) and 243 genes significantly down-regulated (adjusted p-value < 0.05, $Log_2FC < -1$) (Fig. 4.5.1c). Gene set enrichment analysis (GSEA) using the hallmark gene sets in Molecular Signatures Database (MSigDB) identified several pathways significantly altered in CBS-depleted AIS cells compared to control (Fig. 4.5.1d and 4.5.1e). Interestingly, GSEA showed downregulation of the RAS signalling pathway in CBS-depleted AIS cells, which is opposite to the finding that NF1 depletion activated RAS signalling during AIS and caused its escape [121]. However, we evaluated RAS signalling using Western blotting (Fig. 4.5.1f) and showed that, instead, it was activated upon CBS depletion, evidenced by the up-regulation of p-ERK (S202/T204). Similarly, GSEA also showed downregulation of MYC targets following CBS knockdown. However, Western blotting showed a moderate increase of MYC protein in CBS-depleted AIS cells compared to control (Fig. 4.5.1g). These findings highlight the importance of understanding the role of post-transcriptional regulation on protein expression and activity during AIS and its escape, which remains to be further investigated. Furthermore, a panel of genes

which were the top candidates significantly regulated by shCBS in RNAseq analysis were selected and further examined using qPCR (Fig. 4.5.1h). Most of the genes encode extracellular matrix (ECM) proteins. qPCR analysis showed these genes were down-regulated in AIS cells but up-regulated upon CBS knockdown (Fig. 4.5.1i), suggesting that CBS depletion in fibroblasts may potentially impact the stromal microenvironment through secretion of ECM components.

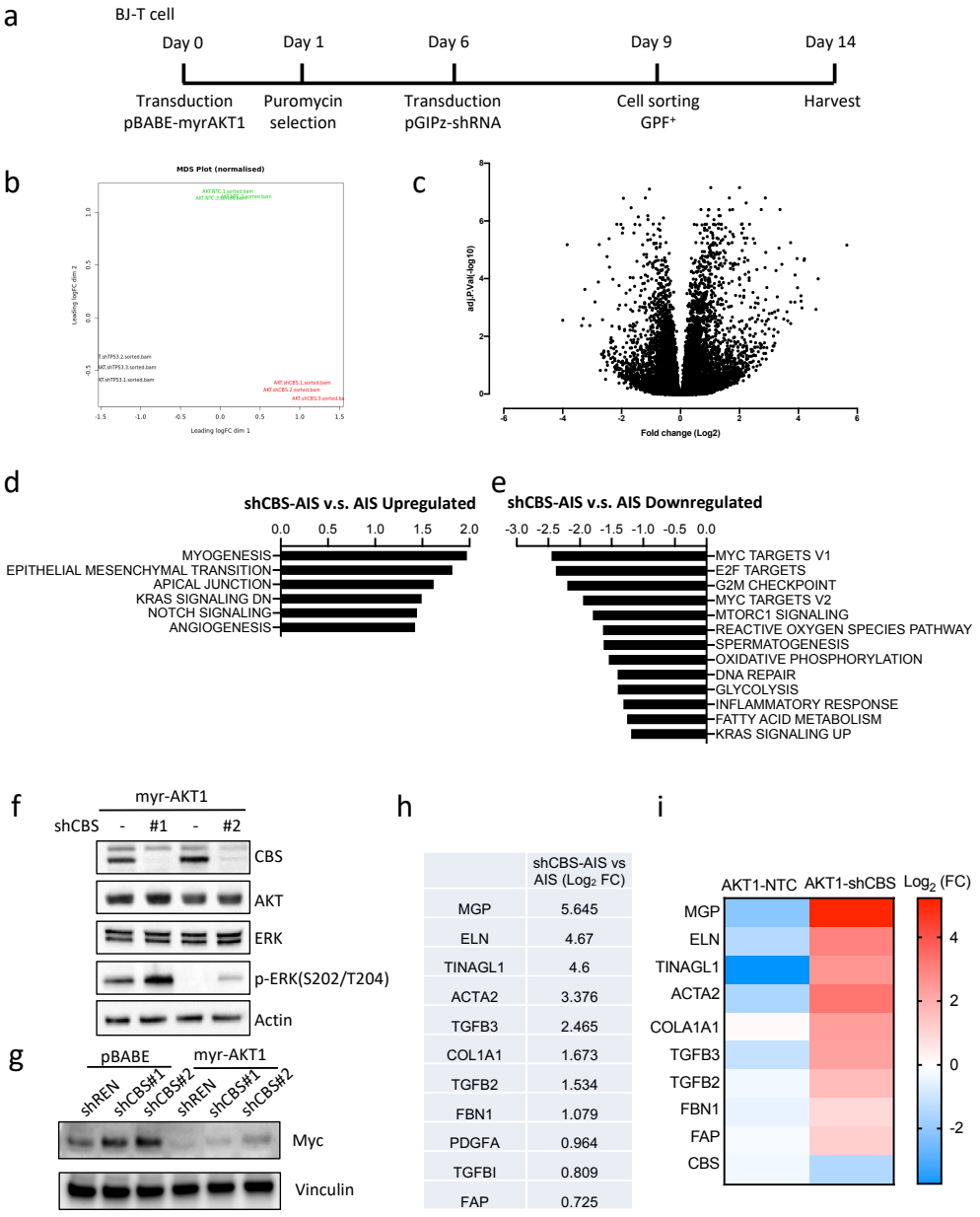


Figure 4.5.1 Inhibition of CBS induces transcriptional changes in AIS cells

BJ-TERT cells transduced with pBabe or myr-AKT1 were transduced with pGIPZ-shCBS (AKT-shCBS) or control vector pGIPZ-NTC (AKT-NTC, pBabe-NTC) on day 6 post-transduction of myr-AKT1 and the transcription profiling was performed on day 14 post-transduction by RNAseq. (a) Timeline representation of the experimental design. (b) The Multidimensional scaling (MDS) plot analysis. (c) Differentially expressed genes between AIS-shCBS with AIS cells plotted in Log_2 Fold Change versus $–Log_{10}$ adjusted p-value. Significantly (d) up- or (e) down-regulated gene sets identified through Gene Set Enrichment Analysis using the MSigDB hallmark gene set. (f) Western blotting showing CBS, AKT, ERK and p-ERK (S202/t204) expression in AIS cells (myr-AKT1) expressing doxycycline-inducible CBS shRNA#1 or #2. Actin was probed as a loading control. (g) Western blotting showing myc expression in proliferating cells (pBabe) or AIS cells expressing shREN control or CBS shRNAs. Vinculin was probed as a loading control. (h, i) The differential mRNA expression of genes encoding extracellular matrix proteins in shCBS-AIS cells compared to AIS cells measured by RNAseq (g) and validated by qRT-PCR (h). n = 3 experiments. cDNA library preparation and RNA sequencing were performed with assistance of by the Molecular Genomics Core Facility (PMCC, Australia). RNA samples were prepared and validated by me. Bioinformatics analysis was performed with the assistance of Dr. Anna Trigos and Dr. Maria Doyle (PMCC, Australia).

Taken together, we propose a model of how CBS contributes to AIS maintenance (Fig.4.5.2). Cells undergoing AIS cells are characterized by increased expression/activity of metabolic enzymes including increased activity of the transsulfuration pathway to enhance GSH biosynthesis. Furthermore, we propose that mitochondria-localized CBS stimulates oxidative phosphorylation through H_2S production and contributes to ROS overproduction. CBS depletion reduces mitochondrial bioenergetic production and oxidative stress in AIS cells. Simultaneously, CBS knockdown causes Hcy accumulation and transmethylation pathway perturbation, accompanied by global DNA/histone demethylation and altered transcriptome. How these epigenetic and genetic changes contribute to CBS deficiency-meditated AIS escape remains unknown.

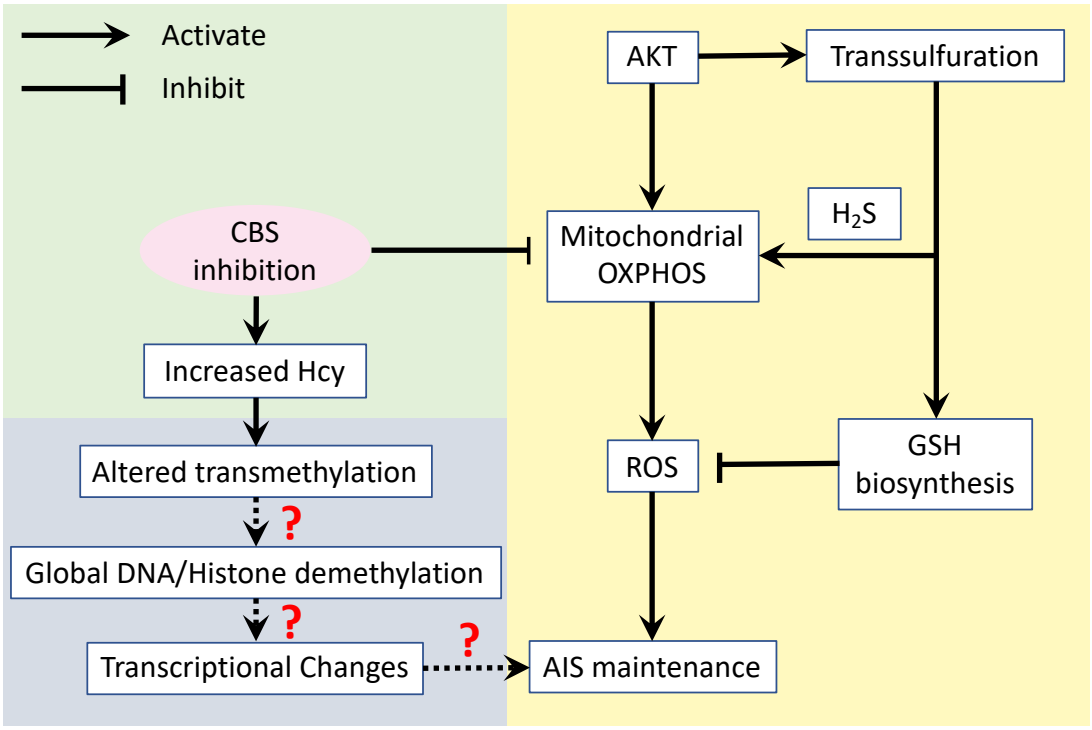


Figure 4.5.2 A model proposed for the role of CBS in AIS maintenance and CBS-depletion mediated AIS escape.

Metabolic alterations during AIS program are shown in the yellow region. The impact of CBS on AIS is demonstrated in the green region. The hypothesises remain to be answered are shown in the grey region.

4.3.6 Loss of CBS synergises with PI3K pathway activation to promote gastric tumour initiation.

We have demonstrated that CBS plays a critical regulatory role in controlling AIS in normal cells with its loss resulting in the release of the senescence brake engaged by AKT oncogenic hyperactivation. We therefore hypothesised that CBS inhibition could cooperate with activation of the PI3K/AKT/mTORC1 pathway to stimulate tumourigenesis. We chose to test this hypothesis in gastric cancer cells, as our TCGA data analysis demonstrated that PI3K/AKT/mTORC1 signalling pathway aberrations occur in 37% (509/1365) of gastric cancer with PIK3CA (20%) and PTEN (11%) aberrations being the most common genetic alterations (Fig. 4.6.1a). CBS deletion was found in 3% (46/1330) of gastric cancers including 35 cases that co-occur with hyperactive PI3K/AKT/mTORC1 signalling. In addition, previous studies have demonstrated CBS deficiency in human gastric cancer cells with hypermethylation at the CBS promoter region, implicating loss of CBS through epigenetic regulation in gastric cancer [281]. Consistent with these findings, TCGA data analysis across different types of tumours indicated CBS deep deletions (7/440) and mutations (6/440) in gastric cancer (Fig. 4.6.1b) when comparing tumour (N=415) to adjacent normal tissue (N=34), CBS mRNA level was also significantly decreased (Fig. 4.6.1c) in tumours compared to normal tissue. To confirm the loss of CBS in human gastric cancer, we evaluated the CBS protein expression level in paired samples of gastric tumours and corresponding adjacent non-cancerous mucosa from 62 gastric cancer patients in a tissue microarray using immunofluorescent staining (Fig. 4.6.1d). The cytosolic CBS protein expression level as measured by fluorescence intensity was significantly down-regulated in tumour tissues compared to adjacent normal gastric tissues. We then examined CBS protein expression in six gastric cancer cell lines compared with an SV40-transformed gastric epithelial cell line GES-1 which was derived from fetal stomach mucosa and was non-tumourigenic in nude mice [270]. Compared to gastric epithelial cells, CBS expression was markedly decreased in all gastric cancer cell lines while the other intracellular L-cysteine supplying enzymes CTH and xCT expression levels were reciprocally upregulated together with an increase of AKT phosphorylation in AGS, Hs746T, KATO III and NCI-N87 gastric cancer cell lines (Fig. 4.6.1e). To confirm whether the loss of CBS expression in gastric cancer is associated with hypermethylation of the CBS promoter, we examined CBS promoter

methylation status in gastric cancer cell lines using Methylation-specific PCR (Fig. 4.6.1f). We showed that the CBS promoter was methylated in all six gastric cancer cell lines tested, and half of them displayed a complete absence of unmethylated CBS promoter (SNU-1, NCI-N87 and AGS) that was associated with lack of CBS transcription. To test whether CBS expression could be rescued by inhibiting promoter hypermethylation, we treated cells with Azacitidine, a DNA methyltransferase (DNMT)-inhibiting cytosine nucleoside analogue (Fig. 4.6.1g). Azacitidine treatment of the gastric cancer cell lines significantly up-regulated CBS mRNA expression in two of the cell lines, whereby SNU-1 cells showed a >50-fold increase. Whether Azacitidine treatment could restore CBS protein expression remains to be investigated.

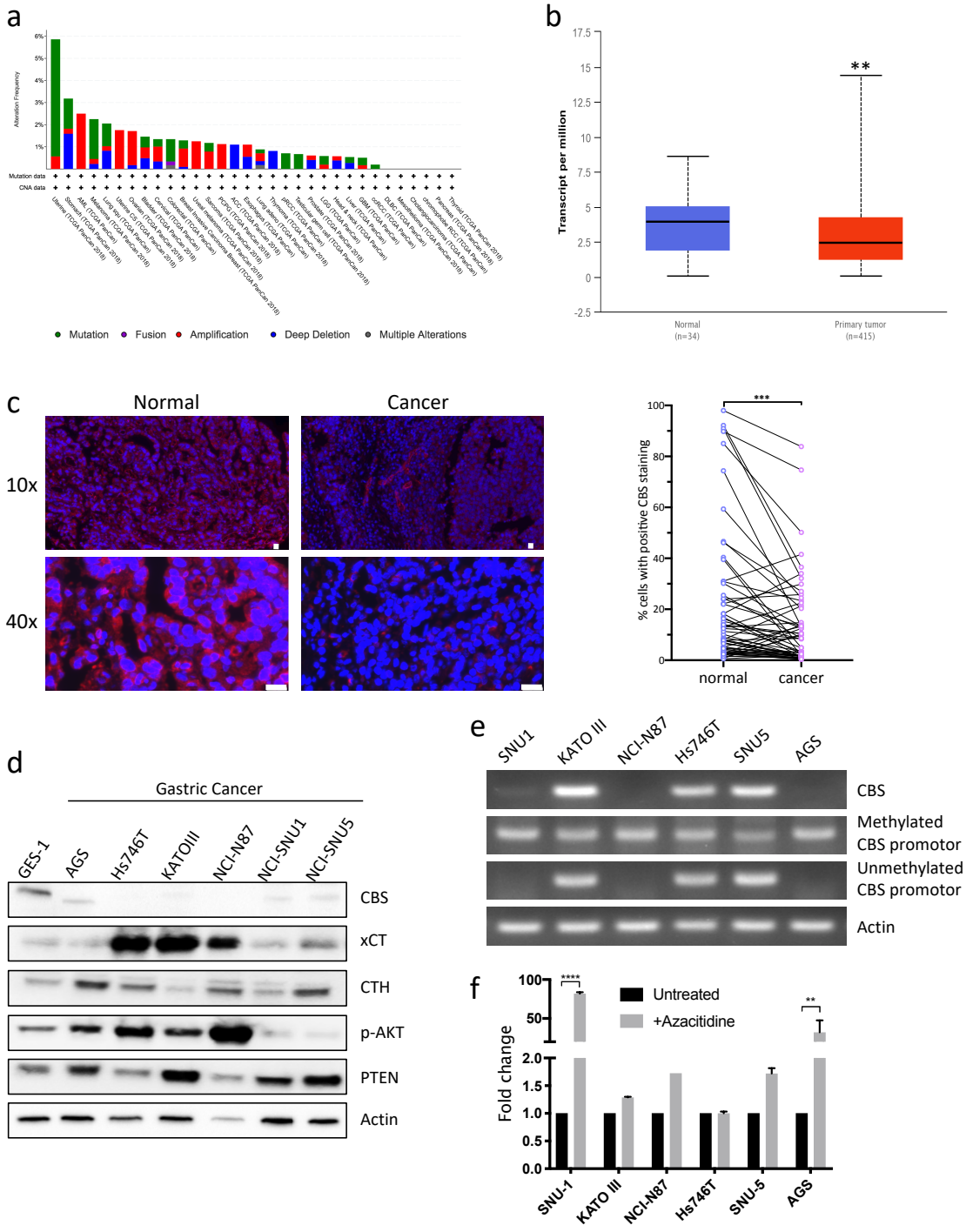


Figure 4.6.1 loss of CBS synergises with activated PI3K pathway to promote gastric tumorigenesis.

TCGA data analysis showing (a) the genetic alteration frequency of CBS in different types of cancer; and (b) CBS mRNA expression in Stomach Adenocarcinoma (STAD) based on tumour or normal adjacent tissues. p=0.0058. (c) Gastric cancer patient tissue microarray was assessed by immunofluorescent staining of CBS (red) and counterstained for the nucleus (DAPI, blue). The representative images of normal or cancer tissues from one gastric cancer patient were shown, Scale bars = 50 μm. The percentage of cytosolic CBS-positive cells in the tumour or adjacent normal tissues from 62 patients were shown. (***) $P < 0.001$ by one-way *ANOVA* as compared with normal gastric tissues. (d) Western blotting showing the expression of CBS, xCT, CTH, p-AKT(S473) and PTEN in One gastric epithelial cell line (GES-1) and six gastric cancer cell lines. Actin was probed as a loading control. (e) The CBS promoter region of six gastric cancer

cell lines was assessed by methylation-specific PCR followed by Agarose gel electrophoresis. Actin was used as a loading control (f) Gastric cancer cells were treated with 2uM Azacitidine for 2 hours and their CBS expression changes were analysed by qRT-PCR, fold changes were quantified against untreated controls. Data are expressed as mean ± SEM. n = 3 experiments.; (****) $P < 0.0001$. Tissue microarray image analysis was conducted with the assistance of A/Prof. Sarah Ellis and her team from Centre for Advanced Histology and Microscopy, PMCC, Australia.

To further test if CBS loss cooperates with PI3K/AKT/mTORC1 hyperactivation in gastric cancer oncogenesis, we transduced myr-AKT1 and CBS shRNA into GES1 cells (Fig. 4.6.2a). Unlike h-TERT-immortalized human fibroblasts (BJ-TERT) where senescence was induced by myr-AKT1 overexpression, AKT1 hyperactivation in the SV40-transformed GES1 cells was sufficient to promote anchorage-independent growth. This finding is consistent with a previous report that OIS cannot be initiated in GES-1 cells by HRAS overexpression, possibly due to the presence of SV40 large T antigen, and RAS-induced transformation was observed [350]. Furthermore, anchorage-independent growth of myr-AKT1-expressing GES-1 cells was significantly enhanced by CBS depletion. CBS depletion also significantly enhanced anchorage-independent growth of GES1 cells with PTEN knockout using CRISPR/Cas9 Gene Knockout technology (Fig. 4.6.2b). Taken together, these results support the concept that CBS loss can cooperate with PI3K/AKT/mTORC1 activation to drive transformation and CBS acts as a tumour suppressor during gastric transformation.

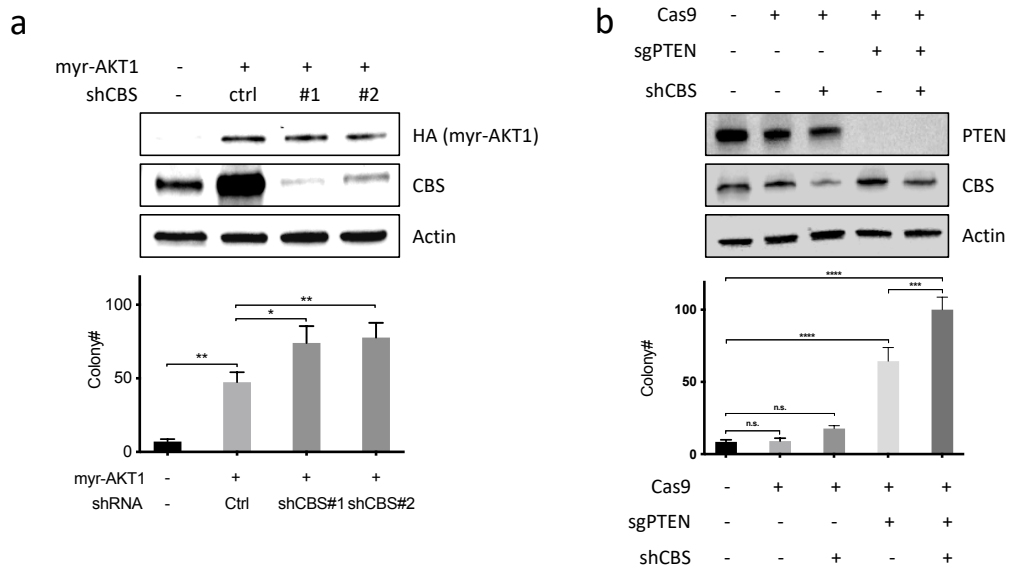


Figure 4.6.2 loss of CBS promotes the transformation of gastric cancer.

(a) Gastric epithelial cells GES-1 were stably transfected with Tetracycline-inducible myr-AKT1 and pGIPZ-shCBS or control pGIPZ-NTC. Cells were plated in soft agar and treated with tetracycline (1ug/mL). After 21 days, the colonies formed were counted. Western blotting showing HA-tagged myr-AKT1 and CBS. Actin was probed as a loading control. (b) GES-1 cells with PTEN knockout by CRISP or Cad9 control were transduced with pGIPZ-shCBS or control pGIPZ-NTC. The anchorage-independent growth was assessed by soft agar colony formation assay. Western blotting showing PTEN and CBS expression. Actin was probed as a loading control. Data are expressed as mean ± SEM. n = 3 experiments. (*) $P < 0.05$; (**) $P < 0.01$; (***) $P < 0.001$; (****) $P < 0.0001$ by one-way *ANOVA* as compared with control.

4.3.7 CBS restoration suppresses gastric tumour growth through H_2S

To further investigate the functional significance of CBS in gastric cancer, we transduced AGS gastric cancer cells harbouring CBS loss with doxycycline-inducible wild type CBS^{wt} or an inactive CBS^{I278T} mutant which is the most frequently observed mutation in cancer cells and exhibits only ~2.4% of the enzyme activity of wild type CBS [351]. Treatment of AGS cells with 0.2ug/ml doxycycline restored CBS^{wt} and CBS^{I278T} protein expression to a level comparable to that of GES1 gastric epithelial cells (Fig. 4.7.1a). A significant increase in CBS function as indicated by increased H_2S production was also observed in cells expressing CBS^{wt} but not in cells expressing CBS^{I278T}, confirming the loss of CBS function in CBS mutant cells (Fig. 4.7.1b). CBS^{wt} restoration significantly suppressed AGS cell proliferation, clonogenic and anchorage-independent growth in soft agar whereas such effects were not observed in the CBS^{I278T}-expressing cells (Fig. 4.7.1c-e). Elevated SA-βGal and reduced EdU staining in CBS^{wt} restored cells suggested that AGS cells underwent a senescence-like phenotype mediated by CBS restoration (Fig. 4.7.1f). Similar results were obtained in an additional two gastric cancer cell lines with hyperactivated AKT, NCI-N87 (Fig. 4.7.2a-c) and Hs-746t (Fig. 4.7.2d-f).

To further test the impact of CBS restoration *in vivo*, we then transplanted AGS cells expressing doxycycline-inducible CBS into immunocompromised mice. Administration of doxycycline in the food and water was carried out for experimental groups when tumours were palpable (38 days post-transplantation), and tumour volumes were measured three-time weekly until reaching the 1000 mm^3 ethical limit. Whereas no significant difference in tumour volume at the endpoint was observed between the untreated parental control group and the group expressing inactive CBS^{I278T}, induction of CBS^{wt} significantly suppressed gastric tumour growth (Fig. 4.7.1g). Likewise, CBS^{wt} but not inactive CBS^{I278T} restoration significantly extended the lifespan of the mice transplanted with AGS cells (Fig. 4.7.1h).

Since the restoration of CBS^{wt} increased H_2S production (4.7.1b) but not GSH biosynthesis (Fig 4.7.1i), we hypothesised that CBS-mediated anti-proliferation occurs through H_2S production. While the treatment of GYY-4137, an H_2S slow-releasing

compound, did not affect the proliferation of non-transformed GES-1 gastric epithelial cells (Fig. 4.7.1j), it significantly decreased proliferation of AGS cancer cells with reduced CBS expression (Fig. 4.7.1k). Consistently, GYY-4137 suppressed the clonogenic growth of AGS cells in a dose-dependent manner (Fig. 4.7.1l). Taken together, our results indicate that CBS performs a tumour-suppressive role in gastric cancer cells through up-regulation of H_2S, and the H_2S slow-releasing compound GYY-4137 may represent a potential therapeutic option in gastric cancer. Whether GYY-4137 treatment can induce gastric cancer cell senescence remains to be investigated.

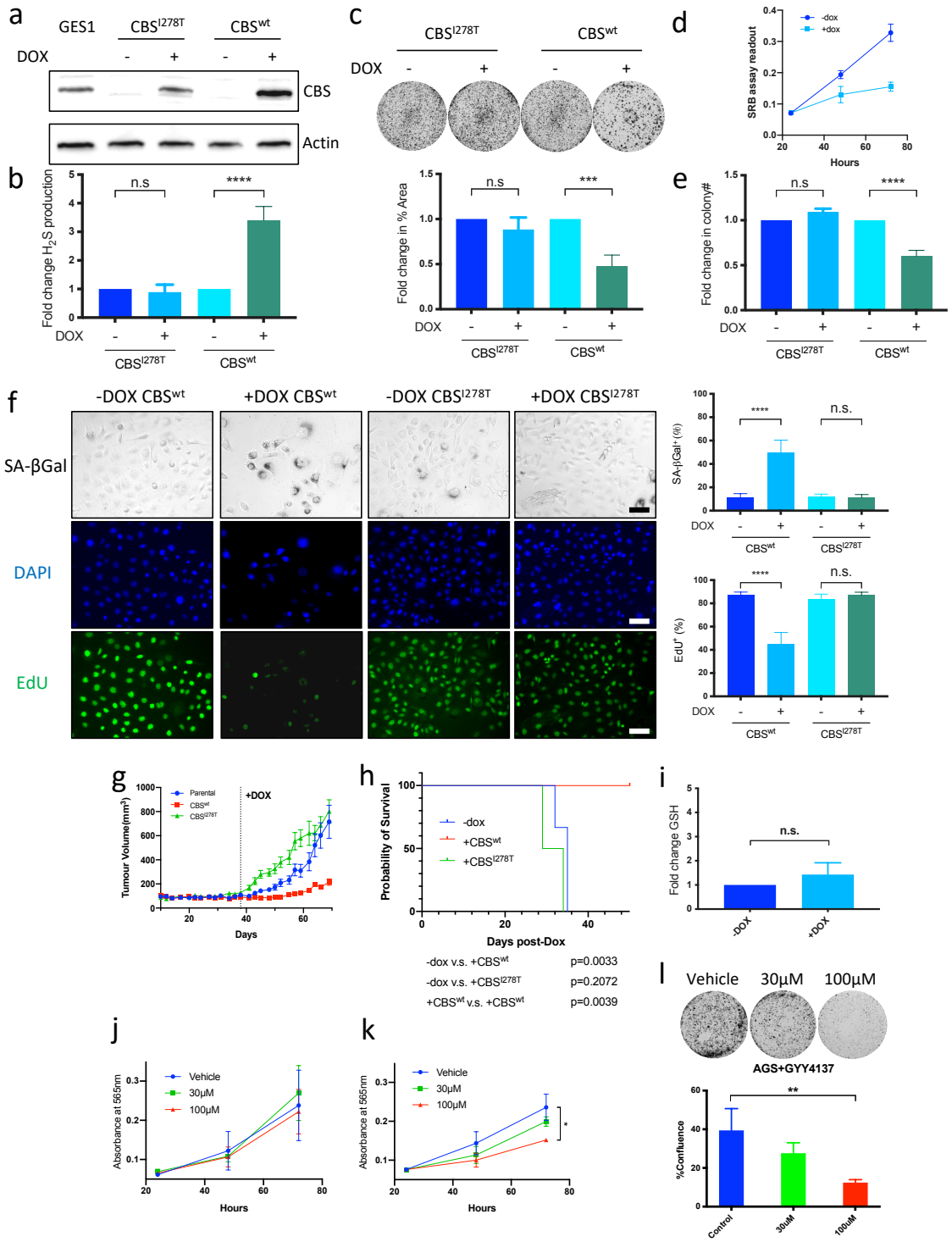


Figure 4.7.1 Restoration of CBS expression in AGS gastric cancer cells suppresses tumour growth through H_2S.

(a-f) AGS gastric cancer cells were stably transfected with doxycycline-inducible CBS^{I278T} or CBS^{wt}. (a) Western blotting showing CBS expression after treatment with doxycycline (200ng/mL) for 10 days. Actin was probed as a loading control (b) H_2S production assay, fold changes in concentration were quantified against the group without doxycycline treatment. (c) The colony formation assays after treatment with doxycycline (200ng/mL) for 10 days. Fold changes in %Area were quantified against the group without doxycycline treatment. (d) The proliferation assays using SRB staining (e) The soft agar anchorage-

independent growth assay, and (f) The SA-βGal and EdU staining assays. (g,h) AGS gastric cancer cells expressing doxycycline-inducible CBS^{I278T} or CBS^{wt} were subcutaneously implanted in BALB/c nude mice. On day 38 post-implantation, mice were supplied with water containing 0.2% doxycycline hyclate and 600mg Doxycycline/kg food. (g) Tumour volume measured in AGS xenografts. Data are expressed as mean ± SEM. n=6 mice per group. (h) The Kaplan-Meier survival curve. Data were analysed by a log-rank (Mantel–Cox) test. (i) GSH level was measured after doxycycline treatment for 7 days. (j) GES-1 and (k) AGS were treated with GYY-4137at 30 uM or 100 uM at different time points as indicated. Cell proliferation was measured by SRB staining. (l) AGS cells were treated with GYY-4137 for 9 days. The clonogenic growth was assessed by colony formation assays. Data are expressed as mean ± SEM. n = 3 experiments. (*) $P < 0.05$; (**) $P < 0.01$; (***) $P < 0.001$; (****) $P < 0.0001$ by either student's t-test or one-way *ANOVA* as compared with control.

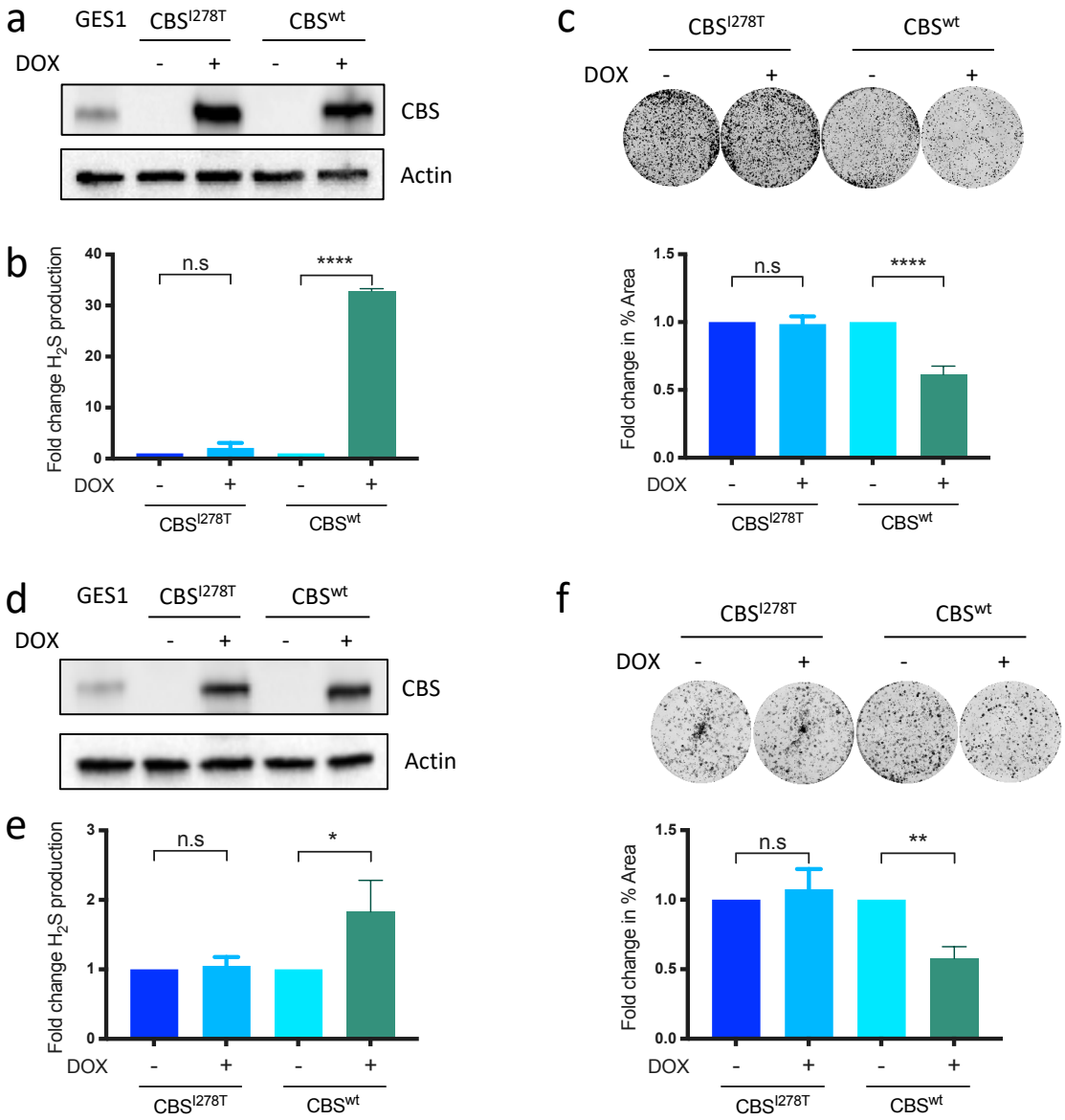


Figure 4.7.2 Restoration of CBS expression in NCI-N87 and Hs 746T gastric cancer cell lines suppresses gastric tumour growth.

(a-c) Gastric cancer cell lines NCI-N87 and (d-f) Hs 746T were stably transfected with doxycycline-inducible CBS^{I278T} or CBS^{wt}. (a, d) Western blotting showing CBS expression. Actin was probed as a loading control. (b, e) H_2S production assays, and (c, f) colony formation assays after treatment with doxycycline (200ng/mL) for 10 days. Data are expressed as mean ± SEM. n = 3 experiments. (*) $P < 0.05$; (**) $P < 0.01$; (***) $P < 0.001$; (****) $P < 0.0001$ by either student's t-test or one-way *ANOVA* as compared with control.

4.4 Discussion

4.4.1 Upregulation of transsulfuration pathway functions as an AIS-specific antioxidant response

Oxidative stress is a key feature of AKT-induced senescence (AIS). Our results demonstrate increased oxygen consumption and ROS accumulation in AIS cells, consistent with others' findings [352]. ROS triggers DNA damage and proliferative arrest in RIS cells [199]. The role of ROS in AIS has not been well studied but was reported to sensitize AIS cells to ROS-induced cell death [352]. We recently showed in a genome-wide RNAi screen that depletion of two genes involved in superoxide production, NADPH oxidase organizer 1 (NOXO1) and NADPH oxidase 5 (NOX5), caused AIS escape, supporting the concept that oxidative stress is required for AIS maintenance. However, excessive ROS can induce cell death and therefore while the increase of ROS is important for AIS maintenance, it must be buffered to prevent ROS-induced cell death.

In this study, we demonstrate that the induction of AIS is characterised by activation of the transsulfuration pathway resulting in an increase of GSH synthesis. We propose that increased levels of GSH (Fig. 4.2.1j) provide the buffering of ROS levels required to maintain intracellular redox balance during AIS maintenance. Upregulation of CBS and CTH expression is associated with activation of the transsulfuration pathway in AIS. This finding is consistent with a previous study showing the transsulfuration pathway enzymes including CBS and CTH are positively regulated through the PI3K/AKT/Sp1 axis and therapeutic inhibition of PI3K pathway remarkably decreases CBS and CTH expression levels [353] [354]. The transsulfuration pathway is a major metabolic pathway that provides cysteine required for de novo GSH synthesis. Meanwhile, the intracellular cysteine level is also regulated by uptake of extracellular cystine through xCT, a cystine transporter encoded by SLC7A11. We found that overexpression of AKT1 markedly increased xCT protein expression, consistent with the increase of cystine uptake observed in AIS. In summary, based on these studies we propose that increased cysteine promotes GSH biosynthesis and enhances antioxidant capacity, which protects senescent cells from ROS-induced cell death.

Interestingly, the LC-MS metabolomics analysis indicated that loss of CBS overcomes AIS cell cycle arrest without affecting the transsulfuration pathway activity and GSH synthesis, indicating these pathways are critical for AIS induction but not maintenance. Instead, the increase in levels of the GSH degradation product, Cys-Gly suggests GSH metabolic turnover is increased. Future studies will examine this further through quantitative metabolomics using isotope labelled L-Cysteine [355]. This maintenance of the GSH pool is possibly achieved by the increase of CTH-mediated cysteine synthesis and xCT-mediated cystine uptake despite no observed changes in levels of CTH and xCT protein expression. A negative correlation between CBS and xCT expression has been recently reported to maintain intracellular cysteine level and sustain cell proliferation [356]. An increased CBS function was previously observed in CTH knockdown cells [357]. Therefore, although our data do not support a role for modulation of GSH synthesis in contributing to CBS deficiency-mediated AIS escape, we have uncovered a critical molecular mechanism which protects cells from oncogene-induced oxidative stress and might promote malignancy through enhancing GSH synthesis via activation of transsulfuration pathway.

Another key metabolite derived from the transsulfuration pathway is H_2S which can be synthesized from cysteine by CBS, CTH and 3-MST (reviewed in Chapter 1.3). We showed that AKT activation increased H_2S production. H_2S acts as a mitochondrial electron donor to mitochondrial complex II, resulting in bioenergetic stimulation [337]. Therefore, an increase in the level of H_2S may contribute to elevated mitochondrial respiration in AIS cells. Our results showed that loss of CBS significantly reduces mitochondrial oxygen consumption rate and ROS level. As CBS has been previously reported to be mitochondrial-localized and regulates mitochondrial function by H_2S production [338], this effect may be partially due to the reduction of mitochondrial H_2S production through depletion of mitochondrial localized CBS. To further support our findings that CBS depletion reduced mitochondrial oxidative stress through H_2S, further experiments could be performed to 1) directly examine mitochondrial H_2S production using the H_2S-specific dye to measure the mitochondrial fractions of CBS-depleted cells [358]; 2) evaluate whether AIS escape could be induced through selective targeting of an antioxidant to mitochondria [359].

Based on these results, we propose that impaired mitochondrial respiration and reduced oxidative stress contribute to CBS deficiency-mediated AIS escape. Taken together, it appears that the transsulfuration pathway functions as a double-edged sword by contributing to GSH biosynthesis to balance the oxidative stress occurring during AIS and, on the other hand, contributing to enhanced mitochondrial respiration and ROS generation through stimulation of H_2S production.

4.4.2 Metabolic reprogramming is coupled to epigenetic alterations during AIS and escape

Besides the transsulfuration pathway, we also found that AKT activated the methionine cycle which produces universal methyl donor SAM, and the metabolites SAH and Hcy. All these metabolites were shown to increase in AIS cells compared to proliferating cells. SAM is a universal methyl group donor for the transmethylation reaction and producing SAH. SAH is a potent and competitive inhibitor of the transmethylation reaction. Methylation capacity is determined by the amount and ratio of SAM/SAH [345]. We found that both the amounts of SAM and SAH and the ratio of SAM/SAH were increased in AIS cells. Unexpectedly, global DNA methylation was decreased during AIS possibly by increased SAH and therefore enhancing the inhibitory effect on methyltransferase activity. Indeed, a persistent increase in Hcy levels has been reported to cause a parallel elevation in intracellular SAH and lead to DNA hypomethylation through inactivation of methyltransferases [360]. It has been reported that OIS cells exhibit global DNA hypomethylation and focal hypermethylation [87] and this DNA methylation pattern was hypothesized to be retained during senescence escape and transformation. Following CBS knockdown in AIS cells, hcy accumulation was further enhanced while there were no significant changes of SAM and SAH abundance in CBS-depleted cells compared to AIS cells. Instead, global DNA methylation was further reduced upon CBS knockdown. It is not clear why the levels and/or ratios of SAM and SAH did not correlate with the methylation pattern. It is possible that the steady-state metabolomic analysis performed is not sensitive enough to detect the dynamic change of the metabolite, therefore not truly reflecting the change of the methylation reactions. These disparate findings will require further investigation, and future studies using bisulfite sequencing will facilitate understanding of genome-wide methylation with single nucleotide

resolution and identification of global hypomethylated and focal hypermethylated DNA regions.

Currently, we do not have evidence to support the impact of epigenetic reprogramming on the transcriptional profile of AIS cells and how this contributes to CBS deficiency-mediated AIS escape. However, we did observe substantial transcriptomic changes in both AIS cells and those depleted of CBS. Notably, although the major SASP factors including IL-1/6/8 were not significantly changed, a panel of genes encoding ECM proteins were up-regulated in AIS-escaped cells, suggesting that CBS depletion in human fibroblasts could potentially modify the interaction with the tissue microenvironment. The particular arrangement and orientation of ECM constituents have been suggested to play a critical role in tumour initiation [361]. Among the ECM protein encoding genes, Platelet-derived Growth Factor A (PDGFA) is of particular interest as it was suggested to be regulated by Hcy [362]. Zhang et al. reported that Hcy accumulation impaired DNMT1 activity, lead to DNA demethylation which promoted PDGFs expression and angiogenesis. In fact, GSEA of our RNA-seq data identified angiogenesis as a significantly up-regulated hallmark in CBS-depleted AIS cells (Fig. 4.5.1d), supporting the hypothesis that depletion of CBS may promote tumourigenesis through up-regulating ECM protein secretion and promoting angiogenesis. Further studies should start with testing whether CBS-depleted AIS cells show a decrease in DNMT1 expression or activity, and in parallel co-cultures with endothelial cells could be performed to assess angiogenic activity.

Certainly, there are many questions required to be addressed in order to understand how metabolic reprogramming influences epigenetic regulation during AIS and escape, such as how modulation of CBS levels alters methyltransferase activities, how the global and focal DNA and histone methylation patterns change in AIS and CBS-depleted cells and whether these epigenetic changes can impact gene expression profiles associated with AIS and AIS escape.

4.4.3 CBS is a novel tumour suppressor in gastric cancer

As we demonstrated previously [121] and in the current study, AIS acts as a critical brake against tumorigenesis and the senescence brake is disengaged during tumorigenesis.

Based on our observation that loss of CBS promotes escape from AIS in normal cells, we have also identified a potential tumour-suppressive role for CBS in gastric cancers harbouring PI3K/AKT pathway activation. We demonstrated the downregulation of CBS protein expression in gastric tumour tissues compared to adjacent normal tissues and in human gastric cancer cell lines compared to immortalised gastric epithelial cells. Loss of CBS cooperates with AKT signalling activation to promote gastric epithelial cell transformation. Overexpressing CBS in gastric cancer cells having negligible levels of CBS induced a senescence-like phenotype and inhibited tumour growth *in vivo*, supporting the important negative regulatory role of CBS in gastric tumour formation and progression. Moreover, we provided a preliminary finding that the epigenetic silencing of CBS can be reversed at the gene expression level through the treatment of hypomethylating agent Azacitidine, and highlighted such agents may potentially be utilised as gastric cancer therapeutics. In fact, a Phase I study of epigenetic priming with Azacitidine prior to chemotherapy for patients with gastric adenocarcinoma revealed significant clinical and epigenetic responses with an overall response rate of 67% [363]. The current study may provide mechanistic insight into the tumour inhibitory effect of Azacitidine in gastric cancer. Further evaluations could begin by evaluating whether Azacitidine restores CBS protein expression and H_2S-producing capacity in CBS-silenced gastric cancer cells.

The tumour suppressive role for CBS has been also reported in glioma [343] and hepatocellular carcinoma [364] while several recent publications reported CBS promoted tumour cell proliferation and survival by regulation of bioenergetic metabolism, antioxidant capacity, apoptosis-related pathways and tumour microenvironment in colon, ovarian and breast cancer cells [266]. Therefore, the effect of CBS is likely tumour type-specific and depends on the metabolic and genetic context of each type of tumour.

Furthermore, we also demonstrated that CBS overexpression in normal BJ-TERT fibroblasts is not sufficient to induce a senescence-like phenotype (Fig 4.1.2f-k), consistent with the concept that the induction of senescence-like phenotype in cancer cells may require hyperactivated PI3K/AKT pathway. Further evaluation of this

hypothesis could be addressed through the utilization of AKT inhibitors, such as MK-2206 [365], in CBS-restored gastric cancer cells which harnessed a hyperactivated PI3K/AKT signalling. This may also begin to answer the question of why the effect of CBS is tumour type-specific and depends on the metabolic and genetic context of each type of tumour.

We demonstrated that restoration of CBS expression inhibited gastric cancer cell proliferation by increasing H_2S production. The control group overexpressing CBS^{I278T}, which has been shown only having 2.4% of enzyme activity of CBS^{wt} [351], suggested the tumour inhibitory effect was possibly due to the lack of H_2S producing capacity of CBS. Further evaluation may be performed using H_SS scavengers in CBS^{WT} restored gastric cancer cells to confirm our findings [366]. In support of this concept, the tumour inhibitory effect was reproduced by treatment with exogenous H_2S using GYY4137. The induction of pro-apoptotic proteins and the impairment of gastric cancer cell metastasis and invasion upon NaHS treatment has been previously reported [367]. The toxic effect of H_2S was suggested to be mediated by inhibition of cytochrome C oxidase in mitochondrial complex IV [337]. Thus, CBS restoration or GYY-4137 treatment may inhibit cytochrome C oxidase and trigger cancer cell death and this should be investigated in future studies. It will be interesting to measure mitochondrial oxidative phosphorylation using the Seahorse assay to examine the effect of CBS overexpression and exogenous H_2S treatment in gastric cancer cells. In addition, it is still unknown whether loss of CBS promotes the transformation of gastric epithelial cells with AKT hyperactivation through the same mechanism employed by fibroblasts. Nevertheless, from our findings we propose a new therapeutic approach for gastric cancer treatment. We demonstrated that the tumour suppressive effect of CBS was recapitulated by treating with GYY4137, a slow releaser of H_2S. Thus, GYY4137 has the therapeutic potential as an anti-tumour agent in gastric cancer. Future studies will investigate the effectiveness of GYY4137 in vivo in comparison with re-constitution of CBS expression.

Although GSH is an important metabolite downstream of CBS, the effect of GSH during transformation or tumour suppression mediated by CBS has not been investigated. However, our data in fibroblasts demonstrated an inverse correlation between CBS

expression and CTH/xCT expression. Elevated CTH and xCT protein expression levels were detected in most of the gastric cancer cell lines showing loss of CBS, and further investigations will examine whether gastric cancer cells maintain cysteine levels and GSH synthesis in the absence of CBS. xCT has been reported to play an important role in the development of different cancer types [368]. Therefore, it will be important to further investigate the therapeutic potential of targeting the GSH synthesis pathway through xCT in gastric cancer.

In conclusion, our study has demonstrated that activation of the transsulfuration and transmethylation pathways play a critical and complex role during AIS maintenance (Table 4.1). In particular, the up-regulated transsulfuration pathway functions as a double-edged sword by contributing to GSH biosynthesis to balance the oxidative stress occurring during AIS, meanwhile, enhancing mitochondrial respiration and ROS generation through stimulation of H_2S production. Elevated transsulfuration may promote transformation if AIS cells disengage the proliferative brake. More importantly, we have identified CBS as a novel metabolic regulator of AIS which represents a new metabolic vulnerability of PI3K/AKT/mTORC1-driven cancers which can be therapeutically targeted.

4.5 Chapter 4 Table

Table 4.1 Summary of findings and future directions.

Metabolic alterations in AIS	Contribution of CBS for AIS metabolic alterations	CBS knockdown-mediated AIS escape	Key questions
Elevated Mitochondrial OXPHOS	Activates OXPHOS through mitochondria-localised CBS	Releases Mitochondrial OXPHOS moderately	Does mitochondrial H_2S decrease?
ROS overproduction	ROS overproduction due to mitochondrial dysfunction	Reduces oxidative stress moderately	Can treatment of anti-oxidants cause AIS escape?
Transsulfuration pathway activation	Activates transsulfuration pathway as anti-oxidant response	No significant change in transsulfuration	Does GSH turnover rate increase?
Transmethylation perturbation	CBS affects the abundance of metabolites in transmethylation.	Only further increases Hcy abundance	Does increased Hcy cause further transmethylation change?
Global hypomethylation/Altered Transcription	Unclear	Further decreased global hypomethylation	Does CBS knockdown cause global hypomethylation and the subsequent transcriptional changes?

CHAPTER 5 Overall discussion and future directions

5.1 Introduction

The studies presented in this thesis aimed to provide more understanding of how metabolism is reprogrammed during AIS and determine the essential metabolic regulators that can be targeted to treat PI3K/AKT/mTORC1-driven cancers. As detailed in Chapter 3, we characterized the global transcriptional and metabolic changes in AIS, demonstrating that AIS and RIS share common senescence hallmarks, including cell cycle arrest, SASP and metabolic reprogramming. Transcriptome profiling showed that unlike RIS cells showing upregulated RAS/ERK and MYC signalling, AIS cells exhibited downregulated RAS/ERK signalling and upregulated mTORC1 signalling, which may contribute to the distinct secretome of each type of OIS. Metabolic profiling demonstrated similar metabolic alterations underpinning AIS and RIS including enhanced glycolysis, TCA cycle and oxidative phosphorylation, reflecting common mechanisms to maximise energy production and generate oxidative stress that contributes to the persistence of the senescence phenotype and is required for AIS and RIS maintenance. Given that AIS and RIS exhibit shared and distinct molecular and metabolic signatures, we highlight that different mechanisms underpin senescence induced by different oncogenes, and suggest the possibility of targeting specific oncogene-driven tumours with potentially reduced side effects.

In Chapter 4, to gain more insight into the metabolic dependency of AIS, we characterized the role of CBS, an enzyme involved in transsulfuration and transmethylation metabolic pathways. Loss of CBS induced AIS escape but did not affect RIS escape, suggesting CBS-coordinated metabolic changes are specifically required for AIS maintenance. We demonstrated that the upregulation of CBS-mediated transsulfuration pathway activity is an AIS-specific antioxidant response. We also showed the metabolic reprogramming occurring during AIS is associated with epigenetic alterations, highlighting another layer of complexity regulating AIS that requires further exploration. Importantly, oxidative stress is essential for AIS maintenance, and CBS depletion causes AIS escape by suppressing mitochondrial oxidative phosphorylation, consistent with release of oxidative stress contributing to AIS escape and tumorigenesis.

We revealed a potential tumour suppressor role of CBS in gastric cancer cells displaying hyperactivated AKT. We also demonstrated *in vitro* and *in vivo* that loss of CBS synergises with PI3K pathway activation to promote gastric cancer initiation and restoration of CBS inhibits gastric tumour growth via H_2S. Our findings not only highlight the critical role of CBS in preventing malignant transformation in cells with activated PI3K/AKT but also the potential to harness key metabolic pathways therapeutically for treating PI3K/AKT-driven cancers. In this chapter, we will further discuss metabolic reprogramming in AIS as illustrated in Fig 5.1 and provide more insights into PI3K/AKT-induced senescence and tumorigenesis.

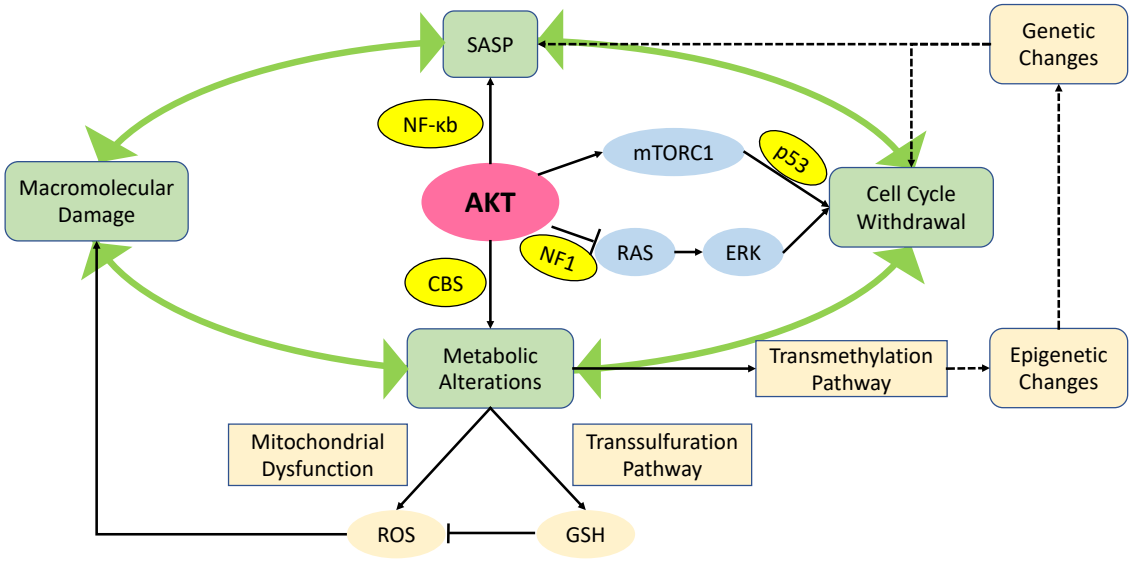


Figure 5.1 Essential pathways and regulators of AIS.

AIS is regulated by a network of four key effectors (Green), including cell cycle withdrawal, metabolic alterations, SASP and macromolecule damage. Disruption of any of these key effectors of AIS releases the senescence brake and facilitates transformation. Our extensive study of AIS has identified the key regulators of AIS (yellow) that impact on these effectors and the loss of which allow AIS escape. Cell cycle withdrawal is governed by the mTORC1-mediated p53 tumour suppressor network as well as the suppression of RAS/ERK signalling through NF1. SASP secretion during AIS is NF-κB pathway dependent. Activation of AKT stimulates the transmethylation pathway, which may contribute to epigenetic changes and subsequently transcriptional alterations in AIS (Dashed lines). Upregulation of CBS mediates metabolic alterations during AIS and functions as a double-edged sword. Upregulation of CBS during AIS induces mitochondrial dysfunction and ROS accumulation, which causes macromolecular damage. Paradoxically, upregulation of the transsulfuration pathway elevates GSH biosynthesis to protect from oxidative stress-induced cell death.

5.2 Transmethylation pathway and epigenetic modifications in AIS

In Chapter 4, we found that while increased CBS levels and transsulfuration and transmethylation pathway activity were associated with AIS establishment, escape from senescence due to CBS deficiency was instead due to its ability to regulate mitochondrial oxidative phosphorylation, suggesting that CBS plays complex roles during AIS initiation and maintenance. We provided substantial evidence supporting the role of CBS in AIS maintenance, and we hypothesise that CBS may be involved in AIS initiation through its ability to regulate transmethylation and the epigenome.

The transmethylation pathway is a critical metabolic pathway supplying methyl groups from the methyl donor SAM to sustain cellular methylation reactions. We demonstrated an altered abundance of SAM and the metabolite SAH during AIS, which could be associated with global demethylation and changes in the epigenome. Studies in Drosophila have demonstrated that accumulation of SAM and/or SAH and subsequent methylome alterations contribute to aging, a process known to be regulated by the epigenome [369] [370]. Furthermore, altering SAM and/or SAH abundance has been utilized in pro-senescence treatment against hepatocellular carcinoma. SAH accumulation caused by genetic depletion [371] or pharmacologic inhibition of SAH [372], or SAM treatment [373] perturbed the SAM/SAH ratio, thereby promoting cellular senescence. Therefore, modulation of the epigenome via targeting transmethylation pathway can be a potential therapeutic approach to treat aging and cancer.

Interestingly, despite a marked increase of SAM and SAH in AIS cells, no significant changes of SAM or SAH levels were detected in AIS escaped cells upon CBS depletion, suggesting that activation of the transmethylation pathway is more likely to contribute to AIS establishment rather than maintenance. In addition, global DNA methylation was decreased during AIS, which was further reduced in CBS-depleted cells. The greater decrease occurred without changes in transmethylation pathway activity, which is inconsistent with the link of the transmethylation pathway to DNA methylation status. Considering the complex role of CBS in regulating multiple metabolic pathways/processes, epigenetic modulation may be an indirect effect downstream of

CBS. Nevertheless, the PI3K/AKT/mTORC1 pathway has been reported to reduce global DNA methylation through phosphorylation of DNA methyltransferases to affect their stability [374], expression [375] and activity [376]. While the role of CBS in regulating the epigenetic changes occurring during AIS is still unclear, our data support a potential role for epigenetic regulation in AIS induction.

Future studies will be required to clarify the roles of transmethylation and epigenetic changes and their contribution to AIS initiation and maintenance. First, we will need to manipulate the activity of the transmethylation pathway through either genetic or pharmacological approaches prior to or after AKT hyperactivation. For example, we can test whether the methylome, transcriptome and chromatin structures change upon SAH accumulation caused by genetic depletion [371] or pharmacologic inhibition of SAHH [372], or SAM treatment [373]. Second, analysing the global methylation landscape using whole genome methylation profiling and assessing chromatin accessibility using Assay for Transposase-Accessible Chromatin using sequencing (ATAC-seq) will help determine whether these epigenetic changes correlate with gene expression and contribute to the senescence phenotype (Fig 5.1).

5.3 Oxidative stress, antioxidant defence and transsulfuration pathway in senescence

While a sub-lethal level of ROS is required for senescence induction, excessive oxidative stress can cause cell apoptosis [377]. However, a fascinating hallmark of OIS cells is that they have an antioxidant system to protect from oxidative stress-induced cell death [378], suggesting the critical importance of redox balance in senescence initiation and maintenance. Indeed, we demonstrated that oxidative stress is a key feature of AIS and identified activation of the transsulfuration pathway, a major metabolic pathway for glutathione (GSH) synthesis, as an AIS-specific antioxidant mechanism (Fig 5.1).

The molecular mechanisms of oxidative stress induced by activation of PI3K/AKT/mTORC1 signalling have been characterized including 1) by directly stimulating ROS-producing enzymes NADPH oxidases (NOXs) [379] [380]; 2) through direct phosphorylation of mitochondrial GSK-3β, reducing its activity and thus alleviating the negative regulation imposed on pyruvate dehydrogenase and α-ketoglutarate

dehydrogenase complexes [381] [382] [383]; and 3) promoting the production of prostaglandins (PGE2) from arachidonic acid by the cyclooxygenases 1 and 2 (COX-1 and COX-2) [384], which results in the generation of superoxide as a by-product [385]. During RIS, ROS induces DNA damage and proliferative arrest but during AIS ROS may induce damage to other macromolecules such as proteins and lipids [386] in the absence of DNA damage. To examine the significance of ROS in AIS initiation and maintenance, future studies will entail treating cells with antioxidant agents such as the glutathione biosynthesis inhibitor buthionine sulfoximine (BSO) [387], and assessing whether they prevent AIS onset or cause AIS escape.

Intriguingly, on the path to transformation, cells that have escaped AIS continue to rely on antioxidant pathways for survival. A study showed that inhibition of GSH biosynthesis in PIK3CA or AKT mutant MCF10A human breast epithelial cells significantly reduced anchorage-independent growth, a hallmark of cell transformation, supporting the dependence of oncogenic PI3K/AKT-mediated tumour initiation on GSH biosynthesis [388]. Furthermore, targeting GSH biosynthesis increased chemotherapy sensitivity in PIK3CA mutant but not wild type breast cancers, highlighting the significant anti-oxidative role PI3K/AKT pathway plays in cancer cell survival. Therefore, the dependence of PI3K/AKT-driven cancers on up-regulated transsulfuration pathway and GSH biosynthesis is a potential metabolic vulnerability that warrants further investigation.

5.4 PI3K/AKT/mTORC1 signalling pathway-induced senescence and cancer

Oncogenic PI3K/AKT signalling exerts tumour-promoting effects in transformed cells while PI3K/AKT-induced senescence plays a tumour-suppressing role in non-transformed cells. Similarly, mTOR inhibitors, such as everolimus and rapamycin, delay senescence and increase lifespan in aged models [34] [389] [218] [390] [391], and on the other hand, restore senescence in cancer cells [392]. The distinctive response to PI3K/AKT pathway activation and its inhibition in normal cells and transformed cells is thought to be dependent on the level of expression of the activated oncogene and the distinct cellular contexts. Increase of endogenous Ras expression enhanced proliferation of primary MEFs whereas ectopic expression of Ras-induced senescence. The study of Ras activation in mammary tumorigenesis provided *in vivo* evidence for different levels

of Ras activation/expression leading to different outcomes. Chodosh *et al* transplanted mammary epithelial cells with inducible Ras expression into mice and observed that high levels of activated Ras caused senescence in the mammary glands while low levels of activated Ras promoted the formation of mammary tumours [393]. The similar dose-effect of AKT activation was also observed in our study (Chapter 3). A more surprising observation was that pathways downstream of Ras were highly activated when mammary epithelial cells ultimately transformed compared to the initial stage of Ras activation. These findings suggested that 1) activated oncogene expressed at different levels may drive different cellular response and 2) the activity/expression level of oncogene is enhanced throughout cancer initiation and progress via a positive feedback loop to allow inactivation of the senescence program. In addition to the dose-dependent effect, cellular context, such as the distinct genetic backgrounds of normal cells and transformed cells, is another key factor to determine the cellular response to activated oncogenes. In normal cells, activation of PI3K/AKT triggers multiple signalling pathways which are essential for senescence initiation and maintenance and disruption of any these pathways allows bypass of OIS (Fig 5.1). Whether these senescence effector programs can be activated depends on the genetic or non-genetic intracellular environment and the intensity and combination of these effectors confer a complex and diverse nature of senescence [394]. We have reported multiple tumour suppressive pathways that can be targeted to release the senescent brake such as p53, CCAR1, FADD, and NF1 [121], and the current study provides additional mechanistic insights into the complexity of oncogene-induced senescence.

However, it should be noted that OIS is not the only barrier for oncogene-induced transformation and escape from OIS is not sufficient to confer susceptibility to oncogenic transformation. We demonstrated that loss of CBS in synergy with PI3K/AKT signalling activation contributed to transformation of gastric epithelium GES1 which harbour SV40 T gene integration, supporting the concept that multiple genetic alterations are required for ultimately oncogenic transformation. Therefore, a better understanding of the molecular basis for oncogene-induced senescence and the events that required for senescence escape and transformation, will facilitate new targets to

improve the clinical efficacy of PI3K/AKT targeted therapy and identify new therapeutic approaches to restore the senescence brake in oncogene-driven cancers.

The majority of the studies, including ours, investigating oncogene-induced senescence have been based on ectopic expression of an activated oncogene in an experimental cell model to induce senescence. To better understand the physiological relevance of OIS it is critical to establish appropriate mouse models to allow us to examine OIS induction and maintenance *in vivo* models and develop sensitive and reliable methods to detect senescent cells in human and mouse tissues. In chapter 1 we have reviewed several landmark studies conducted in different mouse models of OIS and development of non-germline transgenic mouse models using hydrodynamics-based transfection (reviewed in Chapter 1.1.5.2). Therefore, utilising this rapid and reliable non-viral approach to generate transgenic mouse models with activated PI3K/AKT signalling and develop sensitive luciferase or fluorescent protein reporters or probes enabling to real-time visualize senescence *in vivo* will be the priority of our future study of AKT-induced senescence and tumorigenesis.

5.5 Conclusion

The studies presented in this thesis have expanded our understanding of how AIS is initiated and maintained in non-transformed cells and how escaping AIS results in transformation. Through investigating the molecular mechanisms underlying AIS escape induced by CBS depletion, we have identified a critical role for metabolic reprogramming in AIS maintenance and escape. We have also uncovered a potential link between metabolic reprogramming, epigenetic alterations and redox balance in maintaining AIS that together impose a brake against transformation and tumourigenesis (Fig 5.1). These findings not only provide more understanding of PI3K/AKT-driven oncogenesis but also identify exciting potential for exploiting alterations in metabolism for cancer treatment. Further investigation of the molecular mechanisms underpinning PI3K/AKT/mTORC1-driven senescence and tumourigenesis will facilitate developing novel strategies to improve human health in aging, aging-related diseases, and cancer.

Bibliography

1. Hayflick, L. and P.S. Moorhead, *The serial cultivation of human diploid cell strains.* Exp Cell Res, 1961. **25**: p. 585-621.
2. Harley, C.B., A.B. Futcher, and C.W. Greider, *Telomeres shorten during ageing of human fibroblasts.* Nature, 1990. **345**(6274): p. 458-60.
3. Olovnikov, A.M., *A theory of marginotomy. The incomplete copying of template margin in enzymic synthesis of polynucleotides and biological significance of the phenomenon.* J Theor Biol, 1973. **41**(1): p. 181-90.
4. Watson, J.D., *Origin of concatemeric T7 DNA.* Nat New Biol, 1972. **239**(94): p. 197-201.
5. d'Adda di Fagagna, F., et al., *A DNA damage checkpoint response in telomere-initiated senescence.* Nature, 2003. **426**(6963): p. 194-8.
6. Herbig, U., et al., *Telomere shortening triggers senescence of human cells through a pathway involving ATM, p53, and p21(CIP1), but not p16(INK4a).* Mol Cell, 2004. **14**(4): p. 501-13.
7. van Deursen, J.M., *The role of senescent cells in ageing.* Nature, 2014. **509**(7501): p. 439-46.
8. Serrano, M., et al., *Oncogenic ras provokes premature cell senescence associated with accumulation of p53 and p16INK4a.* Cell, 1997. **88**(5): p. 593-602.
9. Denoyelle, C., et al., *Anti-oncogenic role of the endoplasmic reticulum differentially activated by mutations in the MAPK pathway.* Nat Cell Biol, 2006. **8**(10): p. 1053-63.
10. Parrinello, S., et al., *Oxygen sensitivity severely limits the replicative lifespan of murine fibroblasts.* Nat Cell Biol, 2003. **5**(8): p. 741-7.
11. Dimri, G.P., et al., *A biomarker that identifies senescent human cells in culture and in aging skin in vivo.* Proc Natl Acad Sci U S A, 1995. **92**(20): p. 9363-7.
12. Kurz, D.J., et al., *Senescence-associated (beta)-galactosidase reflects an increase in lysosomal mass during replicative ageing of human endothelial cells.* J Cell Sci, 2000. **113 (Pt 20)**: p. 3613-22.
13. Lee, B.Y., et al., *Senescence-associated beta-galactosidase is lysosomal beta-galactosidase.* Aging Cell, 2006. **5**(2): p. 187-95.
14. Coppe, J.P., et al., *Senescence-associated secretory phenotypes reveal cell-nonautonomous functions of oncogenic RAS and the p53 tumor suppressor.* PLoS Biol, 2008. **6**(12): p. 2853-68.
15. Rodier, F., et al., *Persistent DNA damage signalling triggers senescence-associated inflammatory cytokine secretion.* Nat Cell Biol, 2009. **11**(8): p. 973-9.
16. Marechal, A. and L. Zou, *DNA damage sensing by the ATM and ATR kinases.* Cold Spring Harb Perspect Biol, 2013. **5**(9).
17. Collado, M., et al., *Tumour biology: senescence in premalignant tumours.* Nature, 2005. **436**(7051): p. 642.
18. Ait-Si-Ali, S., et al., *A Suv39h-dependent mechanism for silencing S-phase genes in differentiating but not in cycling cells.* EMBO J, 2004. **23**(3): p. 605-15.
19. Michaloglou, C., et al., *BRAFE600-associated senescence-like cell cycle arrest of human naevi.* Nature, 2005. **436**(7051): p. 720-4.

20. Alimonti, A., et al., *A novel type of cellular senescence that can be enhanced in mouse models and human tumor xenografts to suppress prostate tumorigenesis.* J Clin Invest, 2010. **120**(3): p. 681-93.
21. Chen, Z., et al., *Crucial role of p53-dependent cellular senescence in suppression of Pten-deficient tumorigenesis.* Nature, 2005. **436**(7051): p. 725-30.
22. Braig, M. and C.A. Schmitt, *Oncogene-induced senescence: putting the brakes on tumor development.* Cancer Res, 2006. **66**(6): p. 2881-4.
23. Hannan, K.M. and R.B. Pearson, *Too much or too little: harnessing senescence to control oncogene-driven cancer.* Cell Cycle, 2012. **11**(17): p. 3147-8.
24. Di Leonardo, A., et al., *DNA damage triggers a prolonged p53-dependent G1 arrest and long-term induction of Cip1 in normal human fibroblasts.* Genes Dev, 1994. **8**(21): p. 2540-51.
25. Chang, B.D., et al., *A senescence-like phenotype distinguishes tumor cells that undergo terminal proliferation arrest after exposure to anticancer agents.* Cancer Res, 1999. **59**(15): p. 3761-7.
26. Di Micco, R., et al., *Oncogene-induced senescence is a DNA damage response triggered by DNA hyper-replication.* Nature, 2006. **444**(7119): p. 638-42.
27. Lakin, N.D. and S.P. Jackson, *Regulation of p53 in response to DNA damage.* Oncogene, 1999. **18**(53): p. 7644-55.
28. Kamijo, T., et al., *Tumor suppression at the mouse INK4a locus mediated by the alternative reading frame product p19ARF.* Cell, 1997. **91**(5): p. 649-59.
29. Weber, J.D., et al., *Nucleolar Arf sequesters Mdm2 and activates p53.* Nat Cell Biol, 1999. **1**(1): p. 20-6.
30. Wei, S., S. Wei, and J.M. Sedivy, *Expression of catalytically active telomerase does not prevent premature senescence caused by overexpression of oncogenic Ha-Ras in normal human fibroblasts.* Cancer Res, 1999. **59**(7): p. 1539-43.
31. McConnell, B.B., et al., *Induced expression of p16(INK4a) inhibits both CDK4- and CDK2-associated kinase activity by reassortment of cyclin-CDK-inhibitor complexes.* Mol Cell Biol, 1999. **19**(3): p. 1981-9.
32. Lazzerini Denchi, E., et al., *Deregulated E2F activity induces hyperplasia and senescence-like features in the mouse pituitary gland.* Mol Cell Biol, 2005. **25**(7): p. 2660-72.
33. Tu, Z., et al., *Oncogenic RAS regulates BRIP1 expression to induce dissociation of BRCA1 from chromatin, inhibit DNA repair, and promote senescence.* Dev Cell, 2011. **21**(6): p. 1077-91.
34. Astle, M.V., et al., *AKT induces senescence in human cells via mTORC1 and p53 in the absence of DNA damage: implications for targeting mTOR during malignancy.* Oncogene, 2012. **31**(15): p. 1949-62.
35. Bywater, M.J., et al., *Inhibition of RNA polymerase I as a therapeutic strategy to promote cancer-specific activation of p53.* Cancer Cell, 2012. **22**(1): p. 51-65.
36. Fregoso, O.I., et al., *Splicing-factor oncoprotein SRSF1 stabilizes p53 via RPL5 and induces cellular senescence.* Mol Cell, 2013. **50**(1): p. 56-66.
37. Nishimura, K., et al., *Perturbation of ribosome biogenesis drives cells into senescence through 5S RNP-mediated p53 activation.* Cell Rep, 2015. **10**(8): p. 1310-23.

38. Arya, A.K., et al., *Nutlin-3, the small-molecule inhibitor of MDM2, promotes senescence and radiosensitises laryngeal carcinoma cells harbouring wild-type p53.* Br J Cancer, 2010. **103**(2): p. 186-95.
39. Lindstrom, M.S. and Y. Zhang, *Ribosomal protein S9 is a novel B23/NPM-binding protein required for normal cell proliferation.* J Biol Chem, 2008. **283**(23): p. 15568-76.
40. Parisotto, M., et al., *PTEN deletion in luminal cells of mature prostate induces replication stress and senescence in vivo.* J Exp Med, 2018. **215**(6): p. 1749-1763.
41. Orjalo, A.V., et al., *Cell surface-bound IL-1alpha is an upstream regulator of the senescence-associated IL-6/IL-8 cytokine network.* Proc Natl Acad Sci U S A, 2009. **106**(40): p. 17031-6.
42. Lau, L., et al., *Uncoupling the Senescence-Associated Secretory Phenotype from Cell Cycle Exit via Interleukin-1 Inactivation Unveils Its Protumorigenic Role.* Mol Cell Biol, 2019. **39**(12).
43. Acosta, J.C., et al., *A complex secretory program orchestrated by the inflammasome controls paracrine senescence.* Nat Cell Biol, 2013. **15**(8): p. 978-90.
44. Niu, J., et al., *Identification of an autoregulatory feedback pathway involving interleukin-1alpha in induction of constitutive NF-kappaB activation in pancreatic cancer cells.* J Biol Chem, 2004. **279**(16): p. 16452-62.
45. Yang, H., et al., *cGAS is essential for cellular senescence.* Proc Natl Acad Sci U S A, 2017. **114**(23): p. E4612-E4620.
46. Takahashi, A., et al., *Downregulation of cytoplasmic DNases is implicated in cytoplasmic DNA accumulation and SASP in senescent cells.* Nat Commun, 2018. **9**(1): p. 1249.
47. Dou, Z., et al., *Cytoplasmic chromatin triggers inflammation in senescence and cancer.* Nature, 2017. **550**(7676): p. 402-406.
48. Gluck, S., et al., *Innate immune sensing of cytosolic chromatin fragments through cGAS promotes senescence.* Nat Cell Biol, 2017. **19**(9): p. 1061-1070.
49. Li, T. and Z.J. Chen, *The cGAS-cGAMP-STING pathway connects DNA damage to inflammation, senescence, and cancer.* J Exp Med, 2018. **215**(5): p. 1287-1299.
50. Wang, W., et al., *Sequential activation of the MEK-extracellular signal-regulated kinase and MKK3/6-p38 mitogen-activated protein kinase pathways mediates oncogenic ras-induced premature senescence.* Mol Cell Biol, 2002. **22**(10): p. 3389-403.
51. Deng, Q., et al., *High intensity ras signaling induces premature senescence by activating p38 pathway in primary human fibroblasts.* J Biol Chem, 2004. **279**(2): p. 1050-9.
52. Zdanov, S., et al., *Identification of p38MAPK-dependent genes with changed transcript abundance in H2O2-induced premature senescence of IMR-90 hTERT human fibroblasts.* FEBS Lett, 2006. **580**(27): p. 6455-63.
53. Nicke, B., et al., *Involvement of MINK, a Ste20 family kinase, in Ras oncogene-induced growth arrest in human ovarian surface epithelial cells.* Mol Cell, 2005. **20**(5): p. 673-85.
54. Dolado, I., et al., *p38alpha MAP kinase as a sensor of reactive oxygen species in tumorigenesis.* Cancer Cell, 2007. **11**(2): p. 191-205.

55. Freund, A., C.K. Patil, and J. Campisi, *p38MAPK is a novel DNA damage response-independent regulator of the senescence-associated secretory phenotype.* EMBO J, 2011. **30**(8): p. 1536-48.
56. Saxton, R.A. and D.M. Sabatini, *mTOR Signaling in Growth, Metabolism, and Disease.* Cell, 2017. **169**(2): p. 361-371.
57. Laberge, R.M., et al., *MTOR regulates the pro-tumorigenic senescence-associated secretory phenotype by promoting IL1A translation.* Nat Cell Biol, 2015. **17**(8): p. 1049-61.
58. Herranz, N., et al., *mTOR regulates MAPKAPK2 translation to control the senescence-associated secretory phenotype.* Nat Cell Biol, 2015. **17**(9): p. 1205-17.
59. Herranz, N., et al., *Erratum: mTOR regulates MAPKAPK2 translation to control the senescence-associated secretory phenotype.* Nat Cell Biol, 2015. **17**(10): p. 1370.
60. Acosta, J.C., et al., *Chemokine signaling via the CXCR2 receptor reinforces senescence.* Cell, 2008. **133**(6): p. 1006-18.
61. Kuilman, T., et al., *Oncogene-induced senescence relayed by an interleukin-dependent inflammatory network.* Cell, 2008. **133**(6): p. 1019-31.
62. Basu, S.K., et al., *3'UTR elements inhibit Ras-induced C/EBPbeta post-translational activation and senescence in tumour cells.* EMBO J, 2011. **30**(18): p. 3714-28.
63. Chien, Y., et al., *Control of the senescence-associated secretory phenotype by NF-kappaB promotes senescence and enhances chemosensitivity.* Genes Dev, 2011. **25**(20): p. 2125-36.
64. Sebastian, T., et al., *C/EBPbeta cooperates with RB:E2F to implement Ras(V12)-induced cellular senescence.* EMBO J, 2005. **24**(18): p. 3301-12.
65. Lesina, M., et al., *RelA regulates CXCL1/CXCR2-dependent oncogene-induced senescence in murine Kras-driven pancreatic carcinogenesis.* J Clin Invest, 2016. **126**(8): p. 2919-32.
66. Shah, P.P., et al., *Lamin B1 depletion in senescent cells triggers large-scale changes in gene expression and the chromatin landscape.* Genes Dev, 2013. **27**(16): p. 1787-99.
67. Tasdemir, N., et al., *BRD4 Connects Enhancer Remodeling to Senescence Immune Surveillance.* Cancer Discov, 2016. **6**(6): p. 612-29.
68. Kang, T.W., et al., *Senescence surveillance of pre-malignant hepatocytes limits liver cancer development.* Nature, 2011. **479**(7374): p. 547-51.
69. Sagiv, A., et al., *NKG2D ligands mediate immunosurveillance of senescent cells.* Aging (Albany NY), 2016. **8**(2): p. 328-44.
70. Ovadya, Y., et al., *Impaired immune surveillance accelerates accumulation of senescent cells and aging.* Nat Commun, 2018. **9**(1): p. 5435.
71. Di Mitri, D., et al., *Tumour-infiltrating Gr-1+ myeloid cells antagonize senescence in cancer.* Nature, 2014. **515**(7525): p. 134-7.
72. Narita, M., et al., *Rb-mediated heterochromatin formation and silencing of E2F target genes during cellular senescence.* Cell, 2003. **113**(6): p. 703-16.
73. Zhang, R., et al., *Formation of MacroH2A-containing senescence-associated heterochromatin foci and senescence driven by ASF1a and HIRA.* Dev Cell, 2005. **8**(1): p. 19-30.

74. Di Micco, R., et al., *Interplay between oncogene-induced DNA damage response and heterochromatin in senescence and cancer.* Nat Cell Biol, 2011. **13**(3): p. 292-302.
75. Narita, M., et al., *A novel role for high-mobility group a proteins in cellular senescence and heterochromatin formation.* Cell, 2006. **126**(3): p. 503-14.
76. Chandra, T., et al., *Global reorganization of the nuclear landscape in senescent cells.* Cell Rep, 2015. **10**(4): p. 471-83.
77. Chicas, A., et al., *H3K4 demethylation by Jarid1a and Jarid1b contributes to retinoblastoma-mediated gene silencing during cellular senescence.* Proc Natl Acad Sci U S A, 2012. **109**(23): p. 8971-6.
78. Duncan, E.M., et al., *Cathepsin L proteolytically processes histone H3 during mouse embryonic stem cell differentiation.* Cell, 2008. **135**(2): p. 284-94.
79. Yu, Y., et al., *Targeting the Senescence-Overriding Cooperative Activity of Structurally Unrelated H3K9 Demethylases in Melanoma.* Cancer Cell, 2018. **33**(2): p. 322-336 e8.
80. Kosar, M., et al., *Senescence-associated heterochromatin foci are dispensable for cellular senescence, occur in a cell type- and insult-dependent manner and follow expression of p16(ink4a).* Cell Cycle, 2011. **10**(3): p. 457-68.
81. Parry, A.J., et al., *NOTCH-mediated non-cell autonomous regulation of chromatin structure during senescence.* Nat Commun, 2018. **9**(1): p. 1840.
82. Sadaie, M., et al., *Redistribution of the Lamin B1 genomic binding profile affects rearrangement of heterochromatic domains and SAHF formation during senescence.* Genes Dev, 2013. **27**(16): p. 1800-8.
83. Criscione, S.W., et al., *Reorganization of chromosome architecture in replicative cellular senescence.* Sci Adv, 2016. **2**(2): p. e1500882.
84. Xie, W., et al., *DNA Methylation Patterns Separate Senescence from Transformation Potential and Indicate Cancer Risk.* Cancer Cell, 2018. **33**(2): p. 309-321 e5.
85. Gray, M.D., S.A. Jesch, and G.H. Stein, *5-Azacytidine-induced demethylation of DNA to senescent level does not block proliferation of human fibroblasts.* J Cell Physiol, 1991. **149**(3): p. 477-84.
86. Wilson, V.L. and P.A. Jones, *DNA methylation decreases in aging but not in immortal cells.* Science, 1983. **220**(4601): p. 1055-7.
87. Cruickshanks, H.A., et al., *Senescent cells harbour features of the cancer epigenome.* Nat Cell Biol, 2013. **15**(12): p. 1495-506.
88. Tanaka, H., et al., *The SETD8/PR-Set7 Methyltransferase Functions as a Barrier to Prevent Senescence-Associated Metabolic Remodeling.* Cell Rep, 2017. **18**(9): p. 2148-2161.
89. Moiseeva, O., et al., *Mitochondrial dysfunction contributes to oncogene-induced senescence.* Mol Cell Biol, 2009. **29**(16): p. 4495-507.
90. Glick, D., S. Barth, and K.F. Macleod, *Autophagy: cellular and molecular mechanisms.* J Pathol, 2010. **221**(1): p. 3-12.
91. Mizushima, N., et al., *Autophagy fights disease through cellular self-digestion.* Nature, 2008. **451**(7182): p. 1069-75.
92. Kim, Y.M., et al., *Roles of GSK3 in metabolic shift toward abnormal anabolism in cell senescence.* Ann N Y Acad Sci, 2010. **1201**: p. 65-71.

93. Li, T.Y., S.Y. Lin, and S.C. Lin, *Mechanism and physiological significance of growth factor-related autophagy.* Physiology (Bethesda), 2013. **28**(6): p. 423-31.
94. Young, A.R., et al., *Autophagy mediates the mitotic senescence transition.* Genes Dev, 2009. **23**(7): p. 798-803.
95. Dorr, J.R., et al., *Synthetic lethal metabolic targeting of cellular senescence in cancer therapy.* Nature, 2013. **501**(7467): p. 421-5.
96. Kang, C., et al., *The DNA damage response induces inflammation and senescence by inhibiting autophagy of GATA4.* Science, 2015. **349**(6255): p. aaa5612.
97. Azad, M.B., Y. Chen, and S.B. Gibson, *Regulation of autophagy by reactive oxygen species (ROS): implications for cancer progression and treatment.* Antioxid Redox Signal, 2009. **11**(4): p. 777-90.
98. Karna, P., et al., *Induction of reactive oxygen species-mediated autophagy by a novel microtubule-modulating agent.* J Biol Chem, 2010. **285**(24): p. 18737-48.
99. Luo, Y., et al., *Autophagy regulates ROS-induced cellular senescence via p21 in a p38 MAPKalpha dependent manner.* Exp Gerontol, 2011. **46**(11): p. 860-7.
100. Borodkina, A., et al., *Interaction between ROS dependent DNA damage, mitochondria and p38 MAPK underlies senescence of human adult stem cells.* Aging (Albany NY), 2014. **6**(6): p. 481-95.
101. Slobodnyuk, K., et al., *Autophagy-induced senescence is regulated by p38alpha signaling.* Cell Death Dis, 2019. **10**(6): p. 376.
102. Narita, M., et al., *Spatial coupling of mTOR and autophagy augments secretory phenotypes.* Science, 2011. **332**(6032): p. 966-70.
103. Gerland, L.M., et al., *Association of increased autophagic inclusions labeled for beta-galactosidase with fibroblastic aging.* Exp Gerontol, 2003. **38**(8): p. 887-95.
104. Guo, L., B. Xie, and Z. Mao, *Autophagy in premature senescent cells is activated via AMPK pathway.* Int J Mol Sci, 2012. **13**(3): p. 3563-82.
105. Goehe, R.W., et al., *The autophagy-senescence connection in chemotherapy: must tumor cells (self) eat before they sleep?* J Pharmacol Exp Ther, 2012. **343**(3): p. 763-78.
106. Ivanov, A., et al., *Lysosome-mediated processing of chromatin in senescence.* J Cell Biol, 2013. **202**(1): p. 129-43.
107. Dou, Z., et al., *Autophagy mediates degradation of nuclear lamina.* Nature, 2015. **527**(7576): p. 105-9.
108. Barradas, M., et al., *Identification of a candidate tumor-suppressor gene specifically activated during Ras-induced senescence.* Exp Cell Res, 2002. **273**(2): p. 127-37.
109. Nieto, M., et al., *Normal cellular senescence and cancer susceptibility in mice genetically deficient in Ras-induced senescence-1 (Ris1).* Oncogene, 2007. **26**(12): p. 1673-80.
110. Jacobs, J.J., et al., *Senescence bypass screen identifies TBX2, which represses Cdkn2a (p19(ARF)) and is amplified in a subset of human breast cancers.* Nat Genet, 2000. **26**(3): p. 291-9.
111. Peeper, D.S., et al., *A functional screen identifies hDRIL1 as an oncogene that rescues RAS-induced senescence.* Nat Cell Biol, 2002. **4**(2): p. 148-53.
112. Lee, W.J., et al., *Genome-Wide Overexpression Screen Identifies Genes Able to Bypass p16-Mediated Senescence in Melanoma.* SLAS Discov, 2017. **22**(3): p. 298-308.

113. Rual, J.F., et al., *Toward improving Caenorhabditis elegans phenome mapping with an ORFeome-based RNAi library.* Genome Res, 2004. **14**(10B): p. 2162-8.
114. Wang, Y., et al., *A gain-of-function senescence bypass screen identifies the homeobox transcription factor DLX2 as a regulator of ATM-p53 signaling.* Genes Dev, 2016. **30**(3): p. 293-306.
115. Wajapeyee, N., et al., *Oncogenic BRAF induces senescence and apoptosis through pathways mediated by the secreted protein IGFBP7.* Cell, 2008. **132**(3): p. 363-74.
116. Scurr, L.L., et al., *IGFBP7 is not required for B-RAF-induced melanocyte senescence.* Cell, 2010. **141**(4): p. 717-27.
117. Kaplon, J., et al., *Near-genomewide RNAi screening for regulators of BRAF(V600E) -induced senescence identifies RASEF, a gene epigenetically silenced in melanoma.* Pigment Cell Melanoma Res, 2014. **27**(4): p. 640-52.
118. Chan, K.T., et al., *Combining High-Content Imaging and Phenotypic Classification Analysis of Senescence-Associated Beta-Galactosidase Staining to Identify Regulators of Oncogene-Induced Senescence.* Assay Drug Dev Technol, 2016. **14**(7): p. 416-28.
119. Lahtela, J., et al., *A high-content cellular senescence screen identifies candidate tumor suppressors, including EPHA3.* Cell Cycle, 2013. **12**(4): p. 625-34.
120. Bitler, B.G., et al., *A high-content screening assay for small-molecule modulators of oncogene-induced senescence.* J Biomol Screen, 2013. **18**(9): p. 1054-61.
121. Chan, K.T., et al., *A functional genetic screen defines the AKT-induced senescence signaling network.* Cell Death Differ, 2019.
122. Kalathur, M., et al., *A chemogenomic screening identifies CK2 as a target for pro-senescence therapy in PTEN-deficient tumours.* Nat Commun, 2015. **6**: p. 7227.
123. Cho, S.W., et al., *Targeted genome engineering in human cells with the Cas9 RNA-guided endonuclease.* Nat Biotechnol, 2013. **31**(3): p. 230-2.
124. Korkmaz, G., et al., *Functional genetic screens for enhancer elements in the human genome using CRISPR-Cas9.* Nat Biotechnol, 2016. **34**(2): p. 192-8.
125. Liu, X., et al., *A large-scale CRISPR screen and identification of essential genes in cellular senescence bypass.* Aging (Albany NY), 2019. **11**(12): p. 4011-4031.
126. de Graaf, E.L., et al., *Single-step enrichment by Ti4+-IMAC and label-free quantitation enables in-depth monitoring of phosphorylation dynamics with high reproducibility and temporal resolution.* Mol Cell Proteomics, 2014. **13**(9): p. 2426-34.
127. Dieterich, D.C., et al., *Labeling, detection and identification of newly synthesized proteomes with bioorthogonal non-canonical amino-acid tagging.* Nat Protoc, 2007. **2**(3): p. 532-40.
128. Chen, X. and D.F. Calvisi, *Hydrodynamic transfection for generation of novel mouse models for liver cancer research.* Am J Pathol, 2014. **184**(4): p. 912-923.
129. Tordella, L., et al., *SWI/SNF regulates a transcriptional program that induces senescence to prevent liver cancer.* Genes Dev, 2016. **30**(19): p. 2187-2198.
130. Calvisi, D.F., et al., *Increased lipogenesis, induced by AKT-mTORC1-RPS6 signaling, promotes development of human hepatocellular carcinoma.* Gastroenterology, 2011. **140**(3): p. 1071-83.

131. Liu, Y.T., et al., *A novel spontaneous hepatocellular carcinoma mouse model for studying T-cell exhaustion in the tumor microenvironment.* J Immunother Cancer, 2018. **6**(1): p. 144.
132. Munoz-Espin, D., et al., *Programmed cell senescence during mammalian embryonic development.* Cell, 2013. **155**(5): p. 1104-18.
133. Storer, M., et al., *Senescence is a developmental mechanism that contributes to embryonic growth and patterning.* Cell, 2013. **155**(5): p. 1119-30.
134. Demaria, M., et al., *An essential role for senescent cells in optimal wound healing through secretion of PDGF-AA.* Dev Cell, 2014. **31**(6): p. 722-33.
135. Baker, D.J., et al., *Naturally occurring p16(Ink4a)-positive cells shorten healthy lifespan.* Nature, 2016. **530**(7589): p. 184-9.
136. Childs, B.G., et al., *Senescent intimal foam cells are deleterious at all stages of atherosclerosis.* Science, 2016. **354**(6311): p. 472-477.
137. Meylan, E., et al., *Requirement for NF-kappaB signalling in a mouse model of lung adenocarcinoma.* Nature, 2009. **462**(7269): p. 104-7.
138. Harrison, D.E., et al., *Rapamycin fed late in life extends lifespan in genetically heterogeneous mice.* Nature, 2009. **460**(7253): p. 392-5.
139. Alqahtani, A., et al., *Bromodomain and extra-terminal motif inhibitors: a review of preclinical and clinical advances in cancer therapy.* Future Sci OA, 2019. **5**(3): p. FSO372.
140. Mertens, M. and J.A. Singh, *Anakinra for rheumatoid arthritis: a systematic review.* J Rheumatol, 2009. **36**(6): p. 1118-25.
141. Kishimoto, T., *IL-6: from its discovery to clinical applications.* Int Immunol, 2010. **22**(5): p. 347-52.
142. Xu, M., et al., *JAK inhibition alleviates the cellular senescence-associated secretory phenotype and frailty in old age.* Proc Natl Acad Sci U S A, 2015. **112**(46): p. E6301-10.
143. Kim, K.M., et al., *SCAMP4 enhances the senescent cell secretome.* Genes Dev, 2018. **32**(13-14): p. 909-914.
144. Georgilis, A., et al., *PTBP1-Mediated Alternative Splicing Regulates the Inflammatory Secretome and the Pro-tumorigenic Effects of Senescent Cells.* Cancer Cell, 2018. **34**(1): p. 85-102 e9.
145. Schmitt, C.A., *UnSASPing Senescence: Unmasking Tumor Suppression?* Cancer Cell, 2018. **34**(1): p. 6-8.
146. Luo, X., et al., *Stromal-Initiated Changes in the Bone Promote Metastatic Niche Development.* Cell Rep, 2016. **14**(1): p. 82-92.
147. Ruhland, M.K., et al., *Stromal senescence establishes an immunosuppressive microenvironment that drives tumorigenesis.* Nat Commun, 2016. **7**: p. 11762.
148. Toso, A., et al., *Enhancing chemotherapy efficacy in Pten-deficient prostate tumors by activating the senescence-associated antitumor immunity.* Cell Rep, 2014. **9**(1): p. 75-89.
149. Jackson, J.G., et al., *p53-mediated senescence impairs the apoptotic response to chemotherapy and clinical outcome in breast cancer.* Cancer Cell, 2012. **21**(6): p. 793-806.
150. Karimi-Busheri, F., et al., *Senescence evasion by MCF-7 human breast tumor-initiating cells.* Breast Cancer Res, 2010. **12**(3): p. R31.

151. Achuthan, S., et al., *Drug-induced senescence generates chemoresistant stemlike cells with low reactive oxygen species.* J Biol Chem, 2011. **286**(43): p. 37813-29.
152. Baker, D.J., et al., *Clearance of p16Ink4a-positive senescent cells delays ageing-associated disorders.* Nature, 2011. **479**(7372): p. 232-6.
153. Zhang, P., et al., *Senolytic therapy alleviates Abeta-associated oligodendrocyte progenitor cell senescence and cognitive deficits in an Alzheimer's disease model.* Nat Neurosci, 2019. **22**(5): p. 719-728.
154. Roos, C.M., et al., *Chronic senolytic treatment alleviates established vasomotor dysfunction in aged or atherosclerotic mice.* Aging Cell, 2016. **15**(5): p. 973-7.
155. Farr, J.N., et al., *Targeting cellular senescence prevents age-related bone loss in mice.* Nat Med, 2017. **23**(9): p. 1072-1079.
156. Schafer, M.J., et al., *Cellular senescence mediates fibrotic pulmonary disease.* Nat Commun, 2017. **8**: p. 14532.
157. Zhu, Y., et al., *The Achilles' heel of senescent cells: from transcriptome to senolytic drugs.* Aging Cell, 2015. **14**(4): p. 644-58.
158. Baar, M.P., et al., *Targeted Apoptosis of Senescent Cells Restores Tissue Homeostasis in Response to Chemotoxicity and Aging.* Cell, 2017. **169**(1): p. 132-147 e16.
159. Chang, J., et al., *Clearance of senescent cells by ABT263 rejuvenates aged hematopoietic stem cells in mice.* Nat Med, 2016. **22**(1): p. 78-83.
160. Yosef, R., et al., *Directed elimination of senescent cells by inhibition of BCL-W and BCL-XL.* Nat Commun, 2016. **7**: p. 11190.
161. Zhu, Y., et al., *Identification of a novel senolytic agent, navitoclax, targeting the Bcl-2 family of anti-apoptotic factors.* Aging Cell, 2016. **15**(3): p. 428-35.
162. Munoz-Espin, D., et al., *A versatile drug delivery system targeting senescent cells.* EMBO Mol Med, 2018. **10**(9).
163. Schoenwaelder, S.M., et al., *Bcl-xL-inhibitory BH3 mimetics can induce a transient thrombocytopathy that undermines the hemostatic function of platelets.* Blood, 2011. **118**(6): p. 1663-74.
164. Vogler, M., et al., *BCL2/BCL-X(L) inhibition induces apoptosis, disrupts cellular calcium homeostasis, and prevents platelet activation.* Blood, 2011. **117**(26): p. 7145-54.
165. Rudin, C.M., et al., *Phase II study of single-agent navitoclax (ABT-263) and biomarker correlates in patients with relapsed small cell lung cancer.* Clin Cancer Res, 2012. **18**(11): p. 3163-9.
166. Xu, M., et al., *Senolytics improve physical function and increase lifespan in old age.* Nat Med, 2018. **24**(8): p. 1246-1256.
167. Demaria, M., et al., *Cellular Senescence Promotes Adverse Effects of Chemotherapy and Cancer Relapse.* Cancer Discov, 2017. **7**(2): p. 165-176.
168. Hubackova, S., et al., *Selective elimination of senescent cells by mitochondrial targeting is regulated by ANT2.* Cell Death Differ, 2019. **26**(2): p. 276-290.
169. Wakil, S.J. and L.A. Abu-Elheiga, *Fatty acid metabolism: target for metabolic syndrome.* J Lipid Res, 2009. **50 Suppl**: p. S138-43.
170. Quiros, P.M., A. Mottis, and J. Auwerx, *Mitonuclear communication in homeostasis and stress.* Nat Rev Mol Cell Biol, 2016. **17**(4): p. 213-26.
171. Bratic, A. and N.G. Larsson, *The role of mitochondria in aging.* J Clin Invest, 2013. **123**(3): p. 951-7.

172. Cagin, U. and J.A. Enriquez, *The complex crosstalk between mitochondria and the nucleus: What goes in between?* Int J Biochem Cell Biol, 2015. **63**: p. 10-5.
173. Mason, E.F. and J.C. Rathmell, *Cell metabolism: an essential link between cell growth and apoptosis.* Biochim Biophys Acta, 2011. **1813**(4): p. 645-54.
174. Wallace, D.C., *Mitochondria and cancer.* Nat Rev Cancer, 2012. **12**(10): p. 685-98.
175. Bittles, A.H. and N. Harper, *Increased glycolysis in ageing cultured human diploid fibroblasts.* Biosci Rep, 1984. **4**(9): p. 751-6.
176. Goldstein, S., et al., *Energy metabolism in cultured human fibroblasts during aging in vitro.* J Cell Physiol, 1982. **112**(3): p. 419-24.
177. Liao, E.C., et al., *Radiation induces senescence and a bystander effect through metabolic alterations.* Cell Death Dis, 2014. **5**: p. e1255.
178. Wang, D., et al., *Apoptotic transition of senescent cells accompanied with mitochondrial hyper-function.* Oncotarget, 2016. **7**(19): p. 28286-300.
179. James, E.L., et al., *Senescent human fibroblasts show increased glycolysis and redox homeostasis with extracellular metabolomes that overlap with those of irreparable DNA damage, aging, and disease.* J Proteome Res, 2015. **14**(4): p. 1854-71.
180. Takebayashi, S., et al., *Retinoblastoma protein promotes oxidative phosphorylation through upregulation of glycolytic genes in oncogene-induced senescent cells.* Aging Cell, 2015. **14**(4): p. 689-97.
181. Aird, K.M., et al., *ATM couples replication stress and metabolic reprogramming during cellular senescence.* Cell Rep, 2015. **11**(6): p. 893-901.
182. Capparelli, C., et al., *Autophagy and senescence in cancer-associated fibroblasts metabolically supports tumor growth and metastasis via glycolysis and ketone production.* Cell Cycle, 2012. **11**(12): p. 2285-302.
183. Hirschhaeuser, F., U.G. Sattler, and W. Mueller-Klieser, *Lactate: a metabolic key player in cancer.* Cancer Res, 2011. **71**(22): p. 6921-5.
184. Porter, C., et al., *Mitochondrial respiratory capacity and coupling control decline with age in human skeletal muscle.* Am J Physiol Endocrinol Metab, 2015. **309**(3): p. E224-32.
185. Kaplon, J., et al., *A key role for mitochondrial gatekeeper pyruvate dehydrogenase in oncogene-induced senescence.* Nature, 2013. **498**(7452): p. 109-12.
186. Quijano, C., et al., *Oncogene-induced senescence results in marked metabolic and bioenergetic alterations.* Cell Cycle, 2012. **11**(7): p. 1383-92.
187. Kamei, Y., et al., *Changes in transcription and metabolism during the early stage of replicative cellular senescence in budding yeast.* J Biol Chem, 2014. **289**(46): p. 32081-93.
188. Sebastian, D., M. Palacin, and A. Zorzano, *Mitochondrial Dynamics: Coupling Mitochondrial Fitness with Healthy Aging.* Trends Mol Med, 2017. **23**(3): p. 201-215.
189. Westermann, B., *Bioenergetic role of mitochondrial fusion and fission.* Biochim Biophys Acta, 2012. **1817**(10): p. 1833-8.
190. Mai, S., et al., *Decreased expression of Drp1 and Fis1 mediates mitochondrial elongation in senescent cells and enhances resistance to oxidative stress through PINK1.* J Cell Sci, 2010. **123**(Pt 6): p. 917-26.

191. Yoon, Y.S., et al., *Formation of elongated giant mitochondria in DFO-induced cellular senescence: involvement of enhanced fusion process through modulation of Fis1.* J Cell Physiol, 2006. **209**(2): p. 468-80.
192. Lee, S., et al., *Mitochondrial fission and fusion mediators, hFis1 and OPA1, modulate cellular senescence.* J Biol Chem, 2007. **282**(31): p. 22977-83.
193. Park, Y.Y., et al., *Loss of MARCH5 mitochondrial E3 ubiquitin ligase induces cellular senescence through dynamin-related protein 1 and mitofusin 1.* J Cell Sci, 2010. **123**(Pt 4): p. 619-26.
194. Tondera, D., et al., *SLP-2 is required for stress-induced mitochondrial hyperfusion.* EMBO J, 2009. **28**(11): p. 1589-600.
195. Gomes, A.P., et al., *Declining NAD(+) induces a pseudohypoxic state disrupting nuclear-mitochondrial communication during aging.* Cell, 2013. **155**(7): p. 1624-38.
196. Buck, M.D., et al., *Mitochondrial Dynamics Controls T Cell Fate through Metabolic Programming.* Cell, 2016. **166**(1): p. 63-76.
197. Lee, B.S., S.I. Grewal, and A.J. Klar, *Biochemical interactions between proteins and mat1 cis-acting sequences required for imprinting in fission yeast.* Mol Cell Biol, 2004. **24**(22): p. 9813-22.
198. Childs, B.G., et al., *Senescence and apoptosis: dueling or complementary cell fates?* EMBO Rep, 2014. **15**(11): p. 1139-53.
199. Ogrunc, M., et al., *Oncogene-induced reactive oxygen species fuel hyperproliferation and DNA damage response activation.* Cell Death Differ, 2014. **21**(6): p. 998-1012.
200. Stockl, P., et al., *Sustained inhibition of oxidative phosphorylation impairs cell proliferation and induces premature senescence in human fibroblasts.* Exp Gerontol, 2006. **41**(7): p. 674-82.
201. !!! INVALID CITATION !!! [250].
202. Harman, D., *The biologic clock: the mitochondria?* J Am Geriatr Soc, 1972. **20**(4): p. 145-7.
203. Brand, M.D., *The sites and topology of mitochondrial superoxide production.* Exp Gerontol, 2010. **45**(7-8): p. 466-72.
204. Suski, J.M., et al., *Relation between mitochondrial membrane potential and ROS formation.* Methods Mol Biol, 2012. **810**: p. 183-205.
205. Dai, D.F., et al., *Mitochondrial oxidative stress in aging and healthspan.* Longev Healthspan, 2014. **3**: p. 6.
206. Nacarelli, T., A. Azar, and C. Sell, *Mitochondrial stress induces cellular senescence in an mTORC1-dependent manner.* Free Radic Biol Med, 2016. **95**: p. 133-54.
207. Schriner, S.E., et al., *Extension of murine life span by overexpression of catalase targeted to mitochondria.* Science, 2005. **308**(5730): p. 1909-11.
208. Dai, D.F., et al., *Overexpression of catalase targeted to mitochondria attenuates murine cardiac aging.* Circulation, 2009. **119**(21): p. 2789-97.
209. Ge, X., et al., *Mitochondrial catalase suppresses naturally occurring lung cancer in old mice.* Pathobiol Aging Age Relat Dis, 2015. **5**: p. 28776.
210. Ryan, T.E., et al., *Targeted Expression of Catalase to Mitochondria Protects Against Ischemic Myopathy in High-Fat Diet-Fed Mice.* Diabetes, 2016. **65**(9): p. 2553-68.

211. Treuting, P.M., et al., *Reduction of age-associated pathology in old mice by overexpression of catalase in mitochondria.* J Gerontol A Biol Sci Med Sci, 2008. **63**(8): p. 813-22.
212. Dai, D.F., et al., *Age-dependent cardiomyopathy in mitochondrial mutator mice is attenuated by overexpression of catalase targeted to mitochondria.* Aging Cell, 2010. **9**(4): p. 536-44.
213. Kolesar, J.E., et al., *Defects in mitochondrial DNA replication and oxidative damage in muscle of mtDNA mutator mice.* Free Radic Biol Med, 2014. **75**: p. 241-51.
214. Logan, A., et al., *In vivo levels of mitochondrial hydrogen peroxide increase with age in mtDNA mutator mice.* Aging Cell, 2014. **13**(4): p. 765-8.
215. Lee, J.H., et al., *ATP-citrate lyase regulates cellular senescence via an AMPK- and p53-dependent pathway.* FEBS J, 2015. **282**(2): p. 361-71.
216. Mihaylova, M.M. and R.J. Shaw, *The AMPK signalling pathway coordinates cell growth, autophagy and metabolism.* Nat Cell Biol, 2011. **13**(9): p. 1016-23.
217. Burkewitz, K., Y. Zhang, and W.B. Mair, *AMPK at the nexus of energetics and aging.* Cell Metab, 2014. **20**(1): p. 10-25.
218. Han, X., et al., *AMPK activation protects cells from oxidative stress-induced senescence via autophagic flux restoration and intracellular NAD(+) elevation.* Aging Cell, 2016. **15**(3): p. 416-27.
219. Zwerschke, W., et al., *Metabolic analysis of senescent human fibroblasts reveals a role for AMP in cellular senescence.* Biochem J, 2003. **376**(Pt 2): p. 403-11.
220. Jones, R.G., et al., *AMP-activated protein kinase induces a p53-dependent metabolic checkpoint.* Mol Cell, 2005. **18**(3): p. 283-93.
221. Jiang, P., et al., *Reciprocal regulation of p53 and malic enzymes modulates metabolism and senescence.* Nature, 2013. **493**(7434): p. 689-93.
222. Wiley, C.D., et al., *Mitochondrial Dysfunction Induces Senescence with a Distinct Secretory Phenotype.* Cell Metab, 2016. **23**(2): p. 303-14.
223. Clark-Matott, J., et al., *Metabolomic analysis of exercise effects in the POLG mitochondrial DNA mutator mouse brain.* Neurobiol Aging, 2015. **36**(11): p. 2972-2983.
224. Nacarelli, T., et al., *NAD(+) metabolism governs the proinflammatory senescence-associated secretome.* Nat Cell Biol, 2019. **21**(3): p. 397-407.
225. von Sonntag, C., *The chemistry of free-radical-mediated DNA damage.* Basic Life Sci, 1991. **58**: p. 287-317; discussion 317-21.
226. Lee, A.C., et al., *Ras proteins induce senescence by altering the intracellular levels of reactive oxygen species.* J Biol Chem, 1999. **274**(12): p. 7936-40.
227. Richter, C., *Reactive oxygen and DNA damage in mitochondria.* Mutat Res, 1992. **275**(3-6): p. 249-55.
228. Dinkova-Kostova, A.T. and A.Y. Abramov, *The emerging role of Nrf2 in mitochondrial function.* Free Radic Biol Med, 2015. **88**(Pt B): p. 179-188.
229. Monaghan, R.M. and A.J. Whitmarsh, *Mitochondrial Proteins Moonlighting in the Nucleus.* Trends Biochem Sci, 2015. **40**(12): p. 728-735.
230. Atamna, H., et al., *Combined activation of the energy and cellular-defense pathways may explain the potent anti-senescence activity of methylene blue.* Redox Biol, 2015. **6**: p. 426-435.

231. Volonte, D., et al., *Inhibition of nuclear factor-erythroid 2-related factor (Nrf2) by caveolin-1 promotes stress-induced premature senescence.* Mol Biol Cell, 2013. **24**(12): p. 1852-62.
232. Yang, G., et al., *Hydrogen sulfide protects against cellular senescence via S-sulfhydration of Keap1 and activation of Nrf2.* Antioxid Redox Signal, 2013. **18**(15): p. 1906-19.
233. Halliwell, B., *Free radicals, reactive oxygen species and human disease: a critical evaluation with special reference to atherosclerosis.* Br J Exp Pathol, 1989. **70**(6): p. 737-57.
234. Ayala, A., M.F. Munoz, and S. Arguelles, *Lipid peroxidation: production, metabolism, and signaling mechanisms of malondialdehyde and 4-hydroxy-2-nonenal.* Oxid Med Cell Longev, 2014. **2014**: p. 360438.
235. Moller, I.M. and B.K. Kristensen, *Protein oxidation in plant mitochondria as a stress indicator.* Photochem Photobiol Sci, 2004. **3**(8): p. 730-5.
236. Gardner, P.R. and I. Fridovich, *Superoxide sensitivity of the Escherichia coli 6-phosphogluconate dehydratase.* J Biol Chem, 1991. **266**(3): p. 1478-83.
237. Cabiscol, E., et al., *Oxidative stress promotes specific protein damage in Saccharomyces cerevisiae.* J Biol Chem, 2000. **275**(35): p. 27393-8.
238. Deschenes-Simard, X., et al., *Cellular senescence and protein degradation: breaking down cancer.* Cell Cycle, 2014. **13**(12): p. 1840-58.
239. Dhar, S.K., et al., *Specificity protein 1-dependent p53-mediated suppression of human manganese superoxide dismutase gene expression.* J Biol Chem, 2006. **281**(31): p. 21698-709.
240. Zhao, Y., et al., *p53 translocation to mitochondria precedes its nuclear translocation and targets mitochondrial oxidative defense protein-manganese superoxide dismutase.* Cancer Res, 2005. **65**(9): p. 3745-50.
241. Dikalov, S.I., et al., *Mitochondrial reactive oxygen species and calcium uptake regulate activation of phagocytic NADPH oxidase.* Am J Physiol Regul Integr Comp Physiol, 2012. **302**(10): p. R1134-42.
242. Mistry, Y., et al., *A role for mitochondrial oxidants in stress-induced premature senescence of human vascular smooth muscle cells.* Redox Biol, 2013. **1**: p. 411-7.
243. Passos, J.F., et al., *Feedback between p21 and reactive oxygen production is necessary for cell senescence.* Mol Syst Biol, 2010. **6**: p. 347.
244. Correia-Melo, C., et al., *Mitochondria are required for pro-ageing features of the senescent phenotype.* EMBO J, 2016. **35**(7): p. 724-42.
245. Seo, Y.H., et al., *Enhanced glycogenesis is involved in cellular senescence via GSK3/GS modulation.* Aging Cell, 2008. **7**(6): p. 894-907.
246. Moore, S.A., et al., *Glycogen accumulation in tibial nerves of experimentally diabetic and aging control rats.* J Neurol Sci, 1981. **52**(2-3): p. 289-303.
247. Gertz, H.J., et al., *Glycogen accumulation of the aging human brain.* Mech Ageing Dev, 1985. **31**(1): p. 25-35.
248. Spasic, M.R., P. Callaerts, and K.K. Norga, *AMP-activated protein kinase (AMPK) molecular crossroad for metabolic control and survival of neurons.* Neuroscientist, 2009. **15**(4): p. 309-16.
249. Kenyon, C., *The plasticity of aging: insights from long-lived mutants.* Cell, 2005. **120**(4): p. 449-60.

250. Kuk, J.L., et al., *Age-related changes in total and regional fat distribution.* Ageing Res Rev, 2009. **8**(4): p. 339-48.
251. Ogrodnik, M., et al., *Cellular senescence drives age-dependent hepatic steatosis.* Nat Commun, 2017. **8**: p. 15691.
252. Ogrodnik, M., et al., *Obesity-Induced Cellular Senescence Drives Anxiety and Impairs Neurogenesis.* Cell Metab, 2019. **29**(5): p. 1061-1077 e8.
253. Nacarelli, T., A. Azar, and C. Sell, *Aberrant mTOR activation in senescence and aging: A mitochondrial stress response?* Exp Gerontol, 2015. **68**: p. 66-70.
254. Horton, J.D., et al., *Combined analysis of oligonucleotide microarray data from transgenic and knockout mice identifies direct SREBP target genes.* Proc Natl Acad Sci U S A, 2003. **100**(21): p. 12027-32.
255. Shahbazian, D., et al., *The mTOR/PI3K and MAPK pathways converge on eIF4B to control its phosphorylation and activity.* EMBO J, 2006. **25**(12): p. 2781-91.
256. Zmijewski, J.W. and R.S. Jope, *Nuclear accumulation of glycogen synthase kinase-3 during replicative senescence of human fibroblasts.* Aging Cell, 2004. **3**(5): p. 309-17.
257. Shin, S., et al., *Glycogen synthase kinase-3beta positively regulates protein synthesis and cell proliferation through the regulation of translation initiation factor 4E-binding protein 1.* Oncogene, 2014. **33**(13): p. 1690-9.
258. Bussian, T.J., et al., *Clearance of senescent glial cells prevents tau-dependent pathology and cognitive decline.* Nature, 2018. **562**(7728): p. 578-582.
259. Meuth, M., *The molecular basis of mutations induced by deoxyribonucleoside triphosphate pool imbalances in mammalian cells.* Exp Cell Res, 1989. **181**(2): p. 305-16.
260. Aird, K.M., et al., *Suppression of nucleotide metabolism underlies the establishment and maintenance of oncogene-induced senescence.* Cell Rep, 2013. **3**(4): p. 1252-65.
261. Delfarah, A., et al., *Inhibition of nucleotide synthesis promotes replicative senescence of human mammary epithelial cells.* J Biol Chem, 2019. **294**(27): p. 10564-10578.
262. Mannava, S., et al., *Depletion of deoxyribonucleotide pools is an endogenous source of DNA damage in cells undergoing oncogene-induced senescence.* Am J Pathol, 2013. **182**(1): p. 142-51.
263. Mannava, S., et al., *Ribonucleotide reductase and thymidylate synthase or exogenous deoxyribonucleosides reduce DNA damage and senescence caused by C-MYC depletion.* Aging (Albany NY), 2012. **4**(12): p. 917-22.
264. Bester, A.C., et al., *Nucleotide deficiency promotes genomic instability in early stages of cancer development.* Cell, 2011. **145**(3): p. 435-46.
265. Aksoy, O., et al., *The atypical E2F family member E2F7 couples the p53 and RB pathways during cellular senescence.* Genes Dev, 2012. **26**(14): p. 1546-57.
266. Zhu, H., et al., *Cystathionine beta-Synthase in Physiology and Cancer.* Biomed Res Int, 2018. **2018**: p. 3205125.
267. Kruger, W.D., et al., *Cystathionine beta-synthase deficiency in Georgia (USA): correlation of clinical and biochemical phenotype with genotype.* Hum Mutat, 2003. **22**(6): p. 434-41.

268. Millis, S.Z., et al., *Landscape of Phosphatidylinositol-3-Kinase Pathway Alterations Across 19784 Diverse Solid Tumors.* JAMA Oncol, 2016. **2**(12): p. 1565-1573.
269. Hahn, W.C., et al., *Creation of human tumour cells with defined genetic elements.* Nature, 1999. **400**(6743): p. 464-8.
270. Ke, Y., T. Ning, and B. Wang, *[Establishment and characterization of a SV40 transformed human fetal gastric epithelial cell line-GES-1].* Zhonghua Zhong Liu Za Zhi, 1994. **16**(1): p. 7-10.
271. Morgenstern, J.P. and H. Land, *Advanced mammalian gene transfer: high titre retroviral vectors with multiple drug selection markers and a complementary helper-free packaging cell line.* Nucleic Acids Res, 1990. **18**(12): p. 3587-96.
272. Zuber, J., et al., *Toolkit for evaluating genes required for proliferation and survival using tetracycline-regulated RNAi.* Nat Biotechnol, 2011. **29**(1): p. 79-83.
273. Cosset, F.L., et al., *High-titer packaging cells producing recombinant retroviruses resistant to human serum.* J Virol, 1995. **69**(12): p. 7430-6.
274. Kelly, P.F., et al., *Highly efficient gene transfer into cord blood nonobese diabetic/severe combined immunodeficiency repopulating cells by oncoretroviral vector particles pseudotyped with the feline endogenous retrovirus (RD114) envelope protein.* Blood, 2000. **96**(4): p. 1206-14.
275. Dull, T., et al., *A third-generation lentivirus vector with a conditional packaging system.* J Virol, 1998. **72**(11): p. 8463-71.
276. Stewart, S.A., et al., *Lentivirus-delivered stable gene silencing by RNAi in primary cells.* RNA, 2003. **9**(4): p. 493-501.
277. Hanahan, D., J. Jessee, and F.R. Bloom, *Plasmid transformation of Escherichia coli and other bacteria.* Methods Enzymol, 1991. **204**: p. 63-113.
278. Gavrilescu, L.C. and R.A. Van Etten, *Production of replication-defective retrovirus by transient transfection of 293T cells.* J Vis Exp, 2007(10): p. 550.
279. Boussif, O., et al., *A versatile vector for gene and oligonucleotide transfer into cells in culture and in vivo: polyethylenimine.* Proc Natl Acad Sci U S A, 1995. **92**(16): p. 7297-301.
280. Rao, X., et al., *An improvement of the 2^(-delta delta CT) method for quantitative real-time polymerase chain reaction data analysis.* Biostat Bioinforma Biomath, 2013. **3**(3): p. 71-85.
281. Zhao, H., et al., *Frequent epigenetic silencing of the folate-metabolising gene cystathionine-beta-synthase in gastrointestinal cancer.* PLoS One, 2012. **7**(11): p. e49683.
282. Franken, N.A., et al., *Clonogenic assay of cells in vitro.* Nat Protoc, 2006. **1**(5): p. 2315-9.
283. Guzman, C., et al., *ColonyArea: an ImageJ plugin to automatically quantify colony formation in clonogenic assays.* PLoS One, 2014. **9**(3): p. e92444.
284. Borowicz, S., et al., *The soft agar colony formation assay.* J Vis Exp, 2014(92): p. e51998.
285. Debacq-Chainiaux, F., et al., *Protocols to detect senescence-associated beta-galactosidase (SA-betagal) activity, a biomarker of senescent cells in culture and in vivo.* Nat Protoc, 2009. **4**(12): p. 1798-806.

286. Wang, X., et al., *Expression of group IIA phospholipase A2 is an independent predictor of favorable outcome for patients with gastric cancer.* Hum Pathol, 2013. **44**(10): p. 2020-7.
287. Zhang, X., et al., *Reduced group IVA phospholipase A2 expression is associated with unfavorable outcome for patients with gastric cancer.* Med Oncol, 2013. **30**(1): p. 454.
288. Chen, B., et al., *Fluorescent probe for highly selective and sensitive detection of hydrogen sulfide in living cells and cardiac tissues.* Analyst, 2013. **138**(3): p. 946-51.
289. Modis, K., et al., *Effect of S-adenosyl-L-methionine (SAM), an allosteric activator of cystathionine-beta-synthase (CBS) on colorectal cancer cell proliferation and bioenergetics in vitro.* Nitric Oxide, 2014. **41**: p. 146-56.
290. Chong, J., D.S. Wishart, and J. Xia, *Using MetaboAnalyst 4.0 for Comprehensive and Integrative Metabolomics Data Analysis.* Curr Protoc Bioinformatics, 2019. **68**(1): p. e86.
291. Sutton, T.R., et al., *A robust and versatile mass spectrometry platform for comprehensive assessment of the thiol redox metabolome.* Redox Biol, 2018. **16**: p. 359-380.
292. Fruman, D.A. and C. Rommel, *PI3K and cancer: lessons, challenges and opportunities.* Nat Rev Drug Discov, 2014. **13**(2): p. 140-56.
293. Carpten, J.D., et al., *A transforming mutation in the pleckstrin homology domain of AKT1 in cancer.* Nature, 2007. **448**(7152): p. 439-44.
294. Haferkamp, S., et al., *The relative contributions of the p53 and pRb pathways in oncogene-induced melanocyte senescence.* Aging (Albany NY), 2009. **1**(6): p. 542-56.
295. Freund, A., et al., *Lamin B1 loss is a senescence-associated biomarker.* Mol Biol Cell, 2012. **23**(11): p. 2066-75.
296. Larsen, M.R., et al., *Analysis of posttranslational modifications of proteins by tandem mass spectrometry.* Biotechniques, 2006. **40**(6): p. 790-8.
297. Liberti, M.V. and J.W. Locasale, *The Warburg Effect: How Does it Benefit Cancer Cells?* Trends Biochem Sci, 2016. **41**(3): p. 211-218.
298. Liberti, M.V. and J.W. Locasale, *Correction to: 'The Warburg Effect: How Does it Benefit Cancer Cells?': [Trends in Biochemical Sciences, 41 (2016) 211].* Trends Biochem Sci, 2016. **41**(3): p. 287.
299. Wang, Y., Y. Chen, and J. Fang, *Post-Transcriptional and Post-translational Regulation of Central Carbon Metabolic Enzymes in Cancer.* Anticancer Agents Med Chem, 2017. **17**(11): p. 1456-1465.
300. Bartkova, J., et al., *Oncogene-induced senescence is part of the tumorigenesis barrier imposed by DNA damage checkpoints.* Nature, 2006. **444**(7119): p. 633-7.
301. Kotsantis, P., E. Petermann, and S.J. Boulton, *Mechanisms of Oncogene-Induced Replication Stress: Jigsaw Falling into Place.* Cancer Discov, 2018. **8**(5): p. 537-555.
302. Schieber, M. and N.S. Chandel, *ROS function in redox signaling and oxidative stress.* Curr Biol, 2014. **24**(10): p. R453-62.
303. Pluquet, O., A. Pourtier, and C. Abbadie, *The unfolded protein response and cellular senescence. A review in the theme: cellular mechanisms of endoplasmic*

reticulum stress signaling in health and disease. Am J Physiol Cell Physiol, 2015. **308**(6): p. C415-25.
304. Hu, P., et al., *Critical role of endogenous Akt/IAPs and MEK1/ERK pathways in counteracting endoplasmic reticulum stress-induced cell death.* J Biol Chem, 2004. **279**(47): p. 49420-9.
305. Blaustein, M., et al., *Modulation of the Akt pathway reveals a novel link with PERK/eIF2alpha, which is relevant during hypoxia.* PLoS One, 2013. **8**(7): p. e69668.
306. Dörr, J.R., et al., *Synthetic lethal metabolic targeting of cellular senescence in cancer therapy.* Nature, 2013. **501**(7467): p. 421.
307. Tanida, I., T. Ueno, and E. Kominami, *LC3 and Autophagy.* Methods Mol Biol, 2008. **445**: p. 77-88.
308. Kang, R., et al., *The Beclin 1 network regulates autophagy and apoptosis.* Cell Death Differ, 2011. **18**(4): p. 571-80.
309. Tsai, C.C., et al., *Hypoxia inhibits senescence and maintains mesenchymal stem cell properties through down-regulation of E2A-p21 by HIF-TWIST.* Blood, 2011. **117**(2): p. 459-69.
310. Leontieva, O.V., et al., *Hypoxia suppresses conversion from proliferative arrest to cellular senescence.* Proc Natl Acad Sci U S A, 2012. **109**(33): p. 13314-8.
311. Lee, S.H., et al., *Hypoxia inhibits cellular senescence to restore the therapeutic potential of old human endothelial progenitor cells via the hypoxia-inducible factor-1alpha-TWIST-p21 axis.* Arterioscler Thromb Vasc Biol, 2013. **33**(10): p. 2407-14.
312. Gorissen, B., et al., *Hypoxia negatively affects senescence in osteoclasts and delays osteoclastogenesis.* J Cell Physiol, 2018. **234**(1): p. 414-426.
313. Kilic Eren, M. and V. Tabor, *The role of hypoxia inducible factor-1 alpha in bypassing oncogene-induced senescence.* PLoS One, 2014. **9**(7): p. e101064.
314. Kopan, R. and M.X. Ilagan, *The canonical Notch signaling pathway: unfolding the activation mechanism.* Cell, 2009. **137**(2): p. 216-33.
315. Ntziachristos, P., et al., *From fly wings to targeted cancer therapies: a centennial for notch signaling.* Cancer Cell, 2014. **25**(3): p. 318-34.
316. Hoare, M., et al., *NOTCH1 mediates a switch between two distinct secretomes during senescence.* Nat Cell Biol, 2016. **18**(9): p. 979-92.
317. Teo, Y.V., et al., *Notch Signaling Mediates Secondary Senescence.* Cell Rep, 2019. **27**(4): p. 997-1007 e5.
318. Brookes, S., et al., *INK4a-deficient human diploid fibroblasts are resistant to RAS-induced senescence.* EMBO J, 2002. **21**(12): p. 2936-45.
319. Huot, T.J., et al., *Biallelic mutations in p16(INK4a) confer resistance to Ras- and Ets-induced senescence in human diploid fibroblasts.* Mol Cell Biol, 2002. **22**(23): p. 8135-43.
320. Hills, S.A. and J.F. Diffley, *DNA replication and oncogene-induced replicative stress.* Curr Biol, 2014. **24**(10): p. R435-44.
321. Sears, R., et al., *Multiple Ras-dependent phosphorylation pathways regulate Myc protein stability.* Genes Dev, 2000. **14**(19): p. 2501-14.
322. Gregory, M.A., Y. Qi, and S.R. Hann, *Phosphorylation by glycogen synthase kinase-3 controls c-myc proteolysis and subnuclear localization.* J Biol Chem, 2003. **278**(51): p. 51606-12.

323. Bachireddy, P., P.K. Bendapudi, and D.W. Felsher, *Getting at MYC through RAS.* Clin Cancer Res, 2005. **11**(12): p. 4278-81.
324. Zindy, F., et al., *Myc signaling via the ARF tumor suppressor regulates p53-dependent apoptosis and immortalization.* Genes Dev, 1998. **12**(15): p. 2424-33.
325. Larsson, L.G. and M.A. Henriksson, *The Yin and Yang functions of the Myc oncoprotein in cancer development and as targets for therapy.* Exp Cell Res, 2010. **316**(8): p. 1429-37.
326. Land, H., L.F. Parada, and R.A. Weinberg, *Tumorigenic conversion of primary embryo fibroblasts requires at least two cooperating oncogenes.* Nature, 1983. **304**(5927): p. 596-602.
327. Hydbring, P., et al., *Phosphorylation by Cdk2 is required for Myc to repress Ras-induced senescence in cotransformation.* Proc Natl Acad Sci U S A, 2010. **107**(1): p. 58-63.
328. Zhang, F., et al., *MYC and RAS are unable to cooperate in overcoming cellular senescence and apoptosis in normal human fibroblasts.* Cell Cycle, 2018. **17**(24): p. 2697-2715.
329. Delmore, J.E., et al., *BET bromodomain inhibition as a therapeutic strategy to target c-Myc.* Cell, 2011. **146**(6): p. 904-17.
330. TeSlaa, T. and M.A. Teitell, *Techniques to monitor glycolysis.* Methods Enzymol, 2014. **542**: p. 91-114.
331. Teague, W.M., et al., *Function of phosphorylation sites on pyruvate dehydrogenase.* Biochem Biophys Res Commun, 1979. **87**(1): p. 244-52.
332. Cao, W., et al., *Discovery and confirmation of O-GlcNAcylated proteins in rat liver mitochondria by combination of mass spectrometry and immunological methods.* PLoS One, 2013. **8**(10): p. e76399.
333. Anderson, K.A. and M.D. Hirschey, *Mitochondrial protein acetylation regulates metabolism.* Essays Biochem, 2012. **52**: p. 23-35.
334. Iwasaki, Y., et al., *Separation technique for the determination of highly polar metabolites in biological samples.* Metabolites, 2012. **2**(3): p. 496-515.
335. Coulier, L., et al., *Simultaneous quantitative analysis of metabolites using ion-pair liquid chromatography-electrospray ionization mass spectrometry.* Anal Chem, 2006. **78**(18): p. 6573-82.
336. Gorgoulis, V., et al., *Cellular Senescence: Defining a Path Forward.* Cell, 2019. **179**(4): p. 813-827.
337. Szabo, C., et al., *Regulation of mitochondrial bioenergetic function by hydrogen sulfide. Part I. Biochemical and physiological mechanisms.* Br J Pharmacol, 2014. **171**(8): p. 2099-122.
338. Teng, H., et al., *Oxygen-sensitive mitochondrial accumulation of cystathionine beta-synthase mediated by Lon protease.* Proc Natl Acad Sci U S A, 2013. **110**(31): p. 12679-84.
339. Szabo, C., et al., *Tumor-derived hydrogen sulfide, produced by cystathionine-beta-synthase, stimulates bioenergetics, cell proliferation, and angiogenesis in colon cancer.* Proc Natl Acad Sci U S A, 2013. **110**(30): p. 12474-9.
340. Phillips, C.M., et al., *Upregulation of Cystathionine-beta-Synthase in Colonic Epithelia Reprograms Metabolism and Promotes Carcinogenesis.* Cancer Res, 2017. **77**(21): p. 5741-5754.

341. Bhattacharyya, S., et al., *Cystathionine beta-synthase (CBS) contributes to advanced ovarian cancer progression and drug resistance.* PLoS One, 2013. **8**(11): p. e79167.
342. Sen, S., et al., *Role of cystathionine beta-synthase in human breast Cancer.* Free Radic Biol Med, 2015. **86**: p. 228-38.
343. Takano, N., et al., *Decreased expression of cystathionine beta-synthase promotes glioma tumorigenesis.* Mol Cancer Res, 2014. **12**(10): p. 1398-406.
344. Campisi, J., *Aging, cellular senescence, and cancer.* Annu Rev Physiol, 2013. **75**: p. 685-705.
345. Caudill, M.A., et al., *Intracellular S-adenosylhomocysteine concentrations predict global DNA hypomethylation in tissues of methyl-deficient cystathionine beta-synthase heterozygous mice.* J Nutr, 2001. **131**(11): p. 2811-8.
346. Petersen, L.C., *The effect of inhibitors on the oxygen kinetics of cytochrome c oxidase.* Biochim Biophys Acta, 1977. **460**(2): p. 299-307.
347. Hill, B.C., et al., *Interactions of sulphide and other ligands with cytochrome c oxidase. An electron-paramagnetic-resonance study.* Biochem J, 1984. **224**(2): p. 591-600.
348. Chan, K.T., et al., *A functional genetic screen defines the AKT-induced senescence signaling network.* Cell Death & Differentiation, 2019: p. 1-17.
349. Willems, P.H., et al., *Redox Homeostasis and Mitochondrial Dynamics.* Cell Metab, 2015. **22**(2): p. 207-18.
350. Wu, X.Y., et al., *Identification of HRAS as cancer-promoting gene in gastric carcinoma cell aggressiveness.* Am J Cancer Res, 2016. **6**(9): p. 1935-1948.
351. Kruger, W.D. and D.R. Cox, *A yeast assay for functional detection of mutations in the human cystathionine beta-synthase gene.* Hum Mol Genet, 1995. **4**(7): p. 1155-61.
352. Nogueira, V., et al., *Akt determines replicative senescence and oxidative or oncogenic premature senescence and sensitizes cells to oxidative apoptosis.* Cancer Cell, 2008. **14**(6): p. 458-70.
353. Liu, Y., et al., *Pro-inflammatory cytokine-driven PI3K/Akt/Sp1 signalling and H2S production facilitates the pathogenesis of severe acute pancreatitis.* Biosci Rep, 2017. **37**(2).
354. Yin, P., et al., *Sp1 is involved in regulation of cystathionine gamma-lyase gene expression and biological function by PI3K/Akt pathway in human hepatocellular carcinoma cell lines.* Cell Signal, 2012. **24**(6): p. 1229-40.
355. Malmezat, T., et al., *Glutathione turnover is increased during the acute phase of sepsis in rats.* J Nutr, 2000. **130**(5): p. 1239-46.
356. Zhu, J., et al., *Transsulfuration Activity Can Support Cell Growth upon Extracellular Cysteine Limitation.* Cell Metab, 2019. **30**(5): p. 865-876 e5.
357. Li, N., et al., *The H2S Donor NaHS Changes the Expression Pattern of H2S-Producing Enzymes after Myocardial Infarction.* Oxid Med Cell Longev, 2016. **2016**: p. 6492469.
358. Fu, M., et al., *Hydrogen sulfide (H2S) metabolism in mitochondria and its regulatory role in energy production.* Proc Natl Acad Sci U S A, 2012. **109**(8): p. 2943-8.
359. Smith, R.A., et al., *Selective targeting of an antioxidant to mitochondria.* Eur J Biochem, 1999. **263**(3): p. 709-16.

360. Ulrey, C.L., et al., *The impact of metabolism on DNA methylation.* Hum Mol Genet, 2005. **14 Spec No 1**: p. R139-47.
361. Walker, C., E. Mojares, and A. Del Rio Hernandez, *Role of Extracellular Matrix in Development and Cancer Progression.* Int J Mol Sci, 2018. **19**(10).
362. Zhang, D., et al., *Homocysteine activates vascular smooth muscle cells by DNA demethylation of platelet-derived growth factor in endothelial cells.* J Mol Cell Cardiol, 2012. **53**(4): p. 487-96.
363. Schneider, B.J., et al., *Phase I Study of Epigenetic Priming with Azacitidine Prior to Standard Neoadjuvant Chemotherapy for Patients with Resectable Gastric and Esophageal Adenocarcinoma: Evidence of Tumor Hypomethylation as an Indicator of Major Histopathologic Response.* Clin Cancer Res, 2017. **23**(11): p. 2673-2680.
364. Kim, J., et al., *Expression of cystathionine beta-synthase is downregulated in hepatocellular carcinoma and associated with poor prognosis.* Oncol Rep, 2009. **21**(6): p. 1449-54.
365. Ramanathan, R.K., et al., *Phase 2 study of MK-2206, an allosteric inhibitor of AKT, as second-line therapy for advanced gastric and gastroesophageal junction cancer: A SWOG cooperative group trial (S1005).* Cancer, 2015. **121**(13): p. 2193-7.
366. Yang, C.T., et al., *Data-Driven Identification of Hydrogen Sulfide Scavengers.* Angew Chem Int Ed Engl, 2019. **58**(32): p. 10898-10902.
367. Zhang, L., et al., *An Anticancer Role of Hydrogen Sulfide in Human Gastric Cancer Cells.* Oxid Med Cell Longev, 2015. **2015**: p. 636410.
368. Koppula, P., et al., *Amino acid transporter SLC7A11/xCT at the crossroads of regulating redox homeostasis and nutrient dependency of cancer.* Cancer Commun (Lond), 2018. **38**(1): p. 12.
369. Obata, F. and M. Miura, *Enhancing S-adenosyl-methionine catabolism extends Drosophila lifespan.* Nat Commun, 2015. **6**: p. 8332.
370. Parkhitko, A.A., et al., *Tissue-specific down-regulation of S-adenosyl-homocysteine via suppression of dAhcyL1/dAhcyL2 extends health span and life span in Drosophila.* Genes Dev, 2016. **30**(12): p. 1409-22.
371. Beluzic, L., et al., *Knock-down of AHCY and depletion of adenosine induces DNA damage and cell cycle arrest.* Sci Rep, 2018. **8**(1): p. 14012.
372. Wu, G., et al., *Metabolic perturbation of epigenome by inhibiting S-adenosylhomocysteine hydrolase elicits senescence through DNA damage response in hepatoma cells.* Tumour Biol, 2017. **39**(5): p. 1010428317699117.
373. Wang, Y., Z. Sun, and M. Szyf, *S-adenosyl-methionine (SAM) alters the transcriptome and methylome and specifically blocks growth and invasiveness of liver cancer cells.* Oncotarget, 2017. **8**(67): p. 111866-111881.
374. Esteve, P.O., et al., *A methylation and phosphorylation switch between an adjacent lysine and serine determines human DNMT1 stability.* Nat Struct Mol Biol, 2011. **18**(1): p. 42-8.
375. Popkie, A.P., et al., *Phosphatidylinositol 3-kinase (PI3K) signaling via glycogen synthase kinase-3 (Gsk-3) regulates DNA methylation of imprinted loci.* J Biol Chem, 2010. **285**(53): p. 41337-47.
376. Badeaux, A.I. and Y. Shi, *Emerging roles for chromatin as a signal integration and storage platform.* Nat Rev Mol Cell Biol, 2013. **14**(4): p. 211-24.

377. Macip, S., et al., *Influence of induced reactive oxygen species in p53-mediated cell fate decisions.* Mol Cell Biol, 2003. **23**(23): p. 8576-85.
378. Lu, T. and T. Finkel, *Free radicals and senescence.* Exp Cell Res, 2008. **314**(9): p. 1918-22.
379. Chatterjee, S., et al., *Membrane depolarization is the trigger for PI3K/Akt activation and leads to the generation of ROS.* Am J Physiol Heart Circ Physiol, 2012. **302**(1): p. H105-14.
380. Chen, Q., et al., *Akt phosphorylates p47phox and mediates respiratory burst activity in human neutrophils.* J Immunol, 2003. **170**(10): p. 5302-8.
381. Chen, Q., et al., *Production of reactive oxygen species by mitochondria: central role of complex III.* J Biol Chem, 2003. **278**(38): p. 36027-31.
382. Li, C., et al., *PI3K/AKT signaling regulates bioenergetics in immortalized hepatocytes.* Free Radic Biol Med, 2013. **60**: p. 29-40.
383. Starkov, A.A., et al., *Mitochondrial alpha-ketoglutarate dehydrogenase complex generates reactive oxygen species.* J Neurosci, 2004. **24**(36): p. 7779-88.
384. Bhattacharyya, A., et al., *Oxidative stress: an essential factor in the pathogenesis of gastrointestinal mucosal diseases.* Physiol Rev, 2014. **94**(2): p. 329-54.
385. Kukreja, R.C., et al., *PGH synthase and lipoxygenase generate superoxide in the presence of NADH or NADPH.* Circ Res, 1986. **59**(6): p. 612-9.
386. Richardson, A.G. and E.E. Schadt, *The role of macromolecular damage in aging and age-related disease.* J Gerontol A Biol Sci Med Sci, 2014. **69 Suppl 1**: p. S28-32.
387. Reliene, R. and R.H. Schiestl, *Glutathione depletion by buthionine sulfoximine induces DNA deletions in mice.* Carcinogenesis, 2006. **27**(2): p. 240-4.
388. Lien, E.C., et al., *Glutathione biosynthesis is a metabolic vulnerability in PI(3)K/Akt-driven breast cancer.* Nat Cell Biol, 2016. **18**(5): p. 572-8.
389. Kolesnichenko, M., et al., *Attenuation of TORC1 signaling delays replicative and oncogenic RAS-induced senescence.* Cell Cycle, 2012. **11**(12): p. 2391-401.
390. Demidenko, Z.N., et al., *Rapamycin decelerates cellular senescence.* Cell Cycle, 2009. **8**(12): p. 1888-95.
391. Pospelova, T.V., et al., *Suppression of replicative senescence by rapamycin in rodent embryonic cells.* Cell Cycle, 2012. **11**(12): p. 2402-7.
392. Wall, M., et al., *The mTORC1 inhibitor everolimus prevents and treats Emu-Myc lymphoma by restoring oncogene-induced senescence.* Cancer Discov, 2013. **3**(1): p. 82-95.
393. Sarkisian, C.J., et al., *Dose-dependent oncogene-induced senescence in vivo and its evasion during mammary tumorigenesis.* Nat Cell Biol, 2007. **9**(5): p. 493-505.
394. Salama, R., et al., *Cellular senescence and its effector programs.* Genes Dev, 2014. **28**(2): p. 99-114.

Appendices

Hindawi
BioMed Research International
Volume 2018, Article ID 3205125, 11 pages
https://doi.org/10.1155/2018/3205125

Review Article

Cystathionine β-Synthase in Physiology and Cancer

Haoran Zhu,[1,2] Shaun Blake,[1,2] Keefe T. Chan,[1] Richard B. Pearson,[1,2,3,4] and Jian Kang[1]

[1] *Division of Research, Peter MacCallum Cancer Centre, 305 Grattan Street, Melbourne, Victoria 3000, Australia*
[2] *Sir Peter MacCallum Department of Oncology, Australia*
[3] *Department of Biochemistry and Molecular Biology, University of Melbourne, Parkville, Victoria 3052, Australia*
[4] *Department of Biochemistry and Molecular Biology, Monash University, Clayton, Victoria 3168, Australia*

Correspondence should be addressed to Richard B. Pearson; rick.pearson@petermac.org

Received 23 March 2018; Accepted 29 May 2018; Published 28 June 2018

Academic Editor: Maria L. Tornesello

Copyright © 2018 Haoran Zhu et al. This is an open access article distributed under the Creative Commons Attribution License, which permits unrestricted use, distribution, and reproduction in any medium, provided the original work is properly cited.

Cystathionine β-synthase (CBS) regulates homocysteine metabolism and contributes to hydrogen sulfide (H_2S) biosynthesis through which it plays multifunctional roles in the regulation of cellular energetics, redox status, DNA methylation, and protein modification. Inactivating mutations in CBS contribute to the pathogenesis of the autosomal recessive disease CBS-deficient homocystinuria. Recent studies demonstrating that CBS promotes colon and ovarian cancer growth in preclinical models highlight a newly identified oncogenic role for CBS. On the contrary, tumor-suppressive effects of CBS have been reported in other cancer types, suggesting context-dependent roles of CBS in tumor growth and progression. Here, we review the physiological functions of CBS, summarize the complexities regarding CBS research in oncology, and discuss the potential of CBS and its key metabolites, including homocysteine and H_2S, as potential biomarkers for cancer diagnosis or therapeutic targets for cancer treatment.

1. Introduction

Cystathionine β-synthase (CBS) catalyzes the condensation of homocysteine (Hcy) with serine to form cystathionine, which is the initial and rate-limiting step in the transsulfuration pathway. Cystathionine is subsequently cleaved by the enzyme cystathionine gamma-lyase (CTH) to form cysteine, a precursor of glutathione. Besides this canonical pathway, CBS also participates in the desulfuration reactions that contribute to endogenous hydrogen sulfide (H_2S) production (Figure 1). Thus, CBS acting mainly through control of Hcy and H_2S metabolism exerts diverse biological functions including mitochondrial bioenergetics, redox homeostasis, DNA methylation and protein modification. Deregulation of CBS and the associated alterations in Hcy and/or H_2S levels leads to a wide range of pathological disturbances in the cardiovascular, immune, and central nervous systems and contributes to disease development, such as CBS-deficient homocystinuria (CBSDH). It is now becoming clear that CBS activity also plays an important but complex role in cancer biology. This review focuses on the current understanding of the functional role of CBS and the derived metabolites Hcy and H_2S in cancer pathogenesis and provides insight into the development of novel prognostic markers and therapeutic approaches for cancer patients.

2. CBS Protein Structure and Biological Functions

The human *CBS* gene encodes a protein of 551 amino acids. The crystal structure of the active form of human CBS, formed by four of 63-kDa subunits, has been fully characterized [1, 2]. Each subunit consists of three structural domains. The N-terminal domain binds to the cofactor heme, which is required for successful protein folding and assembly but not necessary for catalytic activity [3]. The catalytic domain encompasses a binding site for another cofactor, pyridoxal-phosphate (PLP) [4]. The C-terminal regulatory domain contains two CBS motifs (CBS1 and CBS2) that dimerize to form a Bateman domain. This domain is responsible for CBS

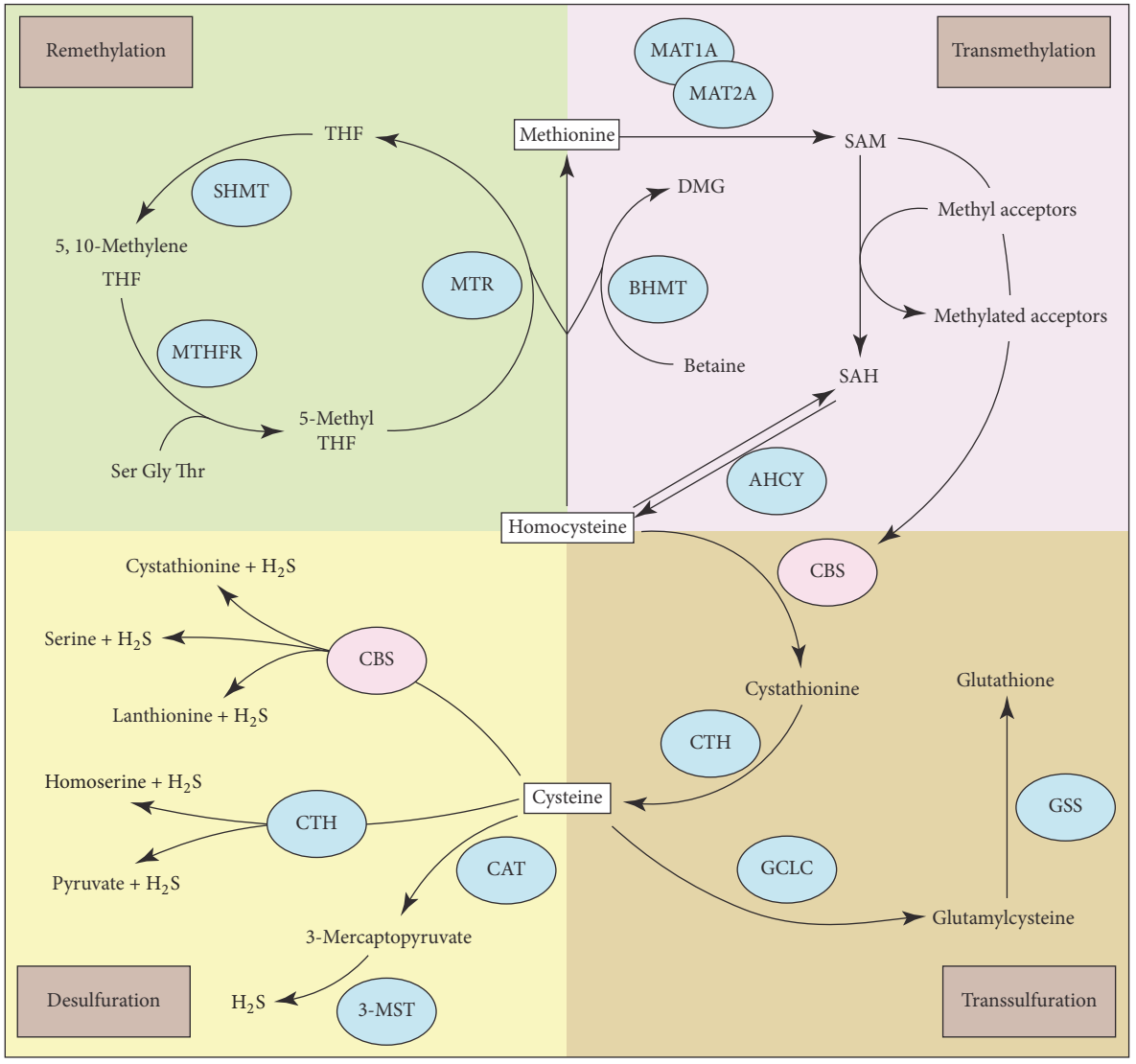


Figure 1: *Metabolic reactions catalyzed by CBS.* CBS catalyzes the condensation of homocysteine (Hcy) with serine to form cystathionine which is subsequently cleaved by cystathionine gamma-lyase (CTH) to form cysteine, a precursor of glutathione. CBS also catalyzes the production of H_2S. In addition to CBS, CTH and 3-mercaptopyruvate sulfurtransferase (3-MST) are also involved in the conversion of cysteine to H_2S. Homocysteine is another key CBS-derived metabolite and is linked to the metabolism of methionine. Methionine is converted to homocysteine via S-adenosyl methionine (SAM) and S-adenosyl homocysteine (SAH), releasing a methyl group that is used in numerous methylation reactions. SAM is an allosteric activator of CBS. 3-MST, 3-mercaptopyruvate sulfurtransferase; AHCY, adenosylhomocysteinase; BHMT, betaine-homocysteine methyltransferase; CAT, cysteine aminotransferase; CBS, cystathionine β-synthase; CTH, cystathionine gamma-lyase; GCLC, gamma-glutamylcysteine synthetase; GSS, glutathione synthetase; MAT1A/2A, methionine adenosyltransferase 1A/2A; MTHFR, methylenetetrahydrofolate reductase; MTR, 5-methyltetrahydrofolate-homocysteine methyltransferase; SAM, S-adenosyl methionine; SAH, S-adenosyl homocysteine; SHMT, serine hydroxymethyltransferase.

subunit tetramerization and contains the binding sites for the allosteric activator S-adenosylmethionine (SAM) [1, 5, 6]. In the native quaternary structure, the access of substrates to the catalytic core is occluded by the C-terminal regulatory motifs and the binding of SAM induces a conformational change that improves the access of the substrates to the catalytic site [2]. The autoinhibitory function of the C-terminal regulatory domain is relieved by the C-terminal truncation that generates a 45 kDa isoform with higher basal catalytic activity than the full-length form [1].

CBS is predominantly expressed in the brain, liver, kidney, and pancreas. It is mainly a cytosolic enzyme, but localization in the nucleus [7] and mitochondria [8] had been detected in specific cell types. CBS can be translocated to the mitochondria in response to hypoxia [9] or nucleolar stress [10]. CBS expression is regulated at multiple levels upon different stimuli. For example, hormonal regulation by glucocorticoids increases CBS expression at the transcriptional level in liver cells, a process that may be perturbed by insulin administration through binding to an

insulin-sensitive sequence localized on the CBS promoter [11]. In addition, testosterone can regulate CBS expression and activity in renal tissue [12]. Growth/differentiation factors such as EGF, TGF-α, cAMP, and dexamethasone induced CBS protein expression in mouse astrocytes [13]. Hypoxia upregulated CBS expression either via hypoxia-inducible factor- (HIF-) 1 at the transcriptional level [14] or decreased degradation of CBS protein by Lon proteases in the mitochondria [9]. Besides HIF-1, the zinc finger transcription factor SP1 binds to the *CBS* gene promoter, establishing its role as a key regulator of CBS expression [15, 16]. Furthermore, CBS activity may be enhanced via posttranslational regulation through S-glutathionylation [17] or inhibited via epigenetic downregulation of CBS expression through promoter methylation [18, 19].

CBS plays a critical role in Hcy elimination. Patients with CBS deficiency exhibit elevated Hcy plasma levels at excess of 200 μM compared to 5-15 μM in healthy adults [20]. CBS-deficient homocystinuria (CBSDH) is an autosomal recessive metabolic disease, resulting from inactivating mutations in the *CBS* gene. CBSDH patients present multiple pathologic changes in the eye, skeleton, central nervous, and vascular systems. Common symptoms in CBSDH patients include thrombosis, osteoporosis, and impaired mental cognitive development (reviewed in [21–23]). Administration of high doses of the PLP precursor, pyridoxine, or vitamin B_6 is common treatment that ameliorates approximately 50% of clinical symptoms. To date, 164 pathogenic genetic variants have been identified (http://cbs.lf1.cuni.cz/mutations.php) of which the predominant mutations are missense mutations. c.833 T > C (p.I278T) is the most frequent mutation detected in many European populations [24]. The I278T missense mutation and many of the less prevalent mutations likely affect the folding or stability of the CBS protein [25] whereas some mutations such as mutant D444N, a missense mutation in the C-terminal regulatory domain, showed an approximately twofold increase in basal CBS activity but impaired response to SAM stimulation [2]. The pathophysiology of CBS deficiency is still not fully understood. As well as the accumulation of Hcy, CBS defects lead to increased concentrations of methionine and S-adenosyl-L-homocysteine (SAH) and depletion of cystathionine and cysteine. These perturbations may act in concert with high Hcy to promote the development and progression of CBSDH (reviewed in [26]).

Accordingly, extensive studies in the mouse models of CBS deficiency showed mice with homozygotic *CBS* deletion (CBS-/-) died within 4 weeks after birth due to severe hepatic dysfunction and exhibited extremely high levels of circulating Hcy (reviewed in [26, 27]). Wang et al. showed that the neonatal lethality could be rescued by decreasing circulating Hcy levels in a transgenic mouse model with inducible CBS expression [28]. They further found that there may be a threshold effect with Hcy, meaning that moderately lowering homocysteinemia can improve mouse viability during the neonatal period [29]. In support of the Hcy threshold effect, CBS+/- heterozygote mice were fully viable with a 3-fold increase of Hcy levels compared to the 8-fold increase in homozygous mice [30].

3. Homocysteine and H_2S, the Major CBS-Derived Metabolites

3.1. Homocysteine. Hcy is a sulfur-containing nonproteinogenic amino acid linked to the metabolism of methionine and cysteine. Methionine is converted to Hcy via S-adenosyl methionine (SAM) and SAH, releasing a methyl group that is used in numerous methylation reactions. Hcy can reform Met by the remethylation pathway either via 5-methyltetrahydrofolate-homocysteine methyltransferase (MTR, 5-methyltetrahydrofolate as the methyl group donor) or betaine-homocysteine methyltransferase (BHMT, betaine as the methyl group donor) (Figure 1). Hcy is also irreversibly metabolized by CBS to cystathionine that subsequently converts to cysteine via CTH in the transsulfuration pathway (Figure 1). Hcy metabolism mainly occurs in the liver and conversion to cystathionine by CBS is a major elimination route of Hcy [31].

Hyperhomocysteinemia (HHcy) is recognized as an independent risk factor for atherosclerotic vascular disease [32]. HHcy may result from mutations in genes encoding enzymes of Hcy biosynthesis and metabolism or deficiencies of vitamin cofactors including vitamin B_{12} and B_6 [33]. The molecular mechanisms underlying HHcy-induced atherosclerosis are complex and multifactorial (Figure 2). Elevated Hcy concentration reduces nitric oxide (NO) bioavailability and causes oxidative stress. HHcy also leads to formation of Hcy thiolactone as a result of error-prone editing by the methionyl-tRNA synthase [34]. This Hcy derivative can cause protein N-homocysteinylation in which the thioester group of thiolactone binds to the lysine residues in proteins, consequently impairing protein function, resulting in unfolded protein response and endoplasmic reticulum stress (reviewed in [35, 36]). Moreover, an elevated Hcy level could lead to accumulation of SAH, a competitive inhibitor of most methyltransferases, consequently inducing DNA hypomethylation [37]. Through this epigenetic mechanism, Hcy has been reported to inhibit endothelial cell growth by decreasing the expression of cyclin A [38], fibroblast growth factor 2 [39], and hTERT expression [40] and by upregulation of platelet-derived growth factors and P66shC [41].

HHcy has also been implicated in the pathogenesis of cancer. Increased release of Hcy by tumor cells is related to their rapid proliferation rate [42]. Hcy accumulation results from defects in methionine synthesis, leading to a methionine-dependent malignant phenotype [43]. A meta-analysis revealed the association of elevated circulating Hcy levels with increased overall risk of cancer [44]. A higher Hcy plasma level has been detected in the patients with hepatocellular carcinoma (HCC) [44] and head and neck squamous cell carcinoma [45]. Although the mechanisms underlying this association between elevated Hcy levels and malignant transformation are unclear, a recent study proposed a mechanism linking Hcy to lipid metabolism and HCC [46]. It demonstrated that Hcy transcriptionally upregulated CYP2J2, a cytochrome P450 (CYP) epoxygenase by stimulating DNA demethylation and increasing SP1/AP1 activity on the promoter of CYP2J2, which promotes epoxyeicosatrienoic acid synthesis and hepatocellular tumorigenesis.

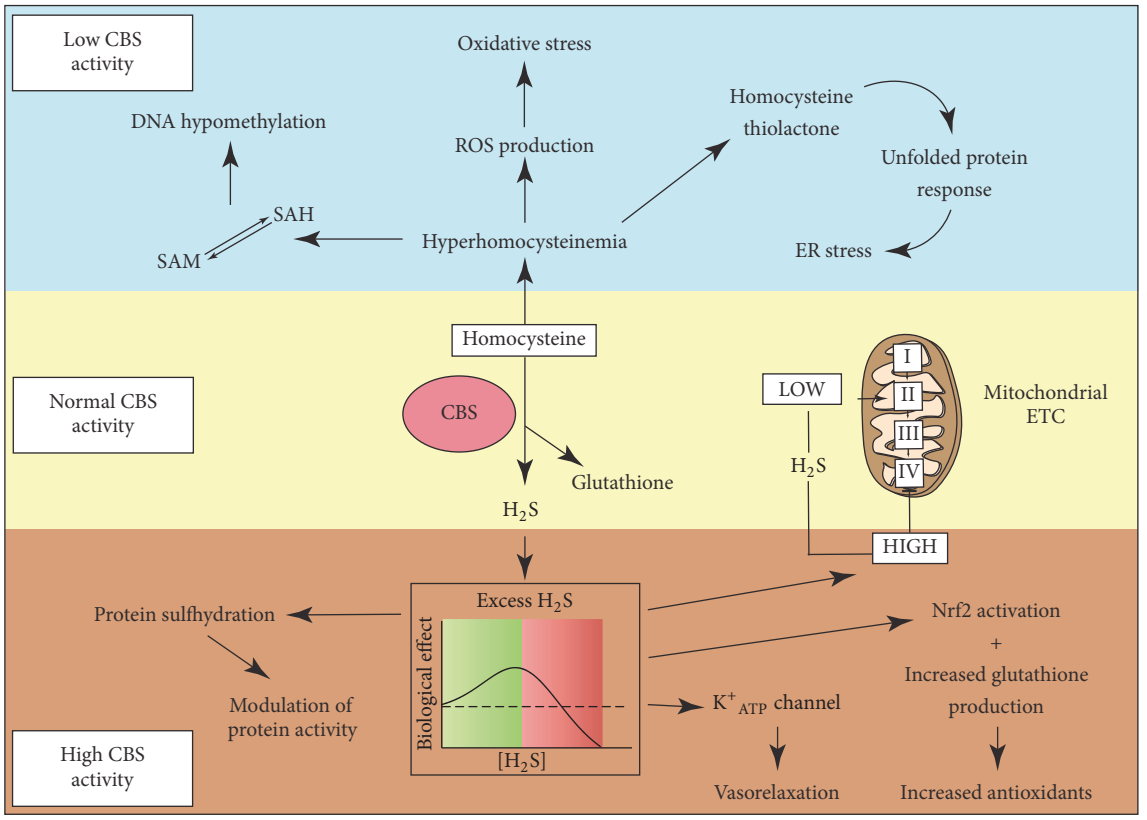


Figure 2: *Potential mechanisms underlying CBS deregulation with alterations of homocysteine and H_2S levels in cancer pathogenesis.* CBS deficiency causes hyperhomocysteinemia. Elevated Hcy concentration can increase reactive oxygen species (ROS) production and induce oxidative stress. Hyperhomocysteinemia also leads to formation of homocysteine thiolactone as a result of error-prone editing by the methionyl-tRNA synthase. This homocysteine derivative can cause protein N-homocysteinylation that impairs protein function, resulting in an unfolded protein response and endoplasmic reticulum (ER) stress. The elevated Hcy level can lead to accumulation of S-adenosyl homocysteine (SAH), a competitive inhibitor of most methyltransferases, consequently inducing DNA hypomethylation and affecting gene transcription. CBS-driven endogenous H_2S production maintains mitochondrial respiration and ATP synthesis, promotes antioxidant production by enhancing Nrf2 activation and increasing glutathione production, and modulates protein activity via protein sulfhydration. Secreted H_2S can cause vasodilation via activation of ATP-sensitive K^+ channels.

3.2. H_2S. Like nitric oxide and carbon monoxide, H_2S is a diffusible gaseous transmitter in the human body and is mainly synthesized during cysteine metabolism and excreted as urinary sulfates by the kidney (reviewed in [47]). CBS catalyzes the production of H_2S via at least three pathways including (i) converting cysteine to serine and H_2S, (ii) condensing cysteine and Hcy to yield cystathionine and H_2S, and (iii) condensing two cysteine molecules to lanthionine and H_2S (Figure 1). In addition to CBS, CTH and 3-mercaptopyruvate sulfurtransferase (3-MST) are also involved in the conversion of cysteine to H_2S (Figure 1).

While H_2S has diverse biological functions in the nervous, cardiovascular, and immune systems, the pathological role of H_2S in cancer biology has attracted substantial attention in recent years. CBS-driven endogenous H_2S production has been reported to support tumor growth by (i) maintaining mitochondrial respiration and ATP synthesis, (ii) stimulating cell proliferation and survival, (iii) redox balance, and (iv) vasodilation (Figure 2). H_2S modulates mitochondrial functions and cellular bioenergetics in a concentration-dependent manner. At low concentrations, H_2S acts as a mitochondrial electron donor to mitochondrial complex II, resulting in bioenergetic stimulation [48, 49]. At higher concentrations, H_2S acts as a mitochondrial poison via the inhibition of cytochrome *c* oxidase in mitochondrial complex IV [50]. H_2S stimulates cell proliferation through activation of specific kinase pathways (e.g., MAPK and PI3K/Akt) and inhibition of selective phosphatases such as PTEN and PTP1B [51–53]. Modulation of protein activity by H_2S either occurs via protein sulfhydration (reviewed in [54]) or intracellular formation of polysulfides by H_2S followed by oxidative inactivation of proteins [55, 56]. The sulfhydration of nuclear factor kappa B (NF-κB) by H_2S has also been shown to inhibit apoptosis and may be of particular relevance to cancer cell survival [57]. The protective effect of H_2S from oxidative stress has been extensively studied in endothelial cells and neurons [58–62]. Studies showed H_2S inhibited H_2O_2-mediated mitochondrial dysfunction by preserving the protein expression levels and activity of key antioxidant enzymes, inhibiting reactive oxygen species

(ROS) production and lipid peroxidation [60]. Additionally, these effects may be associated with sulfhydration of Keap1 and activation of Nrf2 [61] or increasing the production of the antioxidant glutathione. Vasorelaxation is one of the first recognized biological effects of H_2S. The mechanisms of H_2S-mediated vasodilation include the activation of ATP-sensitive K^+ channels, inhibition of phosphodiesterases, and a synergy with NO (reviewed in [63]).

H_2S-donating compounds deliver H_2S exogenously, including fast H_2S donors such as sulfate salts (e.g., NaHS and Na_2S) and naturally occurring compounds (e.g., the garlic constituent diallyl trisulfide, sulforaphane, erucin, and iberin) and slow H_2S-releasing synthetic moieties such as GYY4137 (reviewed in [64]). The cellular response to exogenous H_2S released by the donors has been considered as a biphasic response, in which low H_2S concentrations (or low H_2S production rates) showed enhancement of cell proliferation rates and cell viability whereas high H_2S caused deleterious/adverse effects in cells [50, 65]. This biphasic cellular response is consistent with the special action model of H_2S on mitochondrial respiration described above, that is, stimulation of mitochondrial respiration at low levels and inhibition at high levels. This bell-shape pharmacology of H_2S may, at least in part, explain the inconsistent results of the effect of exogenous H_2S in colon cancer cell line HCT116 reported by different groups including a growth inhibitory effect (using NaHS at 400 μM and 800 μM) by the Deng lab [66] and a growth stimulatory effect (using NaHS at 30-300 μM) by the Szabo lab [49, 65, 67].

4. CBS and Cancer

4.1. Promoting Tumor Growth by Activation of CBS. Elevated expression of CBS in tumor tissues or cell lines has been reported in colon [49, 68], ovarian [8], prostate [69], and breast cancer [70], compared to adjacent normal tissue or nontransformed cells. A series of studies from the Hellmich group characterized the oncogenic role of CBS in colon cancer [49, 68, 71]. Through modification of CBS expression (overexpression or RNAi knockdown) or CBS activity (allosteric activator SAM or the inhibitor aminooxyacetate) in the HCT116 colon cancer cell line, they demonstrated that CBS promoted cancer cell proliferation. The antiproliferative effect observed by silencing or inhibiting CBS was recapitulated in the xenograft mouse models and patient-derived tumor xenografts [49]. CBS not only promotes tumor growth and progression but also initiates tumor formation [68]. Overexpression of CBS in adenoma-like colonic epithelial cell line NCM356 enhanced cell proliferative, anchorage-independent growth and invasive capability *in vitro* and tumorigenicity *in vivo*. Mice heterozygous for CBS showed fewer numbers of mutagen-induced aberrant crypt foci than wild-type controls. Through a similar approach, Bhattacharyya et al. [8] reported that CBS knockdown inhibited cell proliferation and suppressed tumor growth in an orthotopic mouse model of cisplatin-resistant ovarian cancer. Interestingly, in breast cancer silencing CBS did not affect cell proliferation in culture but significantly attenuated tumor growth in a xenograft mouse model [70].

The protumorigenic effect of CBS occurs through an autocrine mechanism by regulation of bioenergetics, antioxidant capacity, and apoptosis-related pathways. Targeting CBS genetically or pharmacologically impairs cellular bioenergetics through inhibiting mitochondrial electron transport, oxidative phosphorylation, and glycolysis. H_2S was identified to be responsible for such metabolic and bioenergetic rewiring in colon cancer cells, as CBS expression and activity correlated with H_2S production and exogenous H_2S stimulated cell proliferation and bioenergetics [49]. Systematic metabolomic analysis of CBS-overexpressing NCM356 cells uncovered an anabolic metabolic phenotype with significantly enhanced glycolysis, nucleotide synthesis, and lipogenesis, which is thought to promote malignant transformation [68]. CBS may also promote tumor cell survival by increasing cell intrinsic antioxidant capacity. Ovarian cancer cells depleted of CBS showed enhanced ROS production. Antioxidant glutathione, but not H_2S, fully rescued viability of CBS-depleted cells, suggesting that the effect of CBS in ovarian cancer cells is mediated through regulation of ROS production by glutathione [8]. Similarly, reduced glutathione abundance was observed in breast cancer cells upon CBS silencing and was accompanied by decreased Nrf2 expression [72]. CBS downregulation reduced antioxidant capacity and enhanced the sensitivity of cancer cells to chemotherapeutic drugs. The cytoprotective effect of CBS is also associated with regulation of NF-κB and p53 apoptosis-related signaling [8]. A recent study further suggested CBS is involved in nucleolar stress-induced apoptosis [10]. The authors demonstrated that treatment of p53-/- colon cancer cells with 5-fluorouracil caused nucleolar stress, which led to accumulation of the ribosome-free form of ribosomal protein L3 (rpL3). rpL3 decreased CBS protein abundance through suppression of SP1-mediated *CBS* gene transcription and increase of CBS protein degradation by translocation of CBS into mitochondria. Decreased CBS abundance and, in turn, reduction of H_2S production have been suggested to contribute to mitochondrial cytochrome C release and induction of the intrinsic cell death pathway [10].

In addition to autocrine regulation, CBS acts via a paracrine mechanism to modulate the tumor microenvironment including stimulating angiogenesis and vasodilation via H_2S production and release as reported in colon and ovarian cancer xenografts [8, 49] and regulating macrophage activation in breast cancer xenograft mouse models [70].

4.2. CBS Associated Oncogenesis Is Tumor Type-Specific. Unlike in colon, ovarian, and breast cancer, CBS does not appear to have a functional role in melanoma [73]. CBS expression is absent in dysplastic nevi, detected in only 25% of primary melanoma samples, and unregulated in four of five melanoma cell lines examined. More importantly, modulation of CBS expression had a minimal effect on melanoma cell proliferation [73].

Downregulation of CBS through promoter methylation has been observed in multiple gastric cancer cell lines and four colon cancer cell lines (including HCT116) [74]. However, the biological consequence of CBS epigenetic silencing in gastric cancer has not been determined. Evidence from

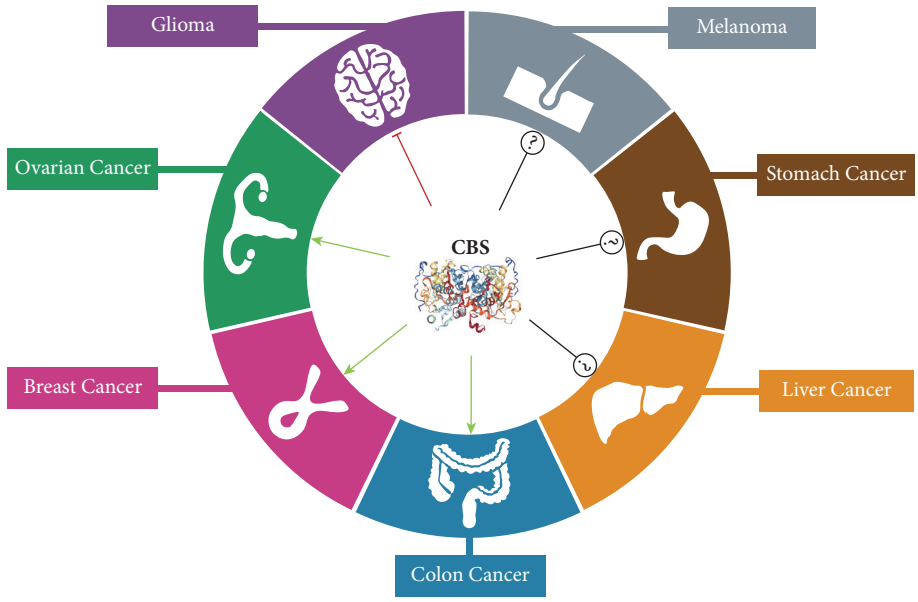


Figure 3: *CBS associated oncogenesis is tumor type-specific.* Activation of CBS promotes tumor growth in colon, ovarian, and breast cancer but suppresses tumor growth in glioma. The role of CBS in liver cancer, gastric cancer, and melanoma is still conflicting and inconclusive.

glioma supports a tumor-suppressive role for CBS [75]. CBS deficiency in U87-MG glioma cells did not affect cell proliferation in 2D culture but increased colony formation in soft agar, indicative of enhanced anchorage-independent growth. Consistently, CBS knockdown decreased tumor latency in U87-MG xenografts and increased tumor volume in an orthotopic model. Enhanced glioma tumorigenicity upon CBS loss was associated with upregulation of HIF-2α protein level and HIF-2α-dependent transcriptional activation of angiopoietin like 4 (ANGPTL4) and vascular endothelial growth factor A (VEGFA). The lack of function or suppression of tumor growth by CBS in certain tumor types indicates that CBS associated oncogenesis is tumor-specific (Figure 3).

4.3. Conflicting Role of CBS in Hepatocellular Carcinoma. Clinical evidence from patient samples strongly supports a negative regulatory role for CBS in hepatocellular carcinoma (HCC). Downregulation of CBS expression and activity contributes to the pathogenesis of multiple liver diseases (Reviewed in [76]). Analysis of 120 HCC specimens found that CBS mRNA was markedly lower in tumor tissues than surrounding noncancerous liver [77]. Reduced CBS expression was significantly correlated with the poor clinic pathological parameters including tumor stage, Edmondson grade, alpha-fetoprotein (AFP) level, and overall survival. Further data analysis suggested that the expression level of CBS mRNA could be used as a prognostic marker for overall survival especially in patients with low AFP levels [77]. Diminished CBS levels were also detected in the tumor tissues from the mouse model of HCC [78–80]. Further supporting the tumor-suppressive role for CBS, exogenous H_2S induced autophagy and apoptosis in HCC cells through the PI3K/Akt/mTOR pathway [81].

Intriguingly, distinct from this clinical data, a recent study showed that several HCC cell lines exhibited higher CBS expression than normal liver cells HL-7702 and QSG-7701 [82]. Both genetic (by siRNA) and pharmacological (by AOAA) inhibition of CBS in the SMMC-7721 HCC cell line with reduced H_2S production decreased cell viability and enhanced ROS production in *vitro*. Another study showing that the PI3K/AKT pathway regulated the CTH/H_2S to promote HCC proliferation also supports the oncogenic role of H_2S in HCC [53]. Clearly, the biological function of CBS in liver cancer is complex and requires further investigation.

5. CBS in Cancer Therapy

Consistent with the complex roles of CBS in cancer biology described above, it is also becoming evident that both the activators and inhibitors of CBS have antitumor activity in different cancer models. This genetic context dependence determines different types of cancer will display distinct efficacy and toxicity profiles in response to CBS-based targeted therapies.

5.1. CBS Inhibitors. Aminooxyacetate (AOAA) is currently considered as the most potent CBS inhibitor compared with the other drugs such as trifluoroalanine and hydroxylamine [65]. It has shown antitumor actions in the mouse xenograft models of colon [49] and breast cancer [83] and patient-derived colon cancer xenografts [49]. Decreased H_2S level in plasma was detected in a colon xenograft mouse model treated with AOAA while the drug effect on circulating Hcy level was not investigated. While these antitumor responses are encouraging, the therapeutic effect of CBS inhibition requires further investigation as AOAA is actually not

selective for CBS [65, 84]. The pharmacological action of AOAA is not limited to suppression of the CBS/ H_2S axis. It binds irreversibly to the cofactor PLP, and therefore, in addition to CBS, it inhibits other PLP-dependent enzymes such as CTH, 3-MST, and glutamate oxaloacetate transaminase 1 (GOT1). AOAA has been reported to target CTH preferentially over CBS (IC50 8.52 μM for CBS versus 1.09 μM for CTH) [85]. Furthermore, inhibition of GOT1 by AOAA disrupted the malate/aspartate shuttle, decreased glucose-derived carbon flux into mitochondrial tricarboxylic acid cycle, and ATP synthesis [83].

To identify new CBS inhibitors, two groups performed small-molecule screening [86, 87]. The Barrios group [87] and the Wu group [86] used recombinant CBS enzymes and employed fluorescent H_2S readouts to screen a composite library of 1900 compounds and a chemical library consisting of 20,000 compounds, respectively. Several compounds showed some selectivity for CBS compared with CTH with IC50 20-50 μM. However, as the studies did not use AOAA as a reference in the screen, whether these drugs are superior to AOAA in terms of potency and selectivity remains unknown.

5.2. CBS Activator S-Adenosyl-L-Methionine (SAM). SAM is a vital molecule for transmethylation and transsulfuration reactions. It is the principle methyl-donor for DNA, amino acid, protein, and lipid methyltransferase and a key precursor for glutathione and polyamine synthesis (reviewed by [88]). It is synthesized from methionine and ATP by methionine adenosyltransferase (MAT, Figure 1). SAM, as an allosteric activator, modulates CBS activity by inducing a conformational change in the C-terminus of CBS that facilitates the entrance of substrates into the catalytic site of the enzyme [1]. Although SAM has been used for treatment of osteoarthritis [89], depression [90], and liver diseases [88], the clinical evidence for its efficacy in these diseases is still inconclusive. Recent data support the concept of using SAM as a chemopreventive agent in HCC and colon cancer, consistent with the proposed tumor-suppressive role of CBS in HCC. The *Mat1a* knockout mice spontaneously develop HCC supporting the fact that hepatic SAM deficiency predisposes to HCC [91]. In several rodent models of HCC, administration of SAM is effective in preventing liver carcinogenesis [92, 93]. One phase II clinical trial is evaluating SAM as a potential chemoprevention agent in patients with hepatitis C cirrhosis [94]. SAM also showed a similar chemoprevention effect in an inflammation induced colon cancer mouse model [95]. In addition to chemoprevention, SAM exerted a proapoptotic effect in liver (at 0.2 mM over 5 days) [96], gastric (10 μM over 7 days) [97], and colon cancer cells (ranging from 0.25 to 5 mM for 24 hours) [98]. Interestingly, similar to the conflicting data regarding CBS function and effects of H_2S donors in colon cancer, the Szabo group [71] reported a biphasic response to SAM in colon cancer cells. At low concentrations for the short-time period (0.1-1 mM for 12 hours or 0.1 mM for 24 hours), SAM induced a stimulatory effect on CBS activation, H_2S production, and cell proliferation, while at higher concentrations or chronic exposure (0.1-5 mM after 24 hours) the inhibitory effects became more prominent and were not attenuated by CBS silencing, suggesting nonspecificity or toxicity [71]. Therefore, more work in multiple experiment models is required to better define the role of SAM/CBS axis in cancer pathogenesis.

6. CBS in Cancer Prognosis

With the identification of the pathogenic role of CBS in cancer, the use of CBS as a prognostic and predictive biomarker is becoming attractive. As described above, the negative correlation of CBS expression with the pathologic parameters in HCC indicates its potential as a prognostic marker in HCC [77]. Modulation of CBS activity can be indicated by the changes of Hcy and/or H_2S levels. The potential prognostic values of Hcy in cancer have been extensively studied [99–101]. However, the biological sources of Hcy were not defined in these studies and, thus, the link between the levels of Hcy and CBS function remains unknown. Nevertheless, significant progress in the detection and quantitation of Hcy from patient samples has been made in recent years. Methods of measuring plasma Hcy have evolved from ion-exchange chromatography to high-performance liquid chromatography (HPLC), gas-chromatography mass spectrometry, liquid chromatography-electrospray tandem mass spectrometry (LC-MS/MS), and fluorescence polarization immunoassay (FPIA) [102]. In terms of H_2S, elevated H_2S in exhaled breath or its degraded form in urine in cancer patients provides support for the clinical utility of H_2S as a marker of cancer [101]. However, in order to determine the prognostic and predictive values of H_2S in cancer, development of the methods that can accurately measure H_2S levels in the circulation or in the targeted organs is imperative.

7. Summary and Future Directions

A functional role for CBS in tumor biology is supported by (i) clinical evidence of altered CBS expression level and CBS-derived Hcy and H_2S levels in cancer patients; (ii) preclinical studies showing dysregulation of CBS function and activity in cancer cell culture and animal models; (iii) mechanistic investigations linking CBS to cancer-related cellular and molecular changes and signaling pathways. The distinct biological effects of CBS alterations in different cancer models reveal the complexity of CBS signaling in cancer pathogenesis. The contradictory role of CBS in cancer biology (Figure 3) is possibly due to the existence of alternative Hcy and H_2S metabolic pathways, and multiple modes of regulation of CBS expression and activity by hormones, growth factors, and other metabolites. Therefore, the functional role of CBS is determined by the distinct metabolic and genetic profiles in different types of cancer and is context-dependent. Furthermore, the current conflicting data adds an additional layer of complexity, indicating that multiple experimental and analytical approaches as well as in-depth mechanistic investigations are required to clarify the role of CBS in cancer biology.

Increased understanding of the role of the CBS-controlled network in cancer biology will greatly promote the development of pharmacological reagents targeting CBS and the identification of appropriate patient populations. CBS acts

through two main metabolites Hcy and H_2S, which have important physiological roles in specific tissues such as the liver, brain, and blood vessels. Given its central metabolic role, it is possible that CBS-based targeted therapy may cause side effects due to accumulation of unfavorable metabolites. For example, CBS inhibitors may elevate Hcy levels with potential risk for developing HHcy. Therefore, further studies will be required to define the therapeutic windows of the novel CBS targeting agents. Additional investigations are clearly required to better elucidate the complex role of CBS in malignant transformation including (i) characterizing the role of CBS-related metabolic signaling in cancer pathogenesis including but not limited to CBS, Hcy, H_2S, and the related enzymes; (ii) determining the interaction of tumor cell-derived CBS and its metabolites with the microenvironment; (iii) identifying biomarkers of CBS-based therapies in clinical samples and cancer models. Certainly, a greater appreciation for the complexity of CBS in cancer biology will give rise to new prospective biomarkers or targets for cancer.

Conflicts of Interest

The authors declare that there are no conflicts of interest regarding the publication of this paper.

Authors' Contributions

Richard B. Pearson and Jian Kang contributed equally to this work.

Acknowledgments

The authors apologize to the authors of many primary research papers that were not cited here due to space constraints but whose work influenced their understanding substantially. This work was supported by the National Health and Medical Research Council (NHMRC) of Australia project and program grants and Cancer Council Victoria. Researchers were funded by NHMRC Fellowships (Richard B. Pearson), a Melbourne International Research Scholarship (Haoran Zhu), and Research Training Program Scholarship (the University of Melbourne) (Shaun Blake).

References

[1] J. Ereño-Orbea, T. Majtan, I. Oyenarte, J. P. Kraus, and L. A. Martínez-Cruza, "Structural basis of regulation and oligomerization of human cystathionine β-synthase, the central enzyme of transsulfuration," *Proceedings of the National Acadamy of Sciences of the United States of America*, vol. 110, no. 40, pp. E3790–E3799, 2013.

[2] J. Ereno-Orbea, T. Majtan, I. Oyenarte, J. P. Kraus, and L. A. Martinez-Cruz, "Structural insight into the molecular mechanism of allosteric activation of human cystathionine β-synthase by S-adenosylmethionine," *Proceedings of the National Acadamy of Sciences of the United States of America*, vol. 111, no. 37, pp. E3845–E3852, 2014.

[3] T. Majtan, L. R. Singh, L. Wang, W. D. Kruger, and J. P. Kraus, "Active cystathionine β-synthase can be expressed in heme-free systems in the presence of metal-substituted porphyrins or a chemical chaperone," *The Journal of Biological Chemistry*, vol. 283, no. 50, pp. 34588–34595, 2008.

[4] M. Meier, M. Janosik, V. Kery, J. P. Kraus, and P. Burkhard, "Structure of human cystathionine β-synthase: a unique pyridoxal 5$\prime$-phosphate-dependent heme protein," *EMBO Journal*, vol. 20, no. 15, pp. 3910–3916, 2001.

[5] V. Kery, L. Poneleit, and J. P. Kraus, "Trypsin cleavage of human cystathionine β-synthase into an evolutionarily conserved active core: Structural and functional consequences," *Archives of Biochemistry and Biophysics*, vol. 355, no. 2, pp. 222–232, 1998.

[6] K.-H. Jhee, P. McPhie, and E. W. Miles, "Domain architecture of the heme-independent yeast cystathionine β-synthase provides insights into mechanisms of catalysis and regulation," *Biochemistry*, vol. 39, no. 34, pp. 10548–10556, 2000.

[7] O. Kabil, Y. Zhou, and R. Banerjee, "Human cystathionine β-synthase is a target for sumoylation," *Biochemistry*, vol. 45, no. 45, pp. 13528–13536, 2006.

[8] S. Bhattacharyya, S. Saha, K. Giri et al., "Cystathionine Beta-Synthase (CBS) Contributes to Advanced Ovarian Cancer Progression and Drug Resistance," *PLoS ONE*, vol. 8, no. 11, Article ID e79167, 2013.

[9] H. Teng, B. Wu, K. Zhao, G. Yang, L. Wu, and R. Wang, "Oxygen-sensitive mitochondrial accumulation of cystathionine β-synthase mediated by Lon protease," *Proceedings of the National Acadamy of Sciences of the United States of America*, vol. 110, no. 31, pp. 12679–12684, 2013.

[10] V. Pagliara, A. Saide, E. Mitidieri et al., "5-FU targets rpL3 to induce mitochondrial apoptosis via cystathionine-β-synthase in colon cancer cells lacking p53," *Oncotarget* , vol. 7, no. 31, pp. 50333–50348, 2016.

[11] S. Ratnam, K. N. Maclean, R. L. Jacobs, M. E. Brosnan, J. P. Kraus, and J. T. Brosnan, "Hormonal regulation of cystathionine β-synthase expression in liver," *The Journal of Biological Chemistry*, vol. 277, no. 45, pp. 42912–42918, 2002.

[12] V. Vitvitsky, A. Prudova, S. Stabler, S. Dayal, S. R. Lentz, and R. Banerjee, "Testosterone regulation of renal cystathionine β-synthase: Implications for sex-dependent differences in plasma homocysteine levels," *American Journal of Physiology-Renal Physiology*, vol. 293, no. 2, pp. F594–F600, 2007.

[13] Y. Enokido, E. Suzuki, K. Iwasawa, K. Namekata, H. Okazawa, and H. Kimura, "Cystathionine β-synthase, a key enzyme for homocysteine metabolism, is preferentially expressed in the radial glia/astrocyte lineage of developing mouse CNS," *The FASEB Journal*, vol. 19, no. 13, pp. 1854–1856, 2005.

[14] N. Takano, Y.-J. Peng, G. K. Kumar et al., "Hypoxia-inducible factors regulate human and rat cystathionine beta-synthase gene expression," *Biochemical Journal*, vol. 458, no. 2, pp. 203–211, 2014.

[15] K. N. Maclean, E. Kraus, and J. P. Kraus, "The Dominant Role of Sp1 in Regulating the Cystathionine β-Synthase -1a and -1b Promoters Facilitates Potential Tissue-specific Regulation by Kruppel-like Factors," *The Journal of Biological Chemistry*, vol. 279, no. 10, pp. 8558–8566, 2004.

[16] Y. Ge, M. A. Konrad, L. H. Matherly, and J. W. Taub, "Transcriptional regulation of the human cystathionine β-synthase -1b basal promoter: Synergistic transactivation by transcription factors NF-Y and Sp1/Sp3," *Biochemical Journal*, vol. 357, no. 1, pp. 97–105, 2001.

[17] W.-N. Niu, P. K. Yadav, J. Adamec, and R. Banerjee, "S-glutathionylation enhances human cystathionine β-synthase

activity under oxidative stress conditions," *Antioxidants & Redox Signaling*, vol. 22, no. 5, pp. 350–361, 2015.

[18] F. Qi, Y. Zhou, Y. Xiao et al., "Promoter demethylation of cystathionine-β-synthetase gene contributes to inflammatory pain in rats," *PAIN*, vol. 154, no. 1, pp. 34–45, 2013.

[19] H.-H. Zhang, J. Hu, Y.-L. Zhou et al., "Promoted interaction of nuclear factor-κB with demethylated cystathionine-β-synthetase gene contributes to gastric hypersensitivity in diabetic rats," *The Journal of Neuroscience*, vol. 33, no. 21, pp. 9028–9038, 2013.

[20] W. D. Kruger, L. Wang, K. H. Jhee, R. H. Singh, and L. J. Elsas II, "Cystathionine β-Synthase Deficiency in Georgia (USA): Correlation of Clinical and Biochemical Phenotype with Genotype," *Human Mutation*, vol. 22, no. 6, pp. 434–441, 2003.

[21] M. Meier, J. Oliveriusova, J. P. Kraus, and P. Burkhard, "Structural insights into mutations of cystathionine β-synthase," *Biochimica et Biophysica Acta (BBA) - Proteins and Proteomics*, vol. 1647, no. 1-2, pp. 206–213, 2003.

[22] M. Yamanishi, O. Kabil, S. Sen, and R. Banerjee, "Structural insights into pathogenic mutations in heme-dependent cystathionine-β-synthase," *Journal of Inorganic Biochemistry*, vol. 100, no. 12, pp. 1988–1995, 2006.

[23] A. A. M. Morris, V. Kozich, S. Santra et al., "Guidelines for the diagnosis and management of cystathionine beta-synthase deficiency," *Journal of Inherited Metabolic Disease*, vol. 40, no. 1, pp. 49–74, 2017.

[24] V. E. Shih, J. M. Fringer, R. Mandell et al., "A missense mutation (I278T) in the cystathionine β-synthase gene prevalent in pyridoxine-responsive homocystinuria and associated with mild clinical phenotype," *American Journal of Human Genetics*, vol. 57, no. 1, pp. 34–39, 1995.

[25] E. W. Miles and J. P. Kraus, "Cystathionine β-synthase: Structure, function, regulation, and location of homocystinuria-causing mutations," *The Journal of Biological Chemistry*, vol. 279, no. 29, pp. 29871–29874, 2004.

[26] W. D. Kruger, "Cystathionine β-synthase deficiency: Of mice and men," *Molecular Genetics and Metabolism*, vol. 121, no. 3, pp. 199–205, 2017.

[27] M. Watanabe, J. Osada, Y. Aratani et al., "Mice deficient in cystathionine β-synthase: animal models for mild and severe homocyst(e)inemia," *Proceedings of the National Acadamy of Sciences of the United States of America*, vol. 92, no. 5, pp. 1585–1589, 1995.

[28] L. Wang, K.-H. Jhee, X. Hua, P. M. DiBello, D. W. Jacobsen, and W. D. Kruger, "Modulation of cystathionine β-synthase level regulates total serum homocysteine in mice," *Circulation Research*, vol. 94, no. 10, pp. 1318–1324, 2004.

[29] S. Gupta, J. Kühnisch, A. Mustafa et al., "Mouse models of cystathionine β-synthase deficiency reveal significant threshold effects of hyperhomocysteinemia," *The FASEB Journal*, vol. 23, no. 3, pp. 883–893, 2009.

[30] N. Tyagi, N. Qipshidze, U. Sen, W. Rodriguez, A. Ovechkin, and S. C. Tyagi, "Cystathionine beta synthase gene dose dependent vascular remodeling in murine model of hyperhomocysteinemia," *International Journal of Physiology, Pathophysiology and Pharmacology*, vol. 3, no. 3, pp. 210–222, 2011.

[31] K. Robert, J. Nehmé, E. Bourdon et al., "Cystathionine β synthase deficiency promotes oxidative stress, fibrosis, and steatosis in mice liver," *Gastroenterology*, vol. 128, no. 5, pp. 1405–1415, 2005.

[32] L. M. Graham, L. E. Daly, H. M. Refsum et al., "Plasma homocysteine as a risk factor for vascular disease: The European Concerted Action Project," *Journal of the American Medical Association*, vol. 277, no. 22, pp. 1775–1781, 1997.

[33] S. Brustolin, R. Giugliani, and T. M. Félix, "Genetics of homocysteine metabolism and associated disorders," *Brazilian Journal of Medical and Biological Research*, vol. 43, no. 1, pp. 1–7, 2010.

[34] H. Jakubowski, "Proofreading in vivo: Editing of homocysteine by methionyl-tRNA synthetase in Escherichia coli," *Proceedings of the National Acadamy of Sciences of the United States of America*, vol. 87, no. 12, pp. 4504–4508, 1990.

[35] W. K. C. Lai and M. Y. Kan, "Homocysteine-induced endothelial dysfunction," *Annals of Nutrition and Metabolism*, vol. 67, no. 1, pp. 1–12, 2015.

[36] X. C. Wang, W. T. Sun, C. M. Yu et al., "ER stress mediates homocysteine-induced endothelial dysfunction: modulation of IKCa and SKCa channels," *Atherosclerosis*, vol. 242, no. 1, pp. 191–198, 2015.

[37] S. Zhou, Z. Zhang, and G. Xu, "Notable epigenetic role of hyperhomocysteinemia in atherogenesis," *Lipids in Health and Disease*, vol. 13, no. 1, article no. 134, 2014.

[38] M. S. Jamaluddin, I. Chen, F. Yang et al., "Homocysteine inhibits endothelial cell growth via DNA hypomethylation of the cyclin A gene," *Blood*, vol. 110, no. 10, pp. 3648–3655, 2007.

[39] P.-Y. Chang, S.-C. Lu, C.-M. Lee et al., "Homocysteine inhibits arterial endothelial cell growth through transcriptional down-regulation of fibroblast growth factor-2 involving G protein and DNA methylation," *Circulation Research*, vol. 102, no. 8, pp. 933–941, 2008.

[40] D. Zhang, X. Sun, J. Liu, X. Xie, W. Cui, and Y. Zhu, "Homocysteine accelerates senescence of endothelial cells via DNA hypomethylation of human telomerase reverse transcriptase," *Arteriosclerosis, Thrombosis, and Vascular Biology*, vol. 35, no. 1, pp. 71–78, 2015.

[41] C.-S. Kim, Y.-R. Kim, A. Naqvi et al., "Homocysteine promotes human endothelial cell dysfunction via site-specific epigenetic regulation of p66shc," *Cardiovascular Research*, vol. 92, no. 3, pp. 466–475, 2011.

[42] C.-F. Sun, T. R. Haven, T.-L. Wu, K.-C. Tsao, and J. T. Wu, "Serum total homocysteine increases with the rapid proliferation rate of tumor cells and decline upon cell death: A potential new tumor marker," *Clinica Chimica Acta*, vol. 321, no. 1-2, pp. 55–62, 2002.

[43] P. Cavuoto and M. F. Fenech, "A review of methionine dependency and the role of methionine restriction in cancer growth control and life-span extension," *Cancer Treatment Reviews*, vol. 38, no. 6, pp. 726–736, 2012.

[44] D. Zhang, X. Wen, W. Wu, Y. Guo, and W. Cui, "Elevated homocysteine level and folate deficiency associated with increased overall risk of carcinogenesis: Meta-analysis of 83 case-control studies involving 35,758 individuals," *PLoS ONE*, vol. 10, no. 5, Article ID e0123423, 2015.

[45] G. Almadori, F. Bussu, J. Galli et al., "Serum folate and homocysteine levels in head and neck squamous cell carcinoma," *Cancer*, vol. 94, no. 4, pp. 1006–1011, 2002.

[46] D. Zhang, J. Lou, X. Zhang et al., "Hyperhomocysteinemia results from and promotes hepatocellular carcinoma via CYP450 metabolism by CYP2J2 DNA methylation," *Oncotarget* , vol. 8, no. 9, pp. 15377–15392, 2017.

[47] C. Szabo, "Gasotransmitters in cancer: From pathophysiology to experimental therapy," *Nature Reviews Drug Discovery*, vol. 15, no. 3, pp. 185–203, 2016.

[48] E. Lagoutte, S. Mimoun, M. Andriamihaja, C. Chaumontet, F. Blachier, and F. Bouillaud, "Oxidation of hydrogen sulfide remains a priority in mammalian cells and causes reverse electron transfer in colonocytes," *Biochimica et Biophysica Acta (BBA) - Bioenergetics*, vol. 1797, no. 8, pp. 1500–1511, 2010.

[49] C. Szabo, C. Coletta, C. Chao et al., "Tumor-derived hydrogen sulfide, produced by cystathionine-β-synthase, stimulates bioenergetics, cell proliferation, and angiogenesis in colon cancer," *Proceedings of the National Acadamy of Sciences of the United States of America*, vol. 110, no. 30, pp. 12474–12479, 2013.

[50] C. Szabo, C. Ransy, K. Módis et al., "Regulation of mitochondrial bioenergetic function by hydrogen sulfide. Part I. Biochemical and physiological mechanisms," *British Journal of Pharmacology*, vol. 171, no. 8, pp. 2099–2122, 2014.

[51] W.-J. Cai, M.-J. Wang, P. K. Moore, H.-M. Jin, T. Yao, and Y.-C. Zhu, "The novel proangiogenic effect of hydrogen sulfide is dependent on Akt phosphorylation," *Cardiovascular Research*, vol. 76, no. 1, pp. 29–40, 2007.

[52] P. Manna and S. K. Jain, "Hydrogen sulfide and L-cysteine increase phosphatidylinositol 3,4,5-trisphosphate (PIP3) and glucose utilization by inhibiting phosphatase and tensin homolog (PTEN) protein and activating phosphoinositide 3-kinase (PI3K)/serine/threonine protein kinase (AKT)/protein kinase Czeta/lambda (PKCzeta/lambda) in 3T3l1 adipocytes," *The Journal of Biological Chemistry*, vol. 286, no. 46, pp. 39848–39859, 2011.

[53] P. Yin, C. Zhao, Z. Li et al., "Sp1 is involved in regulation of cystathionine γ-lyase gene expression and biological function by PI3K/Akt pathway in human hepatocellular carcinoma cell lines," *Cellular Signalling*, vol. 24, no. 6, pp. 1229–1240, 2012.

[54] B. D. Paul and S. H. Snyder, "H 2S signalling through protein sulfhydration and beyond," *Nature Reviews Molecular Cell Biology*, vol. 13, no. 8, pp. 499–507, 2012.

[55] R. Greiner, Z. Pálinkás, K. Bäsell et al., "Polysulfides link H_2S to protein thiol oxidation," *Antioxidants & Redox Signaling*, vol. 19, no. 15, pp. 1749–1765, 2013.

[56] Y. Kimura, Y. Mikami, K. Osumi, M. Tsugane, J.-I. Oka, and H. Kimura, "Polysulfides are possible H_2S-derived signaling molecules in rat brain," *The FASEB Journal*, vol. 27, no. 6, pp. 2451–2457, 2013.

[57] N. Sen, B. D. Paul, M. M. Gadalla et al., "Hydrogen sulfide-linked sulfhydration of NF-κB mediates its antiapoptotic actions," *Molecular Cell*, vol. 45, no. 1, pp. 13–24, 2012.

[58] P. B. L. Pun, J. Lu, E. M. Kan, and S. Moochhala, "Gases in the mitochondria," *Mitochondrion*, vol. 10, no. 2, pp. 83–93, 2010.

[59] K. Suzuki, G. Olah, K. Modis et al., "Hydrogen sulfide replacement therapy protects the vascular endothelium in hyperglycemia by preserving mitochondrial function," *Proceedings of the National Acadamy of Sciences of the United States of America*, vol. 108, no. 33, pp. 13829–13834, 2011.

[60] Y.-D. Wen, H. Wang, S.-H. Kho et al., "Hydrogen sulfide protects HUVECs against hydrogen peroxide induced mitochondrial dysfunction and oxidative stress," *PLoS ONE*, vol. 8, no. 2, Article ID e53147, 2013.

[61] G. Yang, K. Zhao, and Y. Ju, "Hydrogen sulfide protects against cellular senescence via S-sulfhydration of keap1 and activation of Nrf2," *Antioxidants & Redox Signaling*, vol. 18, no. 15, pp. 1906–1919, 2013.

[62] S. Koike, Y. Ogasawara, N. Shibuya, H. Kimura, and K. Ishii, "Polysulfide exerts a protective effect against cytotoxicity caused by t-buthylhydroperoxide through Nrf2 signaling in neuroblastoma cells," *FEBS Letters*, vol. 587, no. 21, pp. 3548–3555, 2013.

[63] R. Wang, "Physiological implications of hydrogen sulfide: a whiff exploration that blossomed," *Physiological Reviews*, vol. 92, no. 2, pp. 791–896, 2012.

[64] K. Kashfi and K. R. Olson, "Biology and therapeutic potential of hydrogen sulfide and hydrogen sulfide-releasing chimeras," *Biochemical Pharmacology*, vol. 85, no. 5, pp. 689–703, 2013.

[65] M. R. Hellmich, C. Coletta, C. Chao, and C. Szabo, "The therapeutic potential of cystathionine β-synthetase/hydrogen sulfide inhibition in cancer," *Antioxidants & Redox Signaling*, vol. 22, no. 5, pp. 424–448, 2015.

[66] Z. W. Lee, J. Zhou, C.-S. Chen et al., "The slow-releasing Hydrogen Sulfide donor, GYY4137, exhibits novel anti-cancer effects in vitro and in vivo," *PLoS ONE*, vol. 6, no. 6, Article ID e21077, 2011.

[67] W.-J. Cai, M.-J. Wang, L.-H. Ju, C. Wang, and Y.-C. Zhu, "Hydrogen sulfide induces human colon cancer cell proliferation: Role of Akt, ERK and p21," *Cell Biology International*, vol. 34, no. 6, pp. 565–572, 2010.

[68] C. M. Phillips, J. R. Zatarain, M. E. Nicholls et al., "Upregulation of cystathionine-β-synthase in colonic epithelia reprograms metabolism and promotes carcinogenesis," *Cancer Research*, vol. 77, no. 21, pp. 5741–5754, 2017.

[69] H. Guo, J.-W. Gai, Y. Wang, H.-F. Jin, J.-B. Du, and J. Jin, "Characterization of hydrogen sulfide and its synthases, cystathionine β-synthase and cystathionine γ-lyase, in human prostatic tissue and cells," *Urology*, vol. 79, no. 2, pp. 483.e1–483.e5, 2012.

[70] S. Sen, B. Kawahara, D. Gupta et al., "Role of cystathionine β-synthase in human breast Cancer," *Free Radical Biology & Medicine*, vol. 86, pp. 228–238, 2015.

[71] K. Módis, C. Coletta, A. Asimakopoulou et al., "Effect of S-adenosyl-l-methionine (SAM), an allosteric activator of cystathionine-β-synthase (CBS) on colorectal cancer cell proliferation and bioenergetics *in vitro*," *Nitric Oxide: Biology and Chemistry*, vol. 41, pp. 146–156, 2014.

[72] B. Kawahara, T. Moller, K. Hu-Moore et al., "Attenuation of Antioxidant Capacity in Human Breast Cancer Cells by Carbon Monoxide through Inhibition of Cystathionine β-Synthase Activity: Implications in Chemotherapeutic Drug Sensitivity," *Journal of Medicinal Chemistry*, vol. 60, no. 19, pp. 8000–8010, 2017.

[73] E. Panza, P. De Cicco, C. Armogida et al., "Role of the cystathionine γ lyase/hydrogen sulfide pathway in human melanoma progression," *Pigment Cell & Melanoma Research*, vol. 28, no. 1, pp. 61–72, 2015.

[74] H. Zhao, Q. Li, J. Wang et al., "Frequent epigenetic silencing of the folate-metabolising gene cystathionine-beta-synthase in gastrointestinal Cancer," *PLoS ONE*, vol. 7, no. 11, Article ID e49683, 2012.

[75] N. Takano, Y. Sarfraz, D. M. Gilkes et al., "Decreased expression of cystathionine β-synthase promotes glioma tumorigenesis," *Molecular Cancer Research*, vol. 12, no. 10, pp. 1398–1406, 2014.

[76] L. K. Sarna, Y. L. Siow, and O. Karmin, "The CBS/CSE system: A potential therapeutic target in NAFLD?" *Canadian Journal of Physiology and Pharmacology*, vol. 93, no. 1, pp. 1–11, 2015.

[77] J. Kim, S. J. Hong, J. H. Park et al., "Expression of cystathionine β-synthase is downregulated in hepatocellular carcinoma and associated with poor prognosis," *Oncology Reports*, vol. 21, no. 6, pp. 1449–1454, 2009.

[78] M. A. Avila, C. Berasain, L. Torres et al., "Reduced mRNA abundance of the main enzymes involved in methionine metabolism in human liver cirrhosis and hepatocellular carcinoma," *Journal of Hepatology*, vol. 33, no. 6, pp. 907–914, 2000.

[79] A. Prudova, Z. Bauman, A. Braun, V. Vitvitsky, S. C. Lu, and R. Banerjee, "S-adenosylmethionine stabilizes cystathionine β-synthase and modulates redox capacity," *Proceedings of the National Acadamy of Sciences of the United States of America*, vol. 103, no. 17, pp. 6489–6494, 2006.

[80] D. F. Calvisi, M. M. Simile, S. Ladu et al., "Altered methionine metabolism and global DNA methylation in liver cancer: relationship with genomic instability and prognosis," *International Journal of Cancer*, vol. 121, no. 11, pp. 2410–2420, 2007.

[81] S. S. Wang, Y. H. Chen, N. Chen et al., "Hydrogen sulfide promotes autophagy of hepatocellular carcinoma cells through the PI3K/Akt/mTOR signaling pathway," *Cell Death & Disease*, vol. 8, no. 3, Article ID e2688, 2017.

[82] H. Jia, J. Ye, J. You, X. Shi, W. Kang, and T. Wang, "Role of the cystathionine β-synthase/H2S system in liver cancer cells and the inhibitory effect of quinolone-indolone conjugate QIC2 on the system," *Oncology Reports*, vol. 37, no. 5, pp. 3001–3009, 2017.

[83] J. M. Thornburg, K. K. Nelson, B. F. Clem et al., "Targeting aspartate aminotransferase in breast cancer," *Breast Cancer Research*, vol. 10, no. 5, article no. R84, 2008.

[84] K. Módis, E. M. Bos, E. Calzia et al., "Regulation of mitochondrial bioenergetic function by hydrogen sulfide. Part II. Pathophysiological and therapeutic aspects," *British Journal of Pharmacology*, vol. 171, no. 8, pp. 2123–2146, 2014.

[85] A. Asimakopoulou, P. Panopoulos, C. T. Chasapis et al., "Selectivity of commonly used pharmacological inhibitors for cystathionine β synthase (CBS) and cystathionine γ lyase (CSE)," *British Journal of Pharmacology*, vol. 169, no. 4, pp. 922–932, 2013.

[86] Y. Zhou, J. Yu, X. Lei et al., "High-throughput tandem-microwell assay identifies inhibitors of the hydrogen sulfide signaling pathway," *Chemical Communications*, vol. 49, no. 100, pp. 11782–11784, 2013.

[87] M. K. Thorson, T. Majtan, J. P. Kraus, and A. M. Barrios, "Identification of Cystathionine β-Synthase Inhibitors Using a Hydrogen Sulfide Selective Probe," *Angewandte Chemie International Edition*, vol. 52, no. 17, pp. 4641–4644, 2013.

[88] S. C. Lu and J. M. Mato, "*S*-adenosylmethionine in liver health, injury, and cancer," *Physiological Reviews*, vol. 92, no. 4, pp. 1515–1542, 2012.

[89] A. W. Rutjes, E. Nüesch, S. Reichenbach, and P. Jüni, "S-Adenosylmethionine for osteoarthritis of the knee or hip.," *Cochrane Database of Systematic Reviews (Online)*, no. 4, p. CD007321, 2009.

[90] I. Galizia, L. Oldani, K. Macritchie et al., "S-adenosyl methionine (SAMe) for depression in adults," *Cochrane Database of Systematic Reviews*, vol. 2016, no. 10, Article ID CD011286, 2016.

[91] M. L. Martínez-Chantar, F. J. Corrales, L. A. Martínez-Cruz et al., "Spontaneous oxidative stress and liver tumors in mice lacking methionine adenosyltransferase 1A," *The FASEB Journal*, vol. 16, no. 10, pp. 1292–1294, 2002.

[92] R. M. Pascale, M. M. Simile, M. R. D. Miglio et al., "Chemoprevention by s-adenosyl-l-methionine of rat liver carcinogenesis initiated by 1,2-dimethylhydrazine and promoted by orotic acid," *Carcinogenesis*, vol. 16, no. 2, pp. 427–430, 1995.

[93] S. C. Lu, K. Ramani, X. Ou et al., "S-adenosylmethionine in the chemoprevention and treatment of hepatocellular carcinoma in a rat model," *Hepatology*, vol. 50, no. 2, pp. 462–471, 2009.

[94] T. R. Morgan, "Chemoprevention of hepatocellular carcinoma in chronic hepatitis C," *Recent Results in Cancer Research*, vol. 188, pp. 85–99, 2011.

[95] T. W. H. Li, H. Yang, H. Peng, M. Xia, J. M. Mato, and S. C. Lu, "Effects of S-adenosylmethionine and methylthioadenosine on inflammation-induced colon cancer in mice," *Carcinogenesis*, vol. 33, no. 2, pp. 427–435, 2012.

[96] Y. Wang, Z. Sun, and M. Szyf, "S-adenosyl-methionine (SAM) alters the transcriptome and methylome and specifically blocks growth and invasiveness of liver cancer cells," *Oncotarget* , vol. 8, no. 67, pp. 111866–111881, 2017.

[97] J. Luo, Y.-N. Li, F. Wang, W.-M. Zhang, and X. Geng, "S-adenosylmethionine inhibits the growth of cancer cells by reversing the hypomethylation status of c-myc and H-ras in human gastric cancer and colon cancer," *International Journal of Biological Sciences*, vol. 6, no. 7, pp. 784–795, 2010.

[98] T. W. H. Li, Q. Zhang, P. Oh et al., "S-adenosylmethionine and methylthioadenosine inhibit cellular FLICE inhibitory protein expression and induce apoptosis in colon cancer cells," *Molecular Pharmacology*, vol. 76, no. 1, pp. 192–200, 2009.

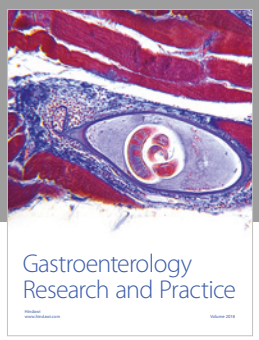
[99] L. L. Wu and J. T. Wu, "Hyperhomocysteinemia is a risk factor for cancer and a new potential tumor marker," *Clinica Chimica Acta*, vol. 322, no. 1-2, pp. 21–28, 2002.

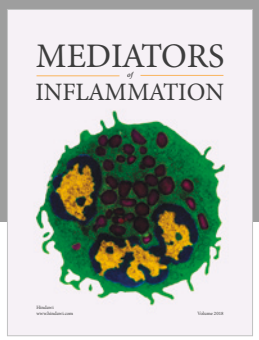
[100] Y. Özkan, S. Yardim-Akaydin, H. Firat, E. Çalişkan-Can, S. Ardiç, and B. Şimşek, "Usefulness of homocysteine as a cancer marker: Total thiol compounds and folate levels in untreated lung cancer patients," *Anticancer Reseach*, vol. 27, no. 2, pp. 1185–1189, 2007.

[101] M. R. Hellmich and C. Szabo, "Hydrogen sulfide and cancer," *Handbook of Experimental Pharmacology*, vol. 230, pp. 233–241, 2015.

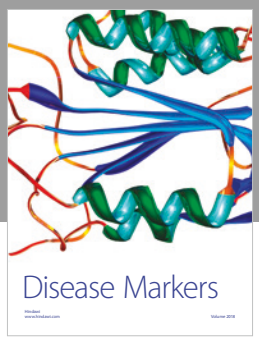
[102] H. J. Powers and S. J. Moat, "Developments in the measurement of plasma total homocysteine," *Current Opinion in Clinical Nutrition & Metabolic Care*, vol. 3, no. 5, pp. 391–397, 2000.



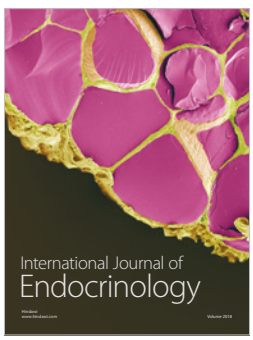






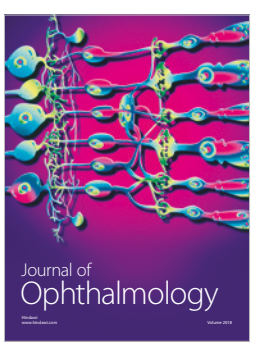


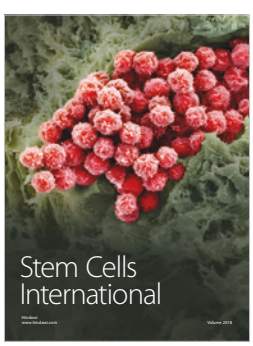


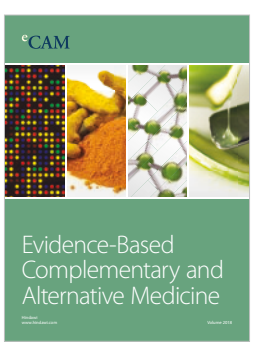






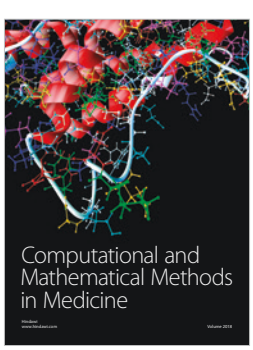


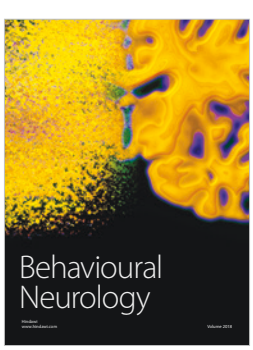




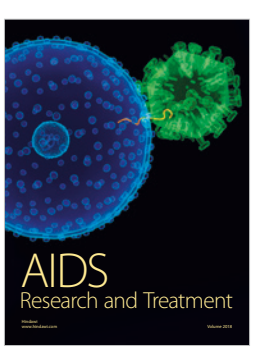


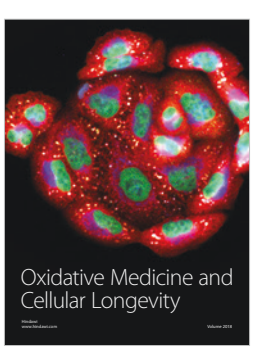












Hindawi

Submit your manuscripts at
www.hindawi.com